



**HAL**  
open science

# Modification of surface properties of biopowders by dry particle coating

Serkan Otles

► **To cite this version:**

Serkan Otles. Modification of surface properties of biopowders by dry particle coating. Chemical and Process Engineering. Institut National Polytechnique (Toulouse), 2008. English. NNT : 2008INPT033G . tel-04525200

**HAL Id: tel-04525200**

**<https://hal.science/tel-04525200v1>**

Submitted on 28 Mar 2024

**HAL** is a multi-disciplinary open access archive for the deposit and dissemination of scientific research documents, whether they are published or not. The documents may come from teaching and research institutions in France or abroad, or from public or private research centers.

L'archive ouverte pluridisciplinaire **HAL**, est destinée au dépôt et à la diffusion de documents scientifiques de niveau recherche, publiés ou non, émanant des établissements d'enseignement et de recherche français ou étrangers, des laboratoires publics ou privés.



# THÈSE

En vue de l'obtention du

## DOCTORAT DE L'UNIVERSITÉ DE TOULOUSE

Délivré par *Institut National Polytechnique de Toulouse*  
Discipline ou spécialité : *Génie des procédés*

---

Présentée et soutenue par *M. Serkan OTLES*  
Le 11 Décembre 2008

Titre : *MODIFICATION OF SURFACE PROPERTIES OF BIOPOWDERS BY DRY PARTICLE COATING*

---

### JURY

<i>Mme. Elisabeth DUMOULIN</i>	<i>Rapporteur</i>
<i>M. Pierre GUIGON</i>	<i>Rapporteur</i>
<i>M. Denis PONCELET</i>	<i>Examineur</i>
<i>M. Gérard THOMAS</i>	<i>Examineur</i>
<i>M. John A. DODDS</i>	<i>Directeur de thèse</i>
<i>M. Olivier LECOQ</i>	<i>Co directeur de thèse</i>

---

**Ecole doctorale :** *Mécanique, Energétique, Génie civil et Procédés*  
**Unité de recherche :** *RAPSODEE (centre de Recherches d'Albi en génie des Procédés, des Solides Divisés, de l'Energie et de l'Environnement), UMR EMAC-CNRS 2392, École des Mines d'Albi*  
**Directeur(s) de Thèse :** *John A. DODDS et Olivier LECOQ*

*Our true mentor in life is the science*

*H. Atatürk*



I would like to express my sincere appreciation to my advisor, Prof. Dr. John A. Dodds, for his insight, encouragement and support throughout my doctoral study. Without his guidance and motivation, this research would not have been accomplished. I am grateful to Dr. Olivier Lecoq, my co–advisor, for the help and inspiration he has brought to this work. I would also like to thank Dr. Alain Chamayou and Dr. Laurence Galet for offering valuable advices.

I would like to thank you Prof. Jacques Fages, Director of the RAPSODEE research centre, for his welcome to the laboratory.

I am grateful to Prof. Dr. Elisabeth Dumoulin from Institut des Sciences et Industrie du Vivant et de l’Environnement (AgroParisTech), Prof. Dr. Pierre Guigon from Université de Technologie de Compiègne and Prof. Dr. Gérard Thomas from Ecole des Mines de St. Etienne for their participation to my PhD defence as the jury members.

Special thanks go to our technicians Sylvie, Séverine, Laurent, Philippe and Christine in Albi and Anne Marie in St. Etienne and our secretary Anne Marie for their help, motivation and trust on me during this research.

I would like to thank you my colleagues Mokrane, Chawki, Leslie, Brice and all PhD students whom I shared unforgettable 3 years for their support during my PhD study. And specially, my dear friend Yamina for her support, friendship, motivation and also scientific advices, thank you very much Yamina. I can not forget also my colleagues whom I spent just couple of weeks in St. Etienne but I got friends for life time.

And of course Marie-France, my french teacher, who allowed me to express myself with a language that I have never used in my life and helped me to adapt myself to this lovely country and people.

I am also grateful to two very special people, first of all, Nadia, without your support I wouldn’t be able to write these sentences, thank you very much for being next to me all the time. And Abdellah of course, thanks a lot for everything you did.

I would like to express my endless gratitude to my parents, Salih and Oya, my sister Yesim and all of my family who have always helped me in everyway possible. And all of my friends, especially to Cem Cakiroglu and Emre Batir for their support and motivation.

Last, but certainly not least, I want to thank you to the person who is my inspiration source, lighthouse in the academic ocean and always holds my hand to show the way, my uncle Prof. Dr. Semih Otles. Thank you Amca for everything, this is your achievement.



**TABLE OF CONTENTS**

	<b>Page</b>
<b>Introduction</b>	<b>9</b>
<b>Chapter I. Background on Dry Particle Coating</b>	<b>15</b>
1. Introduction	17
2. Advantages of dry coating	18
3. Origin of dry coating	18
3.1. Ordered Mixture	18
3.2. Dry Coating Mechanism	20
4. Inter-particular Forces	24
4.1. Van der Waals Forces	24
4.2. Capillary Force	26
4.3. Electrostatic Force	27
4.4. Dependency of Inter-particular Forces on Different Parameters	28
5. Dry Particle Coating Equipments	32
5.1. Mechanofusion	32
5.2. Nara Hybridizer	33
5.3. Hosokawa Cyclomix	36
5.4. Magnetically Assisted Impaction Coater	38
5.5. Theta Composer	40
5.6. V–Blender	41
5.7. Rotating Fluidizer Bed Coater	42
6. Applications on Dry Coating	43
7. Conclusion	45
<b>Chapter II. Materials and Methods</b>	<b>47</b>
1. Introduction	49
2. Dry Particle Coating Equipments	49
2.1. Nara Hybridizer	49
2.2. Hosokawa Cyclomix	51
2.3. Turbula Mixer	52
3. Characterization Methods	53
3.1. Environmental Scanning Electron Microscopy	55
	5

---

3.2. Atomic Force Microscopy	56
a) Tapping Mode	57
b) Contact Mode	59
c) Non – Contact Mode	61
3.3. Laser Diffraction Granulometer	62
3.4. Helium Pycnometer	64
3.5. Tapped Density Tester	64
3.6. Freeman Technology Powder Rheometer	66
3.7. Contact Angle Measurement	68
3.8. Dynamic Vapour Sorption	68
4. Materials	69
4.1. Poly(methyl methacrylate)	70
4.2. Cellets	72
4.3. Talc	73
5. Conclusion	75
<b>Chapter III. Effect of Equipment and Operating Conditions on the End-Use</b>	
<b>Properties of Composite Particles</b>	<b>77</b>
1. Introduction	79
2. Dry Coating of Particles in Hybridizer	80
2.1. Hydrodynamic Properties of Hybridizer	80
2.2. Preliminary Study of Poly(methyl methacrylate) Particles	81
2.2.1. General Mass Balance	82
2.2.2. Effect of Rotational Velocity on the Particle Size Distributions	82
2.3. Preliminary Study of Talc Particles	84
2.4. Dry Coating of Poly(methyl methacrylate) with Talc	86
2.4.1. General Mass Balance	87
2.4.2. Measurement of Solid Densities of the Dry Coated Particles	87
2.4.3. Characterization of Surface Morphology of the Particles	89
2.4.4. Characterization of Particles by Atomic Force Microscopy	90
A) Topographical Analysis of the Particles	91
B) Phase Contrast Analysis of the Particles	96
C) Measurement of Adhesion Forces Between the Particles	102



---

2.4.5. Calculation of Talc Particle Deposition on the Surface of the Coated Particles	110
2.4.6. Characterization of Coating Strength of the Particles	112
A) Effect of Operating Velocity on the Coating Strength of the Particles	113
B) Effect of Mass Percentage of Talc on the Coating Strength of the Particles	116
C) Effect of Equipment on Coating Strength of the Particles	118
2.4.7. Characterization of the Flowability Properties of the Particle	120
A) Effect of Operating Velocity on the Flowability Properties of the Particles	120
B) Effect of Mass Percentage of Talc on the Flowability Properties of the Particles	122
C) Effect of Equipment on the Flowability Properties of the Particles	125
2.5. Conclusion	126
3. Dry Coating of Particles in Cyclomix	130
3.1. Preliminary Study of Poly(methyl methacrylate) Particles	130
3.1.1. General Mass Balance	131
3.1.2. Effect of Rotational Velocity on Particle Size Distributions	131
3.2. Dry Coating of Poly(methyl methacrylate) with Talc	133
3.2.1. General Mass Balance	133
3.2.2. Measurement of Solid Densities of the Dry Coated Particles	134
3.2.3. Characterization of Surface Morphology of the Particles	135
3.2.4. Characterization of Coating Strength of the Particles	136
A) Effect of Operating Velocity on Coating Strength of the Particles	136
B) Effect of Mass Percentage of Talc on Coating Strength of the Particles	138
C) Effect of Equipment on Coating Strength of the Particles	140
3.2.5. Characterization of Flowability Properties of the Particle	141
A) Effect of Operating Velocity on Flowability Properties of the Particles	141
B) Effect of Mass Percentage of Talc on Flowability Properties of the Particles	144

C) Effect of Equipment on Flowability Properties of the Particles	145
3.3. Conclusions	146
4. Dry Coating of Particles in Turbula	148
4.1. Preliminary Study of Poly(methyl methacrylate) Particles	148
4.2. Dry Coating of Poly(methyl methacrylate) with Talc	149
4.2.1. Measurement of Solid Densities of the Dry Coated Particles	150
4.2.2. Characterization of Surface Morphology of the Particles	150
4.2.3. Characterization of Coating Strength of the Particles	151
A) Effect of Mass Percentage of Talc on Coating Strength of the Particles	151
B) Effect of Equipment on Coating Strength of the Particles	153
4.2.4. Characterization of Flowability Properties of the Particles	154
A) Effect of Mass Percentage of Talc on Flowability Properties of the Particles	154
B) Effect of Equipment on Flowability Properties of the Particles	157
4.3. Conclusions	157
5. Conclusions	159
5.1. Visual Analysis of The Dry Coated Particles in Different Equipments	159
5.2. Coating Strength of The Dry Coated Particles in Different Equipments	160
5.3. Modification of Flowability Properties of Dry Coated Particles in Different Equipments	161
<b>Chapter IV. Effect of Particle Size on the End–Use Properties of Composite Particles</b>	<b>163</b>
1. Introduction	165
2. Effect of Host Particle Size on the End – Use Properties of the Dry Coated Particles	166
2.1. Preliminary Study of Cellets 90 and Cellets 200 Particles	166
2.1.1. General Mass Balance	167
2.1.2. Effect of Rotational Velocity on Particle Size Distributions	168
2.2. Dry Coating of Cellets 90 and Cellets 200 with Talc	168
2.2.1. Characterization of Surface Morphology of the Particles	174
2.2.2. Characterization of Particles by Atomic Force Microscopy	176

---

A) Topographical Analysis of the Particles	177
B) Phase Contrast Analysis of the Particles	182
C) Measurement of Adhesion Forces Between the Particles	186
2.2.3. Calculation of Talc Particle Deposition on the Surface of the Coated Particles	189
2.2.4. Calculation of Van der Waals Forces Between the Particles	191
2.2.5. Characterization of Coating Strength of the Particles	192
A) Particles in Hybridizer Trials	192
B) Particles in Cyclomix Trials	195
C) Particles in Turbula Trials	198
D) Particles in Basic Mixing Trials	201
2.2.6. Characterizations of the Hydrophilic Properties of The Particles	205
A) Characterization of the Wettability of the Particles	206
B) Characterization of Water Affinity of the Particles	207
2.3. Conclusions	210
3. Effect of Guest Particle Size on the End – Use Properties of the Dry Coated Particles	213
3.1. Dry Coating of Cellets 200 Particles with Talc and Talc 16000	213
3.1.1. Characterization of Surface Morphology of the Particles	214
3.1.2. Characterization of Coating Strength of the Particle	216
A) Particles in Hybridizer Trials	217
B) Particles in Cyclomix Trials	218
C) Particles in Turbula Trials	220
D) Particles in Basic Mixing Trials	222
3.2. Conclusions	225
4. Conclusions	226
<b>Conclusion &amp; Perspectives</b>	<b>229</b>
<b>Appendices</b>	<b>239</b>
<b>References</b>	<b>277</b>



# INTRODUCTION



For many years, scientists have been mixing powders for different purposes, mainly by the method of stirring. Recently, particle design, structuring and optimization of physical and chemical properties to achieve a combination of the desired effects, has grown in importance. Powder coating is a method that focuses on improving or modifying some specific properties of powders that the natural product does not offer. It is an essential operation in the preparation of pharmaceutical materials for controlled–drug delivery within the body, food manufacture which must combine a desirable appearance, aroma and enhance shelf life, plastic processing, ceramic materials, fertilizer production, mining industry and powder metallurgy industry. The importance of powder coating resides in the fact that it is not only the base material which determines the properties of end products, but also, they are guest materials and process conditions.

At present, most commercial coatings of particles, grains, granules or pellets are done using wet coating processes. The most popular methods employed by industry are pan coaters or fluidized bed coaters with various flow patterns and solution spraying nozzles or by wet chemistry based techniques such as coacervation and interfacial polymerization. These methods need suitable solvents (aqueous or organic based) to form a barrier or film between the host particle and its environment, to dissolve or suspend the coating materials to form the solution/suspension, and the tiny liquid droplets are sprayed to the surface of the substrate particles in the fluidized zone. During processing, the coated particles are simultaneously dried and the end product is obtained. There are several major disadvantages of the existing wet coating techniques. First of all, it is the potential environmental hazard due to the use of volatile solvents. Also, wet coating systems are expensive to operate and it requires a drying stage. The disadvantages of wet coating techniques forced researchers in the field of powder technology to find an alternative or other suitable methods for coating powders. Dry particle coating is the alternative method that does not produce any hazardous waste products and does not require and kind of binders, solvent or even water for coating. It doesn't need any drying step since it doesn't require any kind of solvents, so energy savings makes the dry particle coating process more economical compared to traditional wet coating.

Dry particle coating has been developed from a powder mixing concept that was introduced by Hersey in 1975, which is the “ordered mixture”. In ordered mixing, cohesive fine powder is mixed with coarser particles (the particle size ratio of fine and coarser particles is between 10 and 100), the fine particles (guest) would adhere and create a particle layer on the surface

of the larger particles (host) because of the inter-particle forces between the particles are stronger than the weight of the fine particles (Stephenson et al., 1980, Bannister et al., 1983, Staniforth et al., 1985). In dry particle coating process the same procedure happens but additionally, different equipments, which generate mechanical forces such as impact and shear, are used in order to break the fine agglomerates and coat the coarser particles with them. The surface covering would be more permanent than ordered mixing because of a stronger physical (or chemical) bonding (Alonso et al., 1999).

Dry particle coating process has 3 main terms that are; powder couple (host & guest particles), process (equipment, operating conditions) and the end-use properties of the composite particles. It is very complex to understand the relationship between these parameters. As an example, in order to obtain specific end-use properties for a certain powder couple which equipment and what operating conditions should be chosen? The current state of art approach is to use a trial and error procedure to answer this question. It is necessary to understand the physicochemical principles that govern the coating process to predict the choice of machines and the right combination of process variables needed to produce composite materials with desired end-use properties. In this study, which is a partner of the European Union 6<sup>th</sup> Framework Program-Biopowders Project (Appendix IX), the general aim is to develop a fundamental knowledge in dry particle coating process, to better understand the interactions between the powder couple, process and the end-use properties and also to classify the criteria (operating conditions, equipment used, choice of powders, particle size distribution etc...) that affect the end-use properties of the particles. In order to simplify the complexity of the problem some “model couples” have been chosen. There are some criteria for model couple (host and guest particles) linked to characterization techniques. For example, the particles should have a simple chemical composition and structure; they should be spherical so that the layer of guest particles on the host particles can be characterized by different characterization methods. Moreover, the particles should have certain particle size ratio between them (like 10 times), in order to benefit from the ordered mixture concept in dry particle coating process.

Poly(methyl methacrylate) (PMMA) and talc particles have been chosen as the first model couple because of certain reasons. First of all they are both bio-powders (pharmaceutical, food powders) and they have particle size ratio more than 10 times so that they are available for ordered mixture concept. In addition to being a bio-powder, PMMA particles have a regular



spherical shape and smooth surface which enables us to see the coating performance easily by visual methods and by different characterization techniques.

Cellets particles, which are simply microcrystalline cellulose, and talc particles, have been used as the second model couple since cellets particles are also bio-powder and has a suitable morphology for being analyzed by different characterization methods.

**In the first chapter of the thesis,** a background on the dry particle coating process will be constructed by reviewing early studies in the scientific literature. The description of the dry particle coating process and its advantages, its mechanism, the relationship with different physico-chemical phenomena, different dry particle coating equipments and various dry particle coating applications in different domains will be presented.

**In the second chapter,** the model couples and the equipments that were used for dry particle coating trials will be presented. Moreover, the principles of different characterization methods that were used to study the modification of the end-use properties of the particles will be described in detail.

**In the third chapter,** we focus on the different dry particle coating equipments and their operating conditions influencing the coating phenomena, end-use properties of PMMA and talc particles (first model couple) and to the development of the AFM technique (AFM study has been done with collaboration to Centre CIS, Ecole des Mines de St. Etienne,) to derive coating coverage information. The feasibility of dry coating of PMMA with talc particles using different dry particle coating equipments (Nara Hybridizer, Cyclomix, Turbula) will be studied. Several characterisation methods are used to study the physico-chemical properties (mechanical coating strength and flowability) of the coated PMMA particles in different equipments with different operating conditions.

**In the fourth chapter,** two different particle size distributions of cellets and talc particles (second model couple) are chosen for dry coating process in different equipments in order to study the influence of the size of the host and guest particles on the different end-use properties (mechanical coating strength, wettability and water affinity) of the particles.

**At the end,** the general conclusions of the thesis according to the principle results that were obtained and the future perspectives will be presented.



# CHAPTER I

## *Background on Dry Particle Coating*



## 1. INTRODUCTION

Particle coating or surface modification technology has been used for the synthesis of composite materials with desired end-use properties in many industries, including pharmaceuticals, food, cosmetics, ceramics, electronics and special chemicals. At present, most commercial powder coatings are done by wet coating methods such as sol-gel processes, wet chemical deposition, spray coating, dip coating, spinning disc coaters and a variety of fluidized bed coaters. Wet particle coating is used primarily to form a barrier or film between the host particle and its environment. The coating material usually consists of a solute dissolved in an organic solvent or an aqueous suspension of the solute. The organic solvent is usually highly volatile (VOC). VOCs have been implicated as a major precursor in the production of photochemical smog, which causes atmospheric haze, eye irritation and respiratory problems and even some VOCs are carcinogenic. These environmental drawbacks of wet coating methods have forced researchers in the powder technology field to find alternative methods for coating of powders (Yokoyama et al., 1987, Tanno, 1990, Naito et al., 1993a).

Dry particle coating is a relatively new and alternative approach to wet coating methods and it has drawn attention of many researchers. It uses mechanical forces (mechanical impact, shearing etc.) in order to attach submicron-sized fine particles (guest) on to relatively larger micron-sized (host) particles without using any solvents, binders or even water (Pfeffer et al., 2001). Since the size of the guest particles is so small, Van der Waals interactions are strong enough to keep them firmly attached to the host particles (Ramlakhan et al., 2000). Depending on choice of equipment, operating conditions and particle properties, either a discrete or continuous coating of guest particles can be obtained (figure I.1).

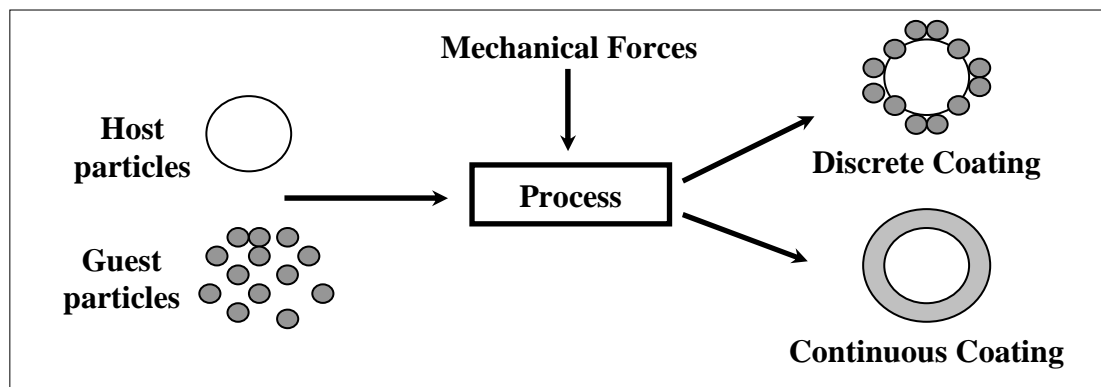


Figure I.1. Dry Particle Coating Process

## **2. ADVANTAGES OF DRY PARTICLE COATING**

Dry particle coating is used to make modifications of the properties or functionality of the host particle and create new generation of composite particles. Some examples of surface properties that can be improved or modified are flowability, dispersibility, solubility, wettability (hydrophilic/hydrophobic properties), electrostatic, electric, magnetic, optical, colour, flavour, taste, particle shape/sphericity, sinterability and solid phase reactivity (Pfeffer et al., 2001). So, dry coating process opens up many different applications in different areas like pharmaceutical, food technology, herbal/cosmetics, agricultural, powder processing industries etc.

In addition to producing materials with different functionality, dry coating process has an advantage of being cost effective due to the reduced use of high-price or rare materials since the more expensive material (guest) can be coated onto the cheaper carrier material (host) and also there is no need for drying the products which results in substantial energy savings. Another major advantage of dry particle coating process is that it is environmentally benign, producing none of the organic (gas or liquid) or aqueous waste streams, which usually are present in wet coating processes (Honda et al. 1994, Sreejith et al., 2000, Pfeffer et al. 2001).

## **3. ORIGIN OF DRY PARTICLE COATING**

The research in dry particle coating process started in Japan about twenty years ago and it is still a developing technology.

### **3.1. Ordered Mixture**

The subject of dry particle coating is closely related to the subject of dry mixing of powders. Theoretically, a binary mixture process should mix two different species of powders so that any sample taken from the mixture would contain the same proportion of the two powders. This is very hard to achieve practically when the powders are either cohesive or they are very different in particle size. When powders are cohesive, they naturally form agglomerates and mixing of these powders requires breaking up of the agglomerates preliminarily. When the powders are very different in particle size, there is an increased tendency for segregation as the particle size becomes larger. However, when the particles to be mixed are very different in particle size (one or two orders of magnitude), then the small particles tend to adhere on the surface of the coarser particles. The adhesion force between the smaller particle and the larger particle is greater than the weight of the smaller particle so the detachment of small particles

from the surface of larger particles is difficult (Pfeffer et al., 2001). Hersey (1975) coined the term “ordered mixture” for this kind of mixture, to distinguish it from the random mixture that results when non-cohesive powders are mixed. Figure I.2 shows the concept of ordered mixture.

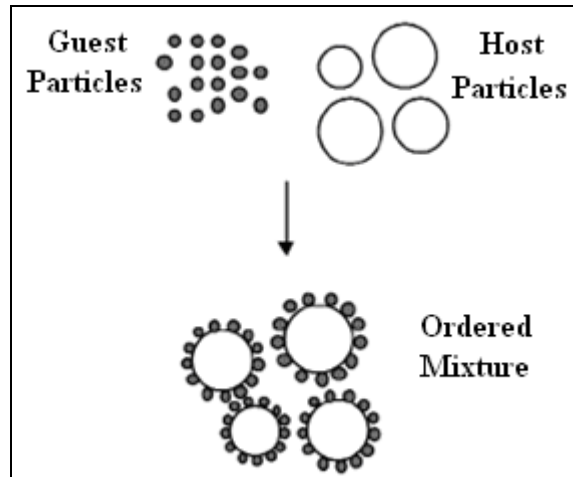


**Figure I.2.** Ordered Mixture

The advantage of ordered mixture is that it provides a much better degree of homogeneity than random mixing as long as the particle size distribution of the larger size particles is not too wide (Hersey, 1975, Bannister et al., 1983). So, in terms of subsequent segregation, ordered mixtures are more stable than random mixtures (Hersey, 1975, Yip et al., 1977, Alonso, 1989a). It was also shown by early researchers that having a very wide size distribution of the large size particles may lead to “ordered unit segregation”, because of the nature of the poly-disperse coarse particles (Hersey, 1977, Yip et al., 1977, Thiel et al., 1982). Egermann (Egermann et al., 1983) called the term “regimented” mix or “interactive mix” for this phenomenon. Staniforth and colleagues also studied ordered mixtures applicable to the pharmaceutical industry (Staniforth et al., 1985).

Bannister and Harnby (1983) explained the ordered mixing process qualitatively. They identified the ordered mixing process in to 3 stages. It starts with separation of the agglomerates of the fine particles in to their primary particles then the bonding of these fines to carrier particles follows. It finishes with redistribution and exchange of fine particles among the carrier particles until a random distribution is achieved. The real process may not take place exactly in that order but it is sure that the de-agglomeration of fine particles must occur in order to have the ordered mixture. Therefore in order to achieve ordered mixing,

sufficient mechanical energy to promote de-agglomeration of fine particles must be used, which means to create particle collisions by mechanical impact and shearing forces. Machines that can be used for this purpose are high shear mixers and grinding machines. Yeung and Hersey (1977) showed that, it is easier to break up fine agglomerates into primary particle size in the presence of coarser particles in the mix when processed in a high shear mixer, than having fine particle agglomerates alone. Since, the host particles act as the media and help the de-agglomeration of the fine particles in this phenomenon.

### 3.2. Dry Particle Coating Mechanism

In a typical dry particle coating process, coarse particles are mechanically mixed with fine cohesive powder. The resulting mixture is expected to have a layer of fine (guest) particles adhering to the surface of large particles. Alonso and colleagues studied the mechanism of dry particle coating (Alonso et al., 1988, 1989a and b, 1990, 1999, 2001). They tried to explain the kinetics of fine particle transfer on carriers in dry particle coating processes by using a statistical model and experimental observations. The model was used to simulate the stages of coating process and understand the influence of some parameters like the effect of the particle size ratio between the coarse and fine particles and the concentration of fine particles in the mixture. They explained the stages of dry particle coating in a special type of mixer, the Angmill Mechanofusion System.

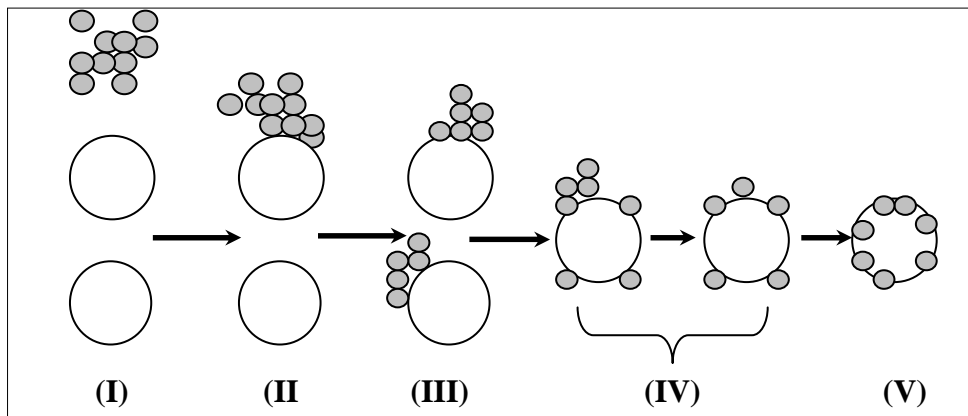


**Figure I.3.** Mechanism of Dry Particle Coating in Mechanofusion

(I) Initial condition, (II) Formation of first carriers, (III) Carriers transferring fines to non-coated particles, (IV) Breaking up of agglomerates and dispersion of fines on the surface of carriers, (V) Mechanofusion



As it can be seen from figure I.3, at the beginning of the operation the fine aggregates adhere to the coarse particles in their immediate vicinity. When a coarse particle carrying fines adheres its surface collides with a non-coated particle, it transfers part of its fines to the latter. By friction and collision between the particles, the agglomerates of fines are gradually dispersed onto the surface of the carriers, which results in an increase in the coated surface area. Afterwards, the mechanofusion system greatly modifies the surface texture by giving a high level of mechanical energy to the particles. Locally melting and a partial or total penetration of the fine component into the body of the larger particles take places. The dispersion of fines actually occurs from the earlier stages of the process. The dispersion rate and the degree to which the agglomerates are broken up depend strongly on the mechanical energy input and therefore, on the type of mixer used.

These authors coated Poly(methyl methacrylate) particles (50  $\mu\text{m}$  mean particle size) with magnetite black spheres (0.17  $\mu\text{m}$  mean particle size) in mechanofusion system in order to analyze the different stages of dry particle coating. From the former experiments and direct observation, they concluded that the spreading of fines within the mixture occurs by collisions between coated and non-coated particles and they found that a reaction of type  $C+N \rightarrow C+C$  between coated (C) and non-coated (N) particles was a suitable analogy to describe the process (Alonso et al., 1989b).

Honda and co-workers (1991, 1994) were interested on the adhesion mechanism of particles by dry particle coating process. They considered that the principal forces involved in dry particle coating process are Coulomb and Van der Waals forces. This study also showed the effect of particle size ratio between the host and guest particles on dry particle coating process.

The concept of ordered mixing and dry coating process were also described in a series of papers by early researchers (Honda et al., 1987, 1988, 1989, 1991, 1992, 1994, 1995, 1997 and 1998). They observed that, an ordinary dry mixing process would result in an ordered mixture, as the fine particles attach to the larger host particles through electrostatic forces (Honda et al., 1991). However, a shear mixer would generate high impulsive forces which cause the fine particles to become attached to the host particle and a coated composite particle is obtained. This device, called the Hybridizer, is manufactured by Nara Machinery of Japan. The hybridizer has proven very useful for pharmaceutical applications; for example, it

accelerated indometacine dissolution when coated onto a carrier particle such as potato starch (Ishizaka et al., 1993a).

However, the earliest reference to a device specifically used for dry particle coating comes from Japan (Yokoyama et al., 1987). The grinding device, called the Angmill, was used for creating particulate materials with different surface properties due to the strong mechanical force acting on the particles. Since the combination of high shear and compression forces acting on the host and guest particles produced some surface fusion, the treatment was termed mechanofusion and the device is also called Mechanofusion which is manufactured by Hosokawa Micron.

On the other hand, Hosokawa recently developed another type of high shear mixer, called the Cyclomix, for dry particle coating applications. It uses mechanical impact and shearing forces in order to mix and coat the particles. It is considered to be a high shear mixer for dry particle coating process (Ghadiri et al., 2007a and b, Hassanpour et al., 2008, Rahmanian et al., 2008). The Mechanofusion and Hybridizer can also produce chemical interactions as well as physical surface interactions between the host and guest particles. These equipments are responsible for the adhesion between the host and guest particles and also the de-agglomeration of the guest particles. Moreover, these devices may cause change in the chemical and electrostatic states of the host and guest particles as a result of the mixing caused by the mechanical forces generated by the machines. In addition to physical adhesion, a chemical reaction may occur at the interface of host-guest particles and causes new surface properties of the composite particles. The process is called mechano-chemical reaction (mechanochemistry). Watanabe and colleagues (2002, 2003) studied the mechano-chemical reaction by mixing indometacine with silica nano-particles. Watano and co-workers (2000) worked on changing the end use properties of some special type of food powder by coating them with hydrophilic silica ( $\text{SiO}_2$ ). They tried to understand the phenomenon of mechano-chemical reaction in dry particle coating processing. They observed that reaction between hydrophilic OH groups of food fibre and silanol groups  $-\text{Si}(\text{OH})-$  results in dehydration (fig. I.4), which leads to suppression of the hygroscopic properties of the food fibre.

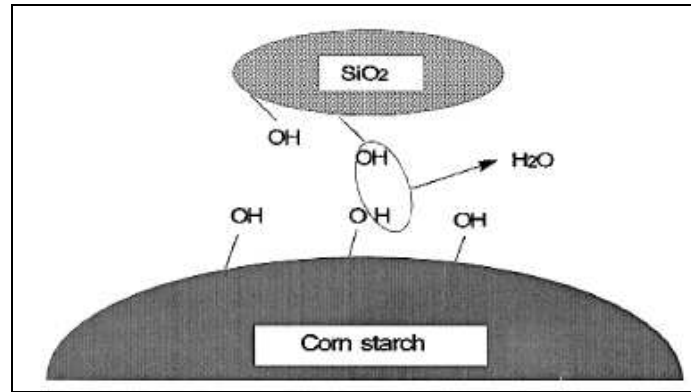


**Figure I.4.** Mechano-chemical Reaction (Watano et al., 2000)

The mechanofusion, hybridizer and cyclomix are considered to be high shear mixers. They produce coated particles by using high level mechanical forces. In certain applications, these high forces are not necessary or they may even cause excessive size reduction of the host particles. For this purpose, there are some other dry particle coating devices that apply smaller level of forces on the particles. For example the theta composer, an elliptical rotor-type powder mixer, was developed for this purpose and manufactured by the Tokuju Company. Several articles describe the operation of the theta composer, which has been found to be very useful for dry coating of certain pharmaceutical and food powders (Fukumori et al., 1998, Kawashima, 1998, Watano et al., 2000).

A V-blender is also another equipment that has been used by early researchers for the purpose of dry coating of particles. The V-blender mixes the powders gently by using rotational movement and achieves good powder mixing at the end (Yang et al., 2005).

There is another softer dry coating method which is called magnetically assisted impaction coater (MAIC) uses a magnetic field to accelerate and spin larger magnetic particles, mixed with the host and guest particles thus promoting collisions between the particles and with the walls of the device (Singh et al., 1997, Ata et al., 1998).

Rotating fluidizer bed coater (RFBC) is also another dry particle coating equipment that applies small level of mechanical forces on the particles. This equipment is developed by New Jersey Institute of Technology and it is based on the principle of centrifugal fluidization (Watano et al., 1998).

During dry particle coating process, individual particles are in contact with each other and with the surface of the equipment used. The degree of interaction between the particles and between the particles and the surfaces of the equipment determines the properties of the

composite particles. Inter-particle forces influence the interaction between the particles and play an important role in the dry particle coating process. In the following section, the adhesion mechanism of particles and the inter-particle forces between the particles will be discussed.

#### **4. INTER-PARTICULAR FORCES**

The nature and degree of particle interactions determine the surface properties of the composite particles (Podczek, 1997). There are two principle interaction mechanisms between the particles, which are adhesion and friction. Adhesion is the result of the inter-particle forces between the particles or a particle with a surface that are in contact. It may occur between the particles and surfaces with different chemical nature or with the same chemical nature which is termed as cohesion. With respect to single particle interactions, the term cohesion is applicable only when the particles are as close as an atomic distance between each other. Friction is the force preventing the tangential displacement of two solid or particle surfaces in contact (Podczek, 1997).

Adhesion between particles and between particles and surfaces are primarily due to Van der Waals Forces, capillary forces, electrical forces and electrostatic coulomb forces. They usually arise because of the interactions between dipole-dipole, charge-dipole, charge-charge, covalent, charge-non-polar, dipolar-non-polar, non-polar-non-polar and also hydrogen bonding (Seville et al., 1997). The inter-particle forces depend on the particle size and the distance between the two acting particles and on the other hand on the shape including surface properties and deformation, as well as the chemical identity of the particles.

In the following section, different inter-particle forces will be introduced and the parameters influencing the forces will be described.

##### **4.1. Van der Waals Forces**

Van der Waals forces ( $F_{vdw}$ ) are a class of intermolecular forces which arise when molecules are polarized and becoming dipoles or multi-poles. Three different Van der Waals forces exist between molecules. These are; Keesom forces, Debye forces and London forces. The Keesom forces are the attractive forces between permanent dipole molecules. The Debye forces are the attractive forces between a permanent dipole molecule and an induced dipole molecule. An induced dipole molecule is a non-polar molecule which was induced to become a dipole molecule by the attractive force of another dipole molecule. London forces are attractive

forces between two non-polar molecules. They are also called as induced dipole-induced dipole forces.

In order to determine the Van der Waals interactions between particles, two different approaches are described in the literature. The microscopic approach, which is also called as the Hamaker integration, is based on the interactions between atoms and molecules (Hamaker, 1937). It can be calculated by integrating the molecular density over the entire volume of the solids (Israelachvili, 1991). The calculation is performed using the Hamaker constant;

$$A_H = \pi^2 C_{AB} \sigma_A \sigma_B \quad (\text{Eqn.I.1})$$

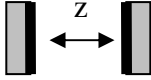
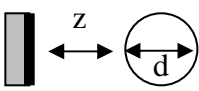
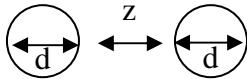
Where  $\sigma_A$  and  $\sigma_B$  are the number of atoms per unit volume of molecule A and B, C is the coefficient in the atom–atom pair potential.

In reality the van der Waals forces between two molecules are changed by the presence of a third molecule. This problem of additivity is completely avoided in the macroscopic theory developed by Lifshitz (1956). Lifshitz neglects the discrete atomic structure and the solids are treated as continuous materials with bulk properties. It is related to the Hamaker coefficient by;

$$A = \frac{3}{4\pi} h\bar{\omega} \quad (\text{Eqn.I.2})$$

Table I.1 shows different models of Van der Waals forces, considering the surface geometry of the two partners (flat surface/flat surface, flat surface/sphere, sphere/sphere). It is assumed that the surfaces are smooth and there is no particle deformation (no surface roughness) and that the distance is between 0.4 nm and 100 nm.

**Table I.1.** Van der Waals Forces ( $F_{vdw}$ ) Between the Model Partners

Model	Microscopic Calculation	Macroscopic Calculation
	$\frac{F_{vdw}}{A_s} = \frac{A_H}{6\pi z^3}$	$\frac{F_{vdw}}{A_s} = \frac{h\bar{\omega}}{8\pi^2 z^3}$
	$F_{vdw} = \frac{A_H d}{6z^2}$	$F_{vdw} = \frac{h\bar{\omega} d}{16\pi z^2}$
	$F_{vdw} = \frac{A_H d}{24z^2}$	$F_{vdw} = \frac{h\bar{\omega} d}{32\pi z^2}$

Fatah (2007) calculated Van der Waals forces between alumina (3 and 13  $\mu\text{m}$ ) and titanium oxide (204, 159 and 167 nm) powders with taking into account the effect of surface roughness. For two identical, spherical particles with a certain surface roughness ( $a$ ), the Van der Waals forces can be calculated by using the equation I.3;

$$F_{vdw} = \frac{A_H R}{12z} \left[ \frac{a}{(z+a)^2} + \frac{a}{(z+a)} \right] \quad (\text{Eqn.I.3})$$

Where,  $R$  is the radius of the identical particles.

#### 4.2. Capillary Forces

Capillary forces ( $F_c$ ) arise from the moisture in the gap between contiguous bodies that form liquid bridges to adhered surfaces (fig.I.5). They are very important for powder flow. Moist powders usually exhibit poor flow properties, sticking to the walls of hoppers or other surfaces during powder handling. In the case of hydrophilic porous materials, moisture is trapped in the pores that build up liquid bridges to adhered surfaces. In some cases, moisture in the gap between contiguous bodies condenses, giving rise to capillary forces (Seville et al., 1997).

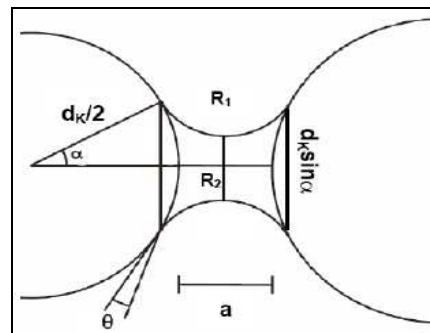


**Figure I.5.** Scheme of a Liquid Bridge (Israelachvili, 1991)

Capillary forces due to moisture condensation depend on the geometry of the gap, properties of the materials in contact, surface free energy, wettability and surface roughness. Moisture starts condensing in the gap in air at a relative humidity of about 50%. Also, above a relative humidity of 65% to 75%, capillary forces dominate the adhesion force (Massimilla et al., 1976).

In the literature different approaches for the calculation of capillary forces are performed considering the geometry of the particles (Naidich, 1967, Toussaint, 1997, Rabinovich, 2005).

When the liquid condenses between a sphere and a surface, the Laplace pressure developed due to the curved liquid surface pulls the sphere and the plane together. A critical distance is described depending on the volume of the liquid bridge. By overstepping this distance the capillary will shear and the force will disappear. Israelachvili (1991) proposed an equation to calculate the capillary force:

$$F_c = 4\pi\gamma_L(\cos\theta) + 4\pi R\gamma_{sl} \quad (\text{Eqn.I.4})$$

Where  $\gamma_L$  is the surface tension of the condensed liquid, and  $\gamma_{sl}$  is the solid/liquid interfacial free energy, R is the radius of the adhered sphere;  $\theta$  is the contact angle between the adhered particle and the liquid. Adamson (1976) proved that capillary forces are proportional to the product of the wetted area of surfaces and the tension arising from the liquid pressure. Consequently, there will be a maximum capillary force at an intermediate value of the liquid tension, which is the quotient between surface tension and the radius of curvature of the liquid meniscus.

### 4.3. Electrostatic Forces

Electrostatic forces (Coulomb forces) ( $F_{el}$ ) emerge between charged particles. When the particles are both either positively or negatively charged, the force is repulsive. When they are of opposite charge, it is attractive. The force can result from friction or even by contacting solid surfaces and building up an electric potential. Due to electron transfers between the particles the potential emerges. The particle, which needs less energy to release the electrons, delivers them to the other particle. The charging of isolators and electronic conductors is depending on the electron surface density (Visser, 1989).

The force acting on one charged particle having charge  $q_1$  by another charged particle having charge  $q_2$  is given by Coulomb's law as;

$$F_e = \frac{1}{4\pi\epsilon_0} \frac{q_1 q_2}{s^2} \quad (\text{Eqn.I.5})$$

Where,  $\epsilon_0$  is the permittivity of vacuum. The force of interaction between a spherical particle of radius R and charge Q, interacting with an adjacent uncharged particle with a separation distance H due to it's own image charge is given by;

$$F_e = \frac{Q^2 \left[ 1 - \frac{H}{(R^2 + H^2)^{1/2}} \right]}{16\pi\epsilon_0 H^2} \quad (\text{Eqn.I.6})$$

However, the electron density of surfaces is inhomogeneous and cannot be determined and the charging can be influenced by adsorbed impurities covering the surfaces. Thus, the calculation of  $F_{el}$  is difficult and often leads to only an approximate value.

#### 4.4. Dependency of Inter-particle Forces on Different Parameters

There are four main mechanical factors influencing adhesion namely: surface roughness, particle size and shape, material hardness and elasticity and the work of adhesion and surface free energy. Surface roughness is one of the most important mechanisms influencing adhesion because it is strongly related to the geometry of contact. As it is illustrated in figure I.6, the Van der Waals forces will be approximately zero for the case (a) and (b), because the surface is rough which limits the approach of two particles and hence low contact area. However for cases (c), (d) and (e), the Van der Waals forces are high, as there is large contact area between the particles.

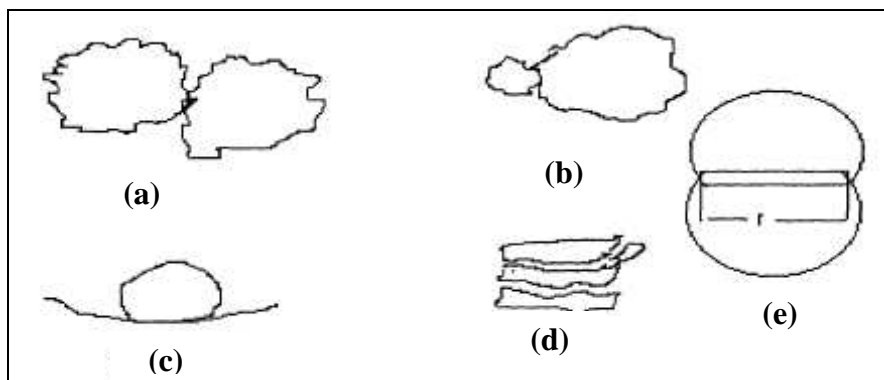


**Figure I.6.** Surface Roughness and Geometrical Factors on Van der Waals Forces (Visser, 1989)

Moreover, the effect of surface roughness on the inter-particle forces is demonstrated by Goetzinger and Peukert (2003), using the model of a flat surface and a spherical particle. The spherical particle has a certain surface roughness, which increases the distance between the particle and the surface. Van der Waals forces are very sensitive on changes in the diameter. By increasing the diameter of the roughness of the spherical particle the amount of the forces is decreased as the distance between the spherical particle and the flat surface enlarges until a



certain surface roughness diameter. The relation between the different diameters and the inter-particle force are shown in figure I.7, showing the proportional relation of the particle's diameter and the inter-particle forces. The curves of the different diameters meet after passing through the minimum due to the fact that the forces in this diagram just depend on the model roughness with a constant diameter. The electrostatic forces show a similar effect passing a minimum at a certain diameter, however, the effect is less intensive as the slope of the electrostatic forces is decreased compared to the slope of the Van der Waals forces.

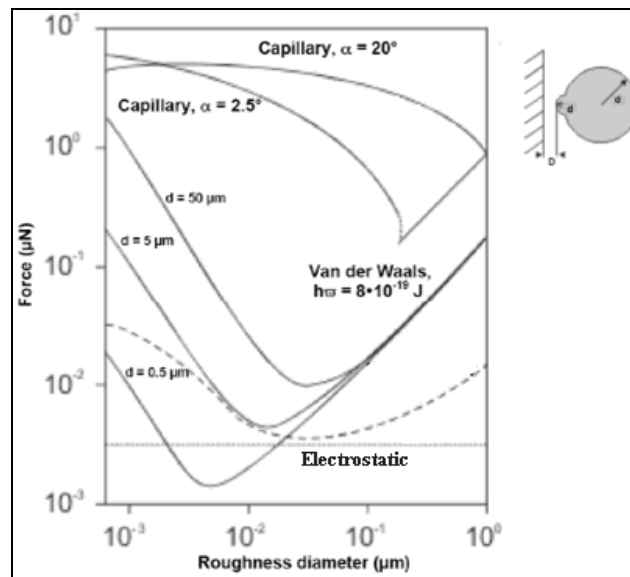


**Figure I.7.** Dependency of the Inter-particle Forces on the Surface Roughness (Schubert, 2003)

The capillary force depends on the volume of the liquid. When the volume is high enough, the liquid will surround the roughness and the force of the capillary will be based on the diameter of the particle and will be slightly decreased by the increase in the diameter of the surface roughness. When the volume is smaller, the capillary force will be build up between the roughness and the flat surface. So, by increasing the diameter of the roughness the force will be decreased. Above a certain diameter of the roughness the capillary force increases linearly with the log diameter of the roughness.

Podczek (1999) proposed that when two particles or a particle and surface are in contact, real contact occurs only at the surface asperities where the contact pressure is very high. If the particle size is much larger than the distance between the asperities, then only few contacts will occur between the particle and the asperities. Thus, the contact area is proportional to the

number of asperities, and increasing the particle size will increase the contact area. If the particle size is smaller than the distance between the asperities, the particles will be placed in the valley between asperities and they have a higher contact area with the surface and though the inter-particle forces will increase. This is called nesting and is showed in figure I.8. This effect is further promoted if the particles are needle shaped. The adhesion force is smallest for ideal spherical particles and largest for cubical shaped particles.

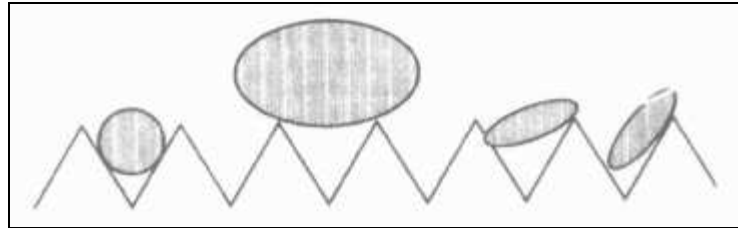


**Figure I.8.** Relationship between Particle Size and Asperity Size (Podczcek, 1999)

The distance between the particles is another parameter that has an important role on inter-particle forces. In figure I.9, the effect of the distance between a spherical particle and a flat surface is shown.

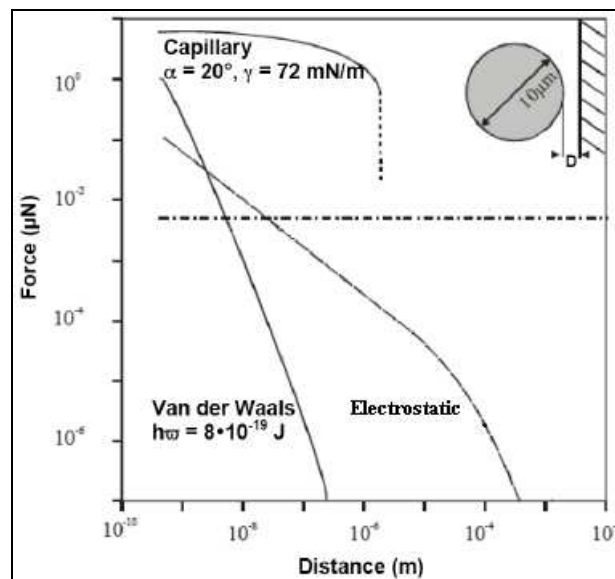


**Figure I.9.** Dependency of the Inter-particle Forces on the Distance between a Flat Surface and a Spherical Particle (Schubert, 2003)

The inter-particle forces decrease by increasing the distance between the sphere and the flat surface. The acting range of Van der Waals forces is very short. At almost distances above

$10^{-7}$  m the Van der Waals force becomes weak and is negligible. The electrostatic forces have a more extensive acting range. For capillary forces, increasing the distance between the partners, the liquid bridge would be pulled off and the capillary force would be vanished.

Particle size is also another factor that affects the adhesion of the particles. Small particles are more strongly affected by inter-particle forces compared to larger particles. Figure I.10 shows the relationship between the particle diameter and the inter-particle forces.

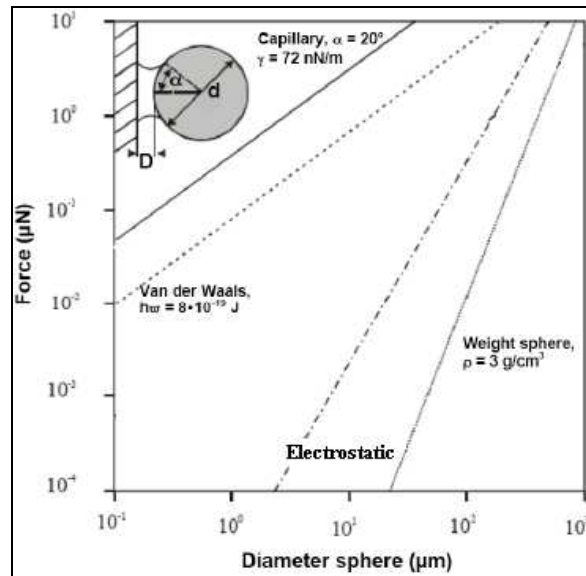


**Figure I.10.** Dependency of the Inter-particle Forces on the Particle Diameter (Schubert, 2003)

With respect to the small diameter, capillary forces are the strongest forces closely followed by the Van der Waals forces. The electrostatic forces are lower compared to the Van der Waals forces but still have an influence on the small particles. Increasing the diameter of the spherical particle (above 100  $\mu\text{m}$ ) changes the relation between the force and the weight of the spherical particle (gravitational force). This is an important phenomenon for the flowability of powders. According to the volume of a spherical particle, the weight increases with the cubic diameter of the sphere in contrast to the inter-particle forces, which are in a linear relation to the diameter. So, the force increases by decreasing the diameter of the spherical particle leading to a stronger adhesion. Consequently, the flowability of the smaller particles is decreased. This phenomenon is the reason, why fine powders flow less well than coarse powders (Castellanos, 2005).

As it has been mentioned before, in dry particle coating process particles are subjected to mechanical forces (mechanical impact, shear, centrifugal force, etc.) greater than their inter-particle forces in order to break them into their primary constituent particles and adhere the fine (guest) particles on the larger (host) particles. There are some devices available for this reason and they will be explained with details in the following part.

## 5. DRY PARTICLE COATING EQUIPMENT

There are several dry particle coating equipments that have been used successfully by many investigators to produce composite particles with improved/modified functionality. These devices, although different in their manner of supplying the necessary mechanical forces, all have the aim of promoting the de-agglomeration of the guest particles and their adhesion onto the surface of the host particles.

### 5.1. Mechanofusion

Mechanofusion is a batch operated device which consists of a cylindrical chamber that rotates at very high-speed (200 to 1600 rpm), while a stationary inner piece (which has a cylindrical surface at the end) creates intense shear of the host and guest powder mix pinned against the cylindrical container. There is also a scraper, which prevents powder from caking against the wall. The clearance space between the inner piece and the chamber inner wall is adjustable, which is generally set to 4 to 5 mm. The clearance between the scraper blade and the chamber is much smaller, usually around 0.5 mm. Those clearances are adjustable and are determined by many factors such as, powder properties, particle size, requirements of final products, etc (Naito et al., 1993b, Pfeffer et al., 2001). A schematic representation of the mechanofusion system is shown in figure I.11.

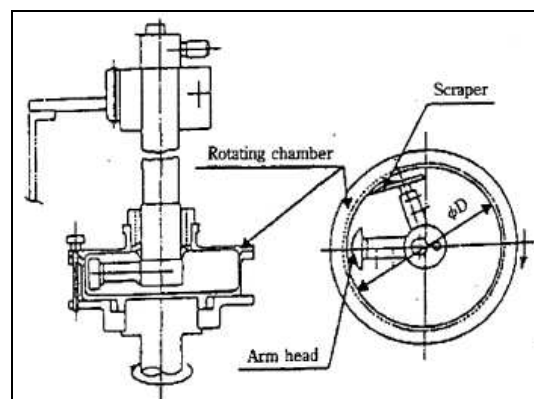
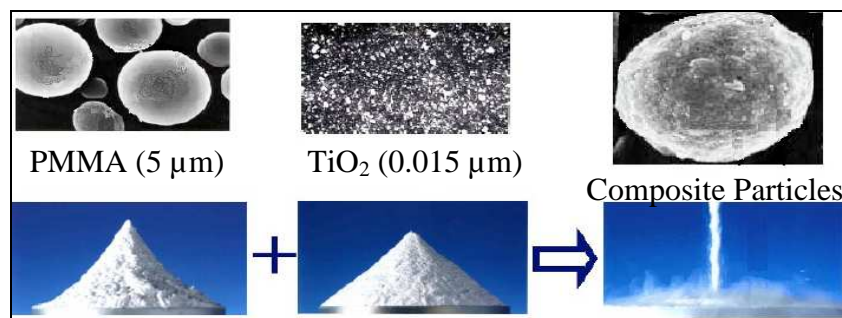


Figure I.11. Mechanofusion System (Pfeffer et al., 2001)

In the mechanofusion process, a measured amount of host and guest particles is placed into the rotating vessel. When the chamber rotates, the powder is forced on the chamber wall by centrifugal action. While particles passing through the converging space between the inner piece and chamber wall; mechanical interactions, mainly in the form of high shear-rate collisions, take place between the particles and between the particles and solid boundaries of the chamber inner wall and the rounded piece. As the particles come out of the space between the inner piece and chamber wall, they adhere to each other and to the chamber wall. The blade helps to scrape off the powders attached to the chamber wall. The powder mixture is then dispersed inside the chamber and gets again into the inner piece region. The powder continuously undergoes this process of compression, attrition, and frictional shearing while the chamber is rotating. As the chamber rotates at high speeds, the interactions are intensive and a considerable amount of thermo-mechanical energy is generated, which results in generation of new composite materials (Chen et al., 2004).

Naito and co-workers (1993b) used mechanofusion in order to investigate qualitatively the dry particle coating process of glass beads and titanium oxide ( $\text{TiO}_2$ ) fine particles. The ratio of fine particles fixed onto host particles and the BET specific surface area of the processed particles were measured as a function of the processing time. They described the process in mechanofusion in two steps; in the first step, the fine particles adhere to the surface of the host particles. The second step is described as the compaction of the fine particle layers. They have found that the BET specific surface area of the processed powder was correlated with the energy consumption per weight of material in the mechanofusion.

Youles (2003) worked on dry coating of PMMA particles (5-15  $\mu\text{m}$ ) with  $\text{TiO}_2$  particles (15-50 nm) in mechanofusion system in order to modify the flowability properties of the particles. It was observed that each component displays a high angle of repose but the composite material is so free-flowing that an angle of repose can no longer be measured (fig.I.12).



**Figure I.12.** Mechanofusion Effect on Flow Properties of the Particles (Youles, 2003)

More recently, Jiang and colleagues (2006) coated micro-size PMMA particles with nano-size  $\text{TiO}_2$ ,  $\text{Al}_2\text{O}_3$  and  $\text{SiO}_2$  particles in mechanofusion in order to study the effect of treatment in mechanofusion on the particle-wall interactions of the composite particles. The particles after treatment were dispersed on a flat metal surface and an experiment on particle entrainment on particle entrainment was carried out in an airflow channel to evaluate particle-wall interaction. Relationship between particle entrainment efficiency and air velocity, which corresponds to the distribution of the particle-wall interaction force, were obtained under various conditions, showing that the particle-wall interaction force tends to decrease with the increase in the concentration of added nano-particles.

## 5.2. Hybridizer

Hybridizer is another dry particle coating equipment that was developed by Nara Machinery, Japan (fig.I.13). In this study, the chosen powder couples (host & guest) have been coated in the hybridizer in order to create new composite particles with different surface properties. The properties of the hybridizer and its methodology will be explained in detail in chapter II.

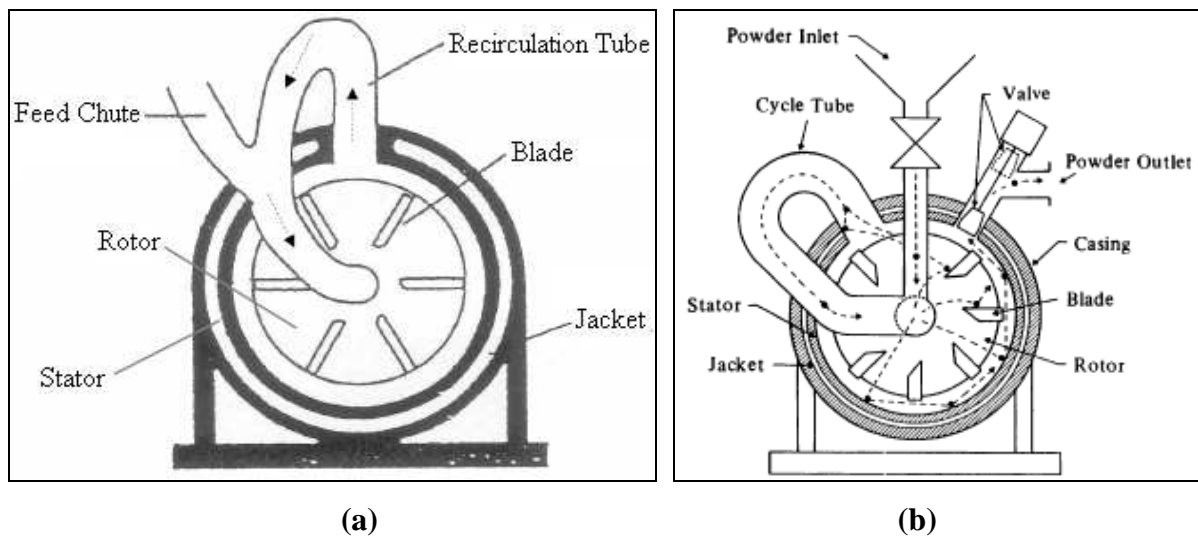


**Figure I.13.** Nara Hybridization Systems

a) NHS – 0 (Honda et al., 1991), b) NHS – 1 (Schmidt et al.,2004)

There are two different types of Nara Hybridization Systems, which are NHS-0 and NHS-1. The main differences between them are the design (place of powder inlet-outlet, recycle tube etc) and the capacity of the equipments. Figure I.13 shows the parts of the NHS-0 and NHS-1 equipments. The hybridizer has several advantages that make it a powerful dry

coating device. The rotor of the hybridizer can rotate at very high speeds (up to 16000 rpm). Due to the strong forces applied to the materials at these high rotational velocities, very short processing times are required to achieve coating. Moreover, the device consists of a recirculating unit that continuously moves the particles in and out of the processing vessel and against the blades of the rotor (Pfeffer et al., 2001).

In the hybridizer, there are three different principle processes;

**Rounding:** In rounding of particles, normally only one material is treated in the hybridizer. The rounding effect is established depending on the material. Its aims are improvement of flow characteristics, adjustment of bulk density and surface area.

Deformable particles like metals and various plastics can be mechanically deformed in a way that the irregular surface is smoothed and rounded by impact forces (Yoshihara et al., 1999).

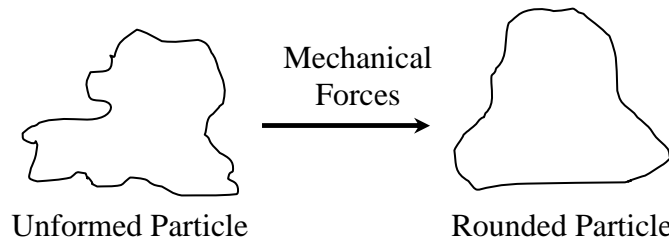


**Figure I.14.** Rounding Effect in the Hybridizer (Yoshihara et al., 1999)

**Embedding:** The guest particles are forced to be embedded to the surface of the host particles by the impact force (fig. I.15). The technique is not only limited to surface modification but also creation of composite material (Yoshihara et al., 1999).

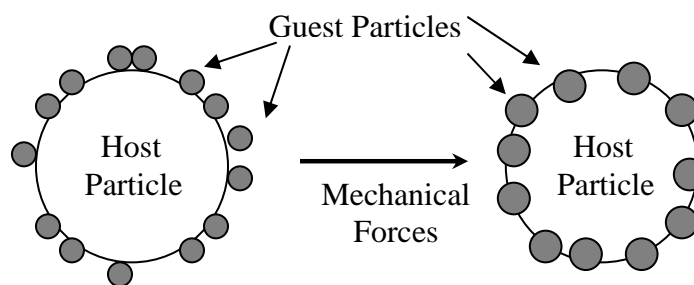


**Figure I.15.** Embedding Process

**Filming:** In the filming process two (usual) or more powders are used as in the embedding process. The upper particle size for the host particle is limited by its stability. If the stability

of the host particle is not strong enough, breakage by impact force may happen. Breakage often occurs for crystalline and agglomerated substances.

For all processes with two or more powders the size ratio of 1/10 for host and guest particles might be used as criteria for the feasibility of the process (Yoshihara et al., 1999).

One main field for hybridizer is pharmaceutical research. In the pharmaceuticals area there are some examples of major concern like the controlled release of a medicine, the change of the mechanical and physical character of a drug as well as the improvement of the properties of the drug and its functionability. Ishizaka and co-workers (1989) coated starch particles in hybridizer with various medicines (oxyphenbutazone, prednisolone, theophylline, indometacin, phenacetin, aspirin, particle sizes < 100  $\mu\text{m}$ ), which are hardly dissoluble in water, in order to increase the solubility of the medicines. They observed that after the process, these medicines dissolved very rapidly. In order to have a long dissolving time or controlled release the hybridizer products were coated by carnauba wax as the first layer then a second layer. They observed that the dissolution is very quick after the medicine is coated on the starch. Moreover, the dissolution time is prolonged very much when the composite particles are coated by one and even more when coated by two carnauba wax layers.

As an interesting application of the hybridizer, Pieper and Mattern (2004) coated potato starch with praziquantel in order to mask the taste of the drug. Analysing the content of praziquantel composite powders with respect to drug content showed that it did not decrease due to processing compared to the weight ratio of the material at the start. Moreover, they observed that the release of praziquantel in water is very fast after hybridizing it with potato starch. On the other hand, although the initial dissolution of the composite particles is rather fast there is tremendous difference in taste compared to the initial states of the particles.

Ouabbas and co-workers (2006) studied the surface modification of silica particles by dry coating with magnesium stearate (MgSt) in hybridizer. Visual analysis showed that MgSt was softened and smeared over host particles after treatment in hybridizer. The flowability of the silica particles was not strongly affected by coating. They also observed that the coating of silica gel particle by hydrophobic MgSt improved the compressibility and moisture resistance of the composite particles.

### **5.3. Cyclomix**

The cyclomix is defined as a high shear mixer/granulator, manufactured by Hosokawa Micron B.V. As it can be seen from figure I.16, it consists of a conical shaped vessel and there is rotor



in the centre of the vessel with an impeller and four sets of blades. It applies high mechanical impact, shearing forces on the particles in order to break the fine agglomerates and coat them on the host particles. In this study cyclomix has also been used an equipment for dry particle coating of the chosen powder couples. The properties and the working principle of the cyclomix will be explained in detail in the chapter II.

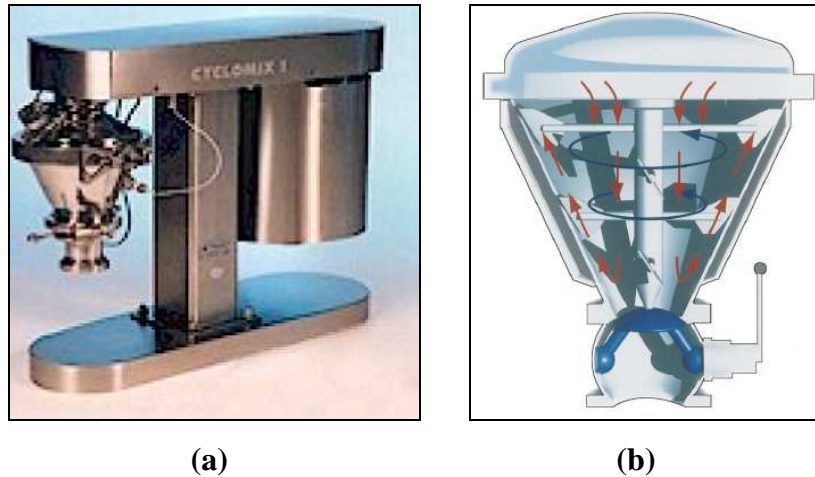


**Figure I.16.** Hosokawa Cyclomix,

(a) Cyclomix, (b) Schematic Representation of Cyclomix (Ghadiri et al., 2007)

Kwan and colleagues (2005) worked on the effect of the scale of cyclomix on the structure, properties and strength of the granules. They treated glass beads particles in two different capacities (1 L and 5 L) of Cyclomix. They observed that the different configurations of the impeller in the 5 L and 1 L Cyclomix affected considerably the flow field of the particles. For the two primary top blade tip speeds (4.1 and 2.1 m/s) they found very different behaviour with the higher tip speed resulting in particles concentrating on top of the lid while at the lower tip speed the particles concentrated at a lower level in the bowl.

Another dry particle coating study with the Cyclomix has been done by Rahmanian and co-workers (2008). They studied the influence of operation scale and impeller speed of high shear mixer granulators on the strength of granules. Calcium carbonate particles were granulated in four scales of a geometrically similar high shear granulator (Cyclomix) with 1, 5, 50 and 250 L capacities. They observed that the granulation operations produce granules with a similar strength of the particles for all four cases.

Ouabbas et al. (2008) coated silica particles with different mass percentages of magnesium stearate in cyclomix in order to understand the effect of coating on surface properties of the

particles. They observed that the flowability of the silica gel powder was significantly decreased after treatment by the Cyclomix mixer with 15% of MgSt.

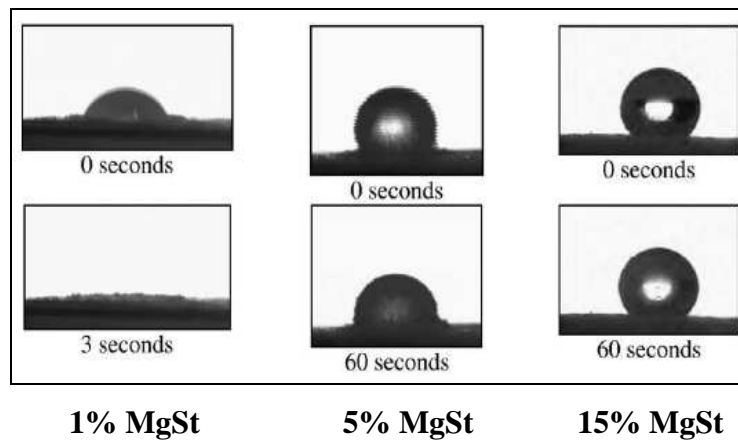


**Figure I.17.** Effect of MgSt Coating on the Wettability of the Particles (Ouabbas et al., 2008)

As it can be seen from figure I.17, they also found that the coating by hydrophobic MgSt in the Cyclomix reduced the high affinity between silica gel and water after treatment with 5% and 15% of MgSt.

#### 5.4. Magnetically Assisted Impaction Coater

Mechanofusion, hybridizer and cyclomix apply high level of mechanical forces on the particles for dry particle coating process. In certain applications (food, pharmaceutical etc.), these high forces are unnecessary or even may damage to the final coated product, for example, excessive size reduction of the host particles. Devices that produce more gentle coating by applying a smaller level of forces have also been introduced. Magnetically assisted impaction coating (MAIC) is one of these methods (Ramlakhan et al., 2000).

It can be used in both continuous mode and in batch mode. Figure I.18 shows the schematic representation of MAIC system. A measured mass of both host and guest particles are placed into a processing vessel (200-ml glass bottle). The magnetic particles are made of barium ferrite and coated with polyurethane to help prevent contamination of the coated particles. An external oscillating magnetic field is created using a series of electromagnets surrounding the processing vessel. When a magnetic field is created, the magnetic particles are excited and move furiously inside the vessel. These agitated magnetic particles then impart energy to the host and guest particles, causing collisions and allowing coating to be achieved by means of impaction of the guest particles onto the host particles (Pfeffer et al., 2001).

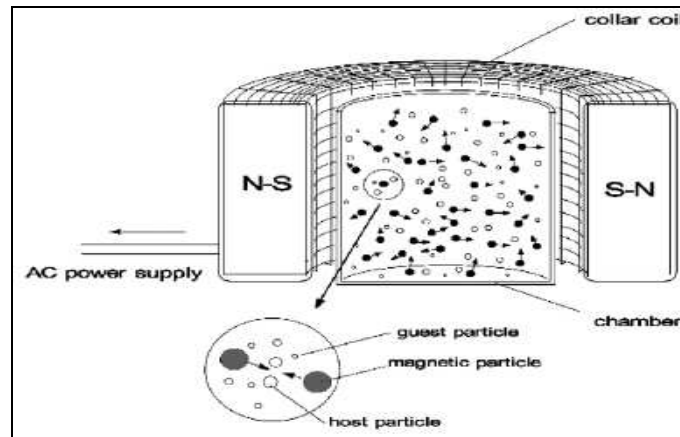


**Figure I.18.** Magnetically Assisted Impaction Coater (Pfeffer et al., 2001)

There are several unique features of MAIC that make it advantageous as a dry particle coating device. Firstly, the MAIC can coat soft organic host and guest particles without causing major changes in the material shape and size. Secondly, although there is some heat generated on a microscopic level due to the collisions of particles, there is negligible heat generation on a macroscopic level and hence no increase in temperature of the material during processing by MAIC. This is desirable when processing temperature sensitive powders such as pharmaceuticals. Lastly, the device can be operated both as a batch and continuous system making it versatile in the amount of material it can process (Ramlakhan et al., 2000).

In the pharmaceutical industry MAIC is used to improve some properties of the powders like flowability and hydrophobicity. In the literature there are examples; one of them is done by M. Ramlakhan and co-workers (2000). In this study they aimed to improve the flowability characteristics of PMMA, cornstarch and cellulose by coating them with alumina guest particles.

The angle of repose (AOR) is a commonly used index for flowability; hence it is used in this work to evaluate the coating effectiveness in terms of improving flow properties. The results for the AOR of cornstarch to powder mass ratios are shown in figure I.19. The AOR for untreated cornstarch is approximately  $59^\circ$ , and it decreases as processing time increases for both magnetic particles to powder mass ratio, indicating improvement in the flow of cornstarch due to a surface coating of silica.

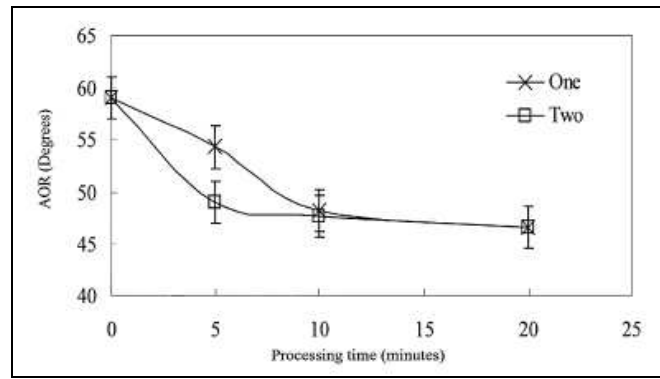


**Figure I.19.** Angle of Repose of Cornstarch as a Function of Processing Time for Two Different Magnetic Particles to Powder Mass Ratios (Ramlakhan et al., 2000)

Chen and colleagues (2006) coated cornstarch and aluminium powders with different types (hydrophilic/hydrophobic) of fumed silica nano-particles in MAIC in order to reduce the cohesion force between the particles and improve the fluidization of the powders. They observed that the dry coating of the particles in MAIC improved the fluidization of cohesive powders dramatically and it appeared that such a coating can transform the behaviour of group C powders (Geldart class of powders) to group A powders.

### 5.5. Theta Composer

Theta composer is considered to be another dry particle coating device that produces gentle coating. The theta composer consists of a slow rotating elliptical vessel (around 30 rpm) and a faster (500–3000 rpm) elliptical rotor. As the rotor rotates inside the vessel, the powder mixture consisting of host and guest particles is subjected to shear and compressive stresses as it is forced into the small clearance between the vessel and the rotor (fig.I.20). As the rotor continues to move and the clearance between the vessel wall and the rotor becomes large, there is bulk mixing of the host and guest particles (Pfeffer et al., 2001).

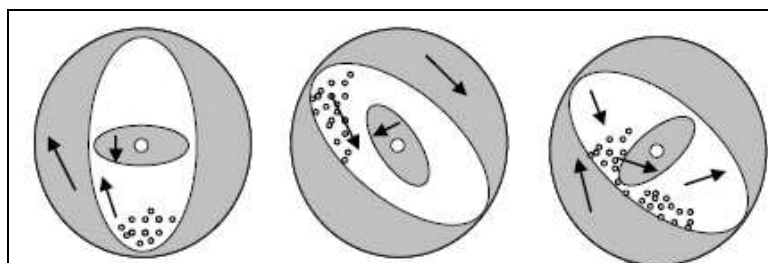


**Figure I.20.** Movements of Powder inside the Theta Composer (Watano et al., 2000)

Watano and co-workers (2000) worked on changing the end use properties of some special type of food powder fibres by coating them with hydrophilic silica ( $\text{SiO}_2$ ). They observed that in dry particle coating processing, between hydrophilic OH groups of food fibre and silanol groups  $-\text{Si}(\text{OH})-$  results in dehydration (mechano-chemical reaction). It leads to suppression of the hygroscopic properties of food fibres. The hygroscopic property was analyzed using a water adsorption method in a temperature and humidity controlled chamber. According to the results it was observed that flowability of the particles was increased because of the good surface coverage of the food fibre by using theta composer.

Another dry particle coating study with theta composer have been done by Coowanitwong and co-workers (2003). They coated  $\text{Al}_2\text{O}_3$  particles with nano-size CuO particles in theta composer and studied the effect of mass percentage of guest particles and operating conditions on the coating obtained. They observed that the product surface area increased with higher nano-particle loadings. They also found that the degree of dispersion and homogeneous distribution of CuO nano-particles on the surface of  $\text{Al}_2\text{O}_3$  particles increased with the processing time.

### 5.6. V-Blender

V-blenders are designed for batch operation. It consists of two cylindrical section joined at an angle of around  $90^\circ$ . The mixer is rotated about a horizontal axis with resulting from the tumbling motion of the particles. Internal baffles are sometimes used to improve mixing performance. The powders are mixed as the vessel is rotated slowly, and during each rotation the powders flow into the two arms followed by powder pouring back towards the apex of the system. A picture of V-blender is shown in figure I.21.



**Figure I.21.** V-Blender (Yang et al., 2005)

In the literature, one of the studies with V-blender was done by J. Yang and co-workers (2005). They tried to understand the effect of dry coating process, the choice of the equipment and the guest particle size on the end-use properties of the composite powders. They coated cornstarch with different types of fumed silica particles by using V-blender and afterwards they studied the modification of flowability properties of the particles by angle of repose measurements. In their apparatus, the vessel was operated at 25 rpm and an agitator bar that rotated at 3600 rpm, was used to enhance the mixing behaviour inside the chamber. The tips of the intensifier bar extend 55 mm from the rotational axis. For each batch, 150 g of particles is charged into a 4-quart vessel and processed for 2 to 40 min.

Figure I.22 shows the results of angle of repose of cornstarch coated with different fumed silica particles with different methods. The angle of repose of coated cornstarch particles in V-blender got lower value than initial cornstarch particles which shows that the flowability of cornstarch particles was improved by dry coating in V-blender.

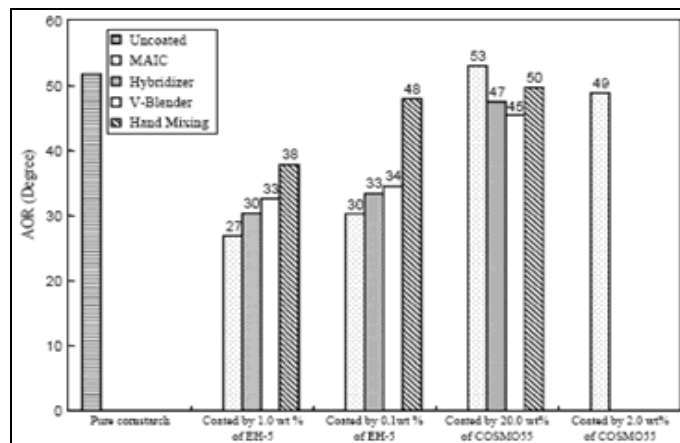


**Figure I.22.** Angle of Repose of Coated Cornstarch Samples in Different Equipments  
(Yang et al., 2005)

### 5.7. Rotating Fluidizer Bed Coater

Rotating fluidizer bed coater (RFBC) is also considered as a gentle coating equipment that were developed recently by New Jersey Institute of Technology (Pfeffer et al., 2001). The host and guest powder mixture are placed into the rotating bed and is fluidized by the radial flow of gas through the porous wall of the cylindrical distributor, as seen in figure I.23.

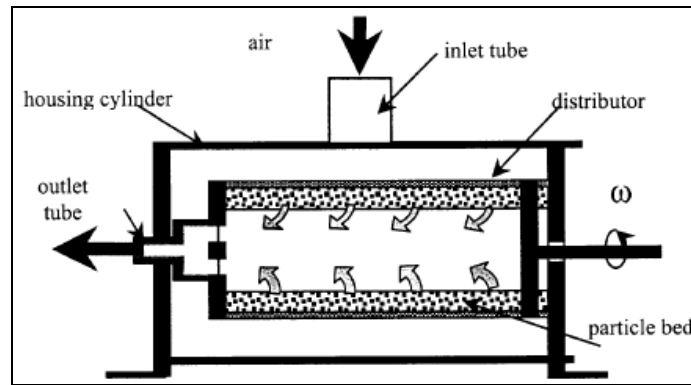


**Figure I.23.** Rotating Fluidizer Bed Coater (Pfeffer et al., 2001)

Due to the high rotating speeds, high centrifugal forces are developed within the fluidized gas-powder system leading to the break-up of the agglomerates of the guest particles and coating them onto host particles (Pfeffer et al., 2001).

The RFBC was used to coat PMMA particles (200  $\mu\text{m}$ ) with alumina particles (0.7  $\mu\text{m}$ ) by Pfeffer and colleagues (2001) in order to analyze the effect of different parameters on the coating performance of the equipment. The measurements of surface morphology (SEM) of the surface of the coated particles showed that the larger and more uniform surface coating of PMMA with alumina was achieved with increases in processing time.

## 6. APPLICATIONS ON DRY PARTICLE COATING

There are many applications of dry particle coating process in different domains. Early work from the Japanese literature report several interesting applications. PMMA particles coated with 10% of  $\text{TiO}_2$  particles using mechanofusion in order to improve the flowability of the particles. They observed that the composite particles flowed freely and had a near zero angle of repose. In contrast, both the original PMMA and  $\text{TiO}_2$  particles did not flow well and had an angle of repose greater than  $30^\circ$  (Yokoyama et al., 1987). It was also reported that processing of ground polystyrene resin of 10  $\mu\text{m}$  size with carbon black in mechanofusion produced easily flowing toner material of rounded shape (Yokoyama et al., 1987).

Mujumdar and co-workers (2004), used mechanofusion to enhance the moisture resistance of ground magnesium powder (primary size 75  $\mu\text{m}$ ) by coating its surface with carnauba wax (primary size 15  $\mu\text{m}$ ). The uncoated and coated samples are characterized by scanning electron microscopy (SEM), humidity tests and X-ray diffraction methods.

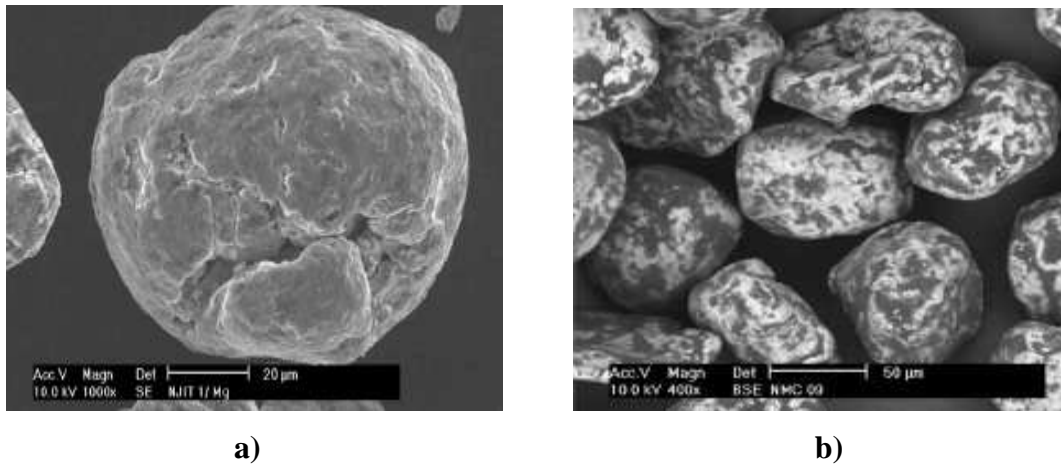


**Figure I.24.** SEM Pictures of a) Ground magnesium particles, b) After Mechanofusion Treatment (Mujumdar et al., 2004)

According to SEM pictures (fig. I.24) they observed that after mechanofusion treatment, magnesium particles were covered with carnauba wax. According to the humidity tests as seen in figure I.25, they indicated that dry coating of magnesium powders with carnauba wax by using mechanofusion generated a material which is much hydrophobic compared to ground magnesium particles.

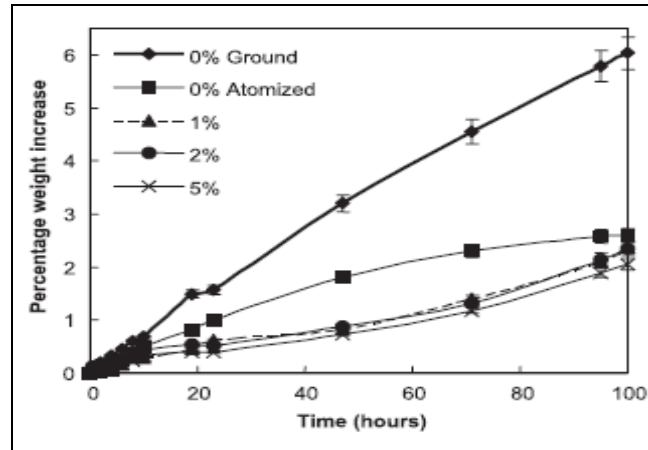


**Figure I.25.** Humidity Tests for the Composite Particles from Mechanofusion (Mujumdar et al., 2004)

Most of the early work reported using the hybridizer involved processing of pharmaceutical drugs to produce controlled-release properties (Ishizaka et al., 1989, 1993a, b). As an example, 5% isoproterenol HCl were coated onto potato starch (70  $\mu\text{m}$ ) followed by a coating of 5% carnauba wax in order to achieve time released control of isoproterenol HCl (Ishizaka



et al., 1989). Moreover, Schmidt et al. (1998) studied many examples of different applications of dry particle coating with hybridizer in different domains (cosmetic, pharmaceutical, toner, electronic).

On the other hand, some researchers showed that multi-layer dry particle coating could also be obtained by using hybridizer system (Kangwabtrakool et al., 2001, 2002, 2003, Tang et al., 2006). In one of the studies, Kangwabtrakool and colleagues (2002) coated WC particles first with TiC and then with Al<sub>2</sub>O<sub>3</sub> in order to modify the hot hardness of the particles. They observed that the hot hardness of the composite particles increased with higher amount of TiC whereas increasing Al<sub>2</sub>O<sub>3</sub> additions reduced the hardness.

The list of different dry particle coating applications in different domains (pharmaceutical, food, ceramic, metallurgy, etc.) with different equipments in order to modify certain surface properties of particles (electrostatic, flowability, wettability, taste masking, solubility, dissolution kinetics etc) is presented in Appendix I.

## **7. CONCLUSION**

Dry particle coating process has been constructed onto the concept ordered mixture which has been introduced to the scientific literature long time ago. Since some years, there are lots of studies about dry particle coating process in the scientific literature. In these studies, different dry particle coating equipments (in lab scale) were used for different applications. Each equipment has a different working principle so the choice of the equipment, the operating conditions and also the powder properties defines what kind of particle coating would be obtained.

There are very few studies about the modelling of the dry particle coating process because of the lack of understanding the physico-chemical interactions between particles in dry particle coating process and also the mechanism of the applied mechanical forces on the particles by each equipment. The understanding of these mechanisms are essential in order to estimate for a given powder couple (host & guest) which equipment and operating conditions should be chosen to achieve desired end-use properties. Since the lack of this information, the dry particle coating process is not commonly used in industry even it has certain advantages from environmental point of view and also being cost effective.

In the following chapter, the materials and the equipments that were used for dry particle coating process and the characterization methods that were used to analyse different properties of the particles will be explained in detail.



## CHAPTER II

### *Materials and Methods*



## 1. INTRODUCTION

In this study, three different mixers have been used to generate composite materials with modified surface properties by dry coating method. Each equipment uses different mechanical forces (mechanical impact, compression, shearing etc) to be able to break up the agglomerates and coat the particles. Different characterization methods have been used, in order to compare the quality of obtained coating from different equipments and study the evolutions of the physicochemical properties of the particles after dry coating process.

In this chapter, the powder couples, the dry coating equipment, that were used for the experiments and different characterization methods, that were used in order to analyze different properties of the particles, will be presented in detail.

## 2. DRY PARTICLE COATING EQUIPMENTS

Two high force mixers (Nara Hybridizer, Hosokawa Cyclomix) and a conventional mixer (Turbula) have been used for dry coating experiments. In this part, it is aimed to present the specifications and methodologies of the dry coating equipments.

### 2.1. Nara Hybridizer

The Nara Hybridization System (NHS) is a machine developed by Nara Machinery for the purpose to create new powder combinations and thereby design particles with new properties. The small (guest) particles are attached to the surface of the core (host) particles by mechanical forces in hybridizer (Pieper, 1996).

The main application areas of the hybridizer are:

- the production of new functional composite materials
- to save high-precise and rare materials by combining cheap raw materials to give hybrid powders
- to improve/modify material properties

The hybridization process is operating in a particle range of 1–500  $\mu\text{m}$  for the host particles which are processed with fine particles in a range of 0.1 to 50  $\mu\text{m}$  as coating material (Yoshihara et al., 1999).

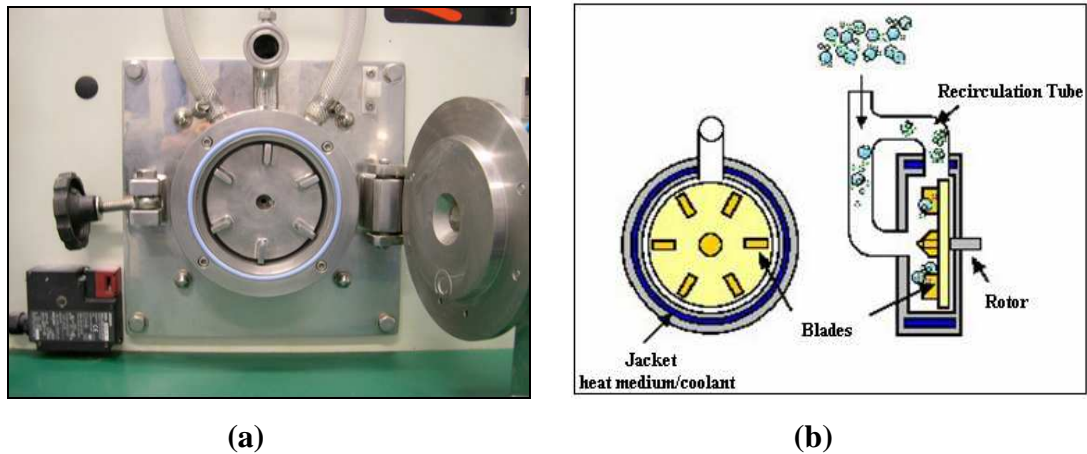


**Figure II.1.** Nara Hybridizer, (a) Stator of Nara Hybridizer (NHS-0), (b) Schematic Representation of Stator and Recirculation Tube of Nara Hybridizer (NHS-0) (Vilela et al., 2005)

In this study NHS-0 type Nara Hybridization System has been used for the experiments. Figure II.1 shows the parts of the Nara Hybridizer (NHS-0) equipment. It can be seen that the hybridizer (NHS-0) itself has three main parts; the rotor (12 cm diameter) with 6 blades, the stator and recycling tube. The stator is jacketed for either cooling or heating. As the rotor is switched on, host and guest particles mix and collide with each other as well as with the walls of the chamber because of the high operating velocity (up to 16000 rpm). Due to high centrifugal forces, particles move to the upper part of the rotating chamber and recycle continuously till the end of the process. The constant recirculation of some particles in this batch process assures that every particle is treated the same way. The hybridization system also has a temperature sensor, which monitors the temperature developed inside the mixing chamber during the operation. The maximum batch size of hybridizer is 50 g. The unique feature of this system is the two-way motion of the particles during the operation, one in the mixing chamber and the other through the recirculating pipe which provides a distinct advantage over the other dry coating machines from the coating point of view as one would expect more collisions between the particles to take place.

The maximum batch size is around 50 g for NHS-0 trials. According to nature of the product, treatments with maximum batch size may cause problems in recirculation of the powders. In order to avoid recirculation problems (have untreated particles), it is advised to use less than the maximum batch size.

The movement of powders inside the hybridizer can be seen in figure II.2. The powder mixture is introduced into the centre of the rotor by feed chute (fig. II.2.a). Afterwards, the

particles collide with each other and the walls of the rotor, because of the high speed of the rotor (up to 16000 rpm) that generates centrifugal force (fig.2.b). Consequently, the powder receives mechanical impact on its surface and is blended, powder reaching the periphery re-enters the recirculation tube and returns to the centre of the rotor. This recycling system is repeated continuously. As the powder is repeatedly impacted, the fine particles become attached to the large host particles (Honda et al., 1991). At the end, the treated powder is transported from the rotor to the powder collector by purging air system and the treated particles can be recovered in the powder collector.

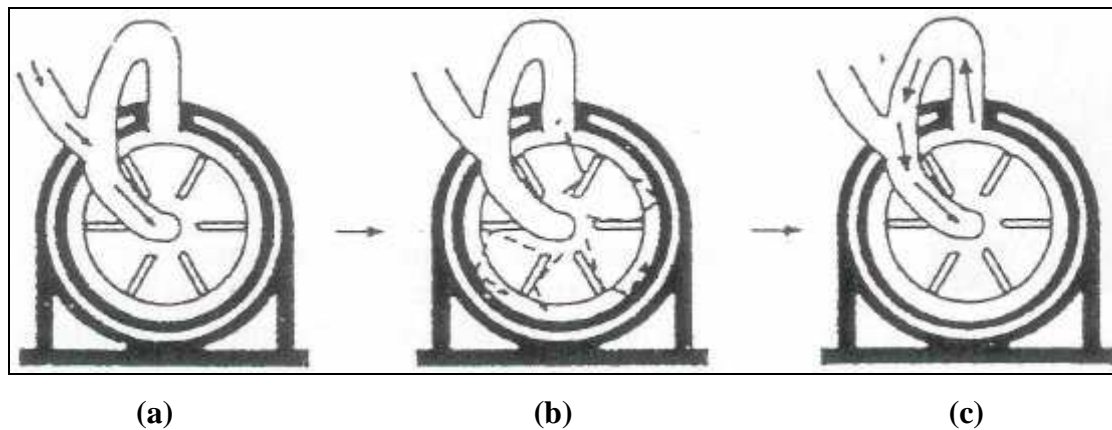


**Figure II.2.** Moving Track of Powder in Nara Hybridization Systems (Honda et al., 1991)

## 2.2. Hosokawa Cyclomix

The cyclomix is a high shear mixer/granulator, manufactured by Hosokawa Micron B.V. Figure II.3 shows the configuration of cyclomix.

The Cyclomix has a conical shaped vessel with 1 L capacity. The vessel is surrounded with a cooling/heating jacket in order to control the temperature of the vessel. At the bottom of the vessel there is a valve in order to recover the powders at the end of the treatment. There is a rotor in the centre of the vessel, consists of an impeller with four sets of blade. The angle of the flat blades is  $30^\circ$  to the vertical axis; the angle of the first (bottom) and the third pairs of the impellers is opposite to that of the second and fourth (top) pairs such that when the shaft is turned clockwise, the first and the third pairs give upwards agitation while the second and fourth pairs give downwards agitation (fig. II.3). The gaps between the impellers and the vessel wall are 5 mm at the side and 2 mm at the bottom.

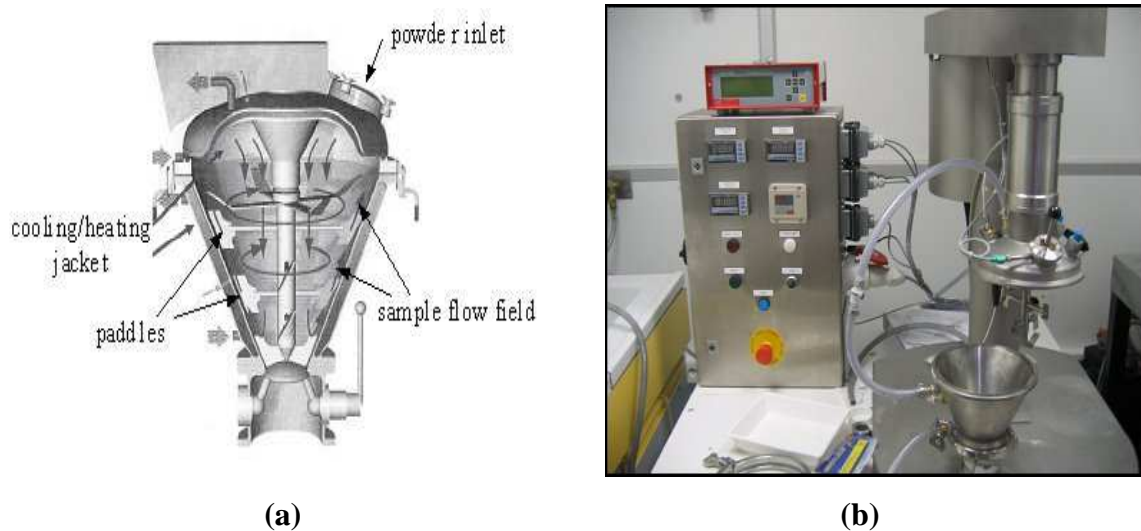


**Figure II.3.** Hosokawa Cyclomix

a) Schematic Diagram of Cyclomix (Ouabbas et al., 2008), b) Cyclomix

The working principle of the cyclomix differs markedly from the existing mixing techniques owing to the specific interaction between mixing element and vessel wall. The powder (host and guest particles) is loaded into the conical mixing vessel from the top; the degree of filling can range between 30 and 100%. Together, the high-speed rotation (up to 3000 rpm) of the paddles and the conical shape of the vessel force the product from the bottom to the upper zone of the vessel. Upon reaching the top, the product flows downwards into the centre of the vessel. This flow pattern results in fast macro-mixing. During the upward motion, the particles are accelerated by the paddles and intensively mixed by friction with vessel walls (Ghadiri et al., 2008).

### 2.3. Turbula Mixer

Turbula is a conventional shaker/mixer, manufactured by WAB (Willy A. Bachofen) AG. It uses centrifugation and gravitational force in order to mix the particles. It has a mixing basket which can hold any form container, from test tubes up to containers having volumes of 2 litres. Containers are held tightly by twisted rubber rings. By adjusting the position of the drive belts on the 5-step pulley, the speed can be varied (22, 32, 46, 68 or 96 rpm). The mixing container is set into three-dimensional movement that exposes the product to always changing, rhythmically pulsing motion. Figure II.4 shows an image of turbula mixer and the possible containers for treatments.





**Figure II.4.** Turbula Mixer (Chéry et al., 2007)

### 3. CHARACTERIZATION METHODS

In this study different characterization methods have been used before and after treatments. The surface morphology of the particles have been analysed by environmental scanning electron microscopy (ESEM) and atomic force microscopy (AFM) techniques. The ESEM allows us to analyse the surface morphology of the particles and also identify the guest particles on the surface of the host particles. The ESEM visual analysis has also been confirmed by AFM. AFM has been used for two different reasons; in the first part we have topographical analysis of the particles (surface roughness) and in the second part we measure the adhesion force between the particles.

Malvern Mastersizer 2000 laser diffraction granulometer has been used in order to analyse the different size distributions (number & volume) of the particles and also to evaluate qualitatively the interactions between the guest and host particles (coating strength) by changing dispersing air pressures.

Modification of different surface properties of the particles has been analysed by using different techniques. Freeman technology powder rheometer (FT4) and Erweka tapped density tester have been used in order to analyse the flowability properties of the powders. The wettability of the powders have been analysed by angle of contact with sessile drop method and the dynamic vapour sorption (DVS) method have been used in order to understand the water affinity of the particles.

### 3.1. Environmental Electron Scanning Microscopy (ESEM)

The ESEM is a common method for visual analysis of the different surfaces. It allows us to observe the surface morphology of the sample with different ambient pressures and in different media (dry & wet). It consists of an electron column that creates a beam of electrons; a sample chamber, where the electron beam interacts with the sample; detectors, that monitor a variety of signals resulting from the beam–sample interaction; and a viewing system that constructs an image from the signal (fig. II.5).

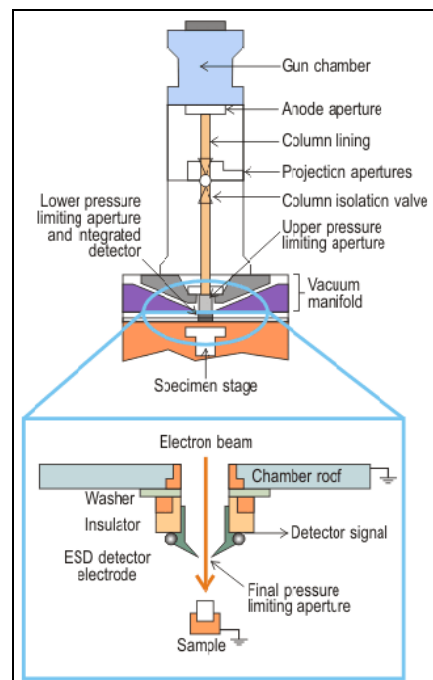


**Figure II.5.** Schematic Representation of ESEM (Techniques de l'ingénieur)

An electron gun at the top of the column generates the electron beam. In the gun, an electrostatic field directs electrons, emitted from a very small region on the surface of an electrode, through a small spot called the crossover. The gun then accelerates the electrons down the column toward the sample with energies typically ranging from a few hundred to tens of thousands of electron volts.

The electrons emerge from the gun as a divergent beam. A series of magnetic lenses and apertures in the column focus and focuses the beam into a de-magnified image of the crossover. Near the bottom of the column a set of scan coils deflects the beam in a scanning pattern over the sample surface. The final lens focuses the beam into the smallest possible spot on the sample surface.

The beam exits from the column into the sample chamber. The chamber incorporates a stage for manipulating the sample, a door for inserting and removing the sample and access ports for mounting various signal detectors and other accessories. As the beam electrons penetrate the sample, they give up energy, which is emitted from the sample in a variety of ways. There are two major ways of emission:

**Secondary Electrons (SE)** are sample atom electrons that have been ejected by interactions with the primary electrons of the beam. They generally have very low energy (by convention less than fifty electron volts). Because of their low energy they can escape only from a very shallow region at the sample surface. As a result they offer the best imaging resolution. Contrast in a secondary electron image comes primarily from sample topography. More of the volume of interaction is close to the sample surface, and therefore more secondary electrons can escape, for a point at the top of a peak than for a point at the bottom of a valley. Peaks are bright and valleys are dark. This makes the interpretation of secondary images very intuitive as they look the same as the corresponding visual image would look (Paqueton et al., 2006).

**Backscattered Electrons (BSE)** are primarily beam electrons that have been scattered back out of the sample by elastic collisions with the nuclei of sample atoms. They have high energy, ranging (by convention) from fifty electron volts up to the accelerating voltage of the beam. Their higher energy results in a larger specific volume of interaction and degrades the resolution of backscattered electron images. Contrast in backscattered images comes primarily from point to point differences in the average atomic number of the sample. High atomic number nuclei backscatter more electrons and create bright areas in the image. Backscattered images are not as easy to interpret, but properly interpreted, can provide important information about sample composition. Each emission mode is potentially a signal from which to create an image (Kimseng et al., 2001).

ESEM also allows us to have elemental analysis or chemical characterization of a sample by Energy dispersive X-ray spectrometer (EDS) technique. As a type of spectroscopy, it relies on the investigation of a sample through interactions between electromagnetic radiation and matter, analyzing x-rays emitted by the matter in response to being hit with charged particles. Its characterization capabilities are due in large part to the fundamental principle that each element has a unique atomic structure allowing x-rays that are characteristic of an element's atomic structure to be identified uniquely from each other.

In this study the ESEM type XL30, manufactured by Philips have been used in order to have the visual analysis of the particles before and after treatments. The ESEM observations have been done all the time in dry media with 1–20 torrs pressure. The EDS method has also been used in order to have chemical characterization of the surface of the particles.

### 3.2. Atomic Force Microscopy (AFM)

Atomic force microscopy (AFM) is an useful tool for investigating both the surface morphological characterizations of solid materials (three dimensional surface topography of the sample) and mechanical interactions occurring at material/tip interfaces at micro- or nano-dimensions. Figure II.6 shows a typical configuration of an AFM. It uses mechanical effects between sample and tip. The tip is mounted on a flexible cantilever which moves along in XYZ directions on the sample. The deflection of the cantilever is recorded with the help of a laser beam and permits the evaluation of the forces between tip and sample. This procedure allows also an investigation of non-conducting samples and the characterization of surfaces with atomic resolution due to the small tip size at the nano scale. It is often used to study surface topography. Specific probes can be used to analyze lateral variations of frictional, elastic, thermal, electrical and magnetic properties. For AFM measurements a special sample treatment is not necessary. Furthermore, the surface analysis can be performed in liquid or gaseous environment. Additionally, AFM can be used to determine inter-particle forces (Butt et al., 2005).

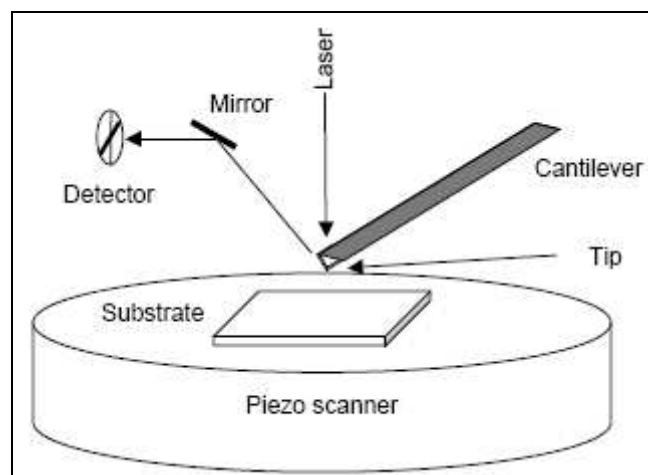


**Figure II.6.** Schematic Representation of Basic Configuration of AFM

AFM has different methods to operate and analyze the different properties of the samples. In this part the different operating methods of AFM will be presented in detail.

### A. Tapping Mode

In the tapping mode, AFM operates by scanning a tip attached to the end of an oscillating cantilever across the sample surface. The cantilever is oscillated at or slightly below its resonance frequency with an amplitude ranging typically from 20 nm to 100 nm. The tip lightly “taps” on the sample surface during scanning, contacting the surface at the bottom of its swing (fig. II.7.a). The feedback loop maintains a constant oscillation amplitude by maintaining a constant root mean square of the oscillation signal acquired by the split photodiode detector. The vertical position of the scanner at each (x,y) data point in order to maintain a constant “set point” (reduced) amplitude is stored by the computer to form the topographic image of the sample surface (fig. II.7.b). By maintaining a constant oscillation amplitude, a constant tip–sample interaction is maintained during imaging. The reflected laser beam reveals different information. The vertical height of the sample surface, the variation in the amplitude and the phase contrast data are taken simultaneously.

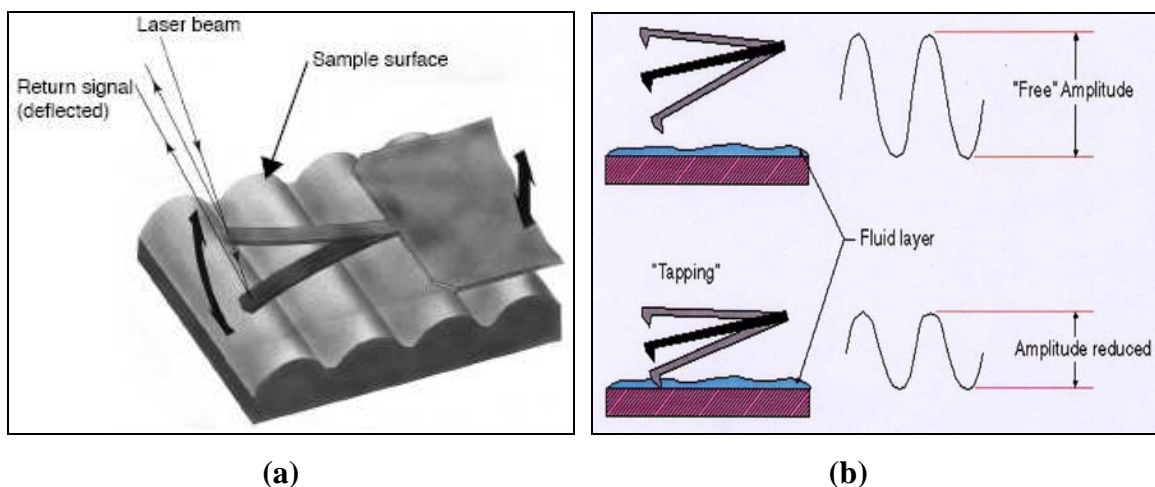


**Figure II.7.** Tapping Mode of AFM

a) AFM Cantilever, oscillating on the Sample b) Free & Reduced Amplitude in Tapping Mode (AFM Manual, Veeco)

The images of the vertical height of the sample surface can be also evaluated in order to find different surface roughness parameters of the sample. There are many statistical values which

define the surface roughness of the samples. The most used surface roughness definitions by the scientists are;

**$R_a$**  : Arithmetic average of the absolute values of the surface height deviations measured from the mean plane.

$$R_a = \frac{1}{n} \sum_{j=1}^n |Z_j| \quad (\text{Eqn.II.1})$$

**$R_{\max}$**  : Maximum vertical distance between the highest and lowest data points in the image.

$$R_{\max} = [Max(z(x, y)) - Min(z(x, y))] \quad (\text{Eqn.II.2})$$

**RMS ( $R_q$ )**: Root mean square average of height deviations taken from the mean data plane, expressed as;

$$RMS = \sqrt{\frac{\sum_i z_i^2}{n}} \quad (\text{Eqn.II.3})$$

The variation in the amplitude signal is used as a feed-back mechanism in order to correct the displacement of the cantilever in z direction and to keep constant amplitude on the sample surface.

The difference in the reference signal and the created signal (by oscillation of the cantilever on the sample surface) is used for phase contrast images as it can be seen in the figure II.8. The phase contrast images of the sample gives some characteristics of the sample material itself. These material characteristics may include elasticity, magnetic and electric forces present (Berquand et al., 2003).

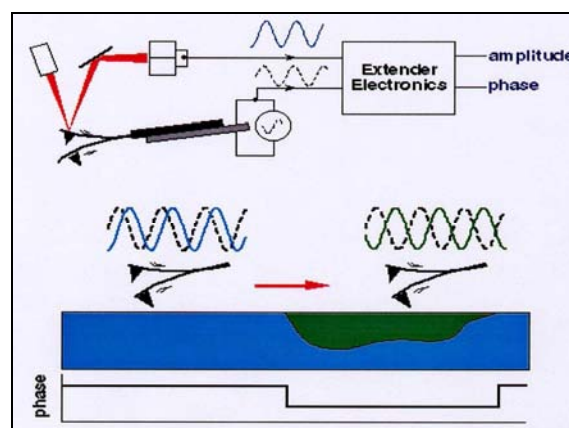


**Figure II.8.** AFM Tapping Mode, Phase Contrast Signal (AFM Manual, Veeco)

The phase angle (contrast) measurements give different information about the interaction between the cantilever tip and the sample surface more specifically for heterogenic materials. Some theoretical studies have been done about derivation of phase contrast signal by different authors (Anczykowski et al, 1996, Burnham et al., 1997, Magonov et al., 1997, Boisgard et al. 1998, Cleveland et al., 1998, Marth et al., 1999, Wang et al., 1999, Garcia et al., 1999 and 2000, Durig, 2000, San Paulo et al., 2001, Sabastian et al., 2001, Yeh et al. 2004, Liu et al. 2005 ). On the other hand, a systematic explanation of the phase angle images is very difficult (Chen et al., 2002), because the difference in the phase angle values could be related to different reasons (viscoelastic properties, surface height etc).

The experimental observations show that the height and phase contrast images depend on the ratio between the free amplitude ( $A_F$ ) and reduced amplitude (set point) ( $A_{SP}$ ) which is used as feed back mechanism (Whangbo et al., 1998). The ratio between these amplitudes has very important role for analysing material surface (Magonov et al., 1997).

## B. Contact Mode

In contact mode, the cantilever tip is placed to contact with the sample surface. Repulsion force ( $F$ ) acting upon the tip is related to the cantilever deflection value ( $x$ ) under Hooke's law;

$$F = -k * x \quad \text{(Eqn.II.4)}$$

where  $k$  is cantilever spring constant. The spring constant value for different cantilevers usually varies from 0.01 to several N/m. The schematic illustration of contact mode can be seen in figure II.9. In contact mode, there are two possible methods for surface imaging:

**Constant force:** the deflection of the cantilever is maintained constant by a feed back mechanism while moving on the sample. The change in the force is interpreted as the topography of the sample. The sensibility of the method is up to 0.1 nm.

**Constant height:** the height of the sample is maintained constant and the deflection of the cantilever is interpreted in order to find the surface characteristic of the sample.

The contact mode has some disadvantages. Speed of scanning is restricted by the response time of feedback system. When exploring soft samples (like polymers, biological samples, Langmuir-Blodgett films etc.) they can be destroyed by the scratching because the probe scanning tip is in direct contact with the surface. Therefore, under scanning soft inhomogeneous samples the local flexure of sample surface varies. As a result acquired

topography of the sample can prove distorted. Possible existence of substantial capillary forces imposed by a liquid adsorption layer can decrease the resolution (AFM manual, Veeco).

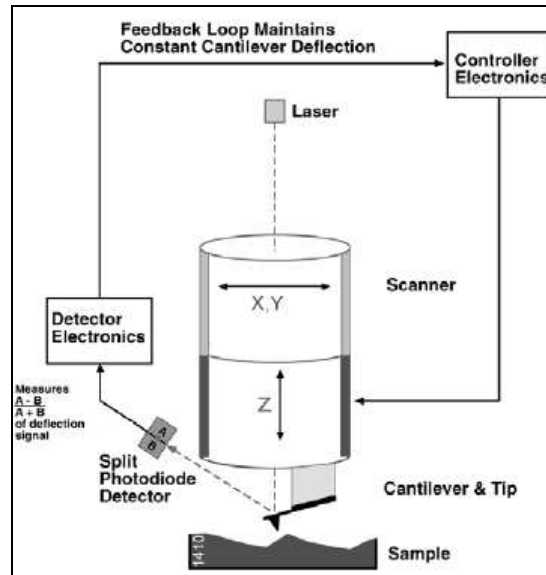


**Figure II.9.** Feed-back Loop of the Contact Mode (AFM Manual, Veeco)

On the other hand, contact mode gives us also the possibility to measure the adhesion force between the cantilever tip and the sample.

### *Adhesion Force Measurements*

Conventional force plots are simply a plot of cantilever deflection on the Y-axis versus Z-piezo position on the X-axis. They normally include two traces, an approach curve and a retract curve. On a hard surface in air, a curve similar to that shown in Figure II.10 is commonly obtained.

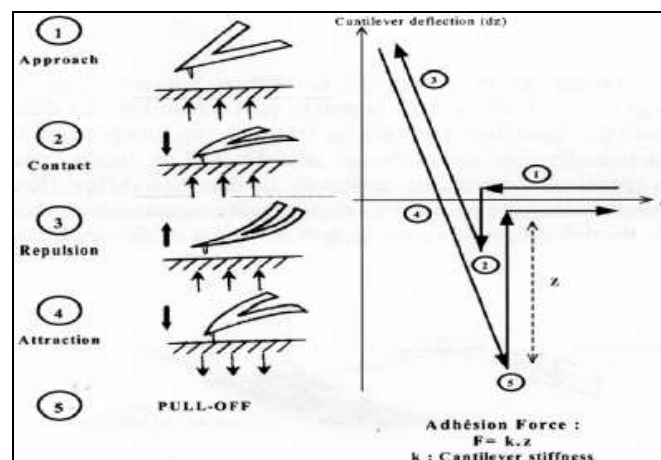


**Figure II.10.** A Force Plot of AFM in Contact Mode (Roberts, 2005)



The tip – sample distance decreases as the curve goes from right to left (approach). Very close to the surface, the tip snaps into contact with the surface due to short range attractive forces (contact). As the piezo continues to extend, the tip is pressed harder into the surface and the cantilever deflection increases (repulsion). The piezo then reverses direction and begins to increase the tip-sample distance, thus decreasing the cantilever deflection (attraction). As the piezo continues to retract, the cantilever strains against this force until it finally breaks free and returns to its non-contact value (pull – off) (Cappela et al., 1999).

### C. Non – Contact Mode

In non – contact mode of AFM, the cantilever is oscillated at a frequency which is slightly above the cantilever’s resonance frequency typically with an amplitude of a few nanometers (<10nm), in order to obtain an AC signal from the cantilever. The tip does not contact the sample surface, but oscillates above the adsorbed fluid layer on the surface during scanning. The cantilever's resonant frequency is decreased by the Van der Waals forces, which extend from 1 nm to 10 nm above the surface, and by other long range forces which extend above the surface. (fig. II.11)

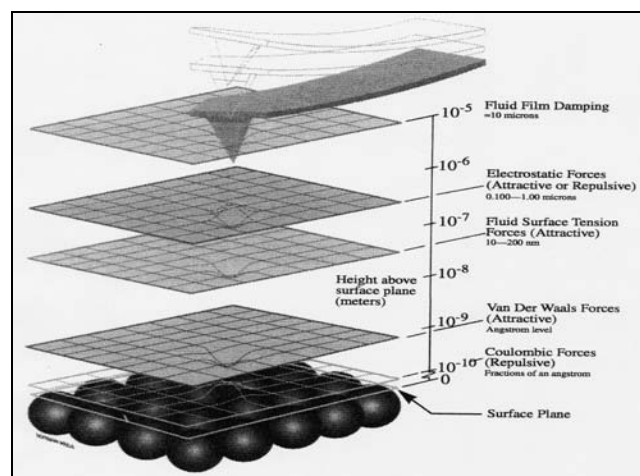


**Figure II.11.** Interparticular Forces Between Cantilever Tip & Sample Surface (Picoforce Manual, Veeco)

The decrease in resonant frequency causes the amplitude of oscillation to decrease. The feedback loop maintains a constant oscillation amplitude or frequency by vertically moving the scanner at each (x,y) data point until a “setpoint” amplitude or frequency is reached. The

distance the scanner moves vertically at each (x,y) data point is stored by the computer to form the topographic image of the sample surface (AFM Manual, Veeco).

In this study, Multimode Nanoscope IIIA atomic force microscopy from Digital Instruments, Veeco Metrology Group® has been used. In tapping mode, MPP 11100, phosphorus (n) doped silicon cantilever probe with spring constant (k) 40 N/m has been used in order to have topographical analysis of the initial host and guest particle surface and also talc coated host particle surface in hybridizer. In contact mode, NP, silicon nitride cantilever probe with spring constant (k) 0.32 N/m was used in order to study the adhesion forces between the particles.

The properties of the used cantilever probes in tapping and contact mode measurements are presented in details in appendix V.

### 3.3. Laser Diffraction Granulometer

The particle size distribution of the powders was measured by a laser diffraction method using the Mastersizer 2000 from Malvern Instruments Ltd. The equipment uses the diffraction of laser beam in order to find the particle size distribution of powders between 0.02  $\mu\text{m}$  and 2000  $\mu\text{m}$  range.

The Mastersizer essentially consists of a laser transmitter and a receiver (300 RF lens) unit, detectors, a dry powder feeder unit with an air venturi in order to control the dispersing air pressure and a cyclone (fig. II.12).

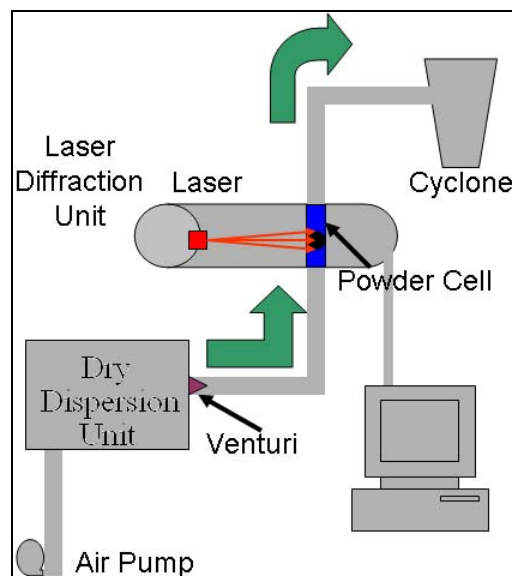


**Figure II.12.** Basic Configuration of Laser Diffraction Granulometer

A representative powder sample is placed in the feeder unit and a vacuum is switched on. The vacuum draws the powder sample into the instrument with chosen dispersing air pressure (up to 4 bars). The dispersed powder passes through the laser beam. The dispersed powder scatters laser light at angles that are inversely proportional to the size of the particles, i.e. large particles scatter light at small forward angles, whereas small particles scatter light at wider angles (Figure II.13). This scattering is captured by an array of detectors. Hence, there is a direct relationship between the distribution of the scattered light energy on these detectors and the particle size distribution (Chatelet, 1996).

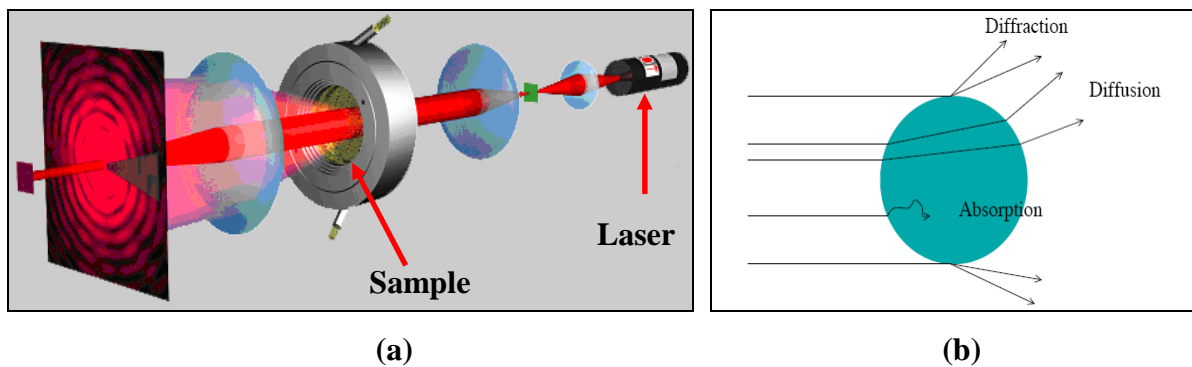


**Figure II.13.** Principle of Laser Diffraction Granulometer

a) Laser Diffraction Unit of the Granulometer b) Interactions of laser light and particles

In this apparatus powder de-agglomeration is controlled by adjusting the dispersing air pressure. The variation of the pressure (P) with corresponding air velocity (V) in the venturi can be seen in figure II.14.b.

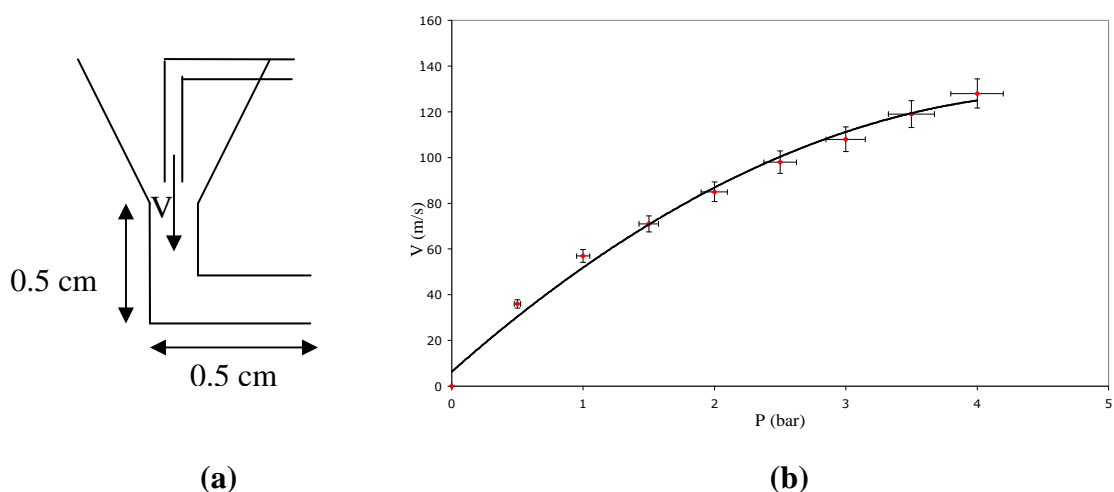


**Figure II.14.** Air Venturi of the Granulometer

a) Dimensions of the Venturi b) Pressure vs. Corresponding Air Velocity in the Venturi

Here we determine at which dispersing air pressure the guest particle start to be liberated from the host particles. The presence of liberated fine particles can be detected by making a comparison between number particle size distributions with different pressures (Vilela, 2006). It is important to note that the diameters from the laser diffraction method are calculated assuming spherical particles, so incorrect values may be obtained for irregular or needle-shaped particles. Thus the size distribution for all the test powders was checked by image analysis using a scanning electron microscope.

### 3.4. Helium Pycnometer

The solid density of the powders was measured using a helium pycnometer (Accupyc 1330, Micromeritics) which works on the basis of gas displacement. The instrument determines the solid density of solid objects or powders based on the following equation assuming an ideal gas:

$$V_p = V_c + \frac{V_a}{1 - \frac{P_1}{P_2}} \quad (\text{Eqn.II.5})$$

The general principle is that the solid powder sample of unknown volume  $V_p$  is placed in a known sample cell volume  $V_c$ , and pressurized with helium gas to the desired target pressure  $P_1$ . The pycnometer has an internal “added volume” chamber ( $V_a$ ) which is added to the cell volume by opening a valve between the two chambers. The resulting lower pressure  $P_2$  is then recorded, allowing the calculation of  $V_p$ . The pycnometer is programmed to perform the above pressurizations and valve 22 openings automatically.  $V_a$  and  $V_c$  are known through accurate calibration using the provided calibration spheres. The helium is able to fill all spaces open to the atmosphere, including the pores inside the powder sample. The solid density is calculated from the volume of sample and the known sample mass. The instrument reports an average value from the number of runs specified by the user. The specified number of runs is input with a numeric keypad on the front of the pycnometer.

### 3.5. Tapped Density Tester

In this study, the tapped density (sample mass/tapped volume of the sample) and apparent density (sample mass/ initial volume of the sample) of the powders have been calculated by using a tapped density tester (Erweka Ltd.) in order to predict the flowability properties of the powders.

The tester essentially consists of 2 graduated cylinders placed on the tester platform. The tapping action is generated by a camshaft which lifts the platform and allows it to drop back to its original position. The normal speed is 300 taps per minute. The number of taps can be selected from a user interface. In this technique, taps were applied until a maximum packing condition was achieved. The level of powder in the graduated cylinder was checked after every 10 taps till there was no further reduction in level. This was taken as the tapped volume which was used for calculating the tapped density. The measurements were done in three times and an average value was reported.

By using tapped and apparent density values, the ability of the powder to flow (table II.1) and its compressibility (table II.2) can be predicted by calculating Carr index ( $I_c$ ) (eqn. II.6) and Hausner Ratio ( $H_r$ ) (eqn. II.7).

$$I_c = \left( \frac{\rho_{tapped} - \rho_{apparent}}{\rho_{tapped}} \right) \quad (\text{Eqn.II.6})$$

$$H_r = \frac{\rho_{tapped}}{\rho_{apparent}} \quad (\text{Eqn.II.7})$$

**Table II.1.** Flowability of the Powders According to Carr Index

Carr Index (%)	Flowability	Powder State
5 – 15	Excellent	Sand-like powder without fibres & fine particles
15 – 18	Good	Sand-like powder without fibres & fine particles
18 – 22	Mediocre	Powder with small amount of fines particles
22 – 35	Bad	Powder with fine particles
35 – 40	Very Bad	Cohesive powder
> 40	Execrable	Very cohesive powder

**Table II.2.** Compressibility of the Powders According to Hausner Ratio

Hausner Ratio	Compressibility
< 1.25	Few compressibility
1.25 – 1.4	Intermediate compressibility
> 1.4	High compressibility

### 3.6. Freeman Technology Powder Rheometer (FT4)

The FT4 Powder Rheometer is a device that is able to classify powders by their flowability. The aim of this device is to provide an automated testing program that is relatively independent of the operator and is quick. It has a special profile propeller type blade which can be rotated and simultaneously moved axially into a powder cell and the axial force and the rotational force can be measured (fig.II.15).



**Figure II.15.** FT4 Powder Rheometer (Freeman, 2006)

There are different kinds of control variables on both axis such as velocity, force and torque. All powder samples are pre-conditioned using the instrument's conditioning methodology to have a homogeneously packed powder bed. The conditioning blade action gently disturbs the powder bed and creates a uniform, lightly packed test sample that can be readily and consistently reproduced. The conditioning cycle comprises a traverse of the blade downward towards to the bottom of the powder cell and then a traverse upward as shown in figure II.16. The downward traverse would typically use a  $5^\circ$  positive helix in order that the blade action is more slicing than compacting. The upward traverse would typically use a  $5^\circ$  negative helix that gently lifts the powder and drops it over the blade. In both upward and downward movement of the blade for conditioning the tip speed of the blade is constant and 100 mm/s. This process removes any packing history such as pre-consolidation or excess air (Freeman, 2008).

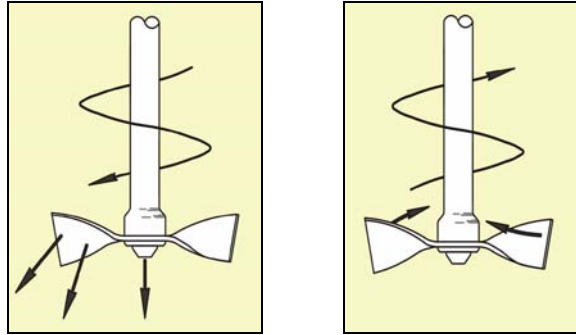


**Figure II.16.** Downward and Upward Conditioning Cycles of FT4 Powder Rheometer  
(Freeman, 2006)

After the conditioning step, there are different types of test programs for different rheological characteristics of powders can be used. In the test programs, the blade moved along a downward helical path, but in the opposite direction, to impose a compaction regime, thereby forcing the powder to flow around the blade. In this study, flow rate index (FRI) program, which includes 4 different test cycles with 4 different blade tip speeds (100 mm/s, 70 mm/s, 40 mm/s, 10 mm/s) has been used in order to characterize the flowability properties of the powders. It allows determining the sensitivity of the powder samples to the stirrer blade speed. The flow rate index values for the powders are calculated by dividing the 11<sup>th</sup> total energy value to the 8<sup>th</sup> total energy value. Higher the FRI value, lower the flowability of the particles (Freeman, 2006). A typical total energy according to tip speed graph can be seen in figure II.17.

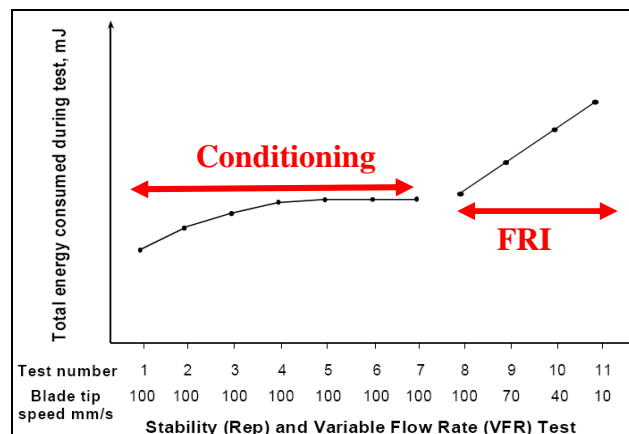


**Figure II.17.** A Typical Graph of Total Energy Consumed vs. Blade Tip Speed

### 3.7. Contact Angle Measurement

The contact angle measurement is used to determine the wettability property of a solid by a liquid. Generally, the determination of the contact angle is conducted using the sessile drop method. The liquid is dropped by a micro syringe on the solid and the contact angle between the baseline of the drop and the tangent at the drop boundary is measured. Young formulated a relation between the interfacial tension  $\gamma$  at a point on a 3 phase contact line (fig.II.18).

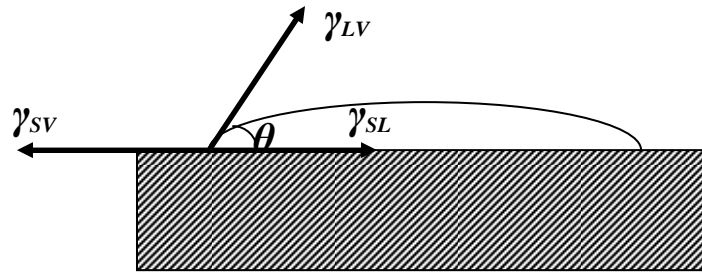


**Figure II.18.** Scheme of the Contact Angle

The indices 'S' and 'L' stand for solid and liquid,  $\gamma_{SL}$  and  $\gamma_{LV}$  describe the surface tension components of the two phases whereas  $\gamma_{SL}$  represents the interfacial tension between the phases and  $\theta$  stands for the contact angle corresponding to the angle between vector  $\gamma_{SL}$  and  $\gamma_{LV}$ . Young formulated the relationship between these quantities;

$$\gamma_{LV} * \cos \theta = \gamma_{SV} - \gamma_{SL} \quad \text{(Eqn.II.8)}$$

In contact angle measurements, powder beds have been prepared for each powder sample. A liquid drop of controlled volume (10  $\mu$ l and around 3 mm diameter) is placed on the powder bed of the particles and then photographed. The contact angle is determined by drawing a tangent to the profile at the point of three-phase contact after the drop profile has been enlarged by image projection.

### 3.8. Dynamic Vapour Sorption (DVS)

Dynamic vapour sorption (DVS) analysis is a technique in which a solid sample is subjected to varying conditions of relative humidity and temperature in order to understand the moisture sorption affinity of solids. A schematic view of a dynamic vapour sorption (DVS) analyser (Surface Measurement Systems Ltd.) is given in figure II.19. The apparatus consists in a twin pan microbalance with a high resolution, housed inside a temperature controlled incubator. A given amount of the solid sample is placed in the sample holder and suspended to one side of



the balance whereas a reference holder is suspended to the other side. A part of carrier gas (usually nitrogen) is bubbled through the test liquid and humidified. The desired humidity of carrier gas is achieved by mixing dry and humid gas flows in the correct proportions using automated mass flow controllers.

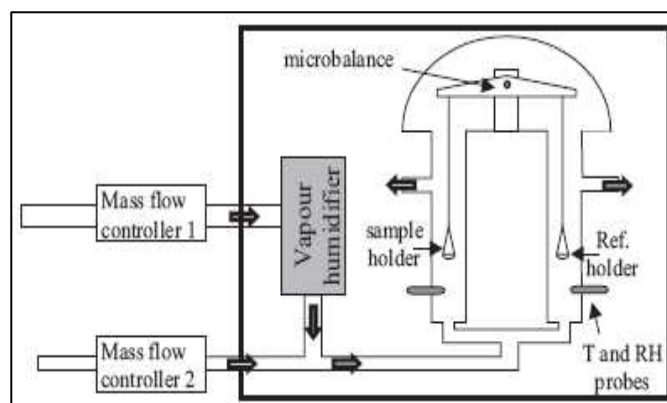


**Figure II.19.** Scheme of the Dynamic Vapour Sorption (Lazghab et al., 2005)

The gas is divided into two equal parts, flowing past the sample holder and the reference holder. In order to reduce uncertainties caused by vapour adsorption/desorption on sample holder's wall, the net liquid uptake is determined by comparing the sample holder to the reference holder. Continuous monitoring of the sample weight permits to follow the liquid adsorption from the beginning up to equilibrium. Prior to being exposed to any vapour, the samples (around 100 mg) are equilibrated at 0% RH to remove any surface adsorbed vapour and to establish a dry mass baseline. Next, the samples are exposed to carrier air with varying relative humidity. The relative humidity is increased step by step during adsorption and decreased during desorption. At each step, the sample mass is allowed to reach equilibrium before humidity is varied. The two basic results can be derived from DVS data is the sorption kinetics and equilibrium adsorption isotherms (Lazghab et al., 2005)

#### 4. MATERIALS

In this study, two different “model couples” have been used for dry coating trials. Poly(methyl methacrylate) (PMMA) with Talc particles (1<sup>st</sup> model couple) and Cellets with Talc particles (2<sup>nd</sup> model couple) have been used as host and guest particles in dry particle coating trials.

#### 4.1. Poly(methyl methacrylate) (PMMA)

Poly(methyl methacrylate) (PMMA) is a thermoplastic and transparent plastic. Chemically, it is the synthetic polymer of methyl methacrylate. It has the chemical formula of  $(C_5O_2H_8)_n$ . The structure of the PMMA can be seen in figure II.20..

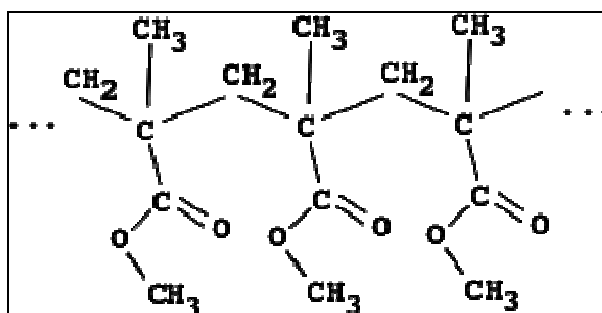


**Figure II.20.** Chemical Structure of PMMA

Methyl methacrylate is the basic molecule, or monomer, from which PMMA is formed (fig.II.21). The chemical formula for this material is  $CH_2=C(CH_3)COOCH_3$ . There are different methods for PMMA synthesis. These techniques have been explained by early researchers (Limmer et al. 2002, Ahmad et al., 2007, Ma et al., 2008, Kuan et al., 2008, Zhu et al. 2008).

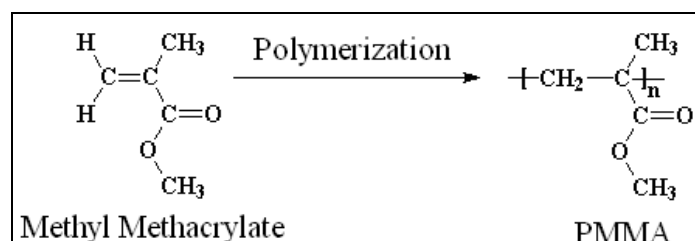


**Figure II.21.** Chemical Structure of Methyl Methacrylate and PMMA

PMMA is an important commercial plastic and it has different properties (odourless, tasteless, nontoxic etc.) which make it very interesting for different applications. It has a good impact strength property. It is softer and can be easily scratched. Zhu et al. (2008) used PMMA particles as filler for improving mechanical properties of PVC matrix. They have observed that the tensile strength of PVC matrix increased from 21.4 MPa to 42.9 MPa and the elongation at break is enhanced greatly from 17.9% to 36.8% because of the PMMA particles in the mixture (5 wt%).

PMMA has been used in a wide range of areas and applications, such as in aircraft windows, signs, lighting, dentures, food-handling equipment and contact lenses. PMMA has also been used as bone cement, to affix implants and to remodel lost bone. It is supplied as a powder with liquid methyl methacrylate (MMA). Surgeons can judge the curing of the PMMA bone cement by pressing their thumb on it. Mendicino et al. (2008) explained the fabrication of an antibiotic impregnated PMMA intramedullary rod. PMMA is also used as carrier for sustained local delivery of drugs (Vallet-Regi et al., 1998, Tao et al., 2003). Elvira et al. (2004) loaded PMMA microspheres with different amounts of cholesterol by using supercritical carbon dioxide in order to understand the drug release properties of the loaded particles. They observed that the drug release rate of PMMA particles decreases significantly when the cholesterol amount on the PMMA carrying particles increases. PMMA has also been used as model particle for studying the surface properties of composite powders by dry coating method in early studies (Ramlakhan et al., 2000, Pfeffer et al., 2001). Horiuchi et al. (1999) used PMMA particle as carrier particle for different pigments. They observed that although PMMA has a high Tg, and high particle size, the pigment coated PMMA particles had a homogeneous coating structure with good integrity.

In this study, PMMA particles from Acros Organics used as the host component in dry coating trials. It has the volume mean diameter ( $d[4;3]_v$ ) 160  $\mu\text{m}$ , average molecular weight (Mw) 35000 g/mol and 1.2 g/ml density ( $\rho$ ). The properties of the PMMA particles are also presented in table II.3.

**Table II.3.** Properties of PMMA Particles

<b>d[4.3] (<math>\mu\text{m}</math>)</b>	<b>d[1.0] (<math>\mu\text{m}</math>)</b>	<b><math>\rho</math> (g/ml)</b>	<b>Mw (g/mol)</b>
160	130	1.24	35000

PMMA particles have a regular spherical shape and smooth surface as it can be seen from figure II.22 that was taken by ESEM. The morphology of the particles enables us to see the coating performance easily by visual methods and it is also suitable for different characterization methods.

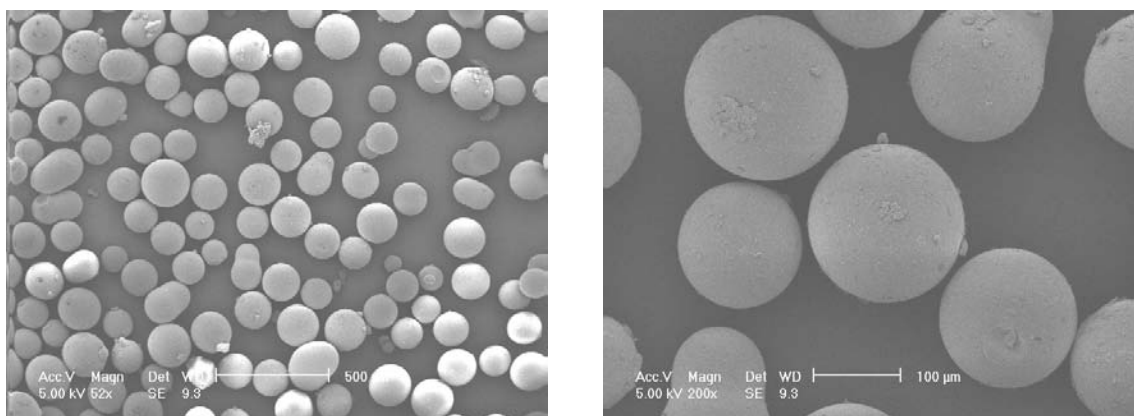


**Figure II.22.** Surface Morphology of PMMA Particles

#### 4.2. Cellets

Cellets are pellets made of microcrystalline cellulose. It has a wide range of particle sizes, the standard types start with Cellets 90 (100–200 µm) and end with Cellets 1000 (1000–1400 µm). It is odourless, tasteless and extremely versatile. It is insoluble in water. As inert carriers, they are mainly used for controlled release formulations, homogeneous distribution of the active agent and for drug delivery. It has high abrasion resistance which improves the coating process. Cellets particles have a regular spherical shape, smooth surface as it can be seen from figure II.23 and they have very high mechanical strength property.

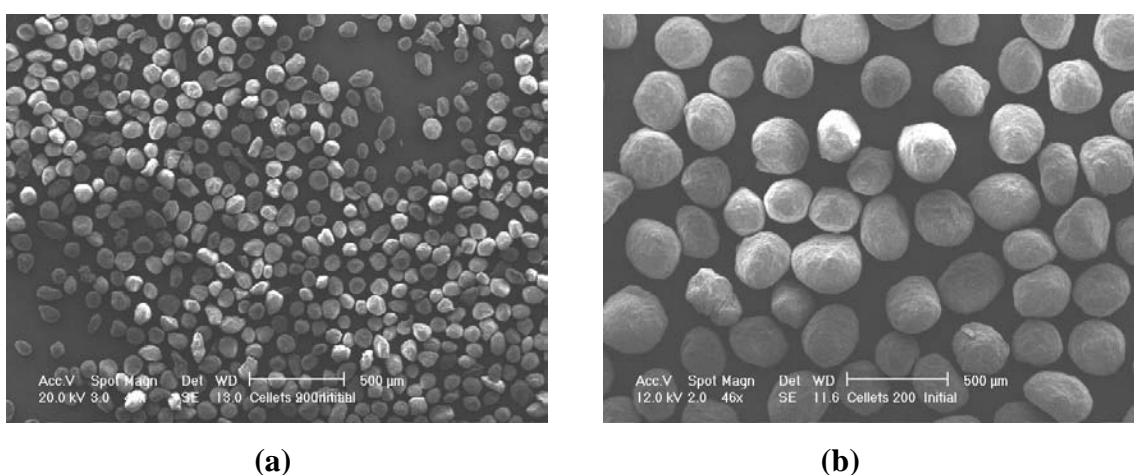


**Figure II.23.** Surface Morphology of Cellets Particles

a) Cellets 90 b) Cellets 200

Laarhoven et al. (2008) coated cellets particles with Poly(vinyl alcohol), Poly(ethylene glycol) and (hydroxypropyl) methyl cellulose in order to study the strength against attraction with a repeated impact tester. They observed that during attraction testing the uncoated cellets

granules do not show any attrition. When cellets particles are coated, all the attrition observed is due to the failure of the coating.

Cellets 90 and cellets 200 particles, from Pharmatrans Sanaq AG, used as two different host components in dry coating trials. Basically, the only difference between the cellets 90 and cellets 200 particles is the particle size distributions. The density ( $\rho$ ) of cellets particles is 1.52 g/ml. The properties of the cellets 90 and cellets 200 particles can also be seen in table II.4.

**Table II.4.** Properties of Cellets Particles

	d[4.3] ( $\mu\text{m}$ )	d[1.0] ( $\mu\text{m}$ )	$\rho$ (g/ml)
<b>Cellets 90</b>	100	74	1.52
<b>Cellets 200</b>	305	217	1.52

### 4.3. Talc

Talc is a mineral composed of hydrated magnesium silicate with the chemical formula  $\text{Mg}_3\text{Si}_4\text{O}_{10}(\text{OH})_2$  which corresponds to 4.8%  $\text{H}_2\text{O}$ , 31.7%  $\text{MgO}$  and 63.5%  $\text{SiO}_2$ . Its elementary sheet is composed of a layer of magnesium-oxygen/hydroxyl octahedra, sandwiched between two layers of silicon-oxygen tetrahedral as it can be seen from the figure II.24.

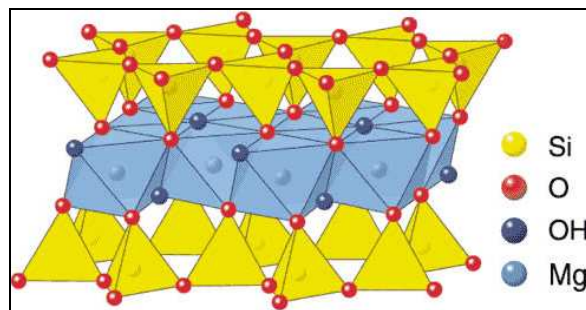


**Figure II.24.** Chemical Structure of Talc (Mulryan, 1992)

The main or basal surfaces of this elementary sheet do not contain hydroxyl groups or active ions, which makes talc very hydrophobic and inert material. Talc is practically insoluble in water and in weak acids and alkalis. It is neither explosive nor flammable. Although it has very little chemical reactivity, talc has a marked affinity for some organic chemicals. Talc's melting point is at  $1500^\circ\text{C}$  and the density is 2.8 g/ml (Balard, 2001).

Talc is the softest material according to Mohs scale of mineral hardness. Its smoothness, high lubricating and hiding power and ability to absorb oil and grease makes it very important

material for industrial applications. It has been used as filling material in paper, plastic and ceramic industries (Lopez, 1998). In the pharmaceutical applications, talc has been used as lubricant, anti-caking agent. It has also been used in order to improve the brightness of the tablets (Kablitz et al., 2006). In food industry, talc is widely used as technological additive in a number of foods and as processing aids in the mechanical extraction of virgin olive oil.

In this study, talc particles from Luzenac S.A have been used as guest particles in dry coating experiments. The volume mean diameter ( $d[4;3]_v$ ) of the particles is 14  $\mu\text{m}$ . In order to obtain talc particles with smaller particle size distributions, some talc particles have been treated in hybridizer at 16000 rpm operating velocity for 6 minutes. At the end, it has been obtained talc particles, which is called as talc 16000, with 4  $\mu\text{m}$  volume mean diameter. The properties of talc particles are presented in table II.5.

**Table II.5.** Properties of Talc Particles

	<b>d[4.3] (<math>\mu\text{m}</math>)</b>	<b>d[1.0] (<math>\mu\text{m}</math>)</b>	<b><math>\rho</math> (g/ml)</b>
<b>Talc</b>	14	8	2.8
<b>Talc 16000</b>	4	1	2.8

It can be seen from the figure II.25, both talc and talc 16000 particles have slab geometry.

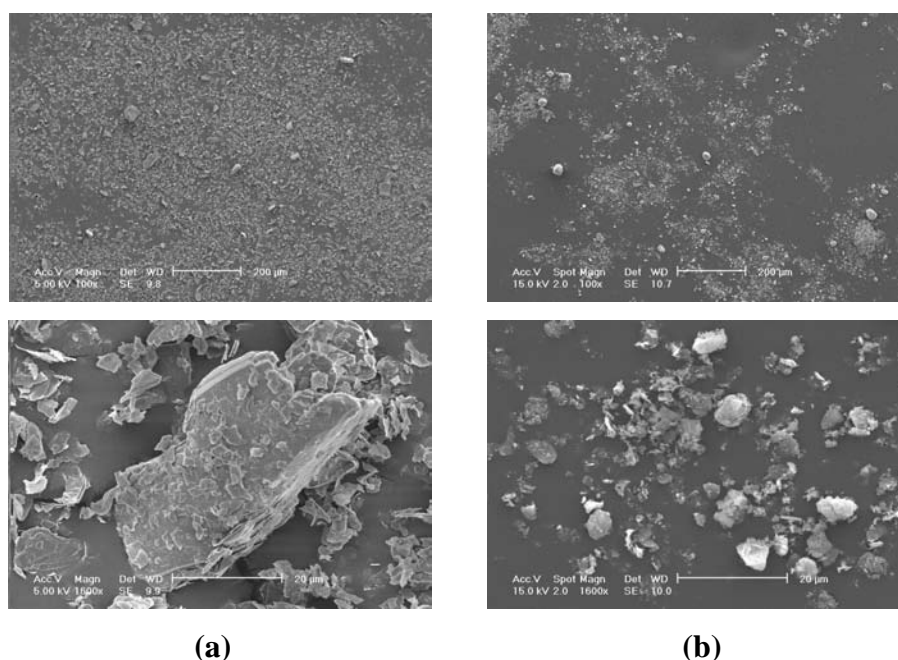


**Figure II.25.** Surface Morphology of Talc Particles

a) Talc b) Talc 16000

## **5. CONCLUSION**

In this chapter, the descriptions of the dry coating equipments, different characterization methods that have been used for analysing different physicochemical properties (flowability, wettability, surface morphology etc.) and the characteristics of the powders that were used for dry coating trials have been explained in detail. In the following chapter the obtained results will be presented and discussed.





## CHAPTER III

### *Effect of Equipment and Operating Conditions on the End–Use Properties of Composite Particles*



## 1. INTRODUCTION

As it has been discussed previously, it is very complex to understand the relationship between the couple (host & guest particles), process (equipment, operating conditions, etc.) and their effect on the end–use properties or for a certain end–use property, the required material properties (size ratio, initial affinity of adhesion etc), process (equipment, energy that the equipment needs to supply, etc.) of the particles. To be able to simplify the problem, it has been chosen some model couples.

In this part of the study, it is aimed to coat the first model couple, poly(methyl methacrylate) (PMMA) (host particle) particles with talc particles (guest particles), by different dry particle coating devices and operating conditions (mass percentage of talc, operating velocity) in order to understand the effect of the equipment and operating conditions on the end–use properties of the new generated particles. Nara Hybridizer (NHS–0), Cyclomix Hosokawa and Turbula mixers have been used as three different dry particle coating equipments (Chapter II). These equipments have certain differences according to the way they function and also the energy that they supply to the powder sample to obtain coating on the surface of the host particles.

The feasibility of dry coating of the PMMA – Talc particles was investigated for each dry particle coating equipment. Several characterisation methods are used to study the physico–chemical properties of the coated particles. Visualisation before and after coating is performed with an Environmental Scanning Electron Microscopy (ESEM), it enables us to qualitatively estimate the type of coating obtained and the amount of deposited guest particles on the host particles. The particle size distributions and coating strength of the composite particles have been studied by using a laser diffraction granulometer (in dry feed mode). In this apparatus the powder de–agglomeration is controlled by adjusting the dispersing air pressure. It has been found the maximum dispersing pressure that the coating can resist.

An Atomic Force Microscopy (AFM) has been used in order to understand guest particle deposition on host particle, analyze the surface morphology of the particles and also to find the adhesion force between the particles. According to the results that have been obtained, it enables us to calculate the amount of guest particles on the surface of the host particles by using a model for adhesion force.

The flowability of the PMMA particles has been analyzed before and after the coating process in different equipments by using a Freeman Technology powder tester (FT4) and a tapped density tester.

## 2. DRY COATING OF PARTICLES IN HYBRIDIZER

The Nara Hybridization System (NHS – 0) has been used as dry coating equipment with different mass percentages of Talc particles. In hybridization, high mechanical impact forces, compression and shearing are used in order to coat the particles.

First of all, it is necessary to find the optimum operating conditions of Hybridizer for the model couple and also to understand the fragmentation behaviour of the powders. For that reason, a preliminary study has been done for PMMA and Talc particles individually. In preliminary study, the PMMA and talc particles are individually treated in the hybridizer at different rotational velocities and their fragmentation characteristics have been studied.

PMMA particles with different mass percentages of talc particles have been treated at different operating velocities for dry coating experiments. In this part, the characterisation of powders before and after coating is presented in detail.

### 2.1. Hydrodynamic Properties of Nara Hybridizer

In order to have an idea about the effect of rotational velocity of hybridizer on generated air velocity, a study of hydrodynamic properties of Hybridizer has been done.

The air velocity inside the hybridizer was measured by using an anemometer. A reference point in order to detect the air velocity has been chosen in the recirculating chamber of the hybridizer as it can be seen from Figure III.1.

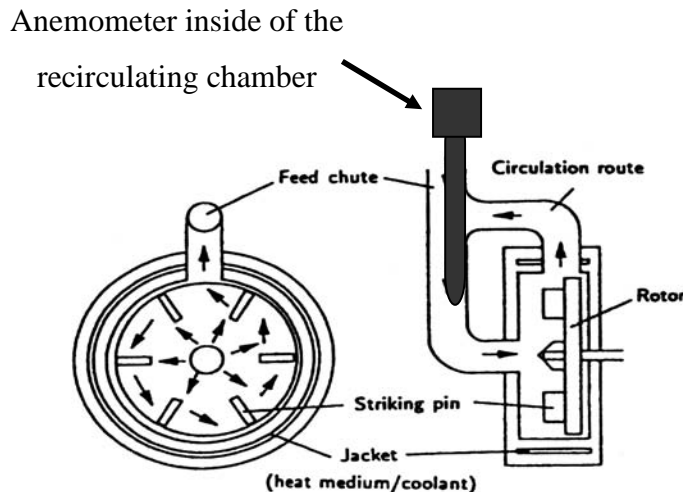


**Figure III.1.** Scheme of Experimental Setup

Nara Hybridizer has been operated (empty) with 10 (from 1000rpm to 9600 rpm) different velocities and 4 different pressures (0 bar, 0.1 bars, 0.2 bars, 0.3 bars).

In the experiments, the anemometer has been used with the time program in which it takes the all data in specific time range (>1 data per second) and after it calculates the mean value for this specific time range. In this study, the time ranges has been defined as 10 seconds (that means for one velocity more that 10 values) and 2 minutes in order to compare the data.

It can be seen from figure III.2 that the velocity of the air increases with increasing rotational velocity of hybridizer as expected. It was observed that there is no significant effect of air (purge) pressure on the circulating air velocity inside the hybridizer. It shows that the de-agglomeration of the particles is affected by rotation of the rotor.

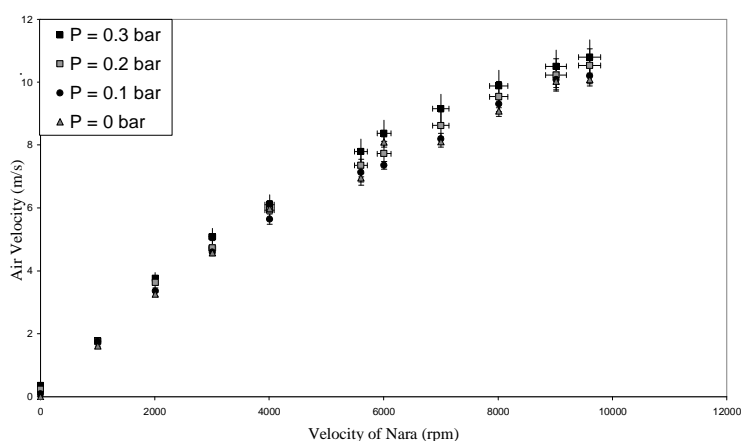


**Figure III.2.** Air Velocity Inside of the Recirculating Chamber of Nara According to Different Air (Purge) Pressures

## 2.2. Preliminary Study of Poly(methyl methacrylate) Particles

In the preliminary study, the PMMA particles have been treated at different rotational velocities. The particle size of the final PMMA has been determined with the Malvern Mastersizer laser diffraction granulometer and expressed as the  $d[3:2]$  or surface weighted mean diameter. In addition, we have determined the yield of the hybridizer that is the percentage of material removed from the device at the end of an experiment with respect to the amount of introduced powders in the beginning.

The rotational velocity of the Hybridizer is up to 16000 rpm, here we used 2500 rpm (15.6 m/s), 4000 rpm (25 m/s), 5600 rpm (35 m/s), 9600 rpm (60 m/s) and 15000 rpm (93.8 m/s) as operating velocities.

The effect of operating time has been also studied. According to early studies that have been done by Vilela et al. (2005), it was seen that the operating time has no significant effect (after

couple of minutes) on the particle fragmentation. In hybridizer treatments, 6 minutes has been chosen as the fixed operating time.

The maximum batch size of the Hybridizer (NHS-0) is about 50 g. According to work has been done by Pfeffer et al. (2001), the advised initial charge should be between 25 and 35 g in order to have a good powder circulation in the mixing chamber. For that reason, the initial charge of the powders has been fixed at 30g.

### 2.2.1. General Mass Balance

The initial charge of 30 g powder is introduced to the Hybridizer. For the each rotational velocity, the percentage of the PMMA removed from the device at the end of the experiment with respect to initial charge has been compared. In the figure III.3, the % of the collected powder according to different operating velocities can be seen.

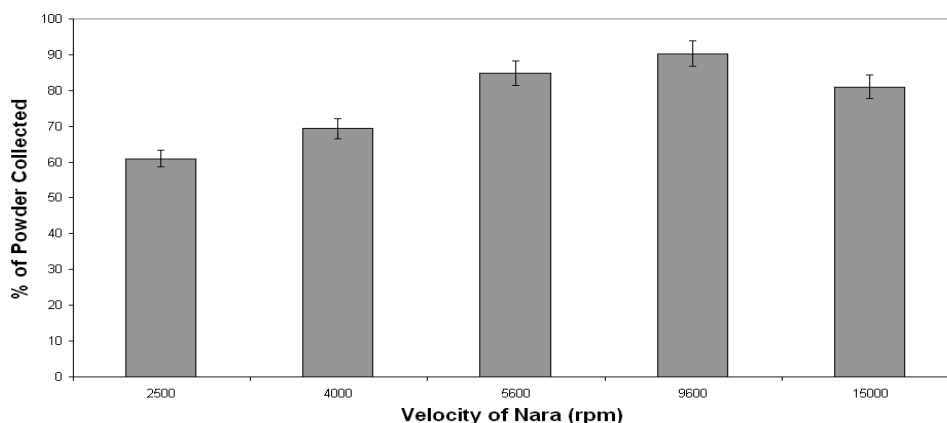


**Figure III.3.** Effect of rotational velocity on Amount of PMMA Collected

It can be seen that the amount of PMMA collected rises from 60 % at low velocities of rotation up to a stable value of about 90 % for rotational velocities greater 5600 rpm. This can be explained by the fact that, air flow generated by rotational velocity of the rotor is not high enough to have a good recirculation of the powder so that some of the powder stays in the recirculation tube.

### 2.2.2. Effect of Rotational Velocity on Particle Size Distributions

Here, it is aimed to understand the fragmentation behaviour of the particles with different operating velocities. The particle size distribution analyses of PMMA particles have been done for each 5 operating velocities of Hybridizer (between 2500 rpm – 15000 rpm). The

figures III.4 and III.5 show the volume and number distributions of PMMA particles before and after treatment in hybridizer with different operating velocities.

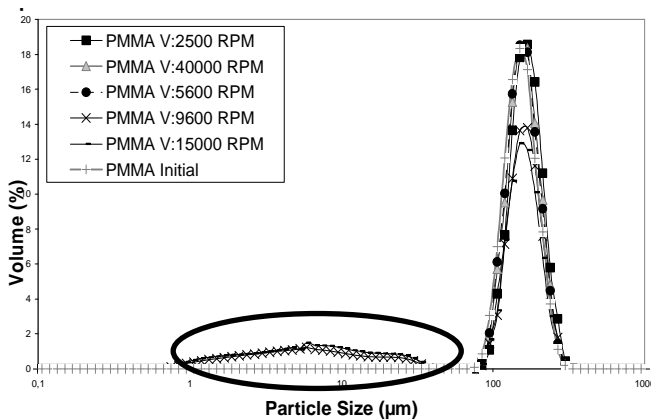


**Figure III.4.** Volume Particle Size Distribution of PMMA Particles Before and After Treatment with Different Operating Velocities

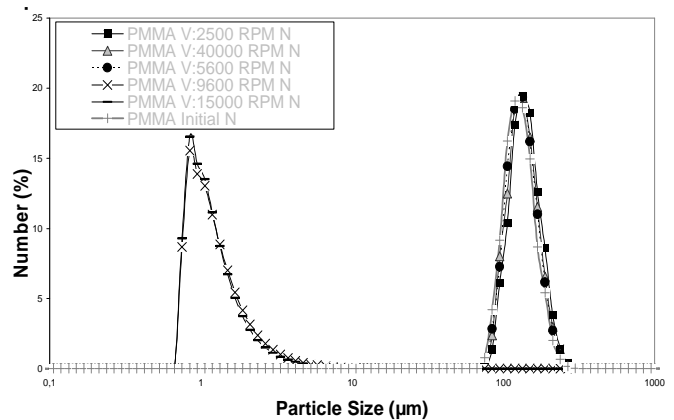


**Figure III.5.** Number Particle Size Distribution of PMMA Particles Before and After Treatment with Different Operating Velocities

It can be seen that the treated PMMA particles at 9600 rpm and 15000 rpm have a fine particle population (<20 µm) compared to other velocities because of the particle breakage. These fine populations can be seen easily in the number particle size distributions (Fig. III.5).

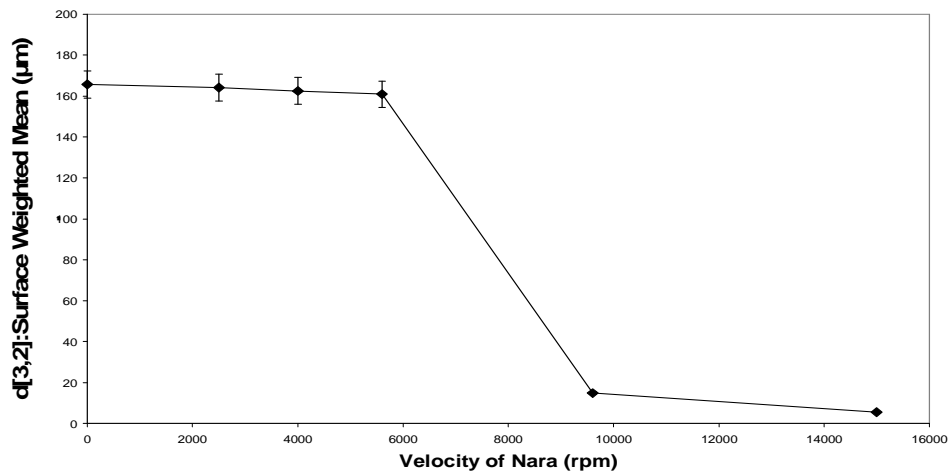


**Figure III.6.** Effect of Rotational Velocity on Particle Sizes of PMMA

The evolution of the surface weighted mean diameter ( $d[3,2]$ ) for PMMA particles before and after the treatments confirms the observations about the particle size distributions (Fig. III.6). The powders, that are produced at low rotational velocities, has an initial particle size  $d[3,2]$  of about 160 µm, but the mean particle size is reduced with higher rotational velocities,

falling to less than 10  $\mu\text{m}$  for rotational velocities greater than 5600rpm. This would indicate particle breakage at these high rotational velocities. It is also confirmed by visual observation with the ESEM as seen in the figure III.7.

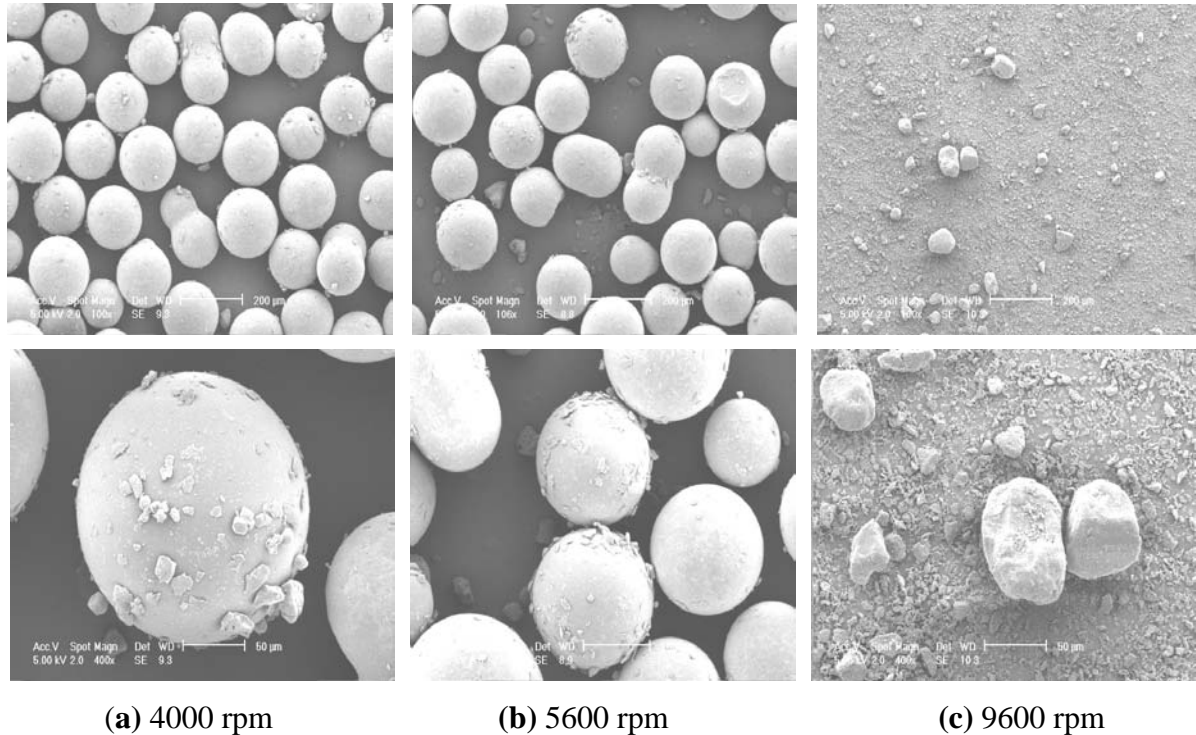


**Figure III.7.** Surface Morphology of PMMA Particles after Treatments in Hybridizer

### 2.3. Preliminary Study of Talc Particles

In the preliminary study with talc particles, the particles has been treated at 4000, 5600 and 9600 rpm operating velocities for 6 minutes operating time as it has been done for PMMA particles. The initial talc particles have a volume mean particle diameter ( $d[4:3]_v$ ) around 14  $\mu\text{m}$ .

The figures III.8 and III.9 show the volume and number particle size distributions of the talc particles before and after the treatments. It can be seen that the talc particles keep their particle size for each operating velocity. It shows us that, up to 9600 rpm operating velocity of Nara Hybridizer talc particles are not broken. It is also confirmed by visual observation as seen in figure III.10.



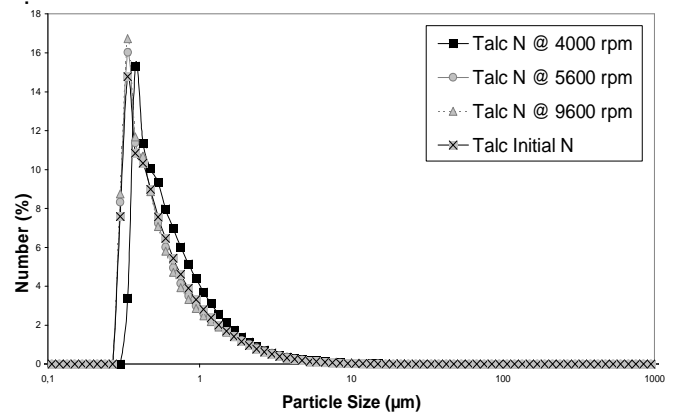
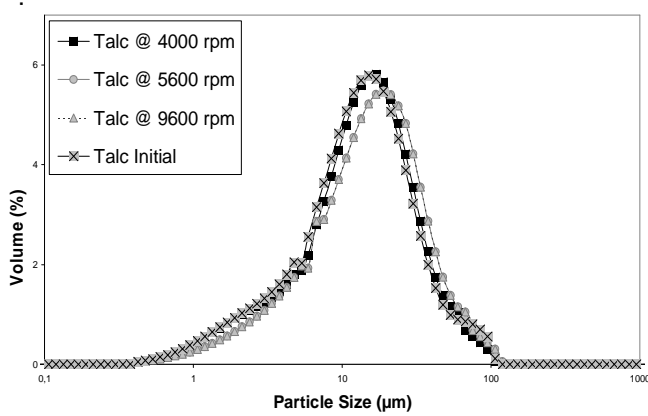


**Figure III.8.** Volume Particle Size Distribution of Talc Particles Before and After Treatment with Different Operating Velocities

**Figure III.9.** Number Particle Size Distribution of Talc Particles Before and After Treatment with Different Operating Velocities

It can be seen that the talc particles are generally agglomerates and have slab morphology.

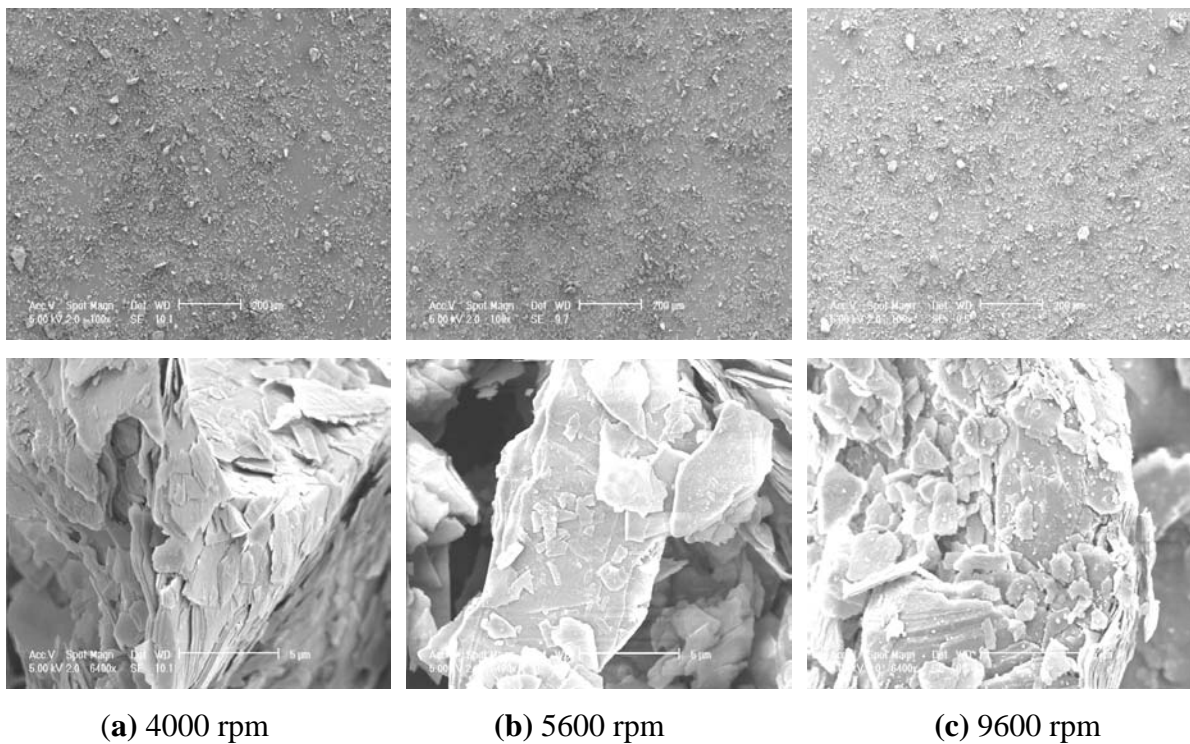


**Figure III.10.** Surface Morphology of Talc Particles after Treatments in Hybridizer

In the preliminary study of the PMMA and talc particles, it has been observed that the particle recovery varies from 60% up to 90%, at 9600 rpm most of the PMMA particles are broken but on the other hand talc particles keep their particle size for each operating velocities.

After the preliminary study, 4000 rpm (25 m/s), 5600 rpm (35 m/s) and 9600 rpm (60 m/s) have been chosen as operating velocities to coat PMMA particles with 2 different mass percentages (1%, 5%) of talc particles for 6 minutes. 5% mass percentage of Talc corresponds to theoretical monolayer coating percentage in hexagonal packing of the PMMA particles. (Appendix II)

#### 2.4. Dry Coating of Poly(methyl methacrylate) with Talc

In this study, it is aimed to understand the effect of the energy that the hybridizer applies to powder sample, which is directly related to the operating velocity, and mass percentage of talc particles on the end-use properties of the generated powders. More precisely, we are interested to analyse the effect of the operating conditions of hybridizer and mass percentage of talc on the coating strength and flowability properties of the particles. On the other hand, we are also interested to analyse the topographical modifications by AFM and afterwards it is also interesting to calculate the amount of talc particles on the surface of PMMA particles by using an adhesion force model. The results of PMMA coated with 1% and 5% talc particles for each operating conditions of hybridizer will be presented (table III.1). Then, the results of the hybridizer trials will be compared with the results of basic mixed PMMA and Talc particles.

**Table III.1.** Operating Conditions of Dry Coating Treatments in Hybridizer

Host Particles	Guest Particles	Operating Velocity (rpm)	Operating Time (min)	Mass % of Guest Particles	Batch Size (g)	Temperature of Cooling Jacket (°C)
PMMA	Talc	4000	6	1 %	30	13
		5600				
		9600				
PMMA	Talc	4000	6	5 %	30	13
		5600				
		9600				

In basic mixing, PMMA particles initially treated (in hybridizer at 4000, 5600, 9600 rpm) and initial talc particles with 2 different mass percentages (1% & 5%) are put into a tube (30 g batch) and they are mixed by shaking by hand for 6 minutes. It can be considered as a simple approach to the concept of ordered mixture.

### 2.4.1. General Mass Balance

In the figure III.11 the results of the percentage of powder recovery of PMMA and PMMA coated with 1% and 5% talc particles for 4000 rpm, 5600 rpm and 9600 rpm rotational velocities are presented.

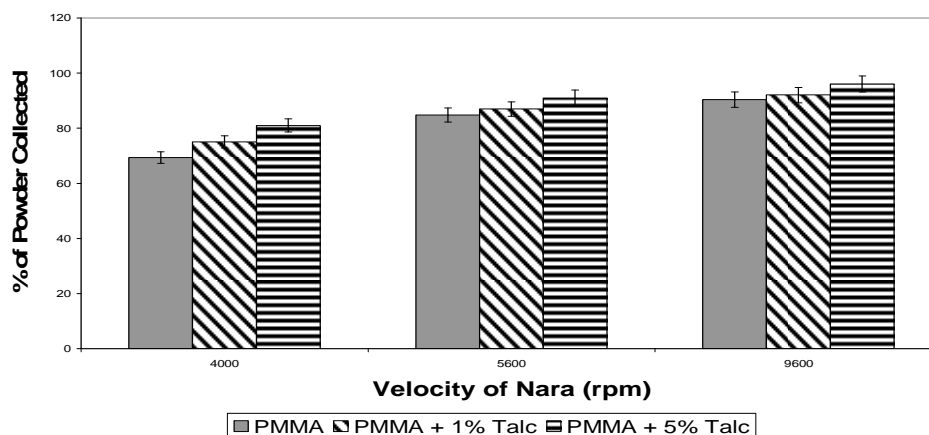


**Figure III.11.** Effect of Rotational Velocity and Mass Percentage of Talc on the Amount of Powder Collected After Treatments in Hybridizer

It can be seen that the percentage of powder recovery increases with increasing operating velocity. It was also observed that the particle recovery of PMMA coated with 5% talc particles is higher than 1% talc coating and alone PMMA particles for each velocity. This is probably due to the lubricant properties of talc particles which helps particles to flow easily inside the recirculation tubes of the hybridizer. On the other hand, it was observed that the unrecovered particles generally stayed on the walls of stator, inside the recirculation tube and the small space between the rotor and stator. In order to understand the reason of particle accumulation on the walls of the stator and inside the recirculation tube, the electrostatic properties of the particles have been analysed by diminution of particle charge method. The method is explained and the results are shown in the Appendix IV. It was found that both lubricant and electrostatic discharging properties of talc particles decreases particle accumulation in hybridizer trials.

### 2.4.2. Measure of Solid Densities of the Dry Coated Particles

The solid densities of PMMA coated with talc particles for each mass percentage of talc particles and for each operating velocities have been determined by using a helium

pycnometer. It was found that the solid density of the PMMA and the talc was unchanged by treating in the Hybridizer for all speeds of rotation. This is not unexpected.

Another measure of the overall performance of the operation is done by comparing the solid densities of the coated particles with the calculated values by assuming all the talc guest particles are fixed on the PMMA host particles.

$$\rho_{Mixture} = \frac{1}{\frac{(1-x)}{\rho_{PMMA}} + \frac{x}{\rho_{Talc}}} \quad (\text{Eqn.III.1})$$

Figure III.12 shows that, the solid density values are close to the expected values for the mixture, indicating that there is good recovery of powders from the Hybridizer.

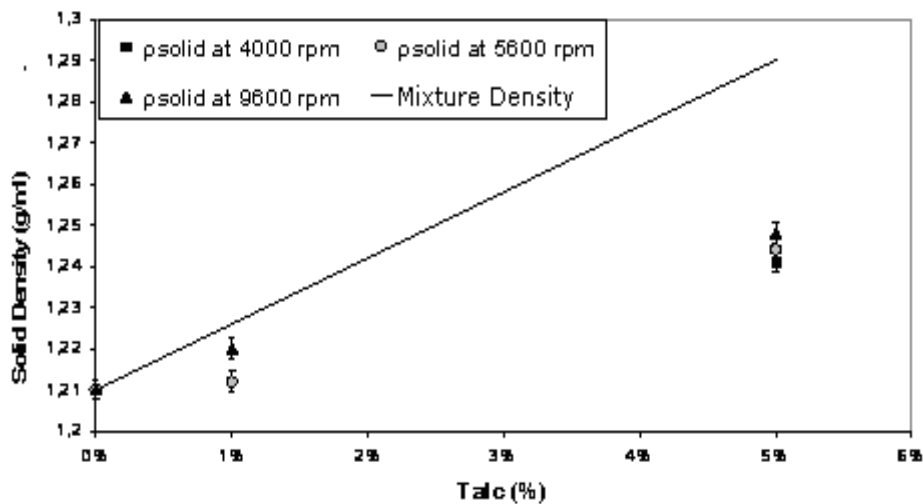


**Figure III.12.** Variation of Solid Densities of Coated Particles According to Talc Percentage

However the densities of the coated particles are always less than the calculated values for the mixture. The tendency is for the experimental values to be closer, the higher the speed of rotation which suggests improved coating with greater mechanical action. In addition, it can be seen that the values for 1 % talc coating are within about 99 % of the theoretical values whereas the values for 5% coating are only with 97 % of the theoretical values. This indicates that it is more difficult to add particles to an existing coating. These conclusions should however be treated with caution as the differences between the density of the talc and the PMMA is not great enough to give a good precision and the values are at the detectable limit of the method.

### 2.4.3. Characterization of Surface Morphology of the Particles

Environmental scanning electron microscopy (ESEM) has been used to observe the surface morphology of the particles as shown in the figure III.13. It can be seen that the hybridizer seems to embed the talc particles on the PMMA particles for each rotational speed. As it would be expected, the amount of talc particles on the surface of the PMMA particles is greater for the 5 % talc coating than 1 % talc coating.

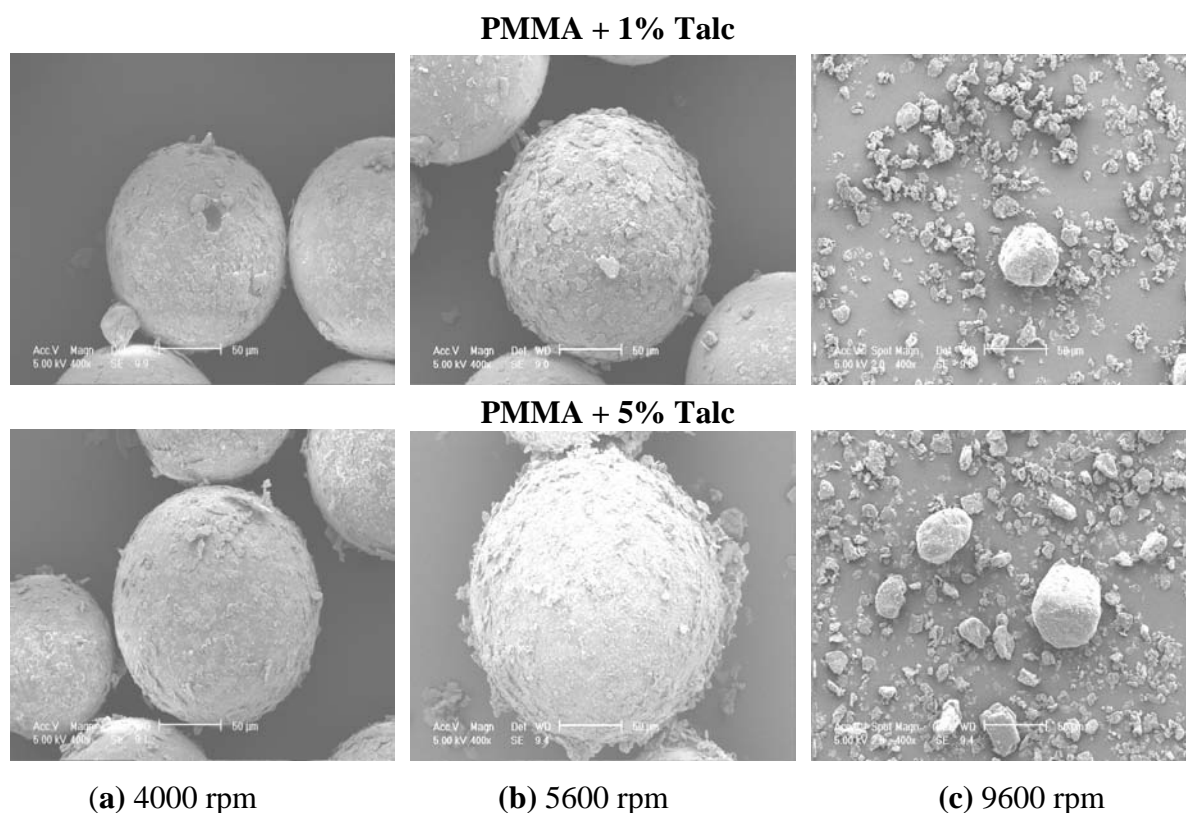


**Figure III.13.** Surface Morphology of PMMA Particles Coated by 1% and 5% Talc Particles in the Hybridizer

The shape and size of the PMMA host particles are not changed by the 4000 rpm and 5600 rpm treatments in hybridizer. However the observation of the results for 9600 rpm treatment shows evidence of big changes both in particle shape and size and the amount of background debris. This confirms the particle size analysis results shown in figure III.6 which suggests extensive breakage of the PMMA particles at 9600 rpm.

The surface morphology analyses have also been done for the basic mixed particles. It can be seen that 9600 rpm pre-treated PMMA particles with talc particles are all broken. It was observed that there are free agglomerates of talc particles for PMMA with 5% talc coating

experiments (for 4000 and 5600 rpm pre-treatments) compared to results of coated particles in the hybridizer (fig.III.14). It shows the effect of mechanical forces of Hybridizer. In basic mixing, the force generated is not sufficient to break the agglomerates of talc particles and attach them on the surface of the PMMA particles, for this reason the agglomerates rest in the powder sample.

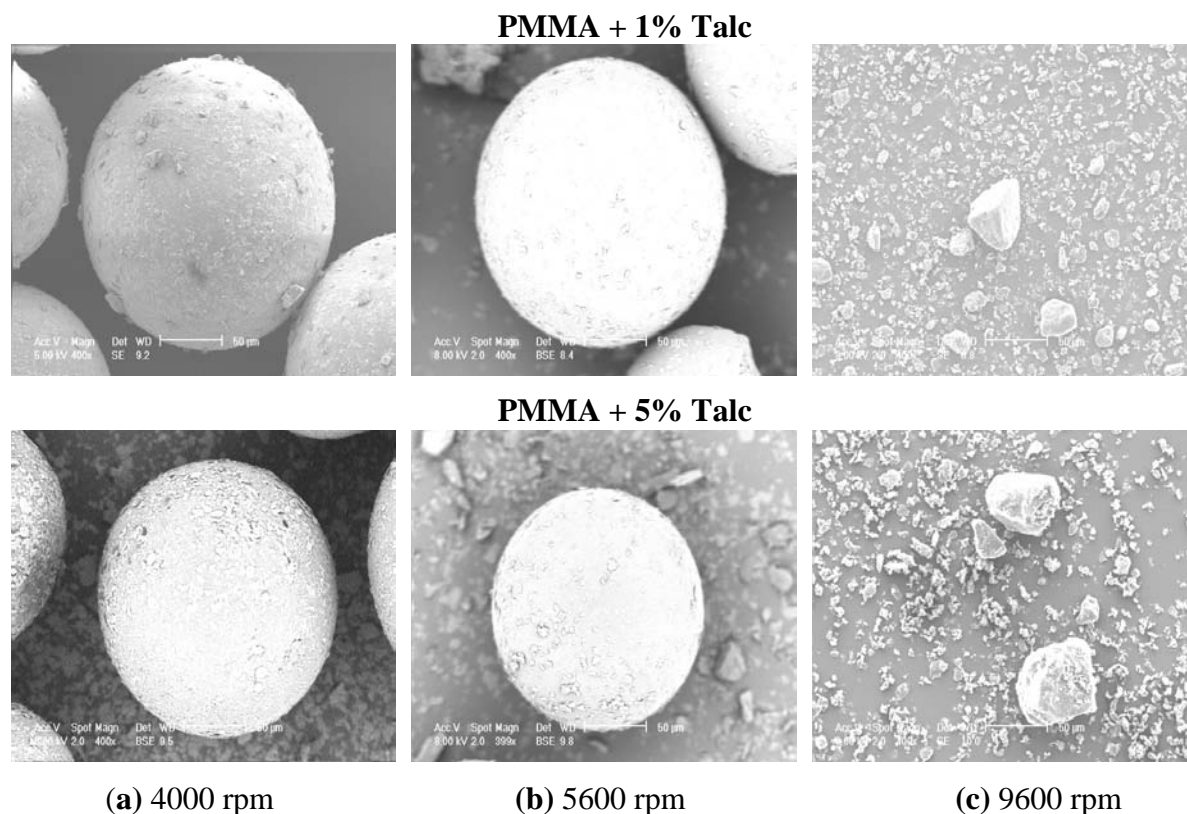


**Figure III.14.** Surface Morphology of PMMA Particles Coated by 1% and 5% Talc Particles by Basic Mixing Method

#### 2.4.4. Characterization of the Particles by Atomic Force Microscopy

In this part of the study, an Atomic Force Microscopy (AFM) has been used in order to examine the topographical analysis of the coated, uncoated particles and to understand the guest particle deposition on host particle, and also to find the adhesion force between the particles. Afterwards, according to the results that have been obtained, the percentage of surface coverage of the particles was calculated by using a model for adhesion force.

### **A. Topographical Analysis of the Particles**

In the topographical analysis of the particles, the AFM has been used on the different surface ranges (from  $10 \times 10 \mu\text{m}^2$  to  $1 \times 1 \mu\text{m}^2$ ) of the PMMA and talc initial particles and also PMMA with 1% and 5% talc coated particles.

The tapping mode of the AFM is used for analysing surface topography of the samples. For each trial, height, amplitude and phase angle values are registered simultaneously. Cantilevers with a phosphorus doped silicon tip of about  $15\text{--}20 \mu\text{m}$  in height and a spring constant of  $0.40 \text{ N/m}$  were used (MPP-11120) (Appendix V). The scan rate of the piezo tube was kept at  $0.6 \text{ Hz}$ , the tip velocity was kept at  $1.20 \mu\text{m/s}$  and the resonant frequency of the tip was between  $275\text{--}325 \text{ kHz}$  (according to the tip) during the measurements. The ratio between the free amplitude ( $A_F$ ) and the amplitude set point ( $A_{SP}$ ) has been chosen as  $0.8$ . This ratio has been found by comparing the quality of surface topography images of several experiments. It is seen that the cantilever probe hasn't got any damage by touching the sample and also it gives remarkable height and phase results at this ratio.

The results of initial PMMA particles, talc particles and PMMA coated with 1% and 5% talc particles will be presented.

#### **A.1. Topographical Analysis of the PMMA Particles**

Surface topography of the initial PMMA sample has been studied by using 10 different representative particles (according to particle shape & size) with 3 different magnitudes of imaging ( $1 \times 1 \mu\text{m}$ ,  $2 \times 2 \mu\text{m}$ ,  $5 \times 5 \mu\text{m}$ ). The AFM cantilever can be seen during a topographical analysis of a PMMA particle in figure III.15.

In figures III.16 and III.17, the height images of a PMMA particle (in 2D and 3D formats) can be seen. According to these images, the surface roughness analysis has been done by an AFM software. There are different values to characterise the surface roughness but most of the time average surface roughness ( $R_a$ ) and root mean square average of surface roughness (RMS) are used by researchers (Heng et al., 2000, Chen et al., 2002, Li et al., 2006, Liang et al., 2007) .

10 different particles with  $5 \times 5 \mu\text{m}^2$  imaging magnitude has been used for surface roughness analysis, a  $R_a$  value has been obtained for the PMMA particles, between  $60 \text{ nm}\text{--}120 \text{ nm}$  ( $R_{a,ave}:86$ ) and the RMS value varies between  $80 \text{ nm}\text{--}160 \text{ nm}$ .(table III.2)

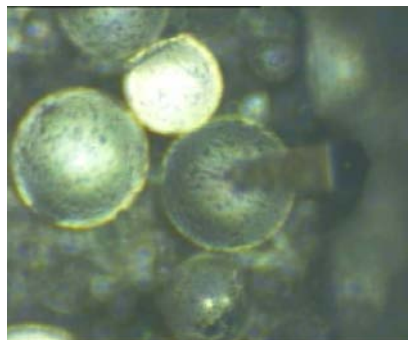


**Figure III.15.** PMMA Particle  
and Cantilever of AFM

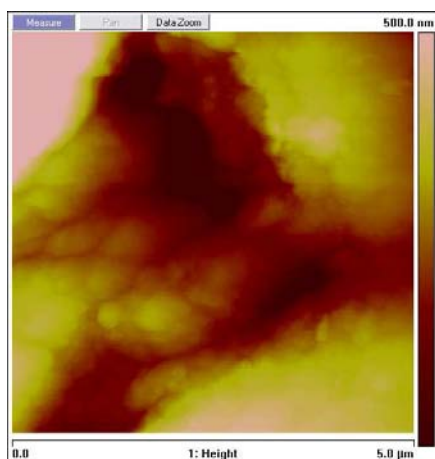


**Figure III.16.** Height Image of  $5 \times 5 \mu\text{m}^2$   
Surface of PMMA Particle by AFM

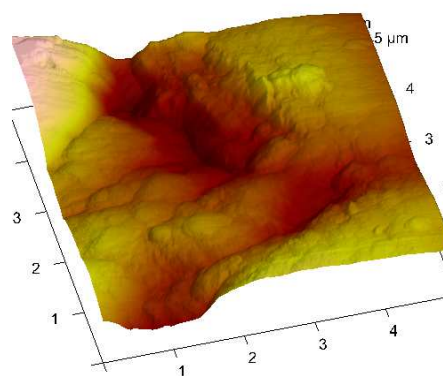


**Figure III.17.** 3D Height Image of  $5 \times 5 \mu\text{m}^2$   
Surface of PMMA Particle by AFM

### A.2. Topographical Analysis of the Talc Particles

Surface topography of the initial talc sample was difficult to analyse more precisely for large magnitudes of imaging like  $5 \times 5 \mu\text{m}^2$ . The talc particles are very soft and have a very small particle size (between  $1 \mu\text{m}$ – $18 \mu\text{m}$ ) compared to PMMA particles and because of that, while the cantilever probe is analysing the particle surface, the cantilever tip may touch to the particles and move them. The AFM cantilever can be seen during a topographical analysis of Talc particles in the figure III.18.



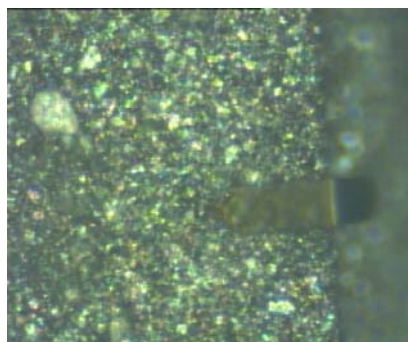


**Figure III.18.** Talc Particles and Cantilever of AFM

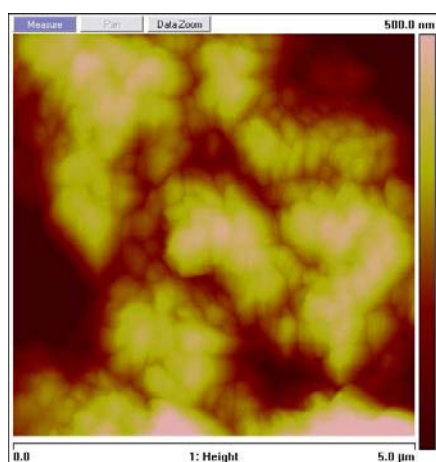


**Figure III.19.** Height Image of  $5 \times 5 \mu\text{m}^2$  Surface of Talc Particle by AFM

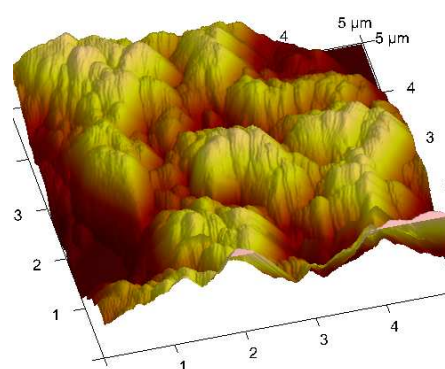


**Figure III.20.** 3D Height Image of  $5 \times 5 \mu\text{m}^2$  Surface of Talc Particle by AFM

In figure III.19 and III.20, images of surface roughness of talc particles can be seen. It is observed that the surface roughness is much higher and more evident for talc particles compared to PMMA particles and it is found the  $R_a$  value for the talc particles is between 100 nm–220 nm ( $R_{a,ave}$ :131) and the RMS value varies between 140 nm–270 nm.(table III.2)

### A.3. Topographical Analysis of the PMMA Coated with 1% and 5% Talc Particles

The topographical analysis has been done also for 1% and 5% talc coated PMMA particles. The idea was to study the effect of talc coating on the surface roughness of the PMMA particles after coating. Figure III.22 and III.23 show the height images of 1% talc coated PMMA particles.

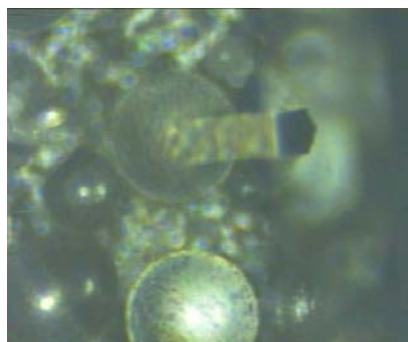


**Figure III.21.** PMMA Coated with 1% Talc Particles and Cantilever of AFM

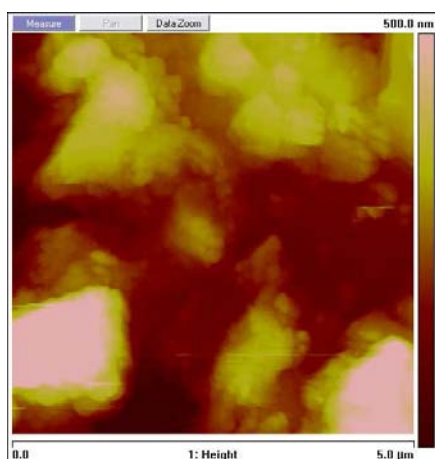


**Figure III.22.** Height Image of 5x5  $\mu\text{m}^2$  Surface of PMMA + 1% Talc Coated Particle by AFM

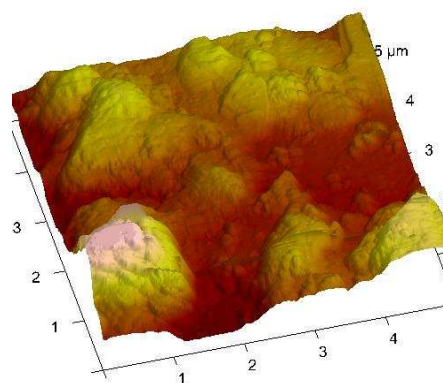


**Figure III.23.** 3D Height Image of 5x5  $\mu\text{m}^2$  Surface of PMMA+1% Talc Coated Particle by AFM

The surface roughness values of PMMA with 1% talc coating has been determined for Ra between 70 nm–140 nm ( $R_{a,ave}$ :91 nm) and RMS varies between 100 nm–190 nm. It is observed that the surface roughness increased because of the existence of talc on the surface. The change in the surface roughness is not much compared to initial PMMA particle which is due to the small amount of talc particles on the surface of PMMA particles.

The height images of 5% talc coated PMMA particles are presented in figure III.25 and III.26. The surface roughness values have been found much higher for the PMMA coated with 5% talc compared to initial PMMA particles as expected. The Ra value is between 88 nm–180 nm ( $R_{a,ave}$ :105 nm) and RMS is between 90 nm–200nm. (Table III.2)

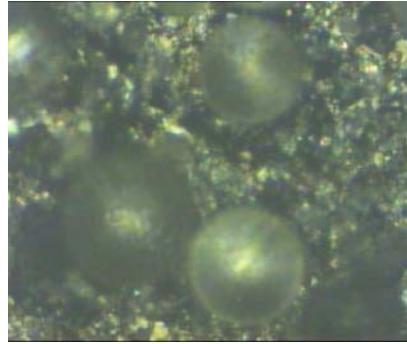


**Figure III.24.** PMMA Coated with 5% Talc Particles

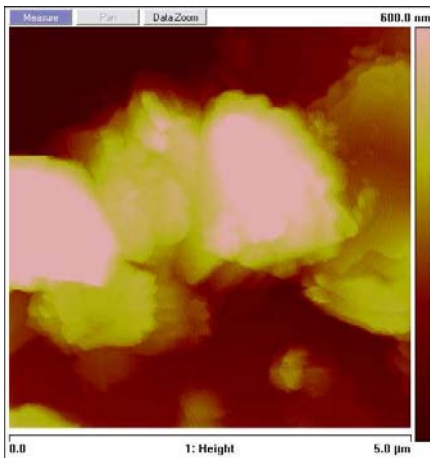


**Figure III.25.** Height Image of 5x5  $\mu\text{m}^2$  Surface of PMMA with 5% Talc Coated Particle by AFM

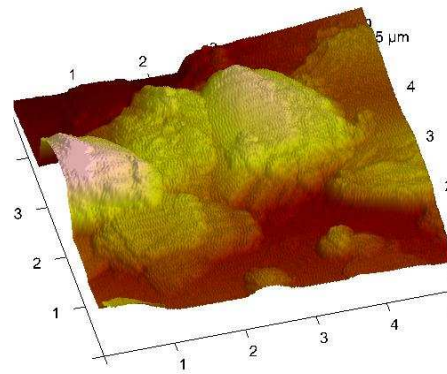


**Figure III.26.** 3D Height Image of 5x5  $\mu\text{m}^2$  Surface of PMMA with 5% Talc Coated Particle by AFM

**Table III.2.** Surface Roughness Values of Uncoated and Coated Particles (5x5  $\mu\text{m}^2$ )

Material	$Ra_{\min} - Ra_{\max}$ (nm)	$Ra_{\text{ave}}$ (nm)	$RMS_{\min} - RMS_{\max}$ (nm)	$RMS_{\text{ave}}$ (nm)
PMMA	60 – 120	86	80 – 160	118
TALC	100 – 220	131	140 – 270	186
PMMA + 1% Talc	70 – 140	91	100 – 190	132
PMMA + 5% Talc	88 – 180	105	90 – 200	155

It has been seen that, coating with talc has certain effects on the surface roughness of the PMMA particles. But, how can we be sure if there are talc particles on the surface? To be able to answer that question, a study has been done to be able to understand the existence of talc

particles on the surface of PMMA particles by comparing height results with phase contrast results.

### B. Phase Contrast Analysis of the Particles

An interesting feature of the AFM tapping mode is its capability of detecting the phase angle of the AFM cantilever oscillation. This phase angle provides information on localized AFM probe-sample interactions and has become an important mode in AFM applications on recognizing heterogeneous (different surface roughness, chemical composition, elasticity etc.) materials. However interpretation of the phase contrast has some difficulties. (Chen et al. 2002)

In this part, it is aimed to distinguish the talc particles deposition on the surface of the PMMA particles according to different surface characteristics of the particles that are obtained in the topographical analysis and phase difference.

It is known that talc particles are much softer than PMMA particles, because of that we suppose phase contrast results would give us different phase angles in the coated particles.

The results of initial PMMA, talc and PMMA coated with 1% and 5% talc particles will be presented in this part.

#### B.1. Phase Contrast Analysis of the PMMA Particles

In the figure III.27, III.28, the height, phase angle and amplitude data of the same PMMA particle with different magnitudes of imaging can be seen.

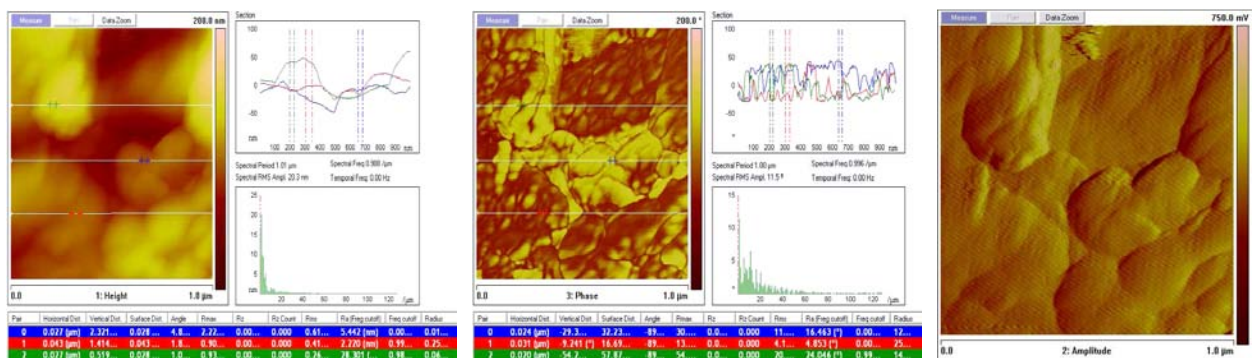
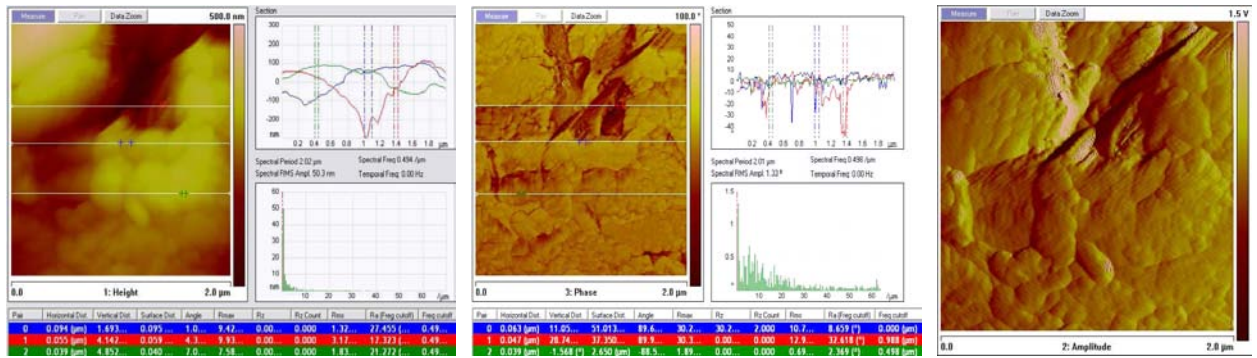


**Figure III.27.** Height, Phase Angle and Amplitude Images of 1x1 μm<sup>2</sup> Surface of PMMA Particle by AFM



Height

Phase Angle

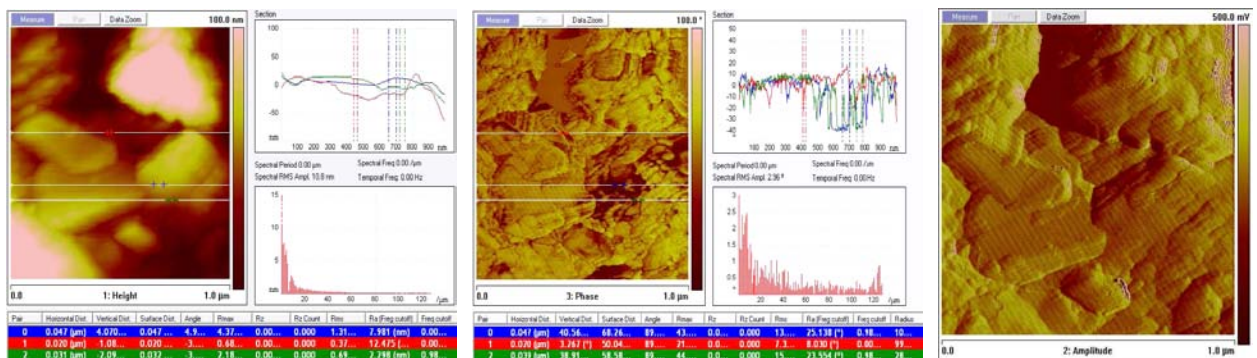
Amplitude

**Figure III.28.** Height, Phase Angle and Amplitude Images of  $2 \times 2 \mu\text{m}^2$  Surface of PMMA Particle by AFM

It was observed that in the same section of images of height and phase angle, the phase angle data varies up to  $40^\circ$  (fig.III.27) which is probably the reason for the difference in height of the surface (surface roughness). The same study has been done for 10 different particles with  $5 \times 5 \mu\text{m}^2$  magnitude of imaging and it is found that the phase angle varies between  $-100^\circ$  and  $40^\circ$  for initial PMMA particles. (table III.3)

### B.2. Phase Contrast Analysis of the Talc Particles

The results of height and phase angle data have also been compared for talc particles. In the figure III.29 and III.30 the images of height, phase angle and amplitude of talc can be seen.

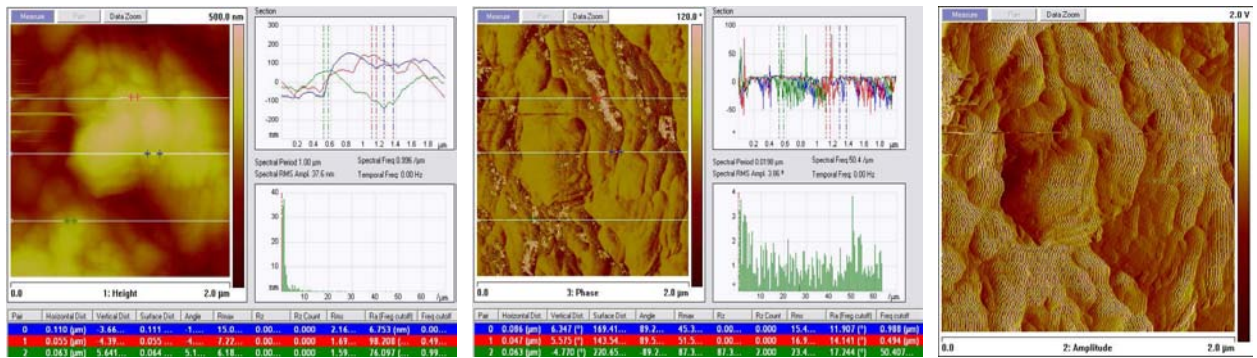


Height

Phase Angle

Amplitude

**Figure III.29.** Height, Phase Angle and Amplitude Images of  $1 \times 1 \mu\text{m}^2$  Surface of Talc Particle by AFM



Height

Phase Angle

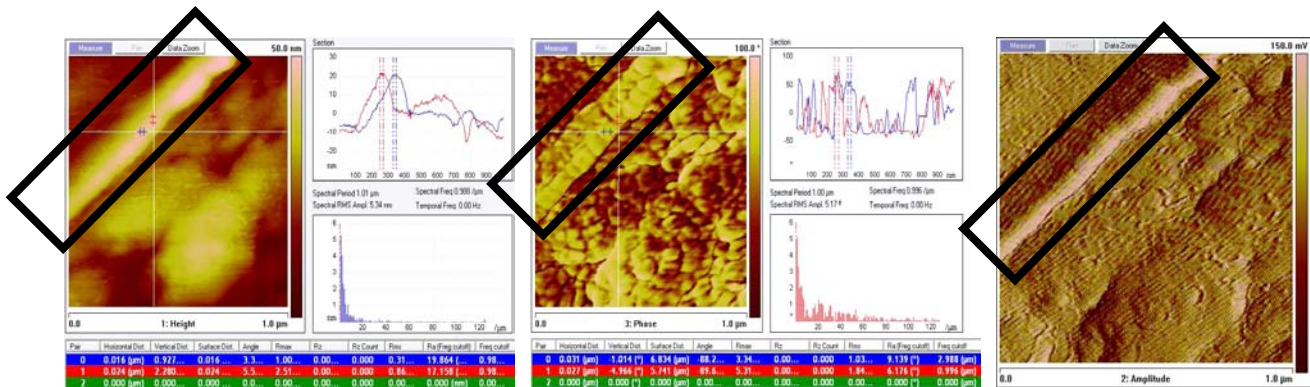
Amplitude

Figure III.30. Height, Phase Angle and Amplitude Images of 2x2  $\mu\text{m}^2$  Surface of Talc Particle by AFM

It has been observed that the phase angle of talc is more evident than PMMA. The reason is the surface roughness and also because of the material surface characteristics. Talc is much softer than PMMA and because of that we have obtained variety of phase angle values (between  $-130^\circ$  and  $110^\circ$ ). (table III.3)

### B.3. Phase Contrast Analysis of the PMMA Coated with 1% and 5% Talc Particles

The results of phase angle, height and amplitude values of PMMA coated with 1% and 5% talc particles can be seen in the figure III.31 and III.32 for  $1 \times 1 \mu\text{m}^2$  magnitude of imaging.



Height

Phase Angle

Amplitude

Figure III.31. Height, Phase Angle and Amplitude Images of  $1 \times 1 \mu\text{m}^2$  Surface of PMMA coated with 1% Talc Particles by AFM

In the figure III.31, a talc particle which is attached vertically on the surface of the PMMA particle can be seen. On the other hand, if we compare the phase angle and height results, we can see that for the same section of the particle the surface roughness seems stable but the

phase angle gives different values between 50° and 60° which is a characteristic result of Talc particles.

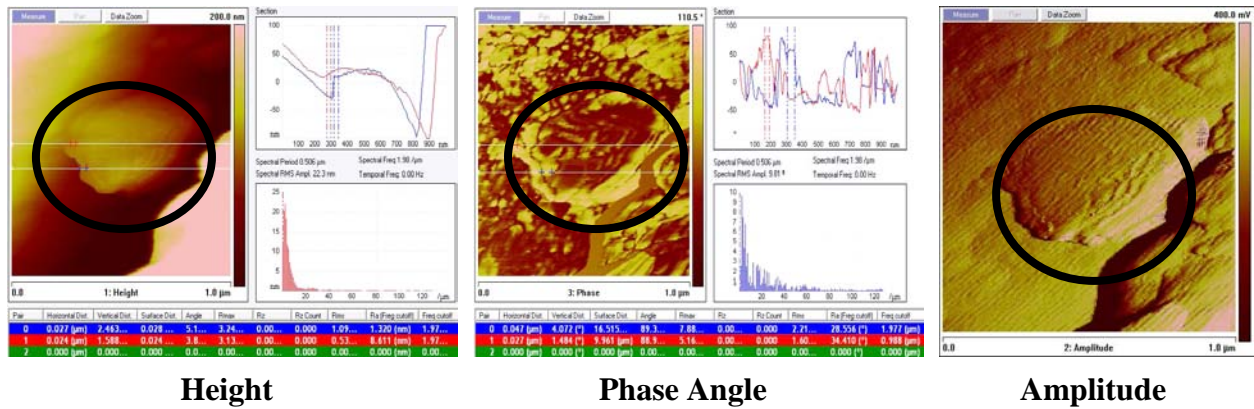


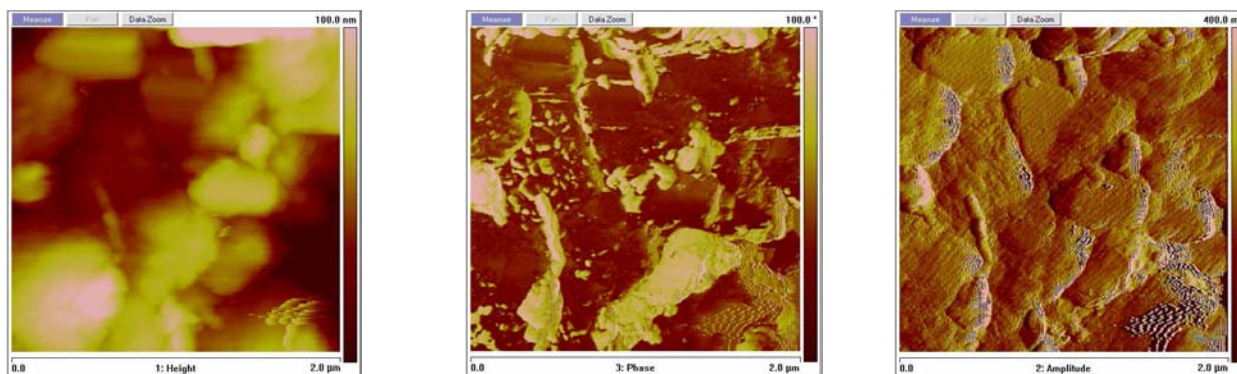
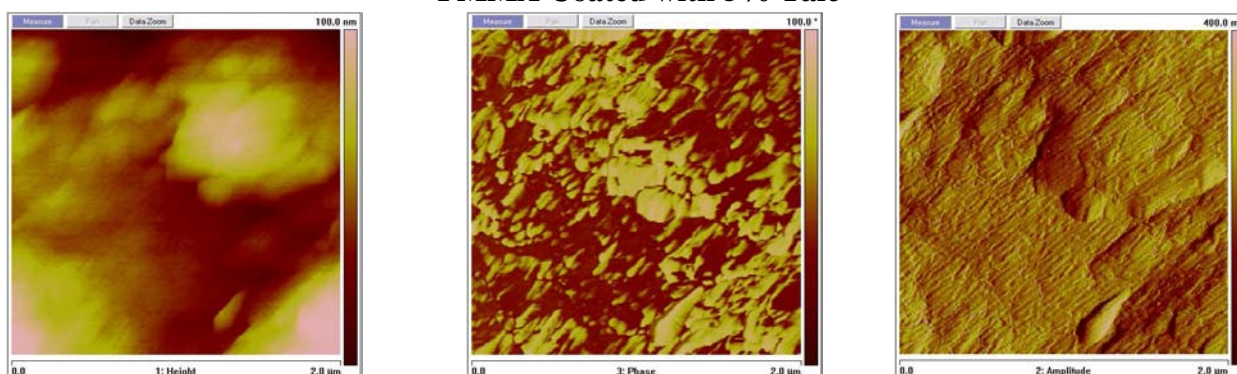
**Figure III.32.** Height, Phase Angle and Amplitude Images of 1x1  $\mu\text{m}^2$  Surface of PMMA coated with 5% Talc Particles by AFM

For 5% talc coating we have also evidence, it shows the existence of talc particles on the surface of PMMA particles. In figure III.32, a single talc particle on the PMMA surface can be easily recognized because of the morphological characteristics. Also the phase angle scale is up to 85° which is much higher than PMMA scale ( $-100^\circ < x < 40^\circ$ ). The results of phase angle, height and amplitude values with 2x2  $\mu\text{m}^2$  imaging magnitude for PMMA coated with 1% and 5% talc particles can be also seen in the figure III.33.

The height and phase angle comparison has been done for 10 different particles with 5x5  $\mu\text{m}^2$  imaging magnitude. It can be seen from table III.3, that for 1% talc coating the phase angle values are between  $-100^\circ$  and  $60^\circ$  but on the other hand for 5% Talc coating the phase angle values are between  $-100^\circ$  and  $85^\circ$ . The probable reason should be the difference in mass percentage of talc particles in the samples.

**Table III.3.** Phase Angle Values of Uncoated and Coated Particles (5x5  $\mu\text{m}^2$ )

Material	Phase Angle <sub>min</sub> (°)	Phase Angle <sub>max</sub> (°)
PMMA	- 100	40
TALC	- 130	110
PMMA + 1% Talc	- 100	60
PMMA + 5% Talc	- 100	85

**PMMA Coated with 1% Talc****PMMA Coated with 5% Talc****Height****Phase Angle****Amplitude**

**Figure III.33.** Height, Phase Angle and Amplitude Images of  $2 \times 2 \mu\text{m}^2$  Surface of PMMA coated with 1% and 5% Talc Particles by AFM

In order to show the existence of talc particles on the surface of PMMA particle, the AFM images has been analysed numerically. In this part of the study, the numerical results of height–phase angle global profiles of the particles ( $5 \times 5 \mu\text{m}^2$  - 10 images) have been taken and converted into a graph of height versus phase angle values. Each image has 256 pixel resolutions so there are  $256 \times 256 \times 10$  points for the height and phase angle graphs of each sample. This allows visualizing the difference between the different samples. At the same imaging magnitude, results of initial PMMA and talc graphs have been compared with 1% and 5% talc coated PMMA particles. In the figure III.34, the graph of initial PMMA and talc particles signature can be seen. It can be observed that the PMMA and talc particles have different phase angle characteristics as it has been observed from the AFM images.



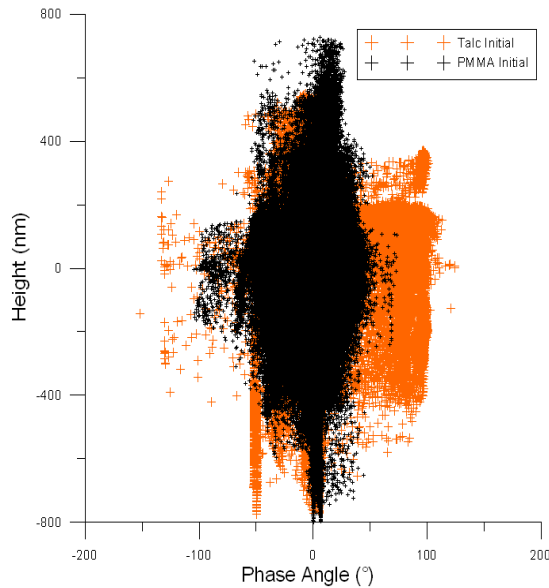


**Figure III.34.** Height vs. Phase Angle Profiles for Initial PMMA and Talc Particles

In figure III.35, the graph of initial PMMA, talc and PMMA coated with 1% and 5% talc particles are shown. It is observed that, the signature of the 1% trial is not very different from the initial PMMA values but when increasing to 5%, the signature gets closer to the signature of the talc. If we compare the signatures of PMMA coated with 1% and 5% talc particles, it can be seen that for PMMA coated with 5% talc particles, there are many more points with high phase angle values which shows us the effect of coating percentage of talc particles.

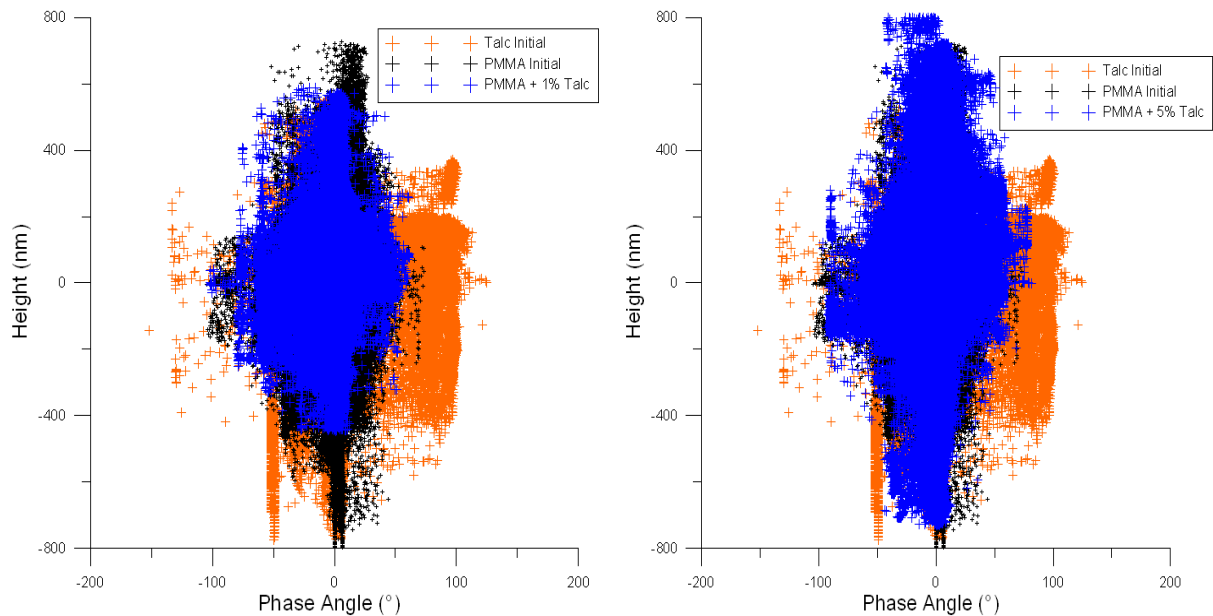


**Figure III.35.** Height vs. Phase Angle Profiles for Initial PMMA, Talc and PMMA Coated with 1% and 5% Talc Particles

As it has been discussed in the literature review, in dry particle coating technology adhesion forces between the particles have very important role. The adhesion forces between the particles were examined by using contact mode of the AFM and the results are presented in the next part.

### C. Measurement of Adhesion Forces Between the Particles

The adhesion forces between the material surface and a fixed particle at the cantilever tip can be measured by using the contact mode of AFM. The piezo scanner moves the substrate on which the adhesion force of the fixed particle is measured in vertical direction. Due to the deflection of the cantilever in relation to the movement of the piezo the adhesion force can be measured. In this study a triangular NP probe (made of silicon nitride) with the spring constant  $k = 0.32$  N/m has been used to determine the adhesion forces between the fixed talc particles at the tip and coated, uncoated PMMA and talc particles.

The accuracy of force measurements depends in part on the sensitivity of the AFM, but also on the accuracy of the value of the spring constant. The value of the spring constant is most sensitive to the variation of the cantilever thickness. The spring constant of an AFM cantilever is usually estimated by the manufacturer, and noted on the documentation that accompanies the probe. Generally, the nominal spring constant values that are supplied by the manufacturer can be in error. In order to calibrate the spring constant of the cantilever probe, thermal tuning has been done. In thermal tuning, the cantilever's mechanical response to thermal noise is measured. This is the cantilever's motion in response to thermal agitation. As it can be seen in the figure III.36, by fitting the frequency spectrum to a Lorentzian line shape, the AFM software arrives at an estimate of the cantilever's spring constant. The spring constant has been found as  $k = 0.51$  N/m by thermal tuning.

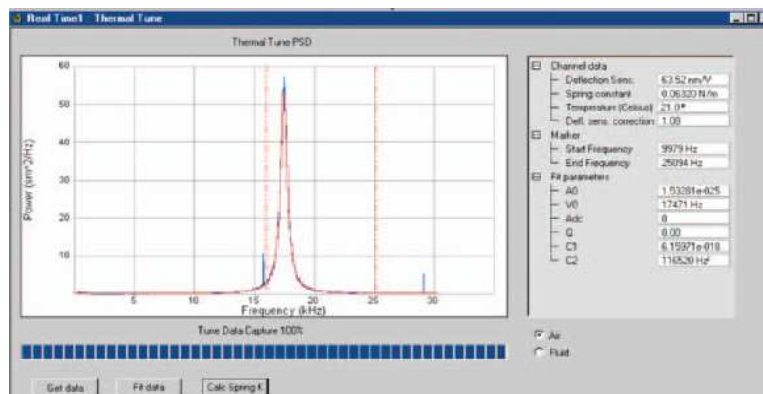


**Figure III.36.** Thermal Tuning of the Cantilever Probe

Adhesion force measurement between a fixed particle at the cantilever tip and a sample has been done previously by other researchers. Aimé et al. (2005) have characterized force–displacement curves on rigid and soft polymer films in controlled atmosphere. The authors point out several causes of misinterpretation of force–displacement curves: the lack of an accurate knowledge of the cantilever stiffness and of the tip size and the difficulty in separating viscoelastic, elastic, and plastic effects. Cleaver et al. (2004) has also studied the adhesion forces by AFM. They studied the influence of relative humidity and applied load on the adhesion forces between individual polystyrene particles. The adhesion forces between the polystyrene particles were found to be between 200 nN–350 nN for 1% relative humidity. Another study has been done for pharmaceutical powders by Louey et al. (2001). They have determined the adhesion forces between a fixed silica particle at the cantilever tip and lactose particles. In their study they used a silicon nitride probe with  $k = 0.42 \text{ N/m}$  and found adhesion force values between 40 nN and 120 nN.

In adhesion force analysis, talc particles have been glued by epoxy resin at the cantilever tip. By using an optical microscopy, the talc particles have been glued at the triangular cantilever tip symmetrically in order to have a representative data. It can be seen in the figure III.37, before and after the adhesion force experiments the cantilever tip has been checked to make us sure that the talc particles stay on the tip after the experiments.

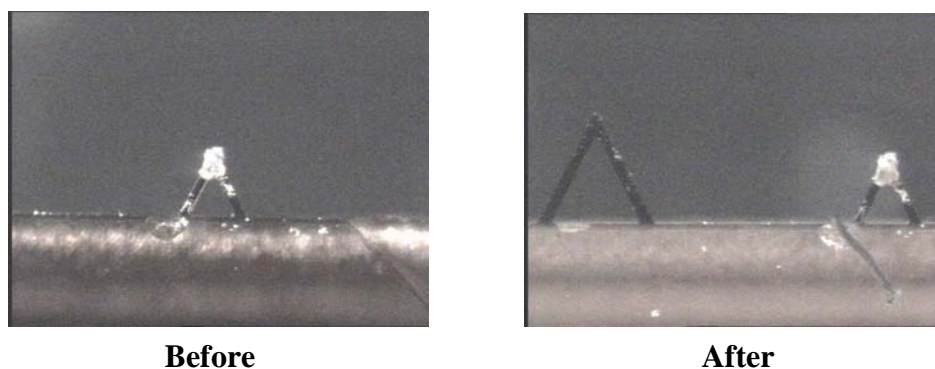


**Figure III.37.** The Talc Particles on the Cantilever Tip Before and After the Analysis

In this study, the adhesion forces between talc particles and the coated and uncoated PMMA particles have been found and also the variation of adhesion forces according to mass percentage of talc in the mixture has been studied. For each powder sample, around 600–700 adhesion force curves have been obtained by analysing minimum 15 particles and 6 different surfaces.

In figure III.38, an example of an adhesion force between talc particles at the cantilever tip and a sample of PMMA, and as the second case the adhesion force between the talc particles at the cantilever tip and a sample of talc can be seen. The force peak between the sample and the cantilever tip corresponds to the pull-off movement of the tip from the sample.

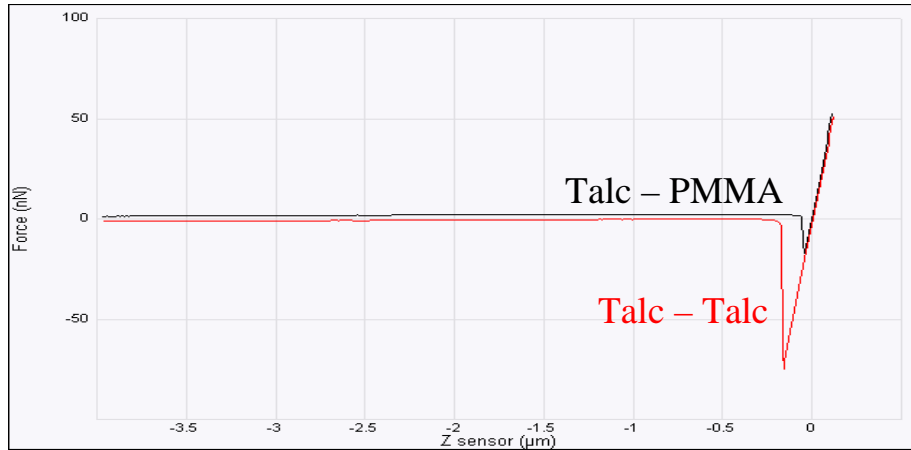


**Figure III.38.** Adhesion Force Curves between Talc-PMMA and Talc-Talc Particles

It has been found that, the adhesion forces between the talc particles vary between 5 nN and 220 nN with an average value of 55 nN. For the case of the adhesion forces between talc and PMMA particles, the data range is between 0 nN and 90 nN with an average value of 13 nN. It has been found that 98% of the adhesion force curves (total 660) between talc and PMMA particles have values between 0 nN and 40 nN and just 2% of adhesion curves have values between 40 nN and 90 nN. According to obtained adhesion force values, it has been observed that the talc particles have much more affinity for adhesion with talc particles than with PMMA particles. (Table III.4). The initial affinity of the particles has also been analysed by theoretically calculating the adhesion energy between the particles. The results can be seen in the Appendix.VI.

**Table III.4.** Adhesion Force Values for Uncoated and Coated Particles

Material	Average Adhesion Force (nN)	Standard Deviation
PMMA	13	14.5
TALC	55	5.2
PMMA + 1% Talc	21	10.6
PMMA + 5% Talc	27	8.3

The adhesion force analysis have been also done for the coated PMMA particles with different mass percentages of talc particles in order to understand the variation of adhesion forces according to different coating percentages. In figure III.39, the distributions of the adhesion forces between the talc particles that are fixed at the cantilever tip and the coated and uncoated PMMA particles are given.

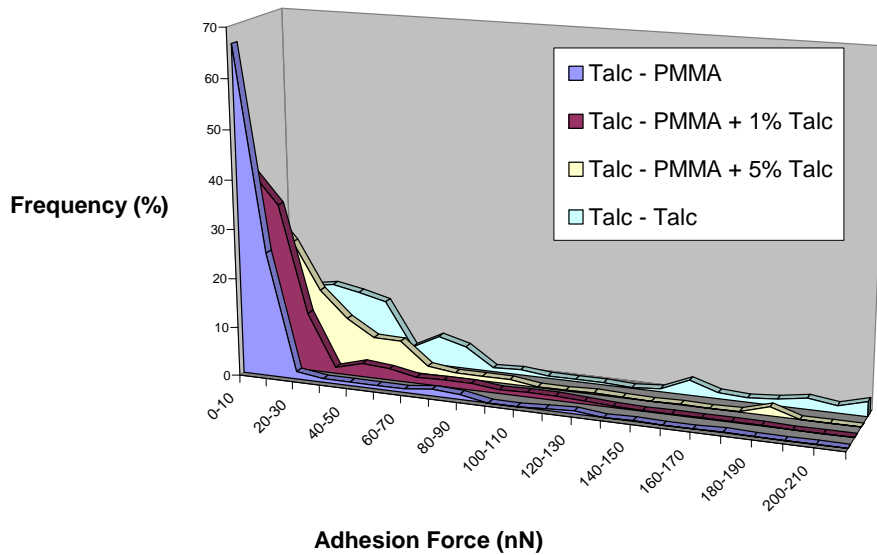


**Figure III.39.** Distributions of Adhesion Forces between Talc and PMMA Coated with 1% & 5% Talc Particles

It can be seen that coating of PMMA particles with talc particles has a certain effect on the distribution of adhesion forces. It was observed that the adhesion force values have a tendency to increase with increasing mass percentage of talc particles in the coating. As it can be seen from the figure III.40, for the initial PMMA particles the 98% of the adhesion forces are between the range of 0–40 nN and this adhesion force frequency decreases to 85% for 1% talc coated PMMA particles and 70% for 5% talc coated PMMA particles. At the end we have obtained average adhesion force values, 21 nN for 1% talc coated PMMA particles and 27 nN for 5% talc coated PMMA particles.

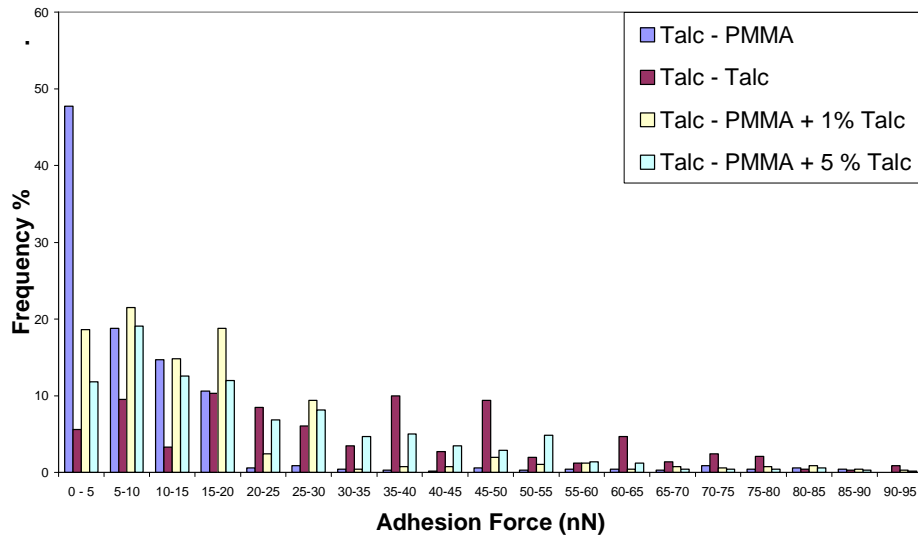


**Figure III.40.** Distributions of Adhesion Forces between Talc and PMMA Coated with 1% & 5% Talc Particles (between 0 – 95 nN)

As it was described in the first chapter, Van der Waals forces have an important role in particle adhesion. The reason of having dry particles and according to particle sizes of PMMA and talc particles, the Van der Waals forces are probably the most dominant adhesion forces for our case. In order to have a rough estimation about the Van der Waals forces between the PMMA and talc particles, Hamaker integration (chapter I) including surface roughness has been used (eqn.I.3).

The average surface roughness values ( $R_a$ ) from AFM measurements have been taken as surface roughness values for the calculations. The Van der Waals forces between the PMMA and Talc particles has been found as 10 nN for 86 nm average surface roughness ( $R_{a,ave}$ ). Compared to the average adhesion force value between the PMMA and talc particles that have been obtained from AFM measurements (13 nN), this rough estimation of Van der Waals forces have a close value.

On the other hand, the AFM results of the particles have been used in order to theoretically calculate the adhesion force by using a model. The model that has been generated by Thomas and Ouabbas (2008) uses the ordered mixture concept. It is assumed that all the particles are spherical and there is monolayer coating as it can be seen in the figure III.41.

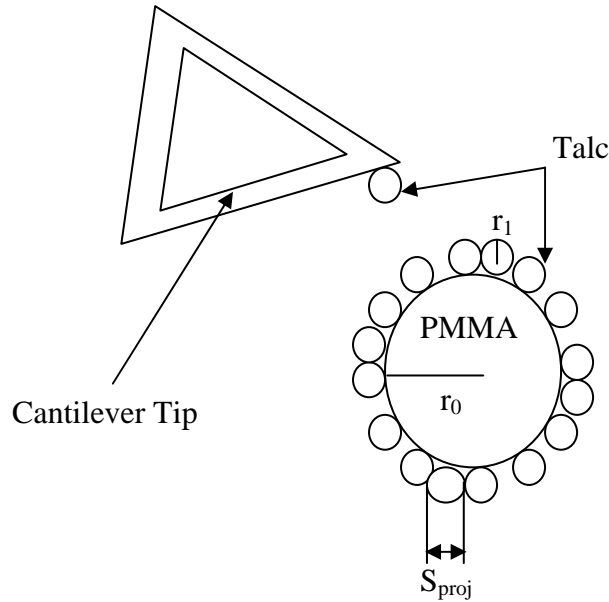


**Figure III.41.** Concept of the Adhesion Force Model

The aim is to calculate the adhesion force values between the fixed talc particles at the cantilever tip and coated PMMA particles according to different mass percentages of talc particles. The total adhesion force between the particles has been described as:

$$F = F_0 S_0 + F_1 S_1 \quad (\text{Eqn.III.2})$$

The equation is based on the idea that, in the AFM adhesion force trials the fixed talc particle at the cantilever may have attraction either with another talc particle on the surface of the PMMA particle or with directly to the PMMA particle. According to this assumption, the total adhesion force has been described as the summation of the force between the PMMA and talc particle ( $F_0$ ) multiplied by the surface fraction of talc free PMMA surface ( $S_0$ ), and the adhesion force between the talc particles ( $F_1$ ) multiplied by the surface fraction of the talc particles on the surface of the PMMA particle ( $S_1$ ).

According to assumptions of monolayer ordered mixture coating (the particles are attached singly on the surface) we have:

$$S_0 + S_1 = 1 \quad (\text{Eqn.III.3})$$

Afterwards by putting equation III.3 inside to equation III.2, it is obtained:

$$F = F_0 + S_1 (F_1 - F_0) \quad (\text{Eqn.III.4})$$

On the other hand, the volume fraction of talc ( $V_1$ ) particles in the mixture has been described according to mass fraction ( $W_1$ ) and the equation III.5 was obtained:

$$V_1 = \frac{W_1}{W_1 + \frac{\rho_1}{\rho_0}(1 - W_1)} \quad (\text{Eqn.III.5})$$

The authors tried to derive the surface fraction of guest particles on the surface of the host particle as a function of volume fraction. The surface fraction of guest particles was taken to be the ratio of projected surface area of guest particles to the total surface area of the host particle;

$$S_1 = \frac{S_{\text{projected}}}{S_{\text{total}}} = \frac{\frac{3}{4} \frac{m_1}{\rho_1 r_1}}{\frac{3}{4} \frac{m_0}{\rho_0 r_0}} = \frac{1}{4} * \frac{m_1}{m_0} * \frac{\rho_0}{\rho_1} * \frac{r_0}{r_1} \quad (\text{Eqn.III.6})$$

Afterwards the surface fraction of talc particles on the surface of the PMMA particle is described as a function of volume fraction as it can be seen in the equation III.7;

$$S_1 = \frac{1}{4} * \frac{r_0}{r_1} * \left( \frac{V_1}{1 - V_1} \right) \quad (\text{Eqn.III.7})$$

At the end the total adhesion force has been described according to adhesion forces between the talc–talc and PMMA–talc particles (they are obtained from AFM measurements) and mass fraction of talc particles;

$$F = F_0 + \left[ (F_1 - F_0) * \frac{1}{4} * \frac{r_0}{r_1} * \frac{W_1}{\frac{\rho_1}{\rho_0}(1 - W_1)} \right] \quad (\text{Eqn.III.8})$$

In our case, the average adhesion force between the PMMA and talc particles ( $F_0$ ) was found to be 13 nN and between the talc particles ( $F_1$ ) it was found to be 55 nN. According the model, the total adhesion force between the talc particles at the cantilever tip and talc coated PMMA particles have been calculated. For 1% talc coated PMMA particles the adhesion force was found to be 15.8 nN and for 5% Talc coated PMMA it was found to be 27.7 nN. It can be seen from figure III.42 that the calculated values are similar to the AFM experimental data (up to 10% coating) when the adhesion force increases linearly. In order to better understand the adhesion force model, 10% and 25% talc coated PMMA particles have also



been analysed. It can be seen that the difference between the calculated and experimental adhesion force values becomes larger for 25% talc coated PMMA particles because the model is only valid for a monolayer coating. The results show that 25% mass percentage of talc particles corresponds to more than a monolayer coating.

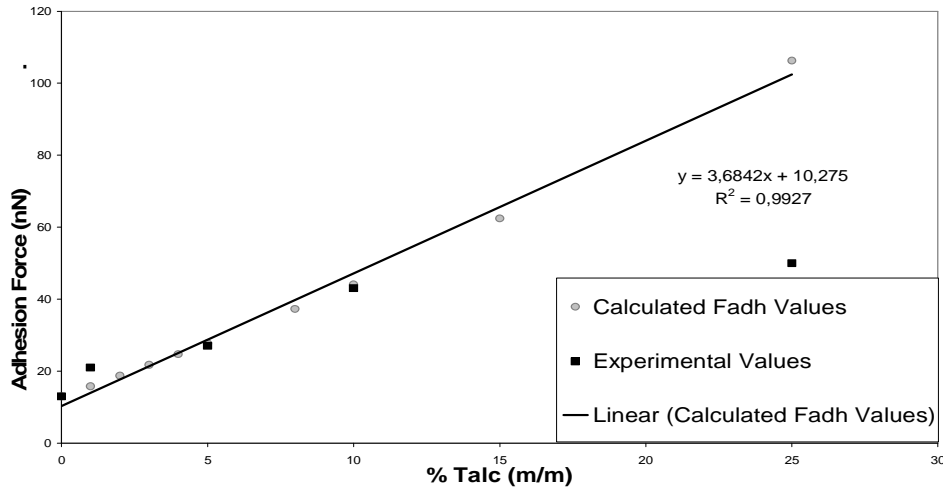


**Figure III.42.** Experimental & Calculated Adhesion Force Values between Talc Coated PMMA Particles and Talc Particles

Figure III.43 shows the evaluation of adhesion force values according to mass percentage of talc in the coating. The 5% talc coating corresponds to the theoretical hexagonal compact monolayer of the particles. But at this level the average force (27 nN) is much less than 55 nN, corresponding to talc–talc interactions. This shows that, there are still low talc–PMMA interaction forces. If we increase the adhesion force linearly with the percentage, we cross the 55 nN level at 26 %. This would correspond to the percentage where the talc headed cantilever probe never comes in contact with PMMA surface, i.e. a continuous coating.

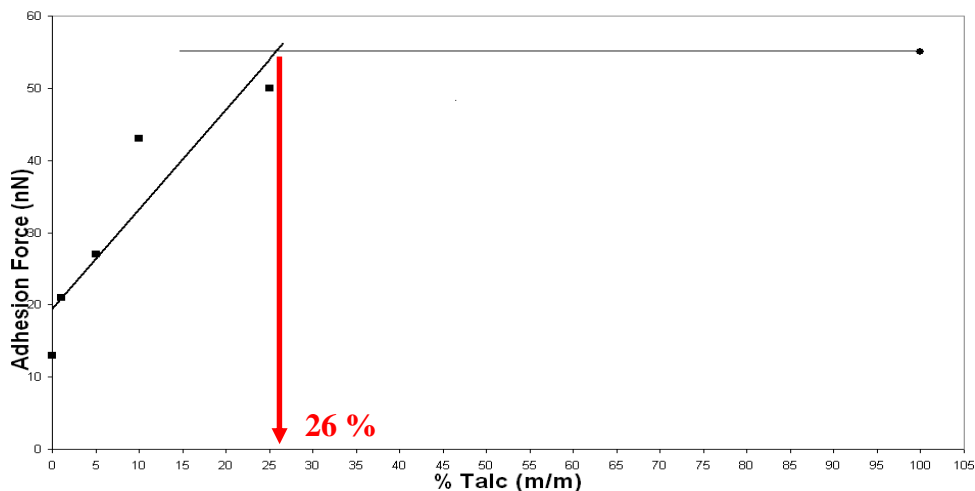


**Figure III.43.** Evaluation of Adhesion Force with Talc Percentage

There is another interesting feature of the adhesion force model. It also allows us to calculate the amount of guest particles on the surface of the host particle according to AFM measured adhesion force values. The results are presented in the next part.

#### 2.4.5. Calculation of Talc Particle Deposition on the Surface of the Coated Particles

This part of the study aims to calculate the amount of talc particles on the surface of the PMMA particles by using the model that has been used for calculation of adhesion forces between the fixed talc particles at the cantilever tip and different mass percentages talc coated PMMA particles.

As described in the early part of the study, the model enables us to calculate adhesion force values according to mass fraction of the guest particles. This means that, it is also possible to calculate the mass fraction of the guest particles on the surface of the host particle if the adhesion forces between the coated particles and the fixed guest particle at the cantilever tip is known.

In the AFM adhesion force measurement for each particle (from 15 different particles), 6 different surfaces have been chosen in order to have representative values as it can be seen in figure III.44. In that case, according to the average adhesion force values which have been obtained from each 6 different surfaces (an average of minimum 100 adhesion force values), the mass fraction of the talc particles for each particle has been calculated.

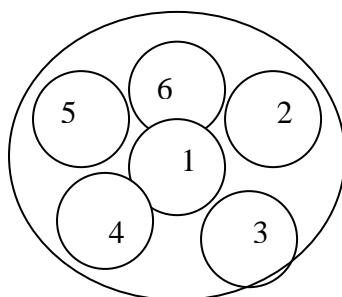


**Figure III.44.** The Different Particle Zones of Adhesion Force Measurements

In equation III.8, the adhesion force between the talc and PMMA ( $F_0$ ) has been taken as 13 nN and the adhesion force between the talc particles ( $F_1$ ) has been taken as 55 nN which are the AFM measured average adhesion force values (table III.4).

Table III.5 shows an example of the calculation of the mass fraction of talc particles according to the adhesion force between the fixed talc particles at the cantilever tip and each chosen surface of a 1% talc coated PMMA particle. According to this example (table III.5), it can be seen that the talc particles are not homogeneously distributed on the PMMA surface. It is observed that at second and sixth surface zones we have much more talc particles compared to other surface zones. The amount of talc particle deposition has been calculated for all 15 different particles of 1% talc coated PMMA particles. It was found that the deposition of talc particles on the surface of the PMMA particles has values between 0.6% and 4% with an average value of 2.3%. The average value is more than the initial mass fraction of the talc particles which is 1%. The possible reason could be the existence of the non analyzed zones on the PMMA particle surface.

**Table III.5.** An Example of Calculated Amount of the Talc Particles on a 1 % Coated PMMA Particle

Surface Number	Measured Average Adhesion Forces (nN)	Real Mass Fraction of Talc Particles
1 <sup>st</sup>	19	2.1 %
2 <sup>nd</sup>	32	6.4 %
3 <sup>rd</sup>	16	1.1 %
4 <sup>th</sup>	15	0.7 %
5 <sup>th</sup>	14	0.4 %
6 <sup>th</sup>	35	7.3 %
<b>Total Surface</b>	21.8	3 %

The amount of talc particle deposition on the PMMA particles has also been calculated for 5% talc coated PMMA particles. In the table III.6, an example of the measured adhesion force for each surface zone of a 5% talc coated PMMA particle and mass fraction of talc particles for can be seen.

**Table III.6.** An Example of Calculated Amount of the Talc Particles on a 5 % Coated PMMA Particle

Surface Number	Measured Average Adhesion Forces (nN)	Real Mass Fraction of Talc Particles
1 <sup>st</sup>	22	3.1 %
2 <sup>nd</sup>	18	1.8 %
3 <sup>rd</sup>	25	4.1 %
4 <sup>th</sup>	36	7.6 %
5 <sup>th</sup>	33	6.7 %
6 <sup>th</sup>	29	5.4 %
<b>Total Surface</b>	27.2	4.8 %

As it can be seen from the table III.6 that the talc particle deposition has been found as 4.8%, which is very close to the initial mass fraction. The same study has also been done for the rest 15 different PMMA coated with 5% talc particles. The talc deposition has been found between 3.9% and 6.5% with an average value of 4.4 %. There is a small difference between the initial mass fraction of talc particles in the system (5%) and the calculated amount of talc deposition on the PMMA surface (average 4.4%). The non analyzed zones of the coated PMMA particles may be one of the reason and also the lost of talc particles after treatment in the Hybridizer has to be considered. On the other hand, agglomeration of talc particles on the surface of the PMMA particle (more than monolayer coating) would prevent the cantilever to reach the PMMA surface and it can be another reason for this result.

#### 2.4.6. Characterization of Coating Strength of the Particles

A Malvern Mastersizer laser diffraction granulometer with dry powder feed has been used to evaluate the strength of the coating on the host particles. In this apparatus powder de-agglomeration is controlled by adjusting the dispersing air pressure. Here we determine at which dispersing air pressure the guest particle start to be liberated from the host particles. The presence of liberated fine particles can be detected by making a comparison between number particle size distributions with different pressures.

In this study, the laser diffraction granulometer has been used with each dispersing air pressure between 0.1 bar and 4.0 bar in order to determine more precisely the liberation pressure for the particles. Afterwards, the pressure of particle liberation, an approach to the

generated kinetic energy of the treatment (according to operating velocity) and mass percentage of talc particles have been compared. The results of hybridizer and basic mixing experiment have also been compared at the end.

### A. Effect of Operating Velocity on Coating Strength of the Particles

The coating strength analysis has been done for each operating velocity for PMMA coated with 1% and 5% talc particles. To be able to understand effect of velocity on the coating strength, PMMA with 1% talc coating results has been chosen to be presented. Analyses have been done for each dispersing pressure. First of all, the results of 0.5, 1.5, 2.5 and 3.5 bar will be presented then the particle liberation pressures for each velocity will be presented more precisely.

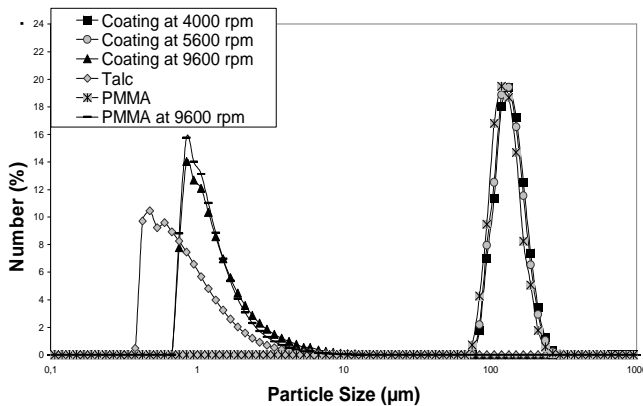


**Figure III.45.** Number Particle Size Distribution of Coated and Uncoated Particles at 0.5 bar Dispersing Pressure

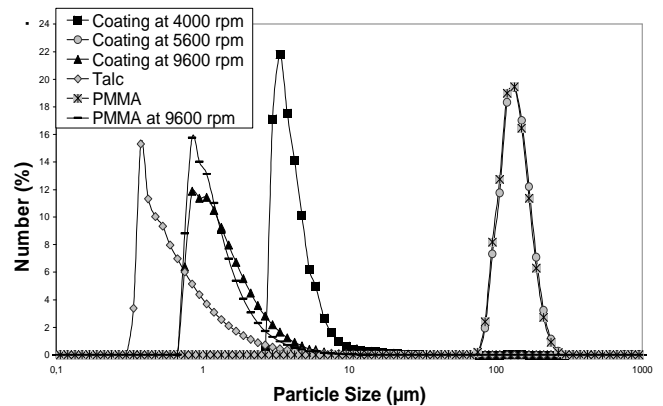


**Figure III.46.** Number Particle Size Distribution of Coated and Uncoated Particles at 1.5 bar Dispersing Pressure

It can be seen in figure III.45, at 0.5 bar, the particle size distributions of coated particles at 4000 rpm and 5600 rpm are similar to initial PMMA particles which are around 145  $\mu\text{m}$ . On the other hand, coated particles at 9600 rpm are smaller in size than those at 4000 and 5600 rpm. At this velocity the particles have also a similar distribution with PMMA treated at the same velocity, it is around 1  $\mu\text{m}$  and the initial talc particles have a number mean particle size distribution at 0.5  $\mu\text{m}$ .

In figure III.46 the particles size distributions of the particles with 1.5 bar dispersing pressure can be seen. It can be observed that there is a shift to the left side for the coated particles at 4000 rpm. It shows a population of particles at around 5  $\mu\text{m}$ . It means that the dispersing pressure for the liberation of the PMMA particles at 4000 rpm is between 0.5 and 1.5 bar. The rest of the particles keep their particle size distributions at that pressure.

At 2.5 bar pressure, it can be seen that for the particles coated at 5600 rpm and 9600 rpm still keep their particle size distributions (fig.III.47). The particle size distribution of coated particles at 4000 rpm have the same fine particle population at 5  $\mu\text{m}$  as it was at 1.5 bar dispersing pressure.

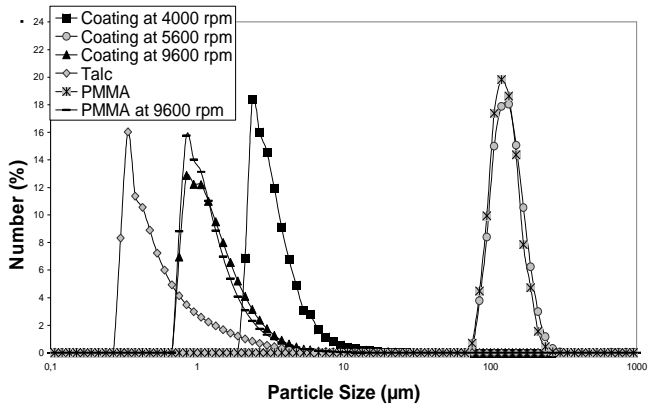


**Figure III.47.** Number Particle Size Distribution of Coated and Uncoated Particles at 2.5 bar Dispersing Pressure

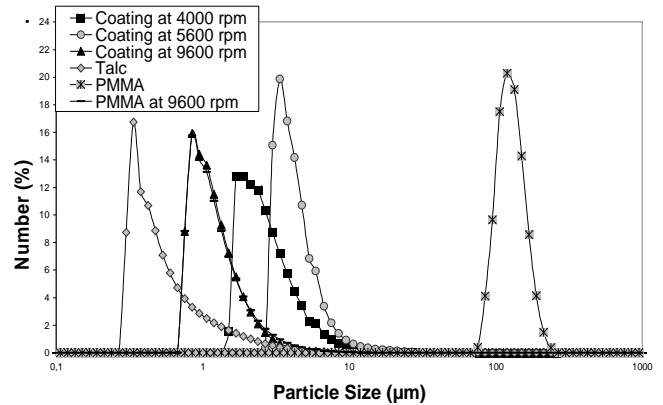


**Figure III.48.** Number Particle Size Distribution of Coated and Uncoated Particles at 3.5 bar Dispersing Pressure

At 3.5 bar pressure, it can be seen that the graph of particles coated at 5600 rpm makes a shift to the left (fig.III.48). It has a fine particle population at around 3  $\mu\text{m}$ . It shows us that the particle liberation pressure is between 2.5 and 3.5 bar for coated particles at 5600 rpm. For particles coated at 9600 rpm, the initial particle size distribution is retained which means even the 3.5 bar pressure is not high enough against the particle interactions between the Talc and PMMA particles. It was also observed that for each operating velocity, the particle size distributions of the coated particles were higher than the particle size distribution of alone talc particles at any pressures. It shows the difficulty of the detachment of talc particles from the surface of the PMMA particles because of the strong interactions between the particles. Figure III.49 gives more precisely the particle liberation pressures for each operating velocity.

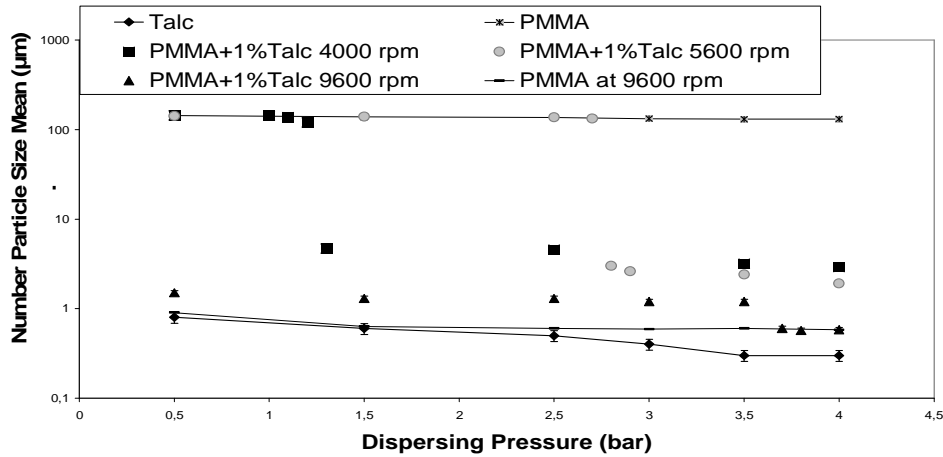


**Figure III.49.** Number Particle Size Mean vs. Dispersing Pressure  
For 1% Coated and Uncoated PMMA Particles

It was observed that the liberation pressure is 1.3 bar for particles treated at 4000 rpm, 2.8 bar for particles treated at 5600 rpm and 3.7 bar for particles treated at 9600rpm. Table III.7 shows the particle liberation pressures and corresponding air velocity in the venturi for 1% talc coated PMMA particle at different operating velocities of the hybridizer. It can be seen that the dispersing pressure for particle liberation increases with increasing rotational velocity. This is probably related to the energy that the system gives to the powder sample. However, it should be remembered that the change in the particle size distribution could be either because of particle detachment or also fragmentation of particles or agglomerates. Especially at 9600 rpm treatments most of the particles are broken and the difference in the particle size distribution could be reason of detachment of talc particles and also breakage of particles.

**Table III.7.** Dispersing Pressures and Air Velocities for Particle Detachment for 1% Talc Coated PMMA Particles in Hybridizer

Material	Dispersing Air Pressure	Air Velocity
PMMA + 1% Talc at 4000 rpm	1.3 bar	64 m/s
PMMA + 1% Talc at 5600 rpm	2.8 bar	107 m/s
PMMA + 1% Talc at 9600 rpm	3.7 bar	122 m/s

### B. Effect of Mass Percentage of Talc on Coating Strength of the Particles

In this part of the study, it is aimed to study the effect of the mass percentage of the talc particles on the coating strength. The PMMA particles have been treated with 1% and 5% Talc particles at 4000, 5600 and 9600 rpm for 6 minutes.

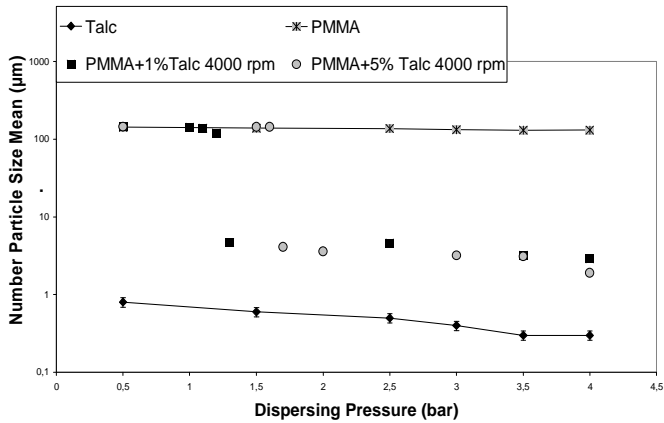


**Figure III.50.** Number Particle Size Mean vs. Dispersing Pressure for 1% and 5% Talc Coated and Uncoated Particles at 4000 rpm

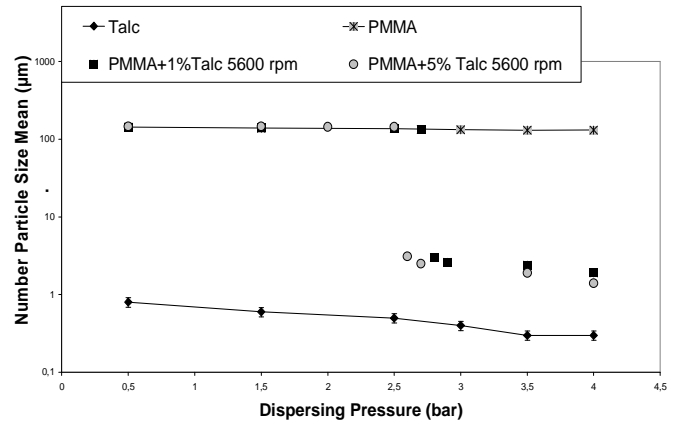


**Figure III.51.** Number Particle Size Mean vs. Dispersing Pressure for 1% and 5% Talc Coated and Uncoated Particles at 5600 rpm

The particle size distributions of particles, that are treated at 4000 and 5600 rpm in the hybridizer, according to dispersing pressures can be seen in the figure III.50 and III.51. It is observed that for 4000 rpm treatments, 1% Talc coated particles start to have particle detachment (or fragmentation) at 1.3 bar dispersing pressure and for 5% coated particles, it is at 1.7 bar. On the other hand, for 5600 rpm treatments, 1% Talc coated particles the particle liberation pressure is 2.8 bar but contrarily to the results of 4000 rpm, for 5% Talc coated particles the liberation pressure is lower than 1% which is 2.6 bar. Figure III.52 shows the number particle size distributions of 1% and 5% talc coated PMMA particles at 9600 rpm in hybridizer. It can be seen that the particle liberation pressure is 3.7 bar for 1% talc coating and 3.4 bar for 5% talc coated PMMA particles. According to results of coated particles in the hybridizer (table III.8), it is concluded that there is no observed effect of mass percentage of talc on the coating strength of the particles that are treated in the hybridizer.



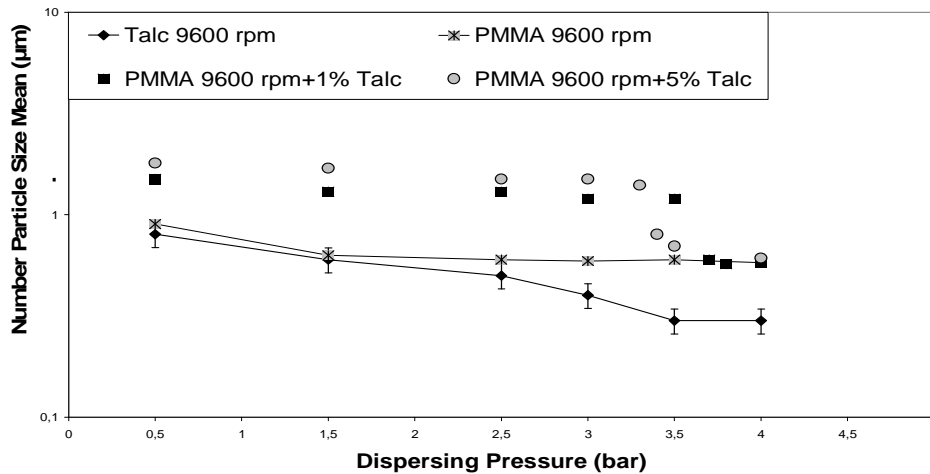


**Figure III.52.** Number Particle Size Mean vs. Dispersing Pressure for 1% and 5% Talc Coated and Uncoated Particles at 9600 rpm

**Table III.8.** Dispersing Pressures and Air Velocities for Particle Detachment for 1% and 5% Talc Coated PMMA Particles in Hybridizer

Material	Dispersing Air Pressure	Air Velocity
PMMA + 1% Talc at 4000 rpm	1.3 bar	64 m/s
PMMA + 1% Talc at 5600 rpm	2.8 bar	107 m/s
PMMA + 1% Talc at 9600 rpm	3.7 bar	122 m/s
PMMA + 5% Talc at 4000 rpm	1.7 bar	77 m/s
PMMA + 5% Talc at 5600 rpm	2.6 bar	103 m/s
PMMA + 5% Talc at 9600 rpm	3.4 bar	118 m/s

In basic mixing trials, it is observed that the particle liberation pressure for PMMA treated at 4000 rpm with 1% talc coating is 0.9 bar and for 5% talc coating the particle liberation pressure is 0.8 bar (Appendix III). For PMMA at 5600 rpm with 1% talc the particle liberation pressure is 1.1 bar and for 5% Talc coating the liberation pressure decreases to 0.7 bar. Also for PMMA at 9600 rpm with 1% talc coating, the particles start to detach (or break up) at 1.9 bar and for 5% talc coating the particle liberation pressure is 1.3 bar. According to these results, for the particles that are treated by basic mixing method, the particle liberation pressure decreases with increasing talc percentage in the coating (Appendix.III).

### C. Effect of Equipment on Coating Strength of the Particles

It was observed that there is a relation between the coating strength of the particles and the operating velocity of the hybridizer in the early part of the study. In this part, we compare the coating strength of the particles that are treated by hybridizer and by basic mixing method. We are interested to compare hybridizer and basic mixing according to a simple approach of the kinetic energy (per mass) that they give to the system. In that case, for the hybridizer the kinetic energy per mass has been simply calculated according to rotational velocity of the blades. The linear velocity ( $V$ ) (m/s) of hybridizer blades was calculated by using equation III.9. Where,  $n$  corresponds to rotational velocity (tours/second) of the rotor.

$$V(m/s) = 2\pi rn \quad (\text{Eqn.III.9})$$

The linear velocities of the hybridizer trials has been found as; 25 m/s (for 4000 rpm), 35 m/s (for 5600 rpm) and 60 m/s (for 9600 rpm). For basic mixing 1 m/s has been assumed as the shaking velocity and the kinetic energy per mass has been calculated according to this value. Afterwards kinetic energy per mass values were calculated by using equation III.10 according to the linear velocities.

$$E_k = \frac{1}{2}V^2 \quad (\text{Eqn.III.10})$$

The particle liberation pressure and the corresponding air velocity according to the kinetic energy per mass that the equipments give to the powder sample can be seen in the figure III.53 and III.54.

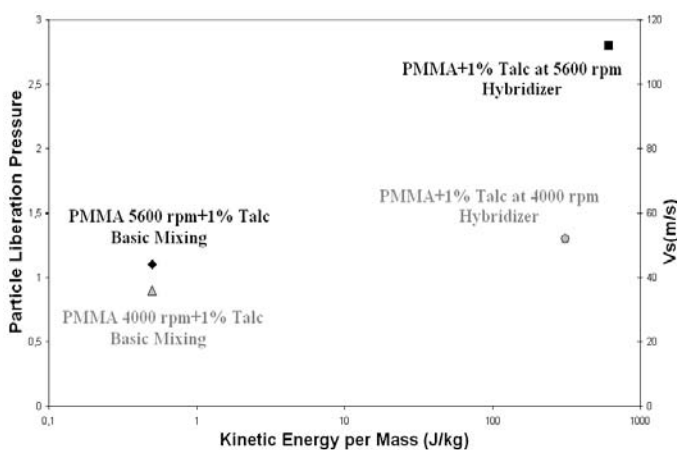


**Figure III.53.** Effect of Equipment on Particle Liberation Pressure for 1% Coated Particles by Hybridizer and Basic Mixing Method

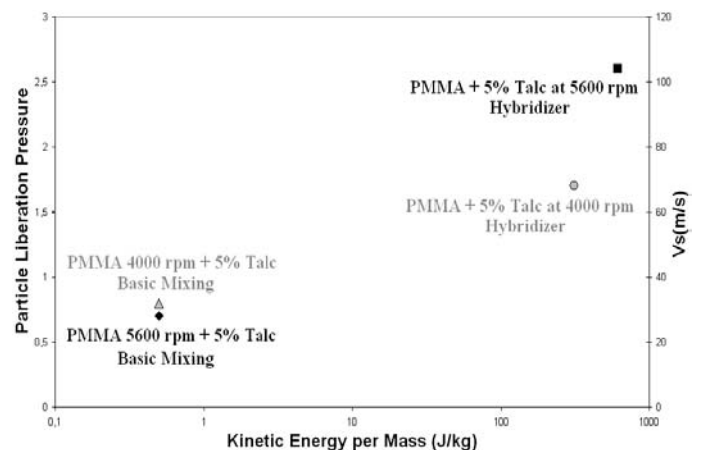


**Figure III.54.** Effect of Equipment on Particle Liberation Pressure for 5% Coated Particles by Hybridizer and Basic Mixing Method

It was observed that the particle liberation pressure increases almost 2 times whenever the assumed kinetic energy generated by hybridizer also increases 2 times. This result shows there is a proportional relation between the particle liberation pressure and the supplied kinetic energy of the system. It is also observed that the particle liberation pressures of the particles that have been treated by hybridizer are higher than basic mixed particles for each case. It is probably related to the mechanical force that the equipment applies to the particles. On the other hand, it should be remembered that there are many factors (elastic properties, surface roughness, surface energy etc.) that affect the mechanical coating strength.

As it was observed from the ESEM images, the talc particles are attached on the surface of the PMMA particles for basic mixing trials but on the other hand talc particles are more embedded on the surface of the PMMA particles for hybridizer trials because of the mechanical forces.

It can be seen from figure III.55, similar results have also been obtained for the particles that are treated at 9600 rpm by hybridizer and PMMA initially treated 9600 rpm and coated with 1% and 5% Talc particles by basic mixing method. In addition, we can see that the particle liberation pressure ratio between the particles from hybridizer and basic mixing increases when the operating velocity gets higher.

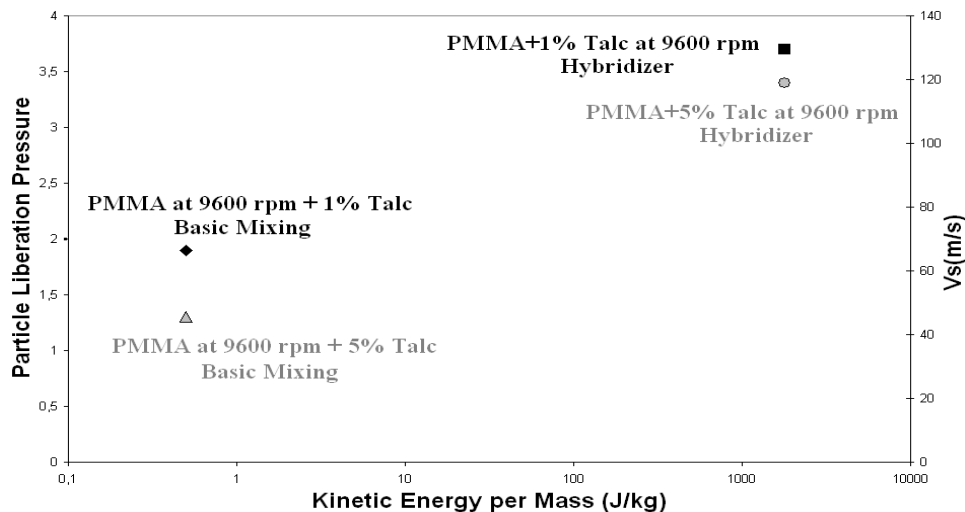


**Figure III.55.** Effect of Equipment on Particle Liberation Pressure for Coated Particles by Hybridizer at 9600 rpm and Basic Mixing Method

### 2.4.7. Characterization of Flowability Properties of the Particles

The flowability properties of the uncoated and coated PMMA particles have been determined by Erweka Tapped Density Tester and Freeman Technology Powder Rheometer (FT4). The methodologies of the flowability analysis have been explained in the chapter II (material and methods). The apparent density is the density that includes the air gaps inside the powder sample. The tapped density has been found by making 600 strokes to the powder samples inside graduated cylinder.

The modification of flowability properties PMMA powders has been analysed according to different operating velocities of hybridizer and different mass percentages of talc particles in the coating. At the end we have also compared the results of powders that have been treated in hybridizer and by basic mixing method.

#### A. Effect of Operating Velocity on Flowability Properties of the Particles

The flowability properties of particles has been analysed for each operating velocity of PMMA coated with 1% and 5% talc particles. To be able to understand effect of velocity on modification of the flowability properties, PMMA with 1% talc coating results has been chosen to be presented. In the figure III.56, the variation of the tapped densities for uncoated and 1% talc coated PMMA particles can be seen.

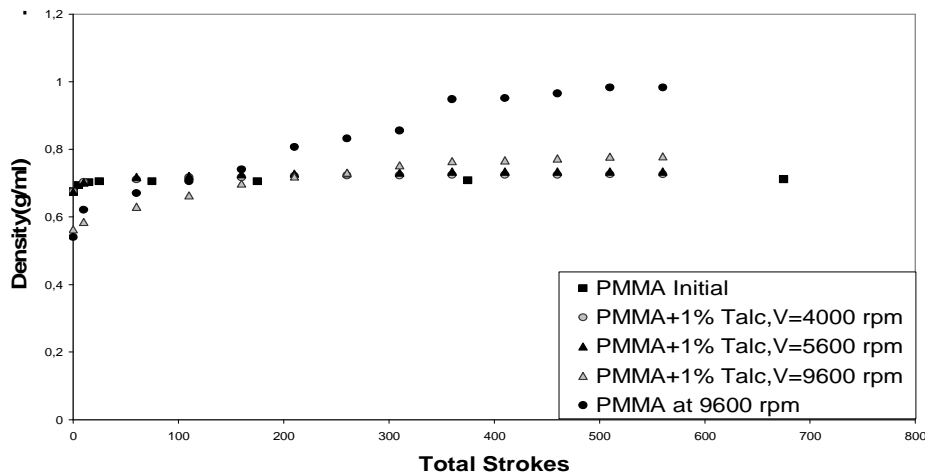


**Figure III.56.** Evaluation of Tapped Densities of PMMA Particles Before and After Coating with Talc According to Different Operating Velocities of Hybridizer

The PMMA particles have a good flowability ( $H_T = 1.01$   $C_T = 0.99$ ) initially. According to the graph, it can be observed that the dry coated PMMA particles by talc have much better

flowability properties than ground PMMA particles. Also it can be observed that the high operating velocities of the hybridizer decrease flowability of the particles due to the particle breakage that causes increase in the contact surface of the particles. The results of Hausner Ratio and Carr Index for each sample can be seen in the table III.9.

**Table III.9.** Carr Index and Hausner Ratio for Uncoated and 1% Coated PMMA Particles

Materials	Carr Index (%)	Flowability	Hausner Ratio
Initial PMMA	0.99 ± 0.02	Excellent	1.01 ± 0.02
PMMA at 4000 rpm	16.03 ± 0.04	Good	1.19 ± 0.04
PMMA at 5600 rpm	18.72 ± 0.05	Mediocre	1.23 ± 0.05
PMMA at 9600 rpm	35.81 ± 0.05	Very Bad	1.56 ± 0.05
PMMA+1% Talc at 4000 rpm	3.04 ± 0.03	Excellent	1.03 ± 0.03
PMMA+1% Talc at 5600 rpm	8.20 ± 0.02	Excellent	1.09 ± 0.02
PMMA+1% Talc at 9600 rpm	27.82 ± 0.04	Bad	1.39 ± 0.04

Figure III.57 and III.58 show the results of FT4 experiments. It can be seen that we have homogeneous mixture at the end of conditioning step for each powder sample.

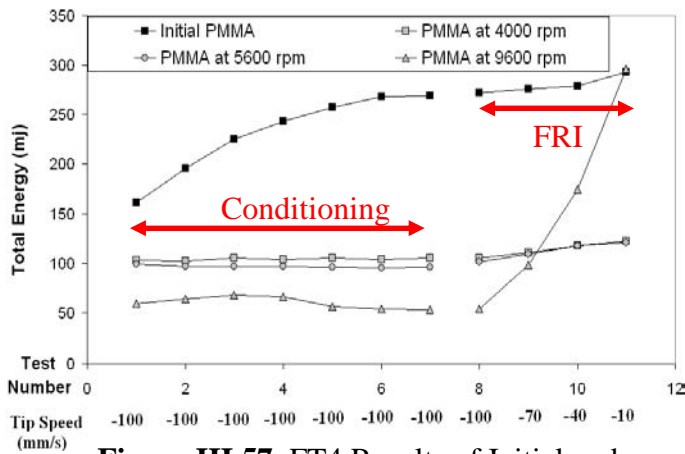


**Figure III.57.** FT4 Results of Initial and Treated PMMA Particles in Hybridizer

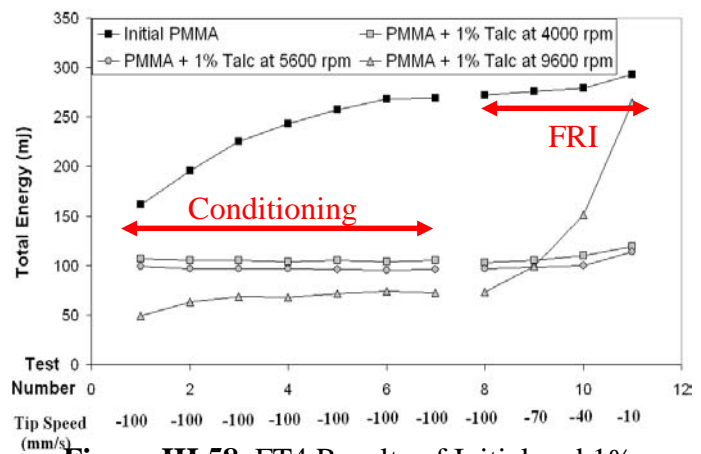


**Figure III.58.** FT4 Results of Initial and 1% Talc Coated PMMA Particles in Hybridizer

The results of the Freeman Technology Powder Tester (FT4) can be seen in the table III.10. The flowability data is inversely proportional with Flow Rate Index data. It is observed that the results of uncoated and coated PMMA particles by FT4 give good correlations with the results of the tapped density tester. It can be observed that the treated PMMA particles in

Hybridizer have a lower flowability than the dry coated particles, at each operating velocity. (4000 rpm, 5600 rpm and 9600 rpm).

**Table III.10.** Evaluation of Flowability of Uncoated and 1% Coated PMMA Particles by FT4

<b>Materials</b>	<b>8<sup>th</sup> Cycle (mj)</b>	<b>11<sup>th</sup> Cycle (mj)</b>	<b>FRI</b>
<b>Initial PMMA</b>	273 ± 0.03	293 ± 0.03	<b>1.10 ± 0.03</b>
<b>PMMA at 4000 rpm</b>	105 ± 0.05	122 ± 0.05	<b>1.16 ± 0.05</b>
<b>PMMA at 5600 rpm</b>	101 ± 0.05	121 ± 0.05	<b>1.20 ± 0.05</b>
<b>PMMA at 9600 rpm</b>	54 ± 0.08	296 ± 0.08	<b>5.48 ± 0.08</b>
<b>PMMA+1% Talc at 4000 rpm</b>	108 ± 0.03	119 ± 0.03	<b>1.08 ± 0.03</b>
<b>PMMA+1% Talc at 5600 rpm</b>	99 ± 0.05	114 ± 0.05	<b>1.15 ± 0.05</b>
<b>PMMA+1% Talc at 9600 rpm</b>	60 ± 0.09	263 ± 0.09	<b>4.39 ± 0.09</b>

The FRI data also shows that the dry coated PMMA particles treated at 9600 rpm have very bad flowability. The reason for this can be attributed to the breakage of the large PMMA particle into fines.

#### **B. Effect of Mass Percentage of Talc on Flowability Properties of the Particles**

This part of the study aims to study the effect of the mass percentage of talc particles on the flowability properties of the coated particles. The results of the tapped and apparent densities of the 1% and 5% talc coated PMMA particles at 4000, 5600 and 9600 rpm operating velocities and for 6 minutes operating time can be seen in the figure III.59.

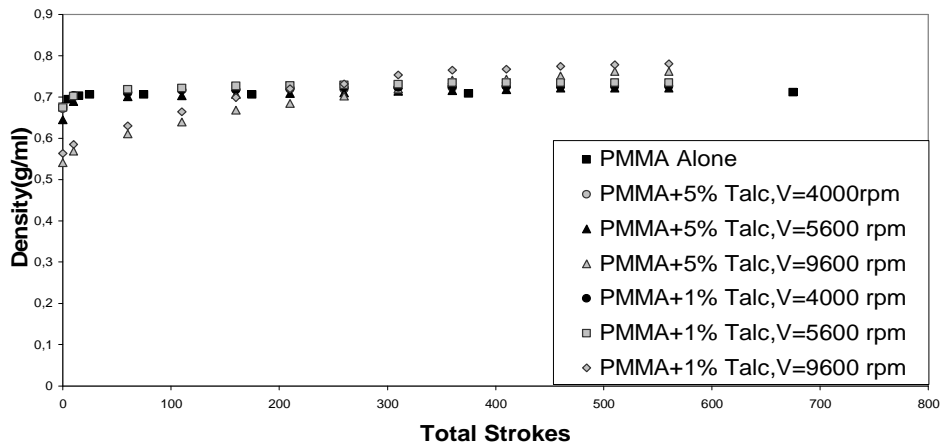


**Figure III.59.** Evaluation of Flowability of PMMA Particles Before and After Coating with 1% and 5% Talc for Each Operating Velocity

According to the graph, it hasn't been seen a significant difference between the 1% and 5% talc coated PMMA particles at any velocities. It can be seen in the table III.11, the Hausner Ratio and Carr Index values of 1% and 5% talc coated PMMA particles are similar.

**Table III.11.** Carr Index and Hausner Ratio for 1% and 5% Talc Coated PMMA Particles

Materials	Carr Index (%)	Flowability	Hausner Ratio
PMMA+1% Talc at 4000 rpm	$3.04 \pm 0.03$	Excellent	$1.03 \pm 0.03$
PMMA+1% Talc at 5600 rpm	$8.20 \pm 0.02$	Excellent	$1.09 \pm 0.02$
PMMA+1% Talc at 9600 rpm	$27.82 \pm 0.04$	Bad	$1.39 \pm 0.04$
PMMA+5% Talc at 4000 rpm	$3.02 \pm 0.03$	Excellent	$1.03 \pm 0.03$
PMMA+5% Talc at 5600 rpm	$8.63 \pm 0.03$	Excellent	$1.09 \pm 0.03$
PMMA+5% Talc at 9600 rpm	$29.01 \pm 0.04$	Bad	$1.41 \pm 0.04$

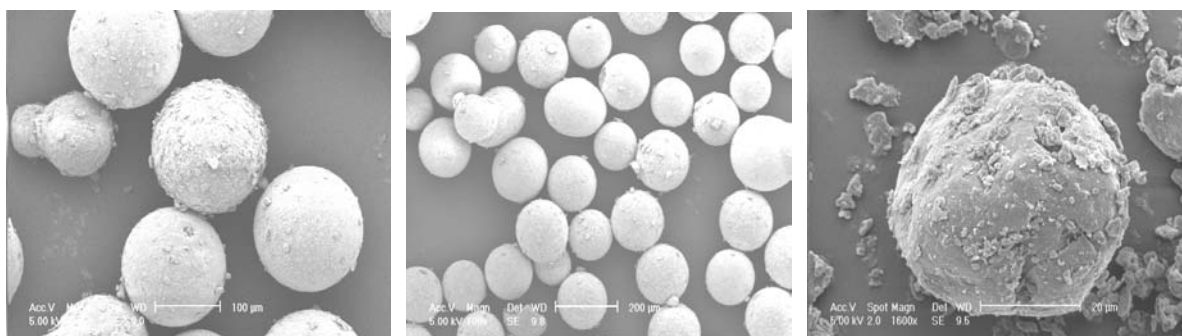
The results of FT4 also shows that for 4000 and 5600 rpm treatments there is no difference between 1% and 5% coatings but contrarily, for 9600 rpm treatments it has been observed that there is a certain effect of coating percentage on the flowability properties of the particles. The results of FT4 can be seen in the table III.12.

**Table III.12.** Evaluation of Flowability of 1% and 5% Coated PMMA Particles by FT4

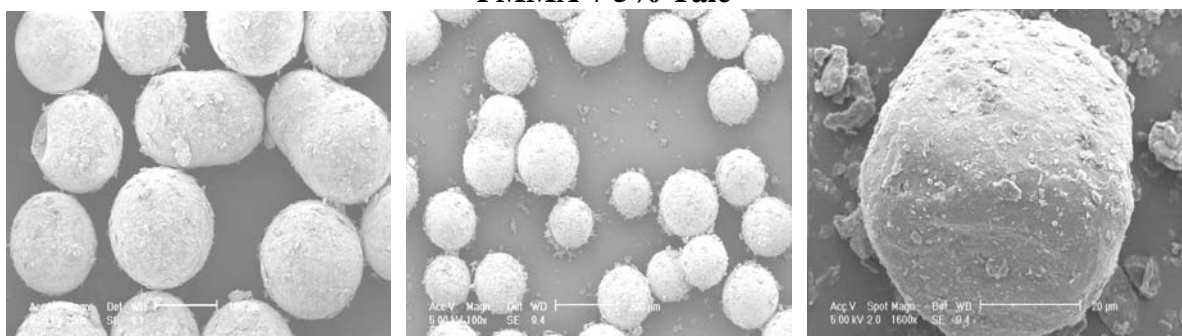
Materials	8 <sup>th</sup> Cycle (mj)	11 <sup>th</sup> Cycle (mj)	FRI
<b>PMMA+1% Talc at 4000 rpm</b>	108 ± 0.03	119 ± 0.03	<b>1.08 ± 0.03</b>
<b>PMMA+1% Talc at 5600 rpm</b>	99 ± 0.05	114 ± 0.05	<b>1.15 ± 0.05</b>
<b>PMMA+1% Talc at 9600 rpm</b>	60 ± 0.09	263 ± 0.09	<b>4.39 ± 0.09</b>
<b>PMMA+5% Talc at 4000 rpm</b>	100 ± 0.04	109 ± 0.04	<b>1.09 ± 0.04</b>
<b>PMMA+5% Talc at 5600 rpm</b>	119 ± 0.03	135 ± 0.03	<b>1.13 ± 0.03</b>
<b>PMMA+5% Talc at 9600 rpm</b>	71 ± 0.08	287 ± 0.08	<b>4.04 ± 0.08</b>

It can be seen that for 9600 rpm treatments, 5% talc coated PMMA particles have better flowability than 1% talc coated particles. In order to verify the effect of FT4 analysis on the coating of the PMMA particles, the coated PMMA particles have been reanalysed visually by ESEM after the analysis with the FT4. The results can be seen in the figure III.60.

#### PMMA + 1% Talc



#### PMMA + 5% Talc



(a) 4000 rpm

(b) 5600 rpm

(c) 9600 rpm

**Figure III.60.** Surface Morphology of PMMA Particles Coated by 1% and 5% Talc

Particles in the Hybridizer after Analysing by FT4



It has been seen that the talc particles are still on the surface of the PMMA particles after analysing with FT4. The coating strength of the particles has been also reanalysed after the measurements with FT4 and no difference is seen before and after analysing with FT4 for the liberation pressures of the particles.

In order to understand the effect of the dry coating equipment on the flowability properties of the particles, the results have been compared with the results of the particles that have been treated by basic mixing method.

### C. Effect of Equipment on Flowability Properties of the Particles

In this part of the study, we compare the flowability properties of the particles that were treated by hybridizer and by basic mixing method. The FT4 analysis of uncoated and 5% talc coated PMMA particles can be seen in the table III.13.

**Table III.13.** Effect of Equipment on the Flowability Properties of Coated PMMA Particles

<b>Materials</b>	<b>8<sup>th</sup> Cycle (mj)</b>	<b>11<sup>th</sup> Cycle (mj)</b>	<b>FRI</b>
<b>PMMA at 4000 rpm</b>	105 ± 0.05	122 ± 0.05	<b>1.16 ± 0.05</b>
<b>PMMA at 5600 rpm</b>	101 ± 0.05	121 ± 0.05	<b>1.20 ± 0.05</b>
<b>PMMA at 9600 rpm</b>	54 ± 0.08	296 ± 0.08	<b>5.48 ± 0.08</b>
<b>PMMA+5% Talc at 4000 rpm</b>	100 ± 0.04	109 ± 0.04	<b>1.09 ± 0.04</b>
<b>PMMA+5% Talc at 5600 rpm</b>	119 ± 0.03	135 ± 0.03	<b>1.13 ± 0.03</b>
<b>PMMA+5% Talc at 9600 rpm</b>	71 ± 0.08	287 ± 0.08	<b>4.04 ± 0.08</b>
<b>PMMA at 4000 rpm + 5% Talc Basic Mixing</b>	102 ± 0.03	115 ± 0.03	<b>1.13 ± 0.03</b>
<b>PMMA at 5600 rpm + 5% Talc Basic Mixing</b>	112 ± 0.04	129 ± 0.04	<b>1.15 ± 0.04</b>
<b>PMMA at 9600 rpm + 5% Talc Basic Mixing</b>	60 ± 0.08	291 ± 0.08	<b>4.88 ± 0.08</b>

It is observed that for each operating velocity, the particles that were coated by hybridizer have better flowability than the particles that were coated by basic mixing method. The possible reason could be that the talc particles are more de-agglomerated and better dispersed on the surface of the PMMA particles in hybridizer trials because of the applied mechanical

forces on the particles. On the other hand, in basic mixing trials the talc particles may rest as agglomerates and not well dispersed on the surface of the PMMA particles.

## **2.5. Conclusions**

The PMMA–talc model couple has been coated successfully by dry coating method in hybridizer and also by basic mixing technique. The effect of the equipment, the operating conditions and the mass percentage of guest particles on the end–use properties of the particles has been studied. A preliminary study was performed in order to determine the optimum operating conditions of Hybridizer for PMMA and talc particles and their fragmentation behaviour. In the preliminary study, the effect of different operating velocities of hybridizer on the particle fragmentation and amount of final powder recovery has been studied for PMMA and talc particles separately. Afterwards, the particles were dry coated with different operating conditions and mass percentages of talc particles.

Several characterisation methods were used to study the physico–chemical properties of the coated particles. Visualisation before and after coating was performed with an Environmental Scanning Electron Microscopy (ESEM), enables us to qualitatively evaluate guest particle deposition on the host particles. It was observed that, for the particles that are processed in hybridizer or generated by the basic mixing method, there is discrete coating of talc particles on the surface of the PMMA particles.

The topographical analysis of the uncoated and coated particles has been done by tapping mode of the AFM. It was observed that the surface roughness is more evident and irregular for Talc particles compared to PMMA particles.

It was seen that the coating of PMMA particles with different mass percentages of talc particles had certain effects on the surface roughness of the PMMA particles. The obtained surface roughness and phase angle values show that the topography of the surface of the PMMA particles has been modified because of coating with talc particles.

Phase angle analysis of tapping mode enables us to distinguish the talc particles deposition on the surface of the PMMA particles. It was observed that the height, phase angle and amplitude data are similar for initial PMMA particles. It was seen that the difference in the phase angle data is due to the surface roughness of the PMMA particles and varies between  $-100^{\circ}$  and  $40^{\circ}$ . On the other hand, it has been observed that the phase angle data of talc particles are more evident than PMMA particles, which is probably due to the surface roughness and also the difference in material surface characteristics. It is known that the talc particles are much softer

than PMMA particles. It was found that the phase angle values go up to  $110^\circ$  for initial talc particles.

The difference in the topographical characteristics of the initial PMMA and talc powders enable us to understand the existence of talc particles on the surface of the PMMA particles by comparing the results of height, phase angle and amplitude for 1% and 5% talc coated PMMA particles. The analyses have been done on many different sections of coated particles. For each section, two different phase angle data ranges at stable surface height prove us the existence of talc particles on the surface of the PMMA particles. In a novel approach, the height and phase angle images have been analysed numerically and the presence of talc particles on the surface and the effect of coating percentage was seen. The results of topographical analysis by AFM also corresponded to the visual observation and showed that discrete coating has been obtained for both 1% and 5% talc coated PMMA particles.

The adhesion forces between talc particles that are fixed at the cantilever tip and coated and uncoated PMMA particles has been measured by using the contact mode of AFM. The results show that the adhesion forces between the talc particles are higher than the adhesion forces between PMMA and talc particles. The effect of mass percentage of talc particles on the evaluation of adhesion forces between the particles has been also studied. It was observed that the adhesion force values have a tendency to increase with increasing mass percentage of talc particles in the coating.

The adhesion force analyses have shown us the effect of the amount of coating on the adhesion force between the particles. It was observed that the adhesion forces increase with increasing mass percentage of talc particles. The reason is the adhesion force between the talc particles is much higher than the adhesion force between the talc and PMMA particles. On the other hand, it should be also considered that in interpreting the results of an AFM experiment is not always straightforward. The absolute distance between the surfaces is usually not known exactly, and neither is the tip geometry. In addition, the fine tips and the surfaces often deform elastically or plastically during a measurement, which further complicates interpretation of the results.

Talc deposition on the surface of the PMMA particles has also been examined by using the adhesion force model. The results show that the talc particles are not homogeneously distributed on the surface of the PMMA particles. At 1% talc coated PMMA particles the calculated talc deposition have been found higher than 1% (2.3%), but for 5% coating we

have calculated a very close value (4.4%). The non analyzed zones of the coated PMMA particles may be one of the reason and also the loss talc particles after treatment in the hybridizer has to be considered. On the other hand agglomeration of talc particles on the surface of the PMMA particle (more than monolayer coating) can be another reason for these results.

The coating strength of the composite particles has been studied by using a Malvern Mastersizer laser diffraction granulometer. We have determined at which dispersing air pressure, the guest particle start to be liberated from the host particles. The effect of operating velocity and mass percentage of talc particles on coating strength was studied. In order to understand the effect of equipment on coating strength of the particles, the coating strength results of the particles that have been treated by hybridizer also compared with the particles that were generated by basic mixing method. It was seen that the dispersing pressure for particle liberation increases with increasing rotational velocity which is probably related to the energy that the system gives to the powder sample. On the other hand, an effect of mass percentage of talc particles on the coating strength of the particles that are treated in the hybridizer has not been observed. At 4000 rpm treatments, the coating strength increases with increasing mass percentage of talc particles but contrary to that result, at 5600 rpm treatments the particle liberation pressure is 2.8 bar for 1% talc coated particles and that value decreases to 1.6 bar for 5% talc coated particles. In addition concerning the particles that are treated in hybridizer, it was seen that the coating strength of the particles is inversely proportional to the mass percentage of talc particles for the particles that are generated by basic mixing method. On the other hand, it was observed that the coating strength of the particles is much stronger for the particles that are treated in the hybridizer than for those generated by the basic mixing method. This is probably related to the kinetic energy that the equipment applies to the particles. On the other hand, when analysing the granulometric results it should be considered that the difference in the particle size distributions of the particles with different dispersing pressure could be either detachment of guest particles or also particle fragmentation.

In order to complete the visual analysis by ESEM, an Atomic Force Microscope (AFM) has been used to study guest particle deposition on host particles and to analyze surface morphology of the particles (surface roughness, phase difference etc.). The evaluation of adhesion forces between particles has also been studied.

The flowability properties of the uncoated and coated PMMA particles have been determined by using a tapped density tester and Freeman Technology Powder Rheometer (FT4). The effects of operating velocity, coating percentage and equipment on the flowability properties of the powders have been studied. It was seen that the dry coated PMMA particles by talc have better flowability properties than grinded PMMA particles. It was seen that that the high operational speeds of the hybridizer decrease flowability of the particles due to particle breakage which causes increase in the contact surface of the particles. No effects of coating percentage have been observed on the flowability properties of the powders for low operating velocity treatments but on the other hand, for 9600 rpm treatments, it was seen that the 5% talc coated particles have better flowability than 1% talc coated particles. The results of tapped and apparent densities and FT4 show us that for each operating velocity, the particles that were coated by hybridizer have better flowability than the particles that were coated by the basic mixing method. The applied mechanical force on the particles by the hybridizer causes de-agglomeration and good dispersion of talc particles on the surface of PMMA particles which is not the case for basic mixing trials so it shows us the reason of the effect of the equipment on the flowability properties of the powders.

As a conclusion, it has been seen that dry coating can be made by simple stirring or with the Nara Hybridizer. The hybridizer uses mechanical forces for dry coating and that gives great coating strength to the coated particles. It was observed that the dry coating of the particles by each method had modified the flowability properties of the particles.

### 3. DRY COATING OF PARTICLES IN CYCLOMIX

The Hosokawa Cyclomix is another type of high force mixer that has been used for dry particle coating process in this study. The Cyclomix uses high mechanical impact forces, compression and especially shearing in order to coat the particles. Cyclomix is a batch system like hybridizer but it has a much larger batch size compared to hybridizer. The batch size of the hybridizer is limited to 50 g powder but the conical shaped mixing vessel of the cyclomix can be filled maximum up to 1 litre powder (about 1 kg). The operating velocity of the cyclomix can reach up to 3000 rpm.

A preliminary study of the model couple (PMMA–talc) in the cyclomix has been made in order to find the optimum operating conditions and the fragmentation behaviour of the particles in the Cyclomix.

Afterwards, according to preliminary study the operating conditions have been defined and the PMMA with (1%, 5%) talc particles were treated in the cyclomix.

The characterizations of the powders were done before and after coating. At the end, the results are compared with the results for the hybridizer in order to understand the effect of equipment on the end – use properties of the powders.

#### 3.1. Preliminary Study of Poly(methyl methacrylate) Particles

The PMMA particles have been processed at 3 different operating velocities of cyclomix for a fixed 6 minutes operating time. The particle size distributions of the treated particles have been analysed by the Malvern Mastersizer laser diffraction granulometer. The visual analyses of the powders have been done by the Environmental Scanning Electron Microscopy (ESEM) before and after the treatments.

The operating velocities of the cyclomix were chosen as 1020 rpm (8.5 m/s), 1600 rpm (13.4 m/s), 3000 rpm (25m/s).

As described in the chapter II, the cyclomix is equipped with a jacket at the vessel, a cover and an outlet valve for cooling/heating purposes. In the trials the temperature of the cooling jacket was fixed at 13°C.

In order to have good recirculation of the powders in cyclomix, it is advised by the company Hosokawa to choose initial filling charges between 500 ml and 700 ml. In this study, the initial filling charges of the powders were fixed at 500 ml.

### 3.1.1. General Mass Balance

The 500 ml PMMA particles were introduced to the cyclomix. After the treatment, the powder exits at the bottom is opened and the treated particles are recovered. The recovered powders after the treatments are compared with the initial charge with different operating velocities. It can be seen from the figure III.61, there is a high percentage of particle recovery for each operating velocity.

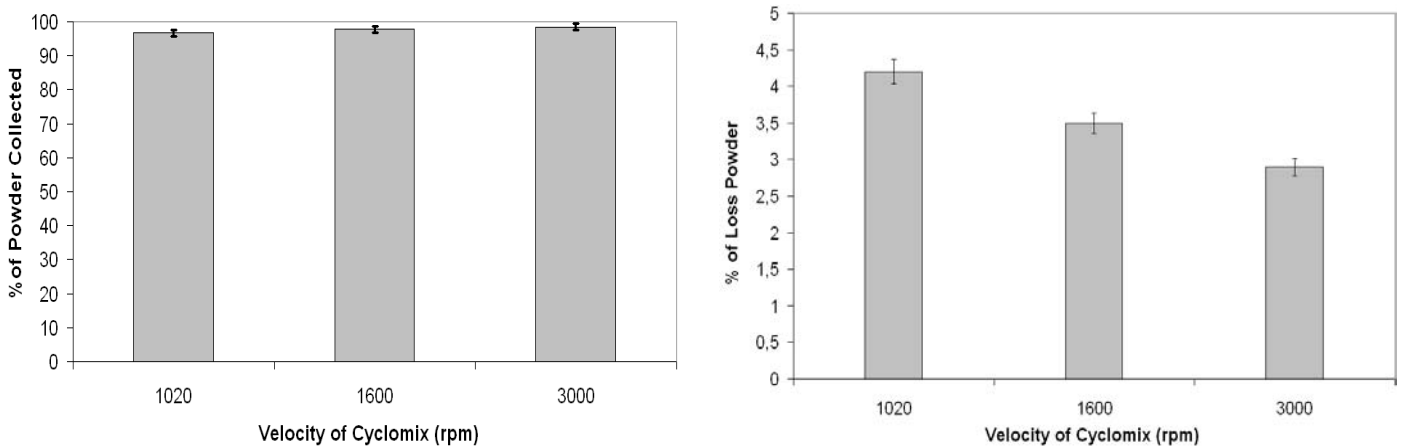


**Figure III.61.** Effect of Rotational Velocity on % of Collected PMMA Particles

### 3.1.2. Effect of Rotational Velocity on Particle Size Distributions

The particle size distribution analyses of PMMA particles have been performed for each operating velocity of the cyclomix (1020 rpm, 1600 rpm, 3000 rpm). The volume and number particle size distributions of PMMA particles before and after treatments in cyclomix can be seen in the figure III.62 and III.63.

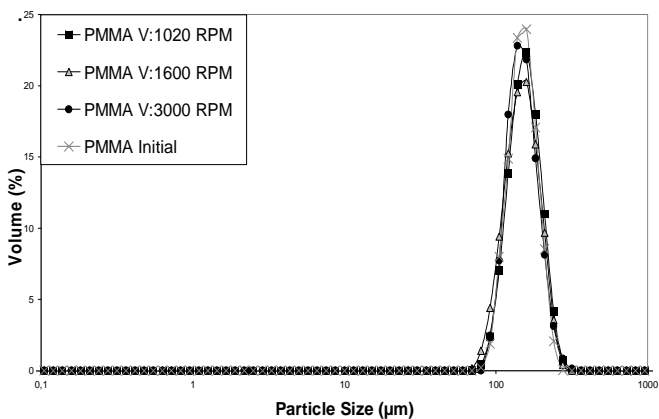


**Figure III.62.** Volume Particle Size Distribution of PMMA Particles Before and After Treatment with Different Velocities

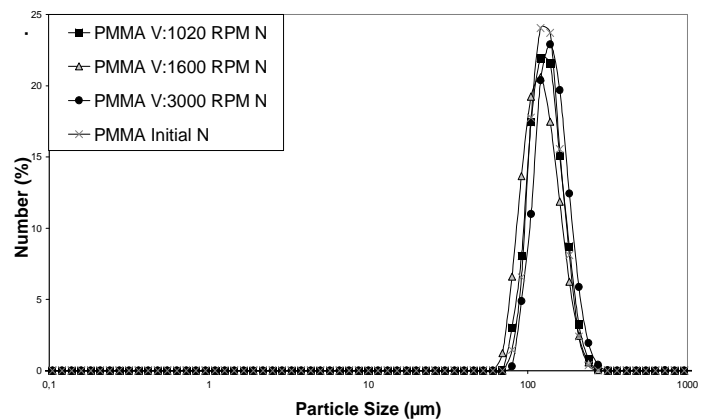


**Figure III.63.** Number Particle Size Distribution of PMMA Particles Before and After Treatment with Different Velocities

According to the volume and number particle size distributions of the treated PMMA particles, there is no particle fragmentation for each velocity of the cyclomix. As it can be seen in the figure III.64, the surface weighted mean particle sizes of the treated PMMA particles also confirm that observation for each velocity.

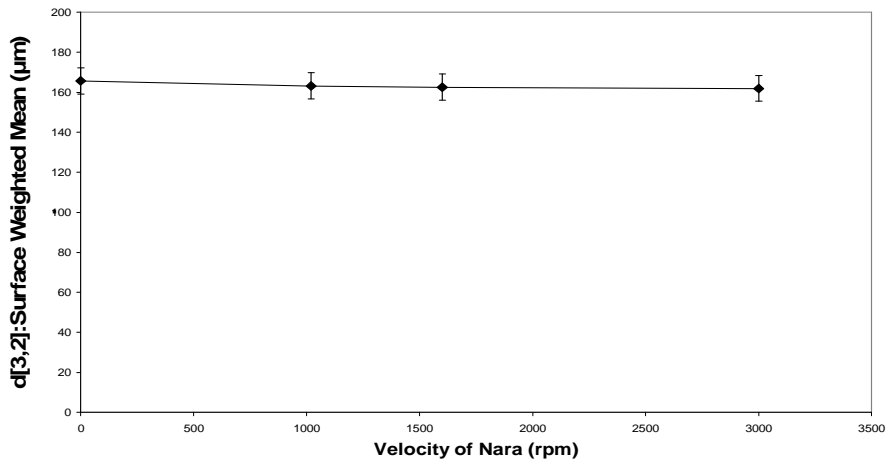


**Figure III.64.** Effect of Rotational Velocity on Particle Sizes of PMMA

The visual observation of the treated PMMA particles has also been done for each operating velocity of the cyclomix. It can be seen from the figure III.65, these show no particle fragmentation for each operating velocity of the cyclomix.

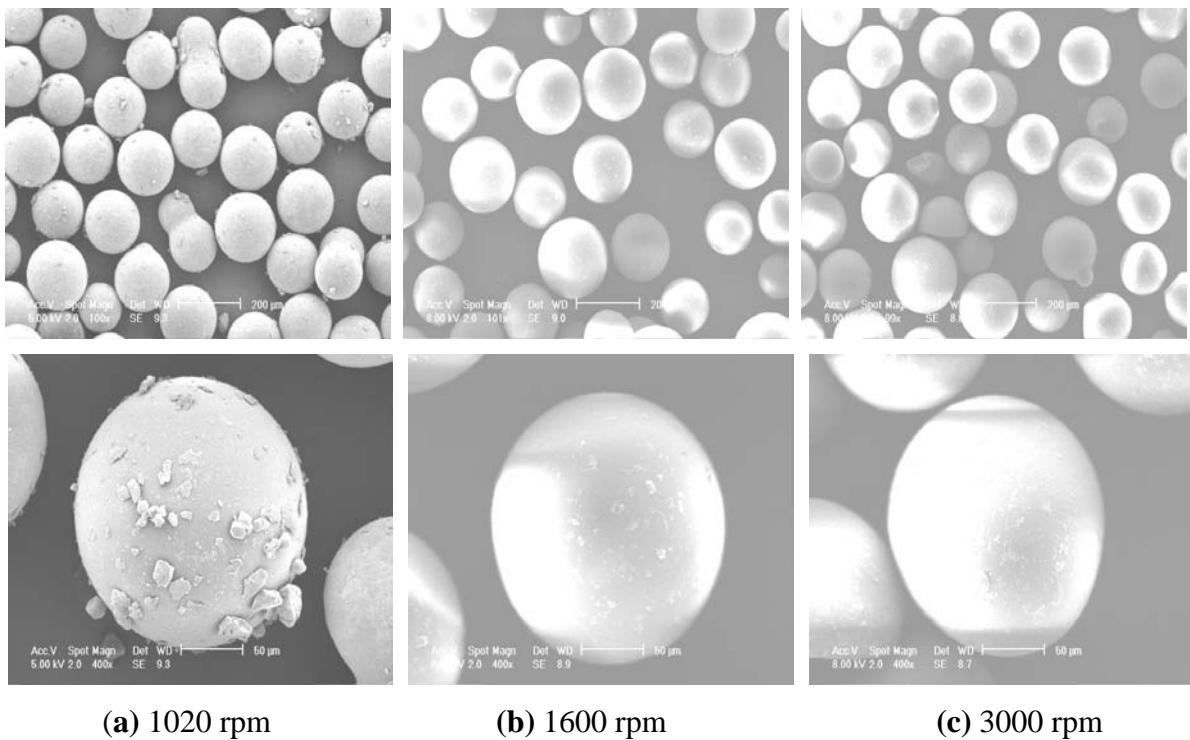


**Figure III.65.** Surface Morphology of PMMA Particles after Treatments in Cyclomix



In the preliminary study, it was observed that the PMMA particles keep their particle size and shape for each operating velocity. Afterwards, PMMA particles have been coated with 1% and 5% talc particles at different operating velocities of cyclomix for 6 minutes fixed operating time.

### 3.2. Dry Coating of Poly(methyl methacrylate) with Talc

In this study, PMMA particles have been coated with 1% and 5% talc particles with different operating velocities of cyclomix (table III.14). The operating time has been fixed at 6 minutes like for the trials with hybridizer. The effects of operating velocities and mass percentages of talc on the end-use properties of the particles have been studied.

At the end, the results of cyclomix trials are compared with hybridizer trials in order to understand the effect of equipment on the coating strength and flowability properties of the particles.

**Table III.14.** Operating Conditions of Dry Coating Treatments in Cyclomix

Host Particles	Guest Particles	Operating Velocity (rpm)	Operating Time (min)	Mass % of Guest Particles	Batch Size (ml)	Temperature of Cooling Jacket (°C)
PMMA	Talc	1020	6	1 %	500	13
		1600				
		3000				
PMMA	Talc	1020	6	5 %	500	13
		1600				
		3000				

#### 3.2.1. General Mass Balance

The figure III.66 shows the percentage of recovered powder after the treatments in cyclomix for each operating velocity. The initial filling charge of the vessel was 500 ml that corresponds to around 620 g particles. It was observed that the recovered powder ratio is very high for each operating velocity and mass percentage of talc particles.

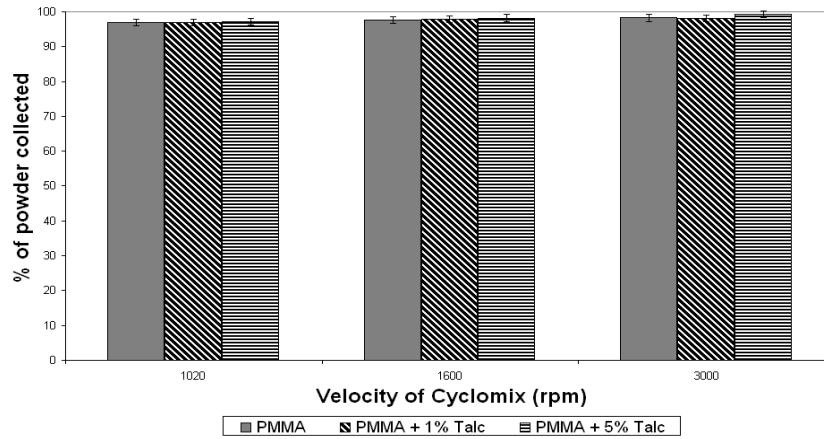


**Figure III.66.** Effect of Rotational Velocity and Mass Percentage of Talc on the % of Powder Recovered After Treatments in Cyclomix

It was also seen that the mass percentage of talc particles in the mixture increases the powder recovery percentage in a very small amount as shown in the figure III.67. It can be seen that the maximum powder recovery was reached for 5% talc coating at 3000 rpm treatments in cyclomix. The effect of lubricant properties of the talc particles may have a role for this result.

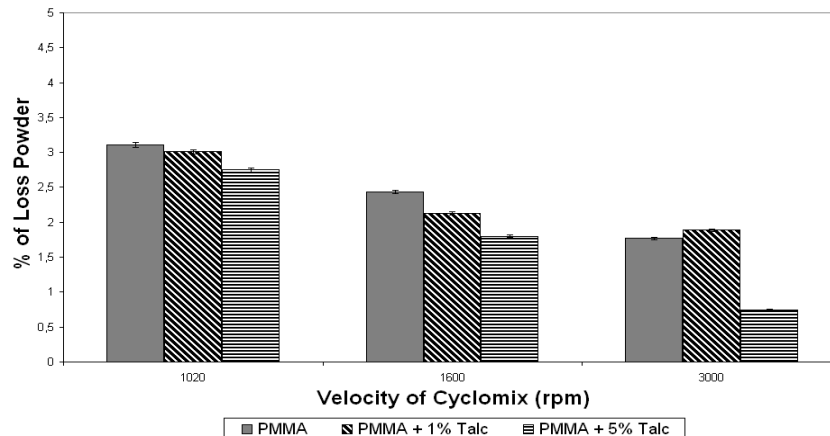


**Figure III.67.** Evaluation of Loss Powder Percentage in Cyclomix

### 3.2.2. Measure of Solid Densities of the Dry Coated Particles

The solid densities of the particles that were treated in cyclomix and hybridizer have been compared. It can be seen from the figure III.68, the solid densities of the particles that were treated in cyclomix or hybridizer are less than the calculated values for the mixture (eqn III.1) and they increase with increasing mass percentage of talc particles in the mixture as expected.

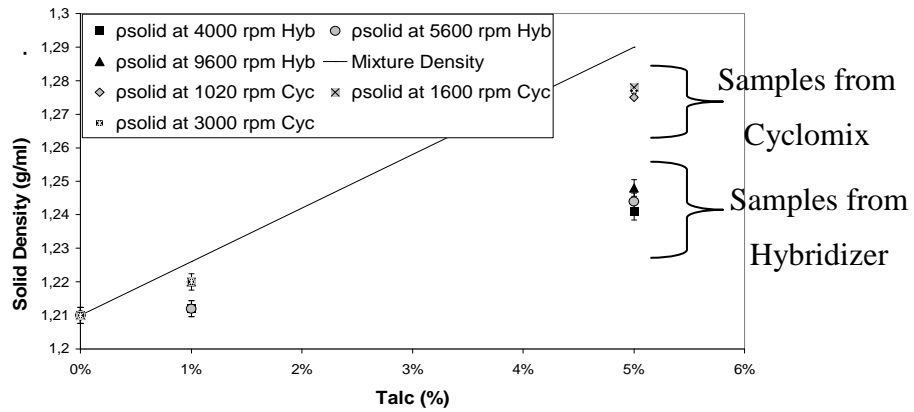


**Figure III.68.** Solid Densities of Coated Particles in Cyclomix and Hybridizer

On the other hand, the solid densities of the particles from cyclomix are higher compared to the particles from hybridizer and or much closer to the perfect coating. The loss of talc particles in hybridizer trials may be a reason for this result, even though the difference between the densities of talc and PMMA is too small to have a good precision.

### 3.2.3. Characterization of Surface Morphology of the Particles

The surface morphology of the particles have been analysed by using ESEM as for the hybridizer trials.

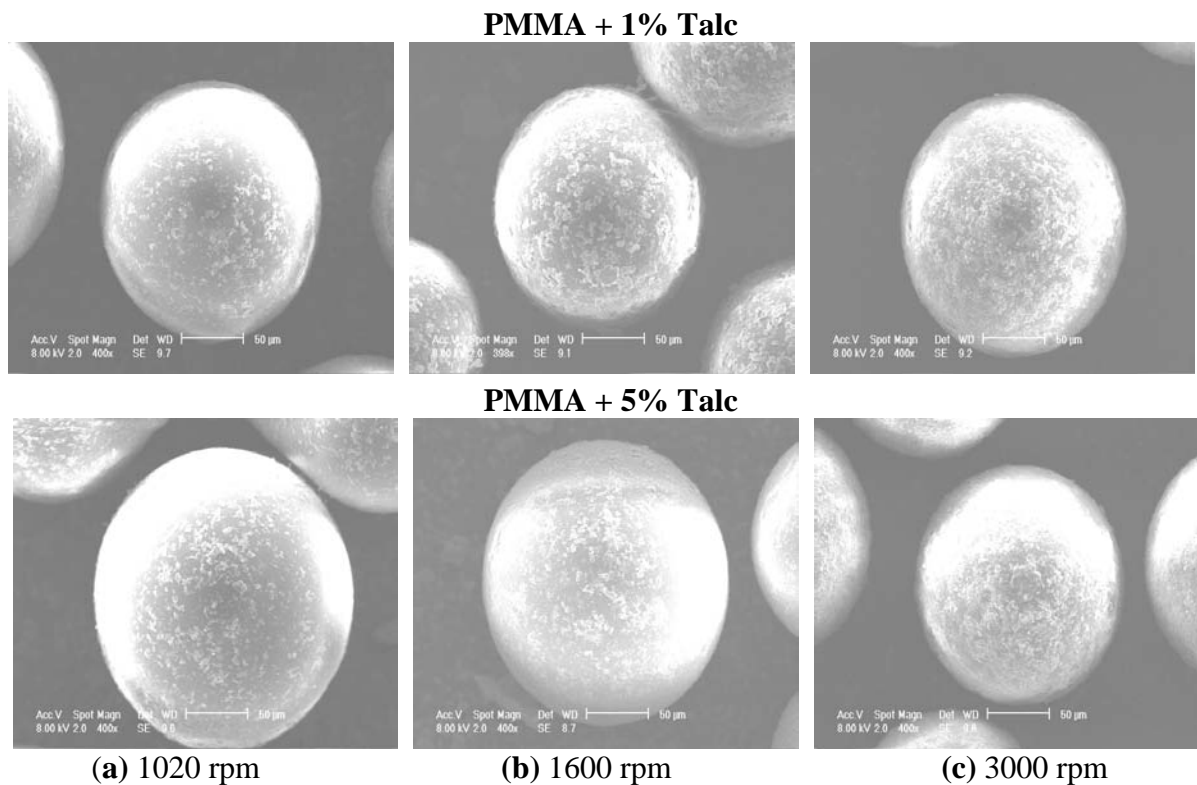


**Figure III.69.** Surface Morphology of PMMA Particles Coated by 1% and 5% Talc

It can be seen from the figure III.69 that the particle size and shape are not changed in all operating velocities of cyclomix. The amount of talc particles on the surface of the PMMA particles is greater for the 5% coating than 1% talc coating as expected.

### 3.2.4. Characterization of Coating Strength of the Particles

The particle liberation pressures have been found by comparing the number particle size distributions with different dispersing air pressures for the coated particles in cyclomix as it was done for the coated particles in hybridizer.

The effects of operating velocity and mass percentage of talc in the mixture on the coating strength have been studied individually for cyclomix treatments. Afterwards, the results of the cyclomix trials are compared with the trials of hybridizer in order to understand the effect of the equipment on the coating strength of the coated particles.

#### A. Effect of Operating Velocity on Coating Strength of the Particles

The coating strength analysis has been done for 1% and 5% talc coated PMMA particles for each operating velocity of the cyclomix. 0.5, 1.5, 2.5, 3.5 bar air dispersing pressures have been chosen in the first part then the particle liberation pressures have been found more precisely.

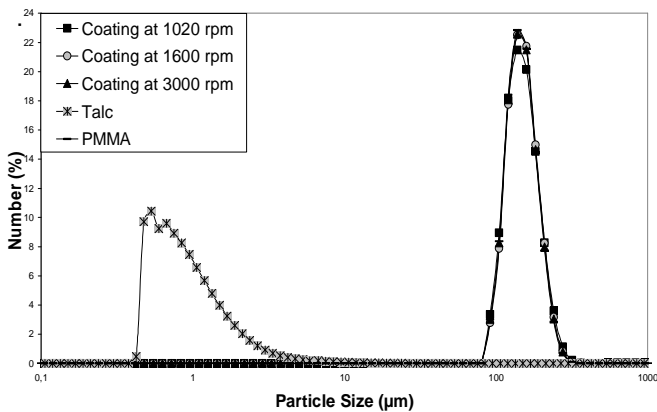


**Figure III.70.** Number Particle Size Distribution of Coated and Uncoated Particles at 0.5 bar Dispersing Pressure

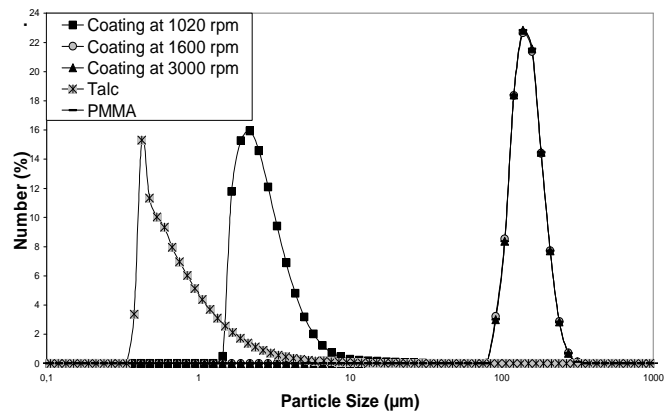


**Figure III.71.** Number Particle Size Distribution of Coated and Uncoated Particles at 1.5 bar Dispersing Pressure

It can be seen from the figure III.70, initial PMMA and 1% talc coated PMMA particles have similar particle size distributions around 160  $\mu\text{m}$ . Afterwards, whenever the dispersing air pressure increases to 1.5 bar, it was observed a shift of particle size distribution to the smaller particle sizes for coated PMMA particles at 1020 rpm (fig.III.71). It shows that the particle

liberation pressure for coated PMMA particles at 1020 rpm is between 0.5 and 1.5 bar. The other talc coated PMMA particles keep their particle size distributions at 1.5 bar pressure.

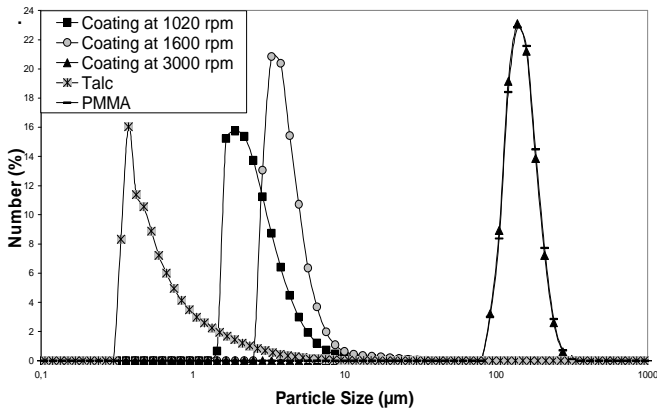


**Figure III.72.** Number Particle Size Distribution of Coated and Uncoated Particles at 2.5 bar Dispersing Pressure

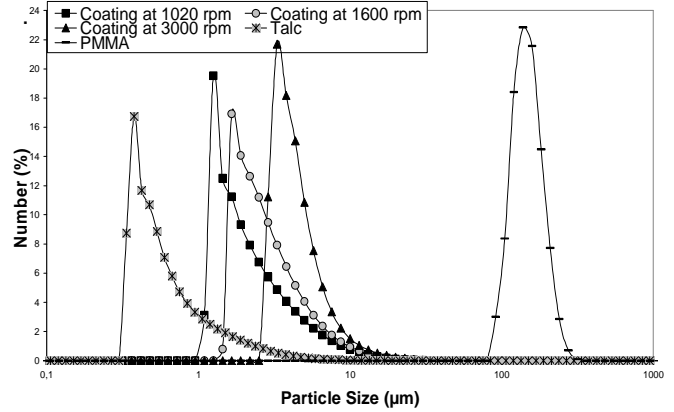


**Figure III.73.** Number Particle Size Distribution of Coated and Uncoated Particles at 3.5 bar Dispersing Pressure

At 2.5 bar pressure, talc coated PMMA particles at 1600 rpm has a smaller particle size distribution (3.8 µm) compared to 1.5 bar pressure because of the particle liberation (fig.III.72). On the other hand, coated PMMA particles at 3000 rpm have still the same particle size distribution at this pressure. But at 3.5 bar pressure the particle size distribution for the coated particles at 3000 rpm decreases to 3 µm. Moreover, other talc coated PMMA particles at 1020 and 1600 rpm become much closer to the talc particle size distribution at 3.5 bar pressure as it can be seen from the figure III.73. In the figure III.74, the particle liberation pressures for each operating velocity can be seen more precisely.

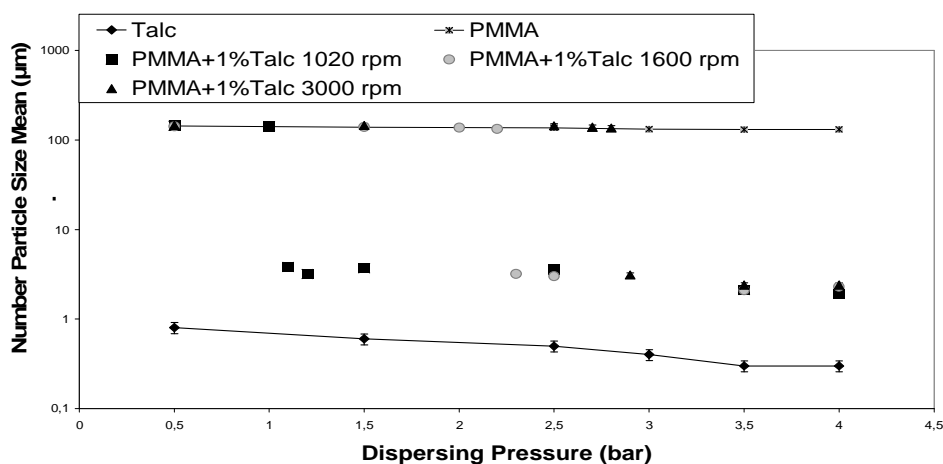


**Figure III.74.** Number Particle Size Mean vs. Dispersing Pressure for 1% Coated and Uncoated PMMA Particles

As it can be seen from the table III.15, the particle liberation pressures increase with increasing operating velocity of cyclomix. The reason is probably the generation of high mechanical impact and shearing forces at high operating velocities. In addition, it should be remembered that the difference in particle size distributions of the particles could be also reason of the particle fragmentation.

**Table III.15.** Dispersing Pressures and Air Velocities for Particle Detachment for Coated Particles in Cyclomix

Material	Dispersing Air Pressure	Air Velocity
PMMA + 1% Talc at 1020 rpm	1.1 bar	56 m/s
PMMA + 1% Talc at 1600 rpm	2.3 bar	95 m/s
PMMA + 1% Talc at 3000 rpm	2.9 bar	109 m/s

**B. Effect of Mass Percentage of Talc on Coating Strength of the Particles**

The effect of mass percentage of talc on the coating strength of the particles has also been studied for cyclomix trials. In the figure III.75, III.76 and III.77 number particle size distributions of particles that were treated at 1020, 1600 and 3000 rpm operating velocities with 1% and 5% talc particles are presented.

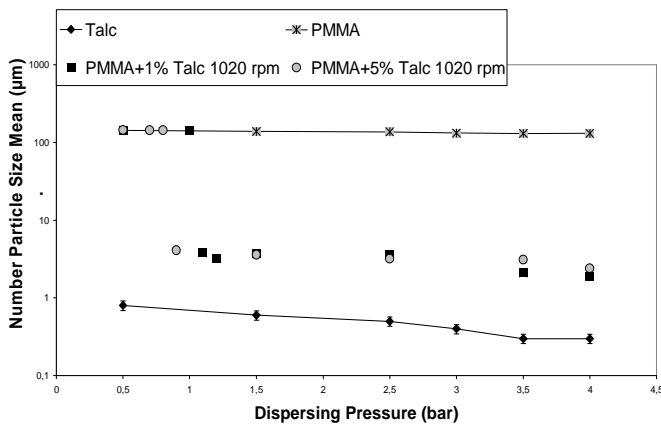


**Figure III.75.** Number Particle Size Mean vs. Dispersing Pressure for PMMA at 1020 rpm with 1% and 5% Talc Coating

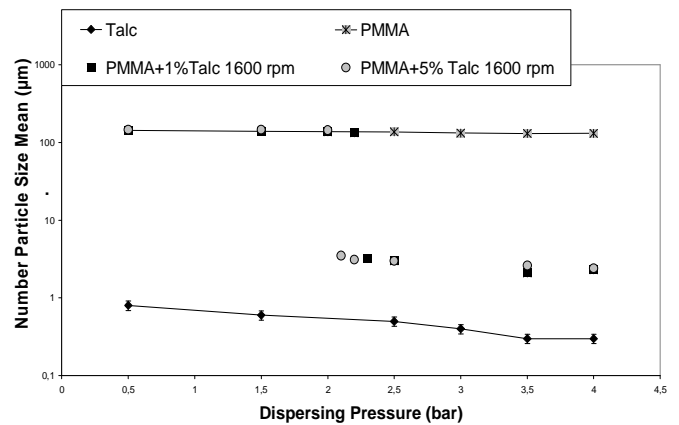


**Figure III.76.** Number Particle Size Mean vs. Dispersing Pressure for PMMA at 1600 rpm with 1% and 5% Talc Coating

It was observed that for 1020 rpm treatments the particle liberation pressure is 1.1 bar for 1% talc coating, whenever the mass percentage of talc particles in the mixture increases to 5%, the particle liberation pressure decreases to 0.9 bar (fig.III.75). At 1600 rpm treatments, we

had the same observation, the particle liberation pressure is 2.3 bar for 1% coating and decrease to 2.1 bar for 5% talc coated particles (fig.III.76). Moreover, at 3000 rpm treatments the particle liberation pressure is 2.9 bar for 1% talc coated particles and decreases to 2.5 bar for 5% talc coated particles (fig.III.77).

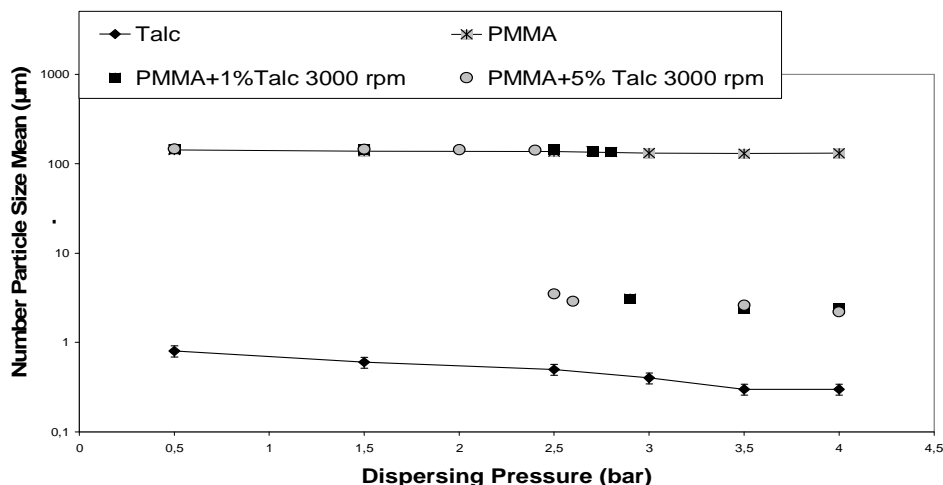


**Figure III.77.** Number Particle Size Mean vs. Dispersing Pressure for PMMA at 3000 rpm with 1% and 5% Talc Coating

As it can be seen from the table III.16, the particle liberation pressures decrease with increasing mass percentage of talc particles in the mixture. The high percentage of talc coating may cause some multi-layering of talc particles (agglomeration) on the surface of PMMA particles. In particle size analysis, there are impacts between particles, particles and the walls of the granulometer and also particles with the dispersing air. Multi-layering may increase the impact shock surface and because of this it would be easier to break up talc particles on the surface at higher coating percentages

As it was seen for the hybridizer trials, for each operating velocity of the cyclomix, the coated PMMA particles always had greater particle size distributions compared to talc particles for all pressures. This is probably the reason of the difficulty to detach talc particles from the surface of PMMA particles because of the strong interactions between talc and PMMA particles. In addition, as it was noticed in the hybridizer trials, the difference in the particle size distributions could be due to particle fragmentation.

**Table III.16.** Dispersing Pressures and Air Velocities for Particle Detachment for 1% and 5% Talc Coated PMMA Particles in Cyclomix

Material	Dispersing Air Pressure	Air Velocity
PMMA + 1% Talc at 1020 rpm	1.1 bar	56 m/s
PMMA + 1% Talc at 1600 rpm	2.3 bar	95 m/s
PMMA + 1% Talc at 3000 rpm	2.9 bar	109 m/s
PMMA + 5% Talc at 1020 rpm	0.9 bar	48 m/s
PMMA + 5% Talc at 1600 rpm	2.1 bar	90 m/s
PMMA + 5% Talc at 3000 rpm	2.5 bar	100 m/s

### C. Effect of Equipment on Coating Strength of the Particles

In this part of the study, in order to understand the effect of equipment on the coating strength of the particles, the results of 1% and 5% talc coated particles in cyclomix have been compared with the hybridizer trials. Figure III.78 and III.79 show the evaluation of the particle liberation pressures of cyclomix and hybridizer trials for 1% and 5% talc coated PMMA particles.

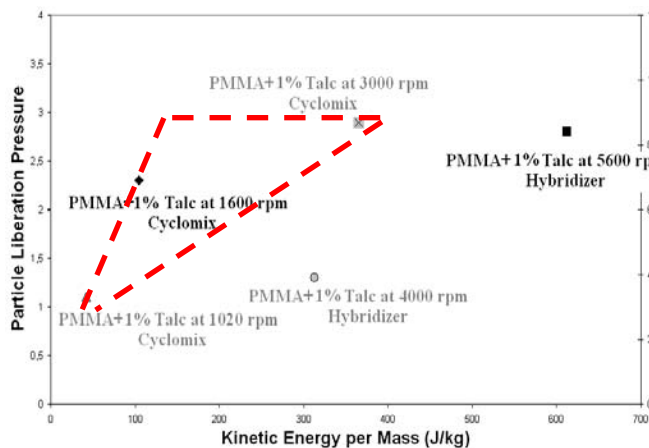


**Figure III.78.** Effect of Equipment on Particle Liberation Pressure for 1% Coated Particles by Cyclomix and Hybridizer

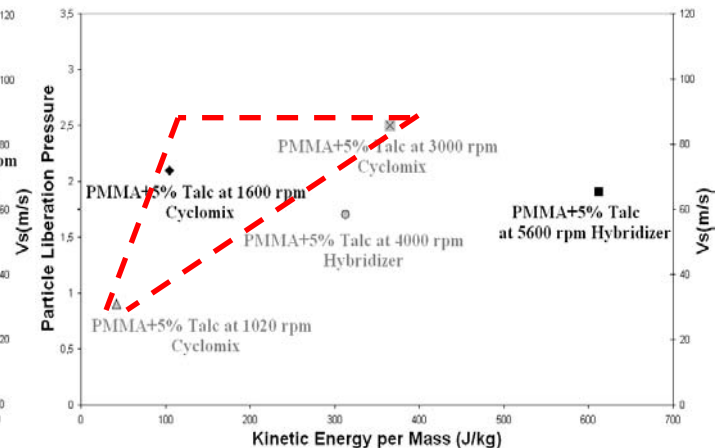


**Figure III.79.** Effect of Equipment on Particle Liberation Pressure for 5% Coated Particles by Cyclomix and Hybridizer

The kinetic energy per mass has also been simply calculated according to rotational velocity of cyclomix as has been done for the hybridizer trials. The linear velocities ( $V$ ) of the



cyclomix blades were calculated for each 3 blades by using the equation III.9. The results are shown in table III.17. ( $d_{\text{blade}}$ : diameter of the blade)

**Table III.17.** Linear Velocities of 3 Blades of the Cyclomix Corresponding to the Rotational Velocities

Rotational Velocity	$V_1$ ( $d_{\text{blade}}$ :12 cm)	$V_2$ ( $d_{\text{blade}}$ :10 cm)	$V_3$ ( $d_{\text{blade}}$ :6.5cm)
1020 rpm	6.4 m/s	5.3 m/s	3.2 m/s
1600 rpm	10.1 m/s	8.4 m/s	5 m/s
3000 rpm	18.8 m/s	15.7 m/s	9.4 m/s

Afterwards the kinetic energy per mass value was calculated for each blade by using the equation III.10. Then the average value has been taken as the energy per mass value of the cyclomix for the given rotational velocity.

The results show us that the coated particles in cyclomix have higher particle liberation pressures at the similar kinetic energy per mass values compared to the coated particles in hybridizer (figure III.78 and III.79). The difference in the operation methodologies of the equipments, usage of different mechanical forces in different orders (impact, shearing) is probably the reason for this result.

### 3.2.5. Characterization of Flowability Properties of the Particles

The flowability properties of the treated particles in cyclomix has been determined by Erweka tapped density tester and Freeman Technology powder rheometer (FT4) as it has been done for treated particles in hybridizer.

The effects of operating velocity of cyclomix and different mass percentages of talc particles in the mixture on the modification of flowability properties of the powders have been studied. The results of flowability properties of treated particles in cyclomix have also been compared with the results of treated particles in hybridizer in order to understand the effect of equipment on the modification of flowability properties of the powders.

#### A. Effect of Operating Velocity on Flowability Properties of the Particles

The flowability properties of 1% and 5% talc coated PMMA particles for each operating velocity of cyclomix have been analysed. The tapped density results of uncoated and 1% talc coated PMMA particles can be seen in the figure III.80.

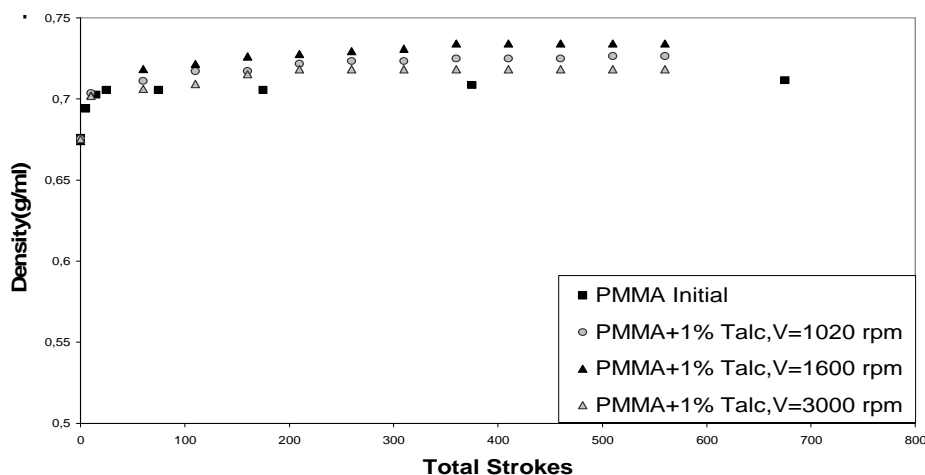


**Figure III.80.** Evaluation of Flowability of PMMA Particles Before and After Coating with Talc According to Different Operating Velocities of Cyclomix

The coated PMMA particles and individually treated PMMA particles in cyclomix have very good flowability properties as it can be seen from the table III.18. The reason is probably, that there is almost no particle fragmentation in cyclomix trials. In addition, at 3000 rpm trials (maximum operating velocity of cyclomix), we can see that the flowability becomes excellent after coating with 1% talc particles.

**Table III.18.** Carr Index and Hausner Ratio for Uncoated and 1% Coated PMMA Particles

Materials	Carr Index (%)	Flowability	Hausner Ratio
Initial PMMA	$0.99 \pm 0.02$	Excellent	$1.01 \pm 0.02$
PMMA at 1020 rpm	$9.63 \pm 0.04$	Excellent	$1.11 \pm 0.04$
PMMA at 1600 rpm	$13.51 \pm 0.04$	Excellent	$1.16 \pm 0.04$
PMMA at 3000 rpm	$19.32 \pm 0.05$	Mediocre	$1.24 \pm 0.05$
PMMA+1% Talc at 1020 rpm	$5.74 \pm 0.03$	Excellent	$1.06 \pm 0.03$
PMMA+1% Talc at 1600 rpm	$8.42 \pm 0.02$	Excellent	$1.09 \pm 0.02$
PMMA+1% Talc at 3000 rpm	$9.10 \pm 0.05$	Excellent	$1.10 \pm 0.05$

The Freeman Technology powder tester (FT4) has also been used in order to complete analysing the flowability properties of the particles (Table III.19).

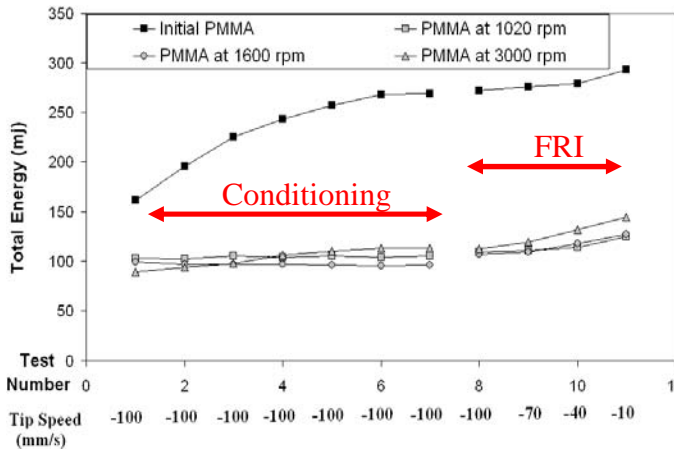


**Figure III.81.** FT4 Results of Initial and Treated PMMA Particles in Cyclomix

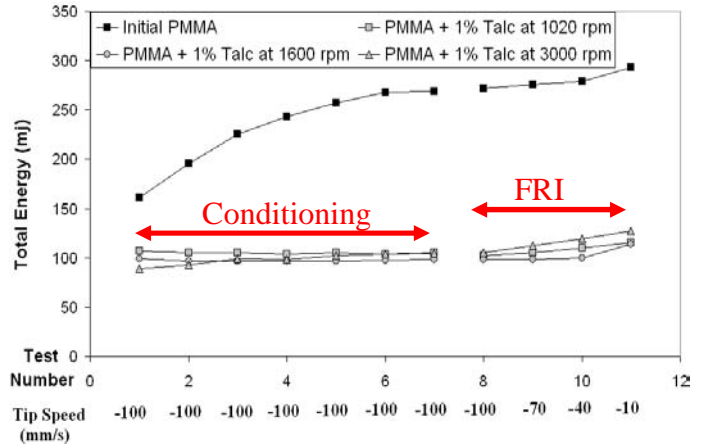


**Figure III.82.** FT4 Results of Initial and 1% Talc Coated PMMA Particles in Cyclomix

Figure III.81 and III.82 show the results of FT4 experiments. It can be seen that we have homogeneous mixture at the end of conditioning step for each powder sample.

**Table III.19.** Evaluation of Flowability of Uncoated and 1% Coated PMMA Particles by FT4

Materials	8 <sup>th</sup> Cycle (mj)	11 <sup>th</sup> Cycle (mj)	FRI
Initial PMMA	273 ± 0.03	293 ± 0.03	1.10 ± 0.03
PMMA at 1020 rpm	109 ± 0.07	125 ± 0.07	1.15 ± 0.07
PMMA at 1600 rpm	107 ± 0.03	127 ± 0.03	1.19 ± 0.03
PMMA at 3000 rpm	112 ± 0.08	144 ± 0.08	1.29 ± 0.08
PMMA+1% Talc at 1020 rpm	102 ± 0.03	115 ± 0.03	1.13 ± 0.03
PMMA+1% Talc at 1600 rpm	98 ± 0.03	114 ± 0.03	1.16 ± 0.03
PMMA+1% Talc at 3000 rpm	105 ± 0.06	127 ± 0.06	1.21 ± 0.06

It was observed that for each operating velocity of cyclomix the talc coated PMMA particles have better flowability than treated PMMA particles in cyclomix. The FRI values of 1020 and 1600 rpm trials don't have much difference. For 3000 rpm treatments the FRI values are higher than other particles and shows little decrease in the flowability properties.

### B. Effect of Mass Percentage of Talc on Flowability Properties of the Particles

In this part of the study, the effect of mass percentage of talc particles on the flowability properties of the coated PMMA particles has been studied. The results of the tapped and apparent densities of 1% and 5% talc coated PMMA particles at 1020, 1600 and 3000 rpm for 6 minutes operating time are shown in the figure III.83.

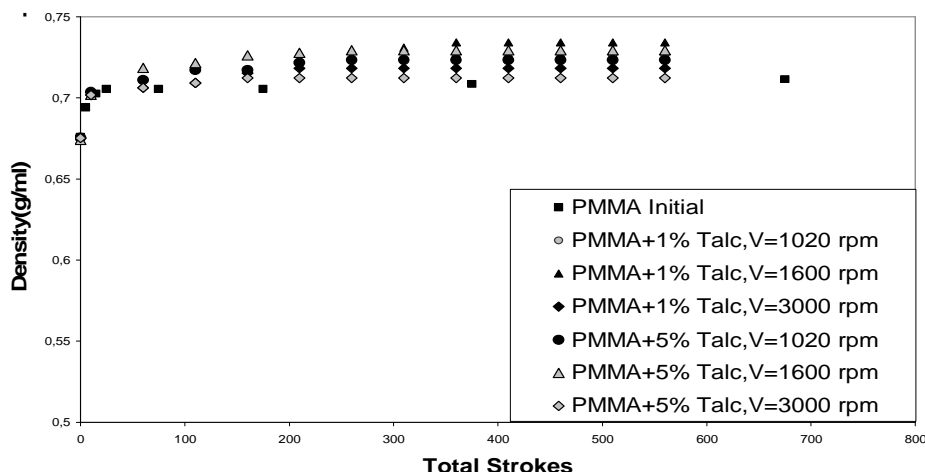


**Figure III.83.** Evaluation of Flowability of PMMA Particles Before and After Coating with 1% and 5% Talc for Each Operating Velocity

The Carr index and Hausner ratio values of 1% and 5% talc coated PMMA particles are presented in the table III.20. It can be seen that for all cases we have excellent flowability according to tapped and apparent density analysis. It hasn't been observed a significant difference of flowability properties between the results of 1% and 5% talc coated PMMA particles.

**Table III.20.** Carr Index and Hausner Ratio for 1% and 5% Coated PMMA Particles

Materials	Carr Index (%)	Flowability	Hausner Ratio
PMMA+1% Talc at 1020 rpm	$5.7 \pm 0.03$	Excellent	$1.06 \pm 0.03$
PMMA+1% Talc at 1600 rpm	$8.4 \pm 0.02$	Excellent	$1.09 \pm 0.02$
PMMA+1% Talc at 3000 rpm	$9.1 \pm 0.05$	Excellent	$1.10 \pm 0.05$
PMMA+5% Talc at 1020 rpm	$4.9 \pm 0.03$	Excellent	$1.05 \pm 0.03$
PMMA+5% Talc at 1600 rpm	$8.1 \pm 0.04$	Excellent	$1.09 \pm 0.04$
PMMA+5% Talc at 3000 rpm	$8.9 \pm 0.04$	Excellent	$1.10 \pm 0.04$

The FT4 has also been used to understand the effect of talc percentage on the flowability properties of the powders. It can be seen that the FRI values are around 1.1 and 1.2, it shows us that the particles have very good flowability for both 1% and 5% talc coatings. On the other hand, we didn't observe much difference between the results of 1% and 5% talc coated PMMA particles since in cyclomix trials; there is no observed particle fragmentation (table III.21).

**Table III.21.** Evaluation of Flowability of 1% and 5% Coated PMMA Particles by FT4

Materials	8 <sup>th</sup> Cycle (mj)	11 <sup>th</sup> Cycle (mj)	FRI
<b>PMMA+1% Talc at 1020 rpm</b>	102 ± 0.03	115 ± 0.03	<b>1.13 ± 0.03</b>
<b>PMMA+1% Talc at 1600 rpm</b>	98 ± 0.03	114 ± 0.03	<b>1.16 ± 0.03</b>
<b>PMMA+1% Talc at 3000 rpm</b>	105 ± 0.06	127 ± 0.06	<b>1.21 ± 0.06</b>
<b>PMMA+5% Talc at 1020 rpm</b>	100 ± 0.01	110 ± 0.01	<b>1.10 ± 0.01</b>
<b>PMMA+5% Talc at 1600 rpm</b>	95 ± 0.04	106 ± 0.04	<b>1.12 ± 0.04</b>
<b>PMMA+5% Talc at 3000 rpm</b>	107 ± 0.06	126 ± 0.06	<b>1.18 ± 0.06</b>

### C. Effect of Equipment on Flowability Properties of the Particles

In this part of the study, the flowability properties of coated particles in cyclomix and hybridizer have been compared with each other in order to understand the effect of the equipment on the flowability properties of the powders.

**Table III.22.** Effect of Equipment on the Flowability Properties of Coated PMMA Particles

Materials	8 <sup>th</sup> Cycle (mj)	11 <sup>th</sup> Cycle (mj)	FRI
<b>PMMA+5% Talc at 4000 rpm Hybridizer</b>	100 ± 0.05	109 ± 0.05	<b>1.09 ± 0.05</b>
<b>PMMA+5% Talc at 5600 rpm Hybridizer</b>	119 ± 0.05	135 ± 0.05	<b>1.13 ± 0.05</b>
<b>PMMA+5% Talc at 9600 rpm Hybridizer</b>	71 ± 0.05	287 ± 0.05	<b>4.04 ± 0.05</b>
<b>PMMA+5% Talc at 1020 rpm Cyclomix</b>	100 ± 0.01	110 ± 0.01	<b>1.10 ± 0.01</b>
<b>PMMA+5% Talc at 1600 rpm Cyclomix</b>	95 ± 0.04	106 ± 0.04	<b>1.12 ± 0.04</b>
<b>PMMA+5% Talc at 3000 rpm Cyclomix</b>	107 ± 0.06	126 ± 0.06	<b>1.18 ± 0.06</b>

The results of FT4 for 5% talc coated PMMA particles in cyclomix and hybridizer can be seen in the table III.22. As it has been observed before, for all operating velocities the coated particles have better flowability properties than treated particles either in cyclomix or hybridizer. The results of cyclomix trials are similar with low operating velocity hybridizer treatments. The only difference between the cyclomix and hybridizer trials is, at high operating velocity of hybridizer (9600 rpm) there is particle fragmentation of PMMA particles that decreases the flowability of the particles and at that velocity the particles have bad flowability than initial state. But for cyclomix trials the particles have good flowability for all operating velocities because we didn't observe any particle fragmentation at any operating velocities of cyclomix.

### **3.3. Conclusions**

The Cyclomix uses mechanical impact forces, compression and shearing as hybridizer does in dry particle coating. The difference between cyclomix and hybridizer probably, in hybridizer the mechanical impact force is more significant but on the other hand in cyclomix shearing is more significant than other mechanical forces. This difference affects the particle fragmentation and end use properties of the powders.

The preliminary study has been done for initial PMMA particles in order to understand its fragmentation behaviour in cyclomix at different operating velocities. It has been observed that contrarily to the hybridizer trials, even at the highest operating velocity there is no particle fragmentation of PMMA particles in cyclomix. It may be explained by the difference of type and amount of mechanical forces that the equipment applies on the particles.

It was observed that the loss particle amount is less in cyclomix treatment than hybridizer treatments. The probable reason is that, in hybridizer there are empty spaces between the rotor and the wall of the hybridizer where the particles may stay but the conical shaped mixing vessel of the cyclomix doesn't have empty spaces between the walls and blades.

Visualisations before and after coating was performed with an ESEM, in order to analyse the morphology of the particles and deposition of guest particles on the host particles. It has been observed that, dry coating of the particles in cyclomix concludes with discrete coating of talc particles on the surface of the PMMA particles.

It has been observed that, like in the hybridizer trials, the particle liberation pressures increase with increasing operating velocity of cyclomix because of the generation of high mechanical impact and shearing forces at high operating velocities. On the other hand, it was found that

for 1% talc coated PMMA particles, after 1900 rpm operating velocity of cyclomix the particle liberation pressure is stable until the maximum operating velocity (3000 rpm). For 5% trials, the particle liberation pressure is stable after 1890 rpm operating velocity until 3000 rpm. On the other hand, it was seen that the particle liberation pressures decrease with increasing mass percentage of talc particles in the mixture. It should be also considered that the particle size difference could be reason of either particle fragmentation or detachment of talc particles or both of them at the same time. At the end, the cyclomix trials have been compared with hybridizer trials in order to understand the effect of equipment on the coating strength of the particles. The kinetic energy per mass values has been simply calculated according to rotational velocity of cyclomix and hybridizer. It was observed that the coated particles in cyclomix have higher particle liberation pressures at similar kinetic energy per mass values compared to the coated particles in hybridizer. The difference in the operation methodologies of the equipments, usage of different mechanical forces in different orders (impact, shearing) can be probably reasons of this result.

Contrary to the coated particles in hybridizer, the coated PMMA particles and individually treated PMMA particles in cyclomix have very good flowability properties because of no particle fragmentation in cyclomix trials. As it has been observed for the hybridizer trials, for each operating velocity of cyclomix the talc coated PMMA particles have also better flowability properties than treated PMMA particles in cyclomix. The effect of mass percentage of talc particles on the flowability of the particles has also been studied. It was seen that there is no significant difference of flowability properties between the results of 1% and 5% talc coated PMMA particles in cyclomix.

As a conclusion, it was seen that the cyclomix is also an useful equipment for dry particle coating process. Cyclomix uses mechanical forces (specially shearing) in order to coat the particles and gives very high coating strength property to the new generated particles. Dry coating of PMMA with talc particles improves their flowability compared to the treated PMMA particles in cyclomix.

#### 4. DRY COATING OF PARTICLES IN TURBULA

Turbula is also another type of mixer that has been used for dry particle coating experiments. It allows us to mix powders by rotational movements of the chamber (chapter II). The particles are mixed in a closed container that has 1L volume. The mixing container is set in three-dimensional movement that exposes the product to an always changing, rhythmically pulsing motion.

In this study, PMMA particles were pre-treated individually in hybridizer in order to be able to compare the results with high force mixers (hybridizer & cyclomix). Afterwards, the treated PMMA particles with 1% and 5% talc particles were mixed by turbula.

The characterization of particles has been done before and after the treatments and the results have been compared with the results of hybridizer and cyclomix trials.

##### 4.1. Preliminary Study of Poly(methyl methacrylate) Particles

In this part, the effect of rotational velocity of turbula on PMMA particles has been studied. PMMA particles have been initially treated in hybridizer at 4000, 5600 and 9600 rpm for 6 minutes. After the hybridizer treatment, PMMA particles have been treated inside a 1L container (30 g) at 96 rpm operating velocity for 6 minutes operating time by turbula. The volume and number particle size distributions of PMMA that were treated by turbula particles can be seen in the figure III.84 and III.85.

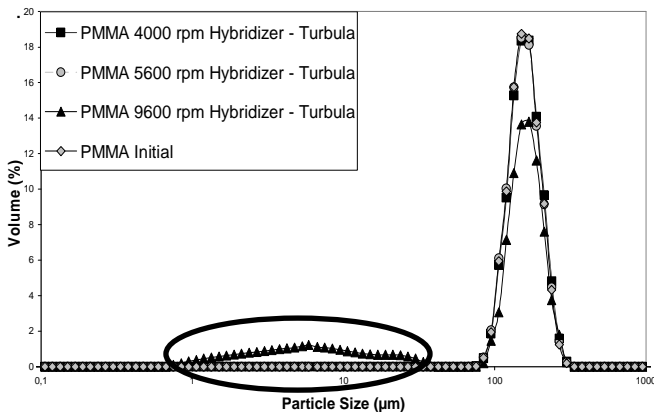


**Figure III.84.** Volume Particle Size Distribution of Treated PMMA Particles by Turbula

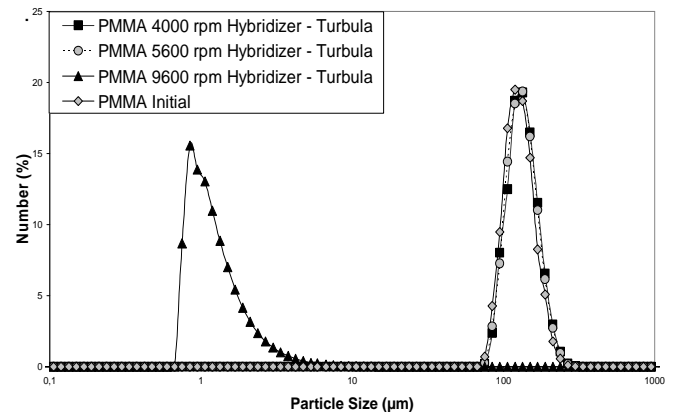
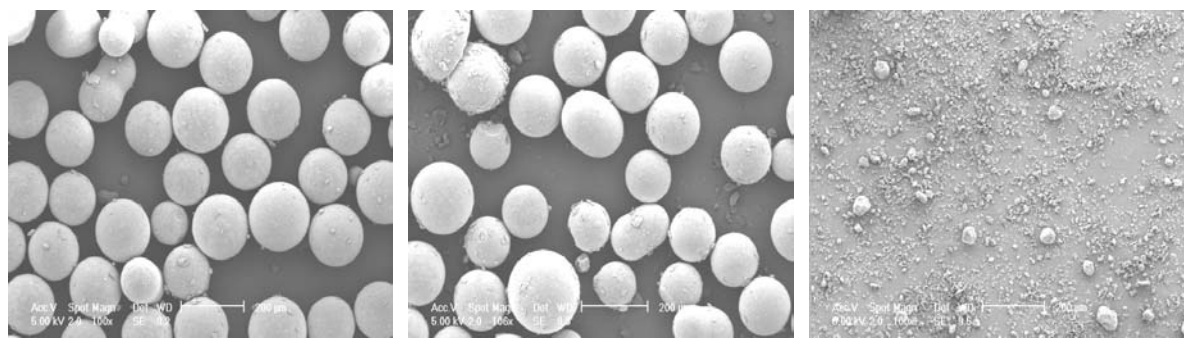


**Figure III.85.** Number Particle Size Distribution of Treated PMMA Particles by Turbula

It can be seen that the particle size distributions of pre-treated particles at 4000 and 5600 rpm in hybridizer then treated by turbula have similar particle size distributions with initial state of PMMA particles. On the other hand, pre-treated particles at 9600 rpm then treated by turbula



has a fine particle population around 8  $\mu\text{m}$ , which shows the particle fragmentation. The visual analysis by ESEM has also been done before and after treatments. As it can be seen from the figure III.86, the results confirm the granulometric analysis.



(a) 4000 rpm Hybridizer – Turbula      (b) 5600 rpm Hybridizer – Turbula      (c) 9600 rpm Hybridizer – Turbula

**Figure III.86.** Surface Morphology of PMMA Particles Pre-Treated in Hybridizer then by Turbula

At the end, if we compare the results of turbula with hybridizer trials (figure III.6 and III.7), it can be observed that there is no effect of operating velocity of turbula on the particle fragmentation as expected. Because turbula is a conventional mixer not a high shear mixer like hybridizer or cyclomix.

#### 4.2. Dry Coating of Poly(methyl methacrylate) with Talc

PMMA particles were pre-treated in hybridizer at different velocities (4000, 5600, 9600 rpm) then treated PMMA particles have been coated with 1% and 5% talc particles by turbula at 96 rpm operating velocity for 6 minutes (table III.23). In turbula trials, 30 g batch mass has been treated as hybridizer trials.

**Table III.23.** Operating Conditions of Dry Coating Treatments in Turbula

Host Particles	Pre-Treatment in Hybridizer Velocity (rpm)	Guest Particles	Mass % of Guest Particles	Operating Velocity of Turbula (rpm)	Operating Time (min)	Batch Size (g)
PMMA	4000	Talc	1 %	96	6	30
	5600		5 %			
	9600					

The effect of mass percentage of talc on the coating strength and flowability properties of particles has been studied as it was done for hybridizer and cyclomix trials. At the end, the results of turbula have been compared with hybridizer, cyclomix and basic mixing trials.

#### 4.2.1. Measure of Solid Densities of the Dry Coated Particles

The solid densities of the particles that were treated by turbula have been measured and compared with the solid densities of the particles that were treated in hybridizer. It can be seen from the figure III.87, the solid densities of coated particle by turbula has similar values with calculated mixture values (eqn III.1). The reason is that, the particles stay inside a closed container so we can have an almost perfect particle recovery in turbula trials.

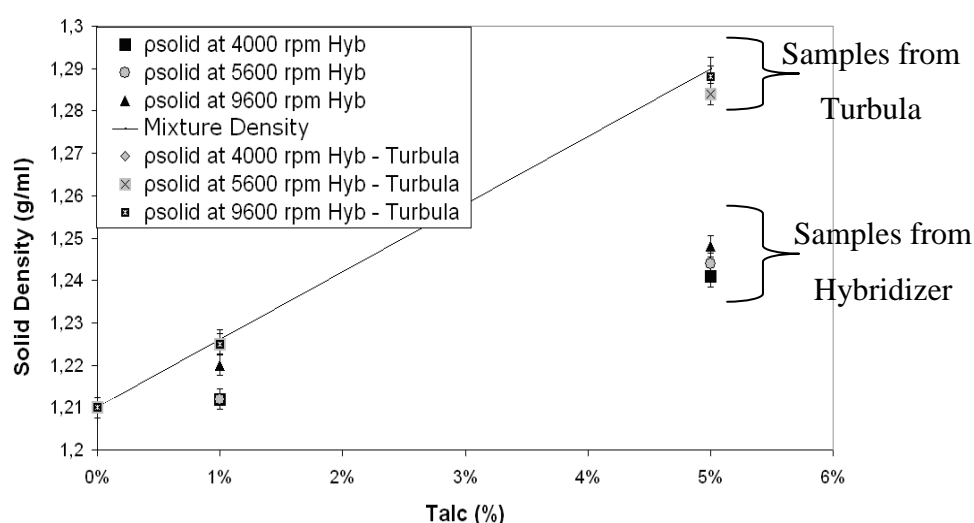


**Figure III.87.** Solid Densities of Coated Particles in Turbula and Hybridizer

It should also be remembered that the difference in the solid densities of the particles can be reason of sampling and inhomogeneity of the mixture.

#### 4.2.2. Characterization of Surface Morphology of the Particles

ESEM has also been used to observe the surface morphology of the coated particles by turbula as shown in the figure III.88. It can be seen that there are free agglomerates of talc particles in the 5% talc mixture because turbula doesn't give enough mechanical energy to de-agglomerate the talc particles.

On the other hand, the effect of pre-treatments in hybridizer can be distinguished easily. It was observed that at 9600 rpm pre-treatments in hybridizer, PMMA particles are broken at this velocity.

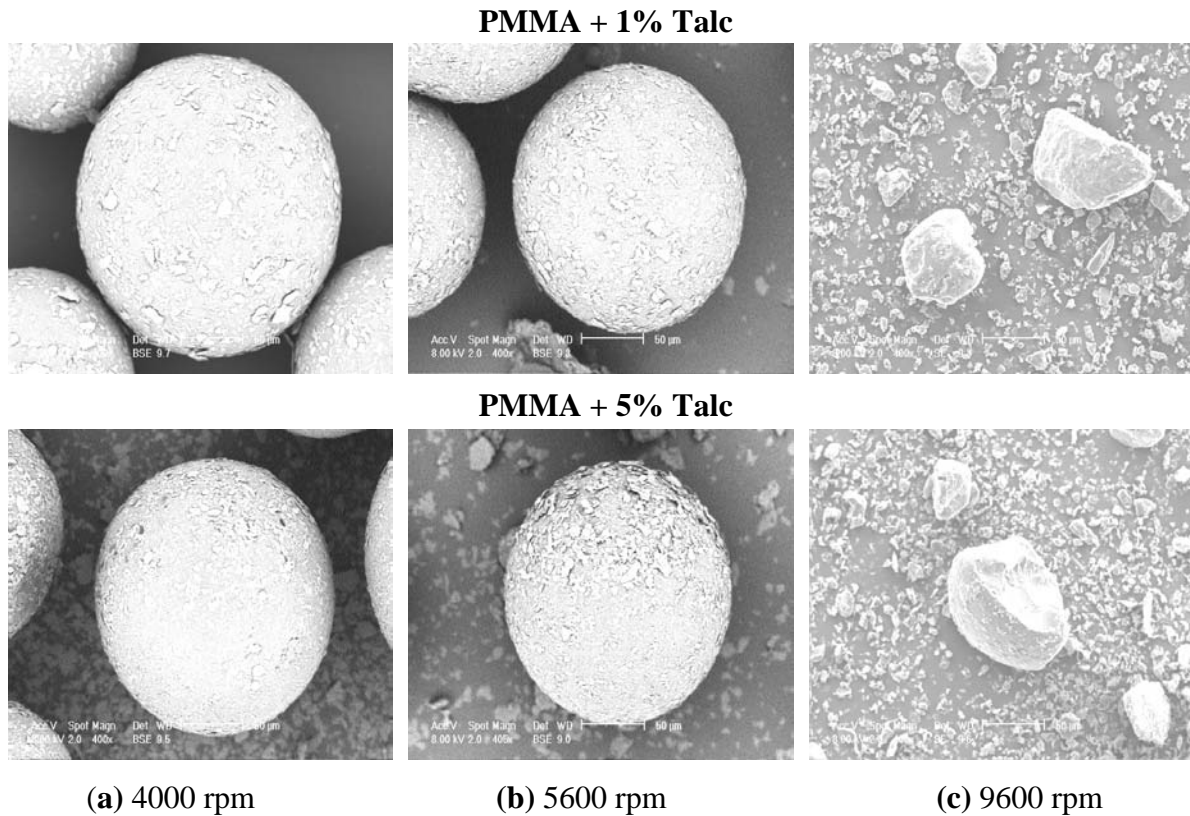


**Figure III.88.** Surface Morphology of Pre-Treated PMMA Particles in Hybridizer and Coated with 1% and 5% Talc Particles in the Turbula

#### 4.2.3. Characterization of Coating Strength of the Particles

The coating strength of the particles has been found by analysing the changes on the number particle size distributions of the particles. The effect of mass percentage of talc particles on the coating strength has been studied. Finally, the coating strength results of the particles that were treated by turbula have been compared with hybridizer, cyclomix and basic mixing trials.

##### A. Effect of Mass Percentage of Talc on Coating Strength of the Particles

The pre-treated PMMA particles (4000, 5600 9600 rpm in hybridizer) with 1% and 5% talc coating by turbula at 96 rpm for 6 minutes operating time can be seen in the figure III.89, III.90 and III.91.

It was observed that the particle liberation pressure is 1.0 bar for pre-treated PMMA particles at 4000 rpm coated with 1% talc by turbula and it decreases to 0.8 bar pressure for 5% talc coating.

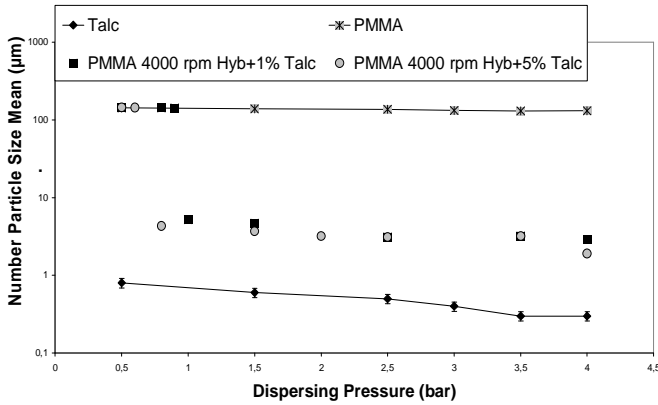


**Figure III.89.** Number Particle Size Mean vs. Dispersing Pressure for 4000 rpm Pre-treated PMMA with 1% and 5% Talc by Turbula

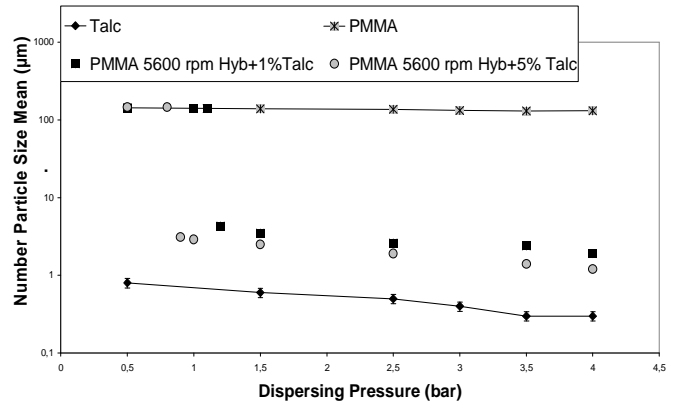


**Figure III.90.** Number Particle Size Mean vs. Dispersing Pressure for 5600 rpm Pre-treated PMMA with 1% and 5% Talc by Turbula

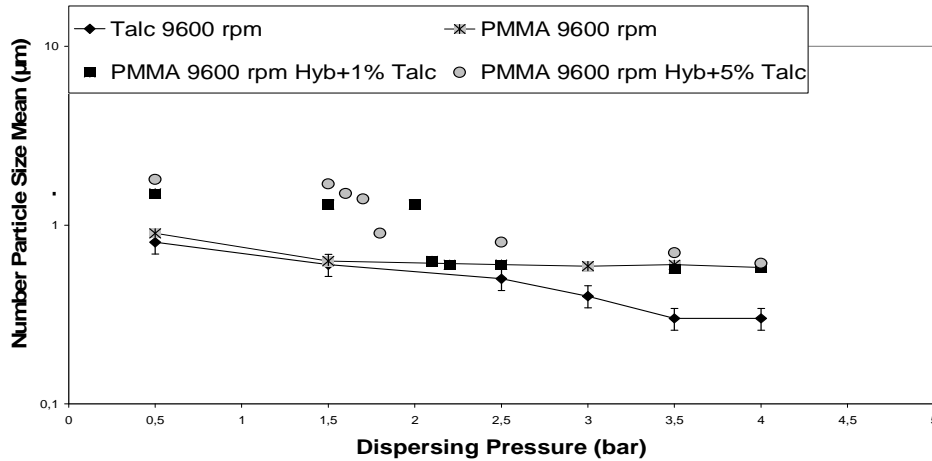


**Figure III.91.** Number Particle Size Mean vs. Dispersing Pressure for 9600 rpm Pre-treated PMMA with 1% and 5% Talc by Turbula

For 5600 pre-treated PMMA particles, the particle liberation pressure is 1.2 bar for 1% coating and 0.9 for 5% talc coating. The 9600 rpm pre-treated PMMA particles coated with talc particles by turbula has also similar coating strength characteristic. The particle liberation pressure is 2.1 bar for 1% talc coating and it decreases to 1.8 bar for 5% talc coating. As it can be seen from the table III.24, the particle liberation (or fragmentation) pressure is higher for 1% talc coatings than 5% talc coating for all the cases.

**Table III.24.** Dispersing Pressures and Air Velocities for Particle Detachment for 1% and 5% Talc Coated Particles by Turbula

Material	Dispersing Air Pressure	Air Velocity
PMMA 4000 rpm+ 1% Talc	1.0 bar	52 m/s
PMMA 5600 rpm+ 1% Talc	1.2 bar	60 m/s
PMMA 9600 rpm+ 1% Talc	2.1 bar	90 m/s
PMMA 4000 rpm+ 5% Talc	0.8 bar	44 m/s
PMMA 5600 rpm+ 5% Talc	0.9 bar	68 m/s
PMMA 9600 rpm+ 5% Talc	1.8 bar	81 m/s

**B. Effect of Equipment on Coating Strength of the Particles**

In order to understand the effect of equipment on the coating strength of the particles, the kinetic energy per mass has been simply calculated for each equipment according to operating velocities. The linear velocities have been calculated by using equation III.9 for corresponding rotational velocities of the equipments. Afterwards the kinetic energy per mass have been calculated by using equation III.10 the high shear mixers apply on the particles probably has an important role for that result.

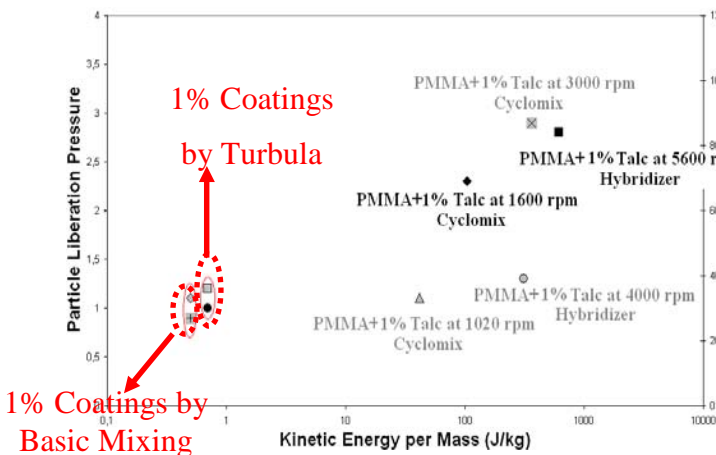


**Figure III.92.** Effect of Equipment on Particle Liberation Pressure for 1% Coated Particles

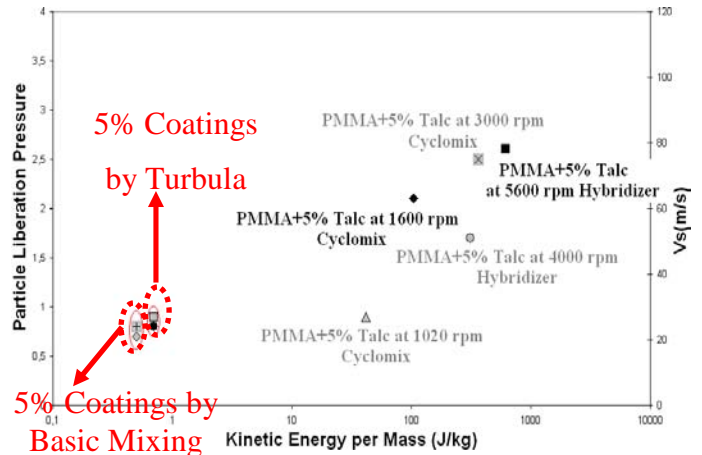


**Figure III.93.** Effect of Equipment on Particle Liberation Pressure for 5% Coated Particles

It can be seen from the figure III.92 and III.93, at 4000 and 5600 rpm pre-treated PMMA with 1% and 5% talc coatings by turbula have a little bit higher particle liberation pressures compared to basic mixing trials. On the other hand, it can be seen that the particle liberation

pressures of the particles that were treated by turbula or basic mixing have similar values with the particles that were treated at 1020 rpm in cyclomix. Moreover, it was observed that at higher velocities of hybridizer and cyclomix, the particle liberation pressures are much higher than turbula trials. The effect of mechanical energy that the high shear mixers apply on the particles probably has an important role for that result.

#### 4.2.4. Characterization of Flowability Properties of the Particles

The flowability properties of the particles have been analysed by using tapped & apparent densities and FT4 results. The effects of mass percentage of talc particles in the mixture and effect of equipment on the flowability properties of the particles has been studied.

##### A. Effect of Mass Percentage of Talc on Flowability Properties of the Particles

In this part of the study, the 1% and 5% talc coated particles have been compared with each other in order to understand the effect of the mass percentage on the flowability properties of the particles. In the figure III.94, evaluations of tapped densities of the coated particles are shown.

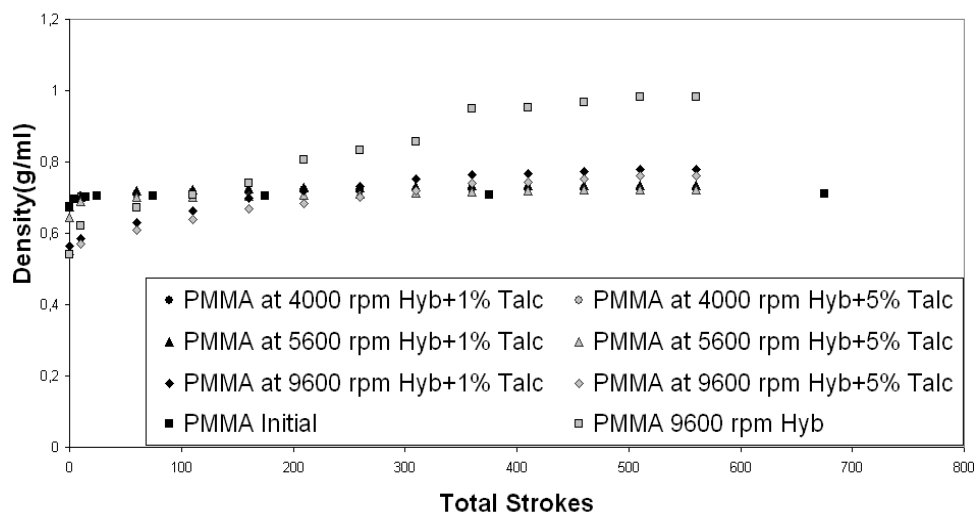


**Figure III.94.** Evaluation of Flowability of PMMA Particles Before and After Coating with 1% and 5% Talc by Turbula

It can be seen from the table III.25, 1% and 5% talc coated PMMA particles have better flowability than pre-treated PMMA particles in hybridizer. It was also observed that at 9600 rpm pre-treated PMMA particles in hybridizer have very bad flowability properties because of the particle fragmentation at this operating velocity of hybridizer. On the other hand, it was

observed that there is no significant difference between the results of 1% and 5% talc coated particles according to tapped and apparent densities.

**Table III.25.** Carr Index and Hausner Ratio for Coated and Uncoated PMMA Particles

Materials	Carr Index (%)	Flowability	Hausner Ratio
Initial PMMA	0.99 ± 0.02	Excellent	1.01 ± 0.02
PMMA at 4000 rpm Hyb	16.03 ± 0.04	Good	1.19 ± 0.04
PMMA at 5600 rpm Hyb	18.72 ± 0.05	Mediocre	1.23 ± 0.05
PMMA at 9600 rpm Hyb	35.81 ± 0.05	Very Bad	1.56 ± 0.05
PMMA 4000 rpm+1% Talc Turbula	3.32 ± 0.04	Excellent	1.03 ± 0.04
PMMA 5600 rpm+1% Talc Turbula	8.91 ± 0.05	Excellent	1.09 ± 0.05
PMMA 9600 rpm+1% Talc Turbula	27.53 ± 0.05	Bad	1.38 ± 0.05
PMMA 4000 rpm+5% Talc Turbula	3.70 ± 0.03	Excellent	1.04 ± 0.03
PMMA 5600 rpm+5% Talc Turbula	8.12 ± 0.03	Excellent	1.09 ± 0.03
PMMA 9600 rpm+5% Talc Turbula	29.40 ± 0.08	Bad	1.42 ± 0.08

The FT4 has also been used to study the flowability properties of the particles. The results of the FT4 trials can be seen from the figure III.95 and III.96. It can be observed that, at the end of the conditioning step we have obtained a homogeneous powder mixture (stable total energy value) for each sample.

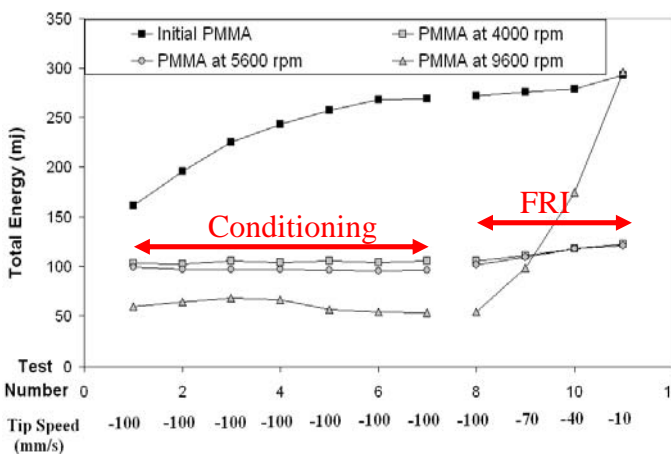


**Figure III.95.** FT4 Results of Initial and Pre - Treated PMMA Particles in Hybridizer

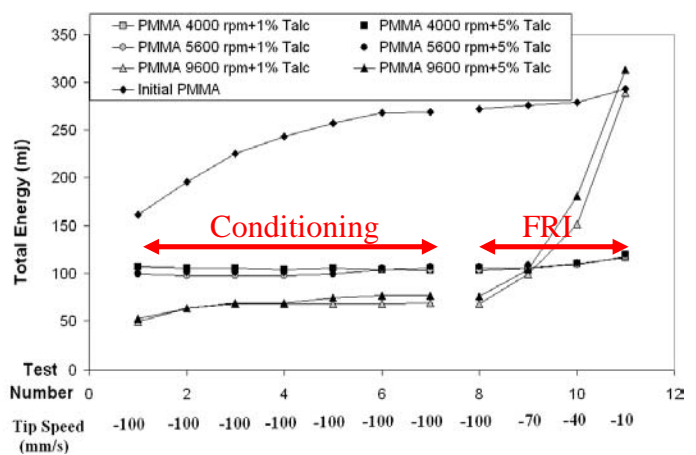


**Figure III.96.** FT4 Results of Initial and 1% & 5% Talc Coated (Pre – Treated) PMMA Particles by Turbula

It was observed that, the 1% and 5% talc coated PMMA particles have better flowability properties than just pre-treated PMMA particles as it was observed from the tapped and apparent density results. On the other hand, we didn't observe much difference between the FRI results of 1% and 5% talc coated PMMA particles. (table III.26)

**Table III.26.** Evaluation of Flowability of 1% and 5% Coated PMMA Particles by FT4

<b>Materials</b>	<b>8<sup>th</sup> Cycle (mj)</b>	<b>11<sup>th</sup> Cycle (mj)</b>	<b>FRI</b>
<b>Initial PMMA</b>	273 ± 0.03	293 ± 0.03	<b>1.10 ± 0.03</b>
<b>PMMA at 4000 rpm Hybridizer</b>	105 ± 0.05	122 ± 0.05	<b>1.16 ± 0.05</b>
<b>PMMA at 5600 rpm Hybridizer</b>	101 ± 0.05	121 ± 0.05	<b>1.20 ± 0.05</b>
<b>PMMA at 9600 rpm Hybridizer</b>	54 ± 0.08	296 ± 0.08	<b>5.48 ± 0.08</b>
<b>PMMA 4000 rpm+1% Talc Turbula</b>	105 ± 0.03	116 ± 0.03	<b>1.11 ± 0.03</b>
<b>PMMA 5600 rpm+1% Talc Turbula</b>	103 ± 0.05	117 ± 0.05	<b>1.14 ± 0.05</b>
<b>PMMA 9600 rpm+1% Talc Turbula</b>	68 ± 0.09	289 ± 0.09	<b>4.25 ± 0.09</b>
<b>PMMA 4000 rpm+5% Talc Turbula</b>	103 ± 0.04	119 ± 0.04	<b>1.16 ± 0.04</b>
<b>PMMA 5600 rpm+5% Talc Turbula</b>	107 ± 0.03	128 ± 0.03	<b>1.20 ± 0.03</b>
<b>PMMA 9600 rpm+5% Talc Turbula</b>	76 ± 0.08	313 ± 0.08	<b>4.12 ± 0.08</b>

### **B. Effect of Equipment on Flowability Properties of the Particles**

In this part of the study, the flowability properties of coated particles by turbula have been compared with the coated particles in hybridizer and cyclomix in order to understand the difference between a conventional mixer and high force mixers for the flowability properties of the particles.

It can be seen from the table III.27, the flowability of the coated particles in the high force mixers (hybridizer & cyclomix) have better flowability than coated particles by turbula. The generated high mechanical forces in high force mixers would cause de-agglomeration and better dispersion of talc particles on the surface of PMMA particles. On the other hand, lack of high mechanical forces causes fine particle agglomeration and a worse dispersion of talc



particles on the PMMA surface compared to composite particles from the high force mixers which would be the probable reason of this result.

**Table III.27.** Effect of Equipment on the Flowability Properties of Coated PMMA Particles

<b>Materials</b>	<b>8<sup>th</sup> Cycle (mj)</b>	<b>11<sup>th</sup> Cycle (mj)</b>	<b>FRI</b>
<b>Initial PMMA</b>	273 ± 0.03	293 ± 0.03	<b>1.10 ± 0.03</b>
<b>PMMA+5% Talc at 4000 rpm Hybridizer</b>	100 ± 0.05	109 ± 0.05	<b>1.09 ± 0.05</b>
<b>PMMA+5% Talc at 5600 rpm Hybridizer</b>	119 ± 0.05	135 ± 0.05	<b>1.13 ± 0.05</b>
<b>PMMA+5% Talc at 9600 rpm Hybridizer</b>	71 ± 0.05	287 ± 0.05	<b>4.04 ± 0.05</b>
<b>PMMA+5% Talc at 1020 rpm Cyclomix</b>	100 ± 0.01	110 ± 0.01	<b>1.10 ± 0.01</b>
<b>PMMA+5% Talc at 1600 rpm Cyclomix</b>	95 ± 0.04	106 ± 0.04	<b>1.12 ± 0.04</b>
<b>PMMA+5% Talc at 3000 rpm Cyclomix</b>	107 ± 0.06	126 ± 0.06	<b>1.18 ± 0.06</b>
<b>PMMA 4000 rpm+5% Talc Turbula</b>	103 ± 0.04	119 ± 0.04	<b>1.16 ± 0.04</b>
<b>PMMA 5600 rpm+5% Talc Turbula</b>	107 ± 0.03	128 ± 0.03	<b>1.20 ± 0.03</b>
<b>PMMA 9600 rpm+5% Talc Turbula</b>	76 ± 0.08	313 ± 0.08	<b>4.12 ± 0.08</b>

### 4.3. Conclusions

PMMA particles have been coated by different mass percentages of talc particles by turbula mixer in order to understand the difference between a conventional mixer and high force mixers (hybridizer & cyclomix) and their effect on the end-use properties of the particles.

The PMMA particles have been pre-treated in hybridizer at 4000, 5600 and 9600 rpm operating velocities (to be able to make a comparison with high force mixer trials) than they were coated with different percentage of talc particles by turbula. In the preliminary study, it was observed that there is no effect of turbula mixer on the fragmentation of the particles. Afterwards, the pre-treated PMMA particles have been coated with 1% and 5% of talc particles by turbula at 96 rpm operating velocity (maximum velocity of turbula) for 6 minutes. The visual analysis has also been done before and after coating. According to the ESEM analysis, it was observed that, we have obtained a discrete talc coating on the surface of PMMA particles in turbula trials like in hybridizer and cyclomix trials. On the other hand, it

was observed that there were free talc agglomerates in the mixture because of insufficient mechanical forces in turbula trials.

The laser diffraction granulometer has been used in order to understand the particle size evaluation and coating strength of the coated particles. The effect of mass percentage of talc particles on the coating strength of the particles has been studied. It was observed that particle liberation pressure decreases with increasing mass percentage of talc particles in the mixture. On the other hand, the results of coated particles by turbula have been compared with the results of coated particles in hybridizer, cyclomix and basic mixing methods in order to understand the effect of equipment on the coating strength of the particles. It was observed that coated particles by turbula have a little bit higher particle liberation pressures compared to basic mixing trials. On the other hand, it was observed that the treated particles by turbula have similar particle liberation pressures with the treated particles in cyclomix at low operating velocity (1020 rpm) but contrarily, at high operating velocities the coated particles in hybridizer and cyclomix have very high particle liberation pressures compared to treated particles by turbula mixer. The effect of mechanical energy that the high shear mixers (hybridizer & cyclomix) apply on the particles probably has an important role for that result. Moreover, as it has been discussed in the hybridizer and cyclomix trials, the granulometric results should be analysed carefully and it should be remembered that either particle breakage or guest particle liberation may cause difference in the particle size distributions of the particles with difference dispersing pressures.

As it was observed for the coated particles in hybridizer and cyclomix, talc coated PMMA particles have better flowability properties than just pre-treated PMMA particles for both 1% and 5% talc coatings. On the other hand, we didn't observe much difference in flowability properties between the results of 1% and 5% talc coated PMMA particles. It was also observed that the flowability properties of the coated particles in the high force mixers (hybridizer & cyclomix) have better flowability than coated particles by turbula since in high force mixers talc particles have better dispersion on the surface of PMMA particles.

At the end, it was seen that the dry coating of PMMA particles with talc particles is also possible by turbula. On the other hand, it was also observed that utilization of conventional mixers or high shear mixers for dry particle coating process modifies the end-use properties of the particles.

## 5. CONCLUSIONS

In this study, PMMA particles (host particle) with a volume mean particle diameter ( $d[4:3]_v$ ) around 160  $\mu\text{m}$  have been coated with 1% and 5% talc particles (guest particles) ( $d[4:3]_v:14\mu\text{m}$ ) by using different dry particle coating equipments in order to understand the effect of mass percentage of talc particles, effect of equipment and their operating conditions on the end-use properties of the new generated particles.

The feasibility of dry coating of the particles and their fragmentation behaviour has been studied in preliminary study of the particles. PMMA and talc particles have been treated individually in hybridizer, cyclomix and turbula with different operating conditions and afterwards, the operating conditions have been determined for dry coating trials.

### 5.1. Visual Analysis of The Dry Coated Particles in Different Equipments

Environmental scanning electron microscopy (ESEM) has been used to observe the surface morphology of the coated particles by each equipment. It was observed that for all the mixers that we have used and also for basic mixing trials, we have obtained a discrete type of talc coating on the PMMA particles.

The difference in the surface coverage of the particles is related to the mechanical force that the equipment applies on the particles coating. Hybridizer and cyclomix uses mechanical impact, compression and shearing forces in order to coat the particles. Due to these mechanical forces, the talc particles are forced on the surface of the PMMA particles and we have obtained embedded talc particles on the PMMA particles.

On the other hand, turbula is a conventional mixer and it uses very low centrifugal forces to coat the particles. As it would be expected, the impact of the particles is much less and softer compared to high force mixers. Because of that reason, it was observed that the talc particles are just firmly attached on the surface of PMMA particles in turbula and basic mixing trials. In addition, the lack of applied mechanical forces on the particles in turbula and basic mixing trials, we have observed that there are some free talc agglomerates in the mixture. The generated force is not sufficient to break the agglomerates of talc particles and attach them on the surface of the PMMA particles, because of that reason the agglomerates rest in the powder sample in turbula and basic mixing.

## 5.2. Coating Strength of The Dry Coated Particles in Different Equipments

The coating strength of the coated particles by different dry coating equipments have been analysed by using a laser diffraction granulometer with dry feed mode. According to evaluation in the particle size distributions of the particles, the particle liberation pressures have been found.

The effect of operating velocity on the particle liberation pressure has been studied. It was seen that the particle liberation pressure increases with increasing operating velocity for hybridizer and cyclomix trials. The generated mechanical forces by the mixers are directly related to the operating velocity of the equipments. So, higher velocity would generate higher mechanical forces and higher mechanical forces would cause stronger interactions between the host and guest particles. As it was observed in the visual analysis, high mechanical forces in hybridizer and cyclomix enables us to obtain embedded talc particles on the PMMA surface.

The effect of mass percentage of talc particles on the coating strength of the particles has also been studied. It was observed that particle liberation pressure decreases with increasing mass percentage of talc particles in the mixture for cyclomix, turbula and basic mixing trials. But for dry coated particles in hybridizer, it was observed that for different operating velocities, mass percentages of talc particles have different effects on the coating strength of the particles.

In order to understand the effect of equipment on the coating strength of the particles, the kinetic energy that the equipment generates was simply calculated by using the operating velocity of the equipment. It was seen that the dry coated particles in hybridizer and cyclomix have much higher particle liberation pressures compared to coated particles by turbula and basic mixing method. It was observed that the particle liberation values increase with increasing calculated kinetic energy per mass values which is directly related to operating velocity of the equipment.

There is an important point that should be remembered that the evolution of the particle size distributions with different dispersing pressures could be related to particle detachment and also particle fragmentation.

### **5.3. Modification of Flowability Properties of Dry Coated Particles in Different Equipments**

The flowability properties of PMMA particles before and after dry coating with talc particles in different equipments has been analysed by using Freeman Technology powder tester (FT4) and a tapped density tester.

In hybridizer trials, it was observed that the dry coated PMMA particles with talc (1% & 5%) have better flowability properties than treated PMMA particles in hybridizer. Also it can be observed that the high operating velocities of the hybridizer decrease flowability of the particles due to the particle breakage that causes increase in the contact surface of the particles.

In cyclomix trials, it was observed that both the dry coated PMMA particles (1% & 5%) and individually treated PMMA particles (except at 3000 rpm) in cyclomix have very good flowability properties. In cyclomix trials, there is almost no particle fragmentation at any operating velocities so it would be the reason for the particles to have good flowability properties. At 3000 rpm, (maximum velocity of cyclomix), the flowability becomes mediocre for individually treated PMMA particles at this operating velocity but it becomes excellent after dry coating with talc particles.

In turbula trials, it was seen that the dry coated PMMA particles (1% & 5%) have better flowability than pre-treated PMMA particles in hybridizer. The flowability properties of dry coated particles in different equipments have also been compared. It was seen that the dry coated particles in hybridizer and cyclomix have better flowability properties than dry coated particles by turbula. As it has been discussed before, high force mixers apply high mechanical force on the particles which causes de-agglomeration and good dispersion of talc particles on the surface of the PMMA particles. On the other hand, in turbula trials there are some talc agglomerates because the mechanical energy that the turbula generates is not high enough to break the agglomerates and disperse them on the PMMA surface. So this may explain the difference between flowability properties of particles from hybridizer, cyclomix and conventional turbula mixer.

The host and guest particle size on the end–use properties of the particles may also have an important role. In Chapter IV, 2 different particle size distributions of Cellets and Talc particles has been chosen as the second model couple, in order to understand influence of particle size ratio between the host and guest particles on the end–use properties of the

particles. Mechanical strength is tried to be related to an estimation of the energy provided in every process, and to the theoretical calculation of the van der Waals forces (initial 'affinity'). The hydrophilic properties of the powders will be studied by dynamic vapour sorption and angle of contact characterization methods.

## CHAPTER IV

### *Effect of Particle Size on the End–Use Properties of the Composite Particles*





## 1. INTRODUCTION

In the second part of this thesis, the aim is to understand the effect the particle size of host and guest particles on the end–use properties of the dry coated particles. For this reason, Cellets particles (with 2 different particle size distributions) and Talc particles (with 2 different particle size distributions) have been chosen as the second model couple of the study for dry coating.

In the first part, in order to understand the effect of host particle size on the end–use properties of the particles, Cellets 90 ( $d_{[4;3]_v}:100 \mu\text{m}$ ) and Cellets 200 ( $d_{[4;3]_v}:305 \mu\text{m}$ ) particles have been coated with talc particles ( $d_{[4;3]_v}:14 \mu\text{m}$ ) by different dry particle coating equipments. The Nara Hybridizer, Hosokawa Cyclomix and a Turbula Mixer have been used to coat the particles. In addition, Cellets 90 and Cellets 200 particles have also been mixed with talc particles by basic mixing method. These samples will be compared with those prepared with the Hybridizer, Cyclomix and Turbula.

In the second part, Cellets 200 ( $d_{[4;3]_v}:305 \mu\text{m}$ ) particles and talc particles with 2 different particle size distributions ( $d_{[4;3]_v}:14 \mu\text{m}$  and  $d_{[4;3]_v}:4 \mu\text{m}$ ) were chosen for dry coating trials to study the influence of the guest particle size on the end–use properties of the particles. Hybridizer, Cyclomix and Turbula have also been used for dry coating of the Cellets 200 particles with different particles sizes of talc particles.

The preliminary study of the particles was investigated in order to understand fragmentation behaviour of the particles and also to define the operating conditions for dry coating trials in different equipments. Several characterisation methods have been used to study the physico–chemical properties of the initial and coated particles. Environmental Scanning Electron Microscopy (ESEM) was used before and after dry coating trials for visual analysis of the particles. An Atomic Force Microscopy (AFM) has also been used in order to understand the guest particle deposition on the host particle surface, to analyse the surface morphology of the particles and also to find the adhesion forces between the particles. The initial affinity of the powders has been studied by calculation of Van der Waals forces between the particles. The particle size distributions and coating strength of the composite particles have been studied by laser diffraction (in dry feed mode). Coating strength is tried to be related to an estimation of the energy provided in each process to understand the effect of equipment. Also the hydrophilic properties of the powders have been studied before and after the coating by dynamic vapour sorption (DVS) and contact angle characterization methods. The amount of

guest particle deposition on the host particle has also been calculated by using the model for adhesion force.

## **2. EFFECT OF HOST PARTICLE SIZE ON THE END – USE PROPERTIES OF THE DRY COATED PARTICLES**

Here, Cellets 90 ( $d_{[4;3]_v}$ :100  $\mu\text{m}$ ) and Cellets 200 ( $d_{[4;3]_v}$ :305  $\mu\text{m}$ ) particles have been coated with talc particles ( $d_{[4;3]_v}$ :14  $\mu\text{m}$ ) by different dry particle coating equipments in order to understand the effect of host particle size on the end–use properties of the coated particles. In the preliminary study, Cellets 90 and Cellets 200 particles have been individually treated in Hybridizer and Cyclomix with different operating velocities. At the end of the preliminary study, the optimum operating conditions for the dry coating trials have been defined.

The theoretical monolayer coating percentage for hexagonal surface packing has been calculated for Cellets 90 and Cellets 200 particles and the mass percentages of talc particles for each dry coating trial has been found. In this part, the results of the different characterization methods for powders before and after talc coating have been presented in details.

### **2.1. Preliminary Study of Cellets 90 and Cellets 200 Particles**

In the preliminary study, Cellets 90 and Cellets 200 particles have been individually treated with different operating velocities of the different dry coating equipments for 6 minutes operation time. The particle size of the final cellets particles have been determined with the Malvern Mastersizer laser diffraction granulometer and expressed as the  $d_{[4;3]_v}$  or volume mean diameter. In addition, we have also determined the yield of the hybridizer and cyclomix trials which is the percentage of material removed from the devices at the end of an experiment with respect to the introduced amount at the start.

In Hybridizer trials, samples of Cellets 90 and Cellets 200 have been processed alone for 6 minutes at 4000 rpm (25 m/s), 5600 rpm (35 m/s), and 9600 rpm (60 m/s) rotational velocities. For each trial, initial powder charge was fixed at 30 g.

In Cyclomix trials, 1600 rpm (13.4 m/s), 1900 rpm (15.9 m/s) and 2600 rpm (21.8 m/s) rotational velocities and 6 minutes operating time have been chosen as operating conditions for preliminary study of the Cellets particles. The initial filling of the equipment has been fixed at 500 ml for the treatments.

### 2.1.1. General Mass Balance

In hybridizer trials, 30 g of cellets 90 and cellets 200 particles were individually processed in the hybridizer at 4000 rpm, 5600 rpm and 9600 rpm operating velocities for 6 minutes. At the end, the treated particles were recovered from the powder collector. For each operating velocity, the percentage of recovery for cellets 90 and cellets 200 particles has been calculated by dividing the amount of recovered powder to the initial charge (30g). In the figure IV.1, the % of the recovered powder according to different operating velocities is presented.

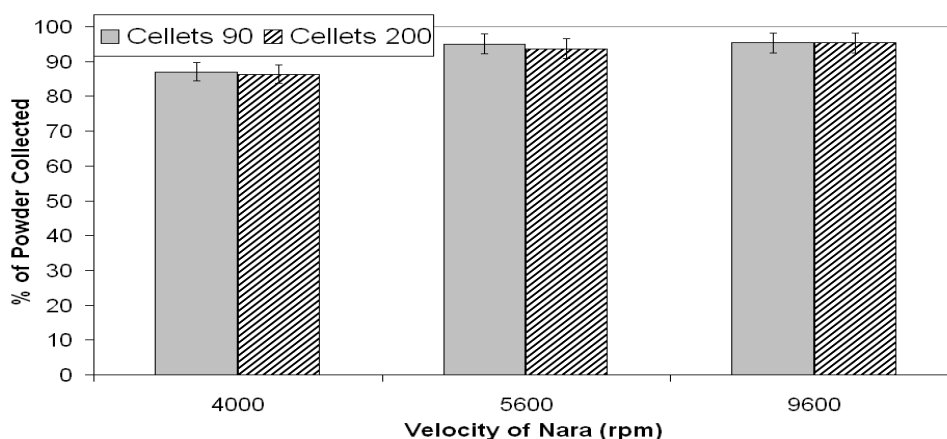


**Figure IV.1.** Effect of Rotational Velocity of Hybridizer on the Amount of Collected Particles

It can be seen that the percentage of recovery for hybridizer trials are very high for both cellets 90 and cellets 200 particles. It was observed that the percentage of recovery is about 87% at 4000 rpm and it increases to 95% at 9600 rpm operating velocity. High operating velocity causes good recirculation of the powders inside the hybridizer, so higher the operating velocity the higher the percentage of particle recovery.

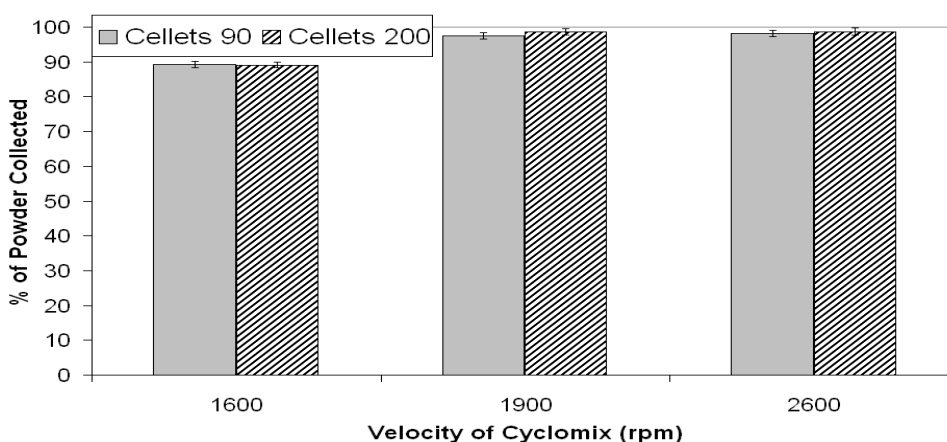


**Figure IV.2.** Effect of Rotational Velocity of Cyclomix on the Amount of Collected Particles

In cyclomix trials, 500 ml cellets 90 and cellets 200 particles have been individually treated at 1600 rpm, 1900 rpm and 2600 rpm for 6 minutes operating time. The results of particle recovery for each operating velocity are shown in the figure IV.2. It can be seen that there is a high percentage of particle recovery (between 89% and 98%) for each operating velocity.

### 2.1.2. Effect of Rotational Velocity on Particle Size Distributions

The particle size distribution analyses of cellets 90 and cellets 200 particles have been measured for each chosen operating velocities of hybridizer and cyclomix by using the laser diffraction granulometer. The figures IV.3 and IV.4 show the volume and number particle size distributions of cellets 90 and cellets 200 particles before and after treatments in hybridizer with different operating velocities.

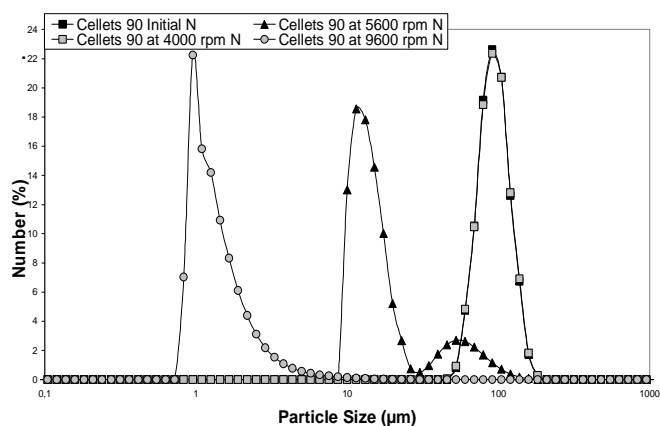
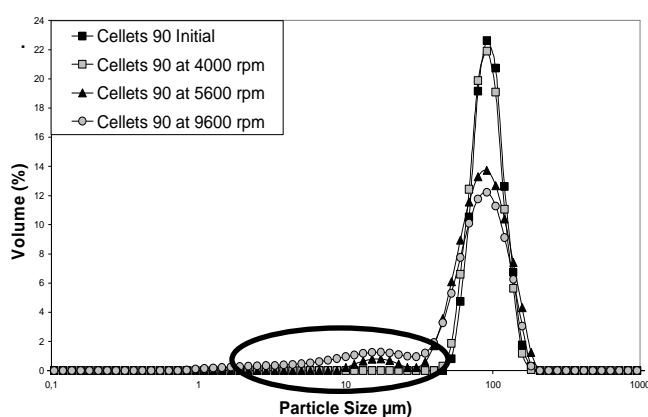


**Figure IV.3.** Volume Particle Size Distribution of Cellets 90 Particles Before and After Treatments in Hybridizer

**Figure IV.4.** Number Particle Size Distribution of Cellets 90 Particles Before and After Treatments in Hybridizer

It can be seen that the treated cellets 90 particles at 5600 rpm and 9600 rpm have a fine particle population compared to initial and 4000 rpm treated cellets 90 particles because of particle fragmentation. The fine population can be distinguished easily by the number particle size distributions (Fig. IV.4).

At 4000 rpm, the particles have the same particle size distribution with initial cellets 90 particles, because of no particle breakage at this operating velocity. For 5600 rpm treatments, there are two different particle populations, big particles at around 90–100 µm and a fine population at around 20 µm. This shows that some of the particles are broken in the treatments. For 9600 rpm processing the fine particle population decreases to 1 µm and it also shows that most of the particles are broken.

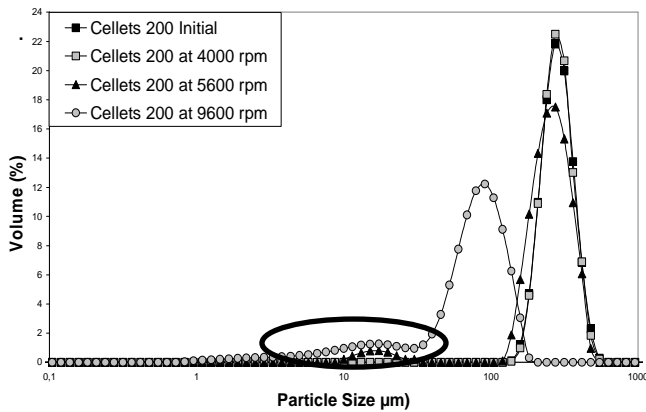


**Figure IV.5.** Volume Particle Size Distribution of Cellets 200 Particles Before and After Treatments in Hybridizer

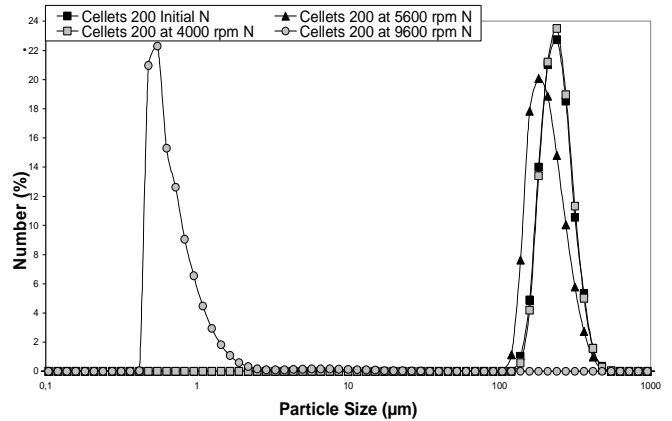


**Figure IV.6.** Number Particle Size Distribution of Cellets 200 Particles Before and After Treatments in Hybridizer

Figure IV.5 and IV.6 show the volume and number particle size distributions of treated cellets 200 particles in hybridizer with different operating velocities. It can be seen that, 4000 rpm treatments doesn't cause particle fragmentation. On the other hand, for 5600 rpm and 9600 rpm treatments, a fine particle population was observed because of particle breakage at these operating velocities. The volume mean diameter of the treated cellets 90 and cellets 200 particles and the percentage of recovery after the trials in hybridizer for each operating velocity can be seen in the figure IV.7 and IV.8.

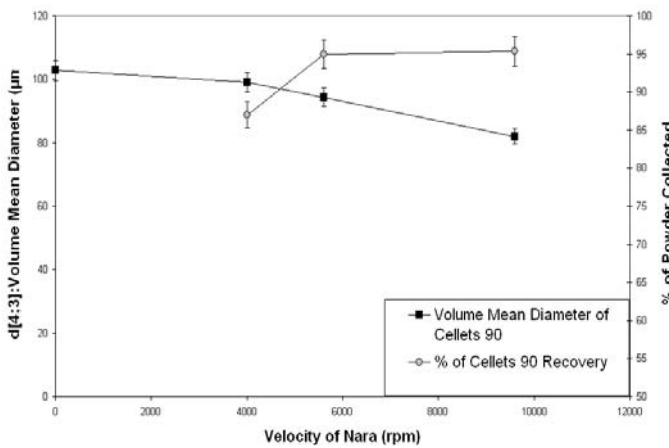


**Figure IV.7.** Volume Mean Diameter vs. % of Recovery for Treated Cellets 90 Particles in Hybridizer

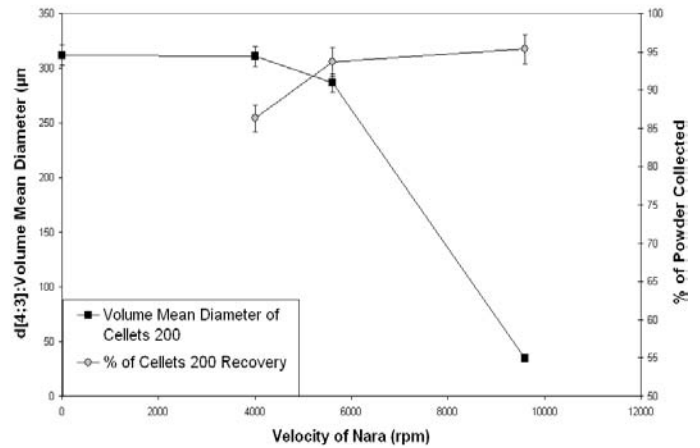


**Figure IV.8.** Volume Mean Diameter vs. % of Recovery for Treated Cellets 200 Particles in Hybridizer

It can be seen that the powders, which were processed at low speeds of rotation, have an initial particle size  $d[4;3]$  of about 100 µm for Cellets 90 and 305 µm for Cellets 200, but the

mean particle size reduces with rotational velocities greater than 5600 rpm. This indicates that there is particle breakage at these high operating velocities. This is confirmed by visual observations with ESEM as shown in the fig. IV.9. It was observed that there are some particle fragments in 5600 and 9600 rpm treatments for cellets 90 and cellets 200 particles because of the generation of high mechanical forces by the equipment at these velocities. It can be seen that there are more cellets 90 fragments at 9600 rpm treatment compared to 5600 rpm treatments as expected.

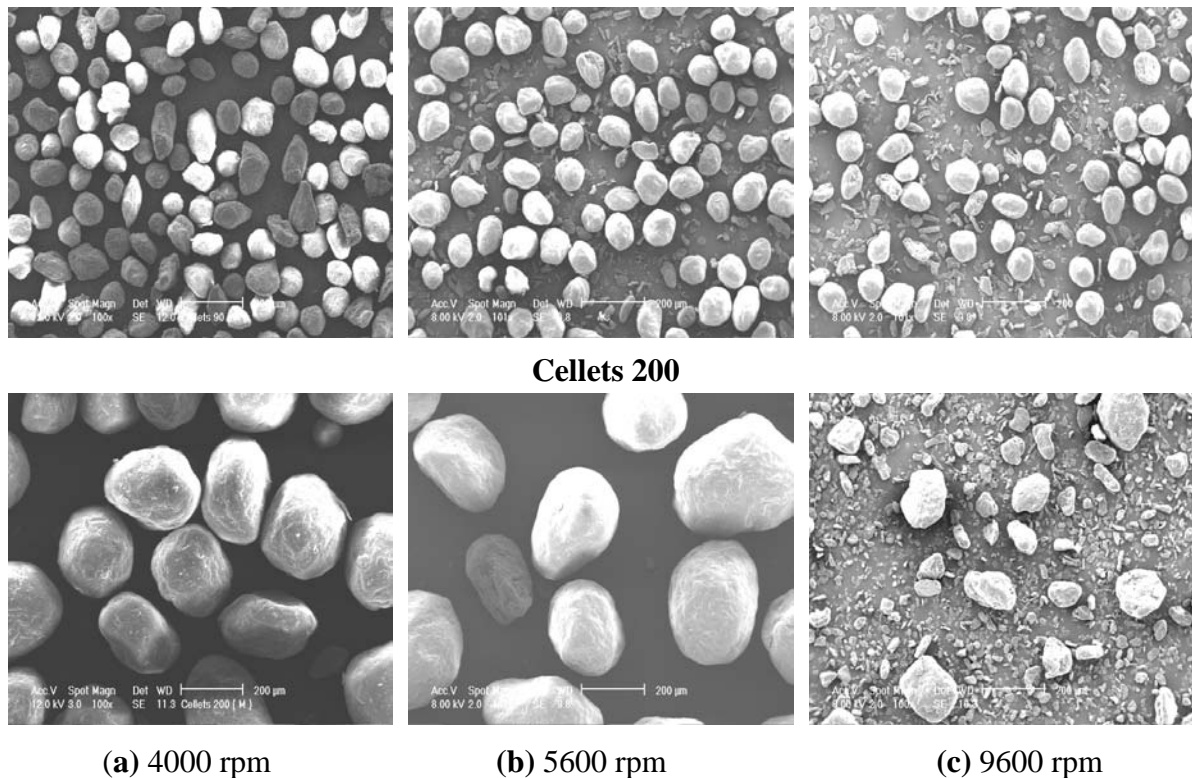


**Figure IV.9.** Surface Morphology of Cellets 90 and Cellets 200 Particles after Treatments in Hybridizer

The volume and number particle size distributions of treated particles in cyclomix have also been determined. The particle size distributions of cellets 90 and cellets 200 particles before and after treatments in cyclomix with different operating velocities can be seen in the figure IV.10 and IV.11.

It was observed that, the initial and treated cellets 90 particles have the same particle size distributions (volume) for all operating velocities of cyclomix. On the other hand, at 1900 and 2600 rpm treatments the number particle size distributions are around 70  $\mu\text{m}$ . This may indicate a slight fragmentation of the particles at these velocities.

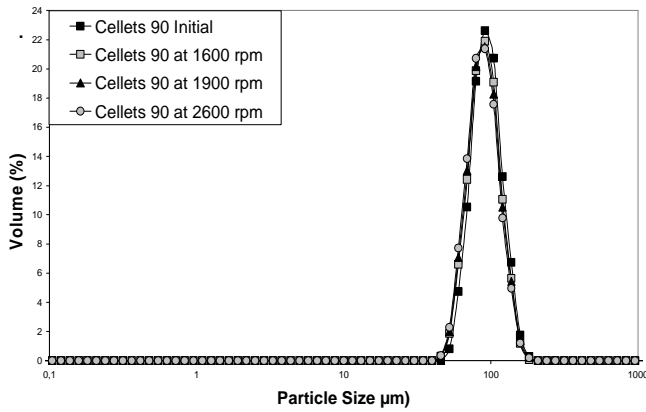


**Figure IV.10.** Volume Particle Size Distribution of Cellets 90 Particles Before and After Treatments in Cyclomix

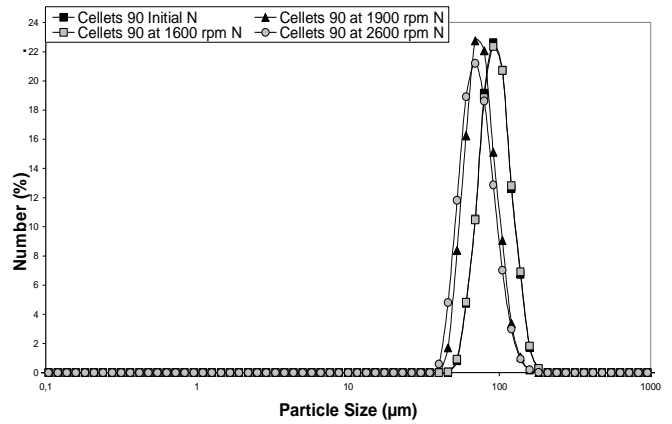


**Figure IV.11.** Number Particle Size Distribution of Cellets 90 Particles Before and After Treatments in Cyclomix

Figure IV.12 and IV.13 show the particle size distributions of initial and treated cellets 200 particles in the cyclomix. It was observed that, at 1600 rpm treatments the cellets 200 particles keep initial particle size distribution. Contrary to 1600 rpm treatments, at 1900 and 2600 rpm treatments there are fine particle populations.

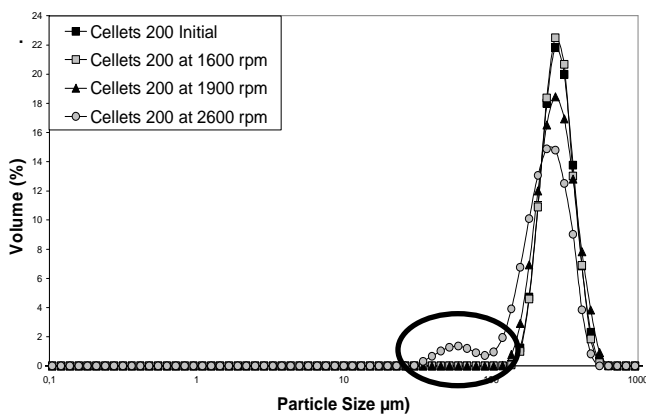


**Figure IV.12.** Volume Particle Size Distribution of Cellets 200 Particles Before and After Treatments in Cyclomix

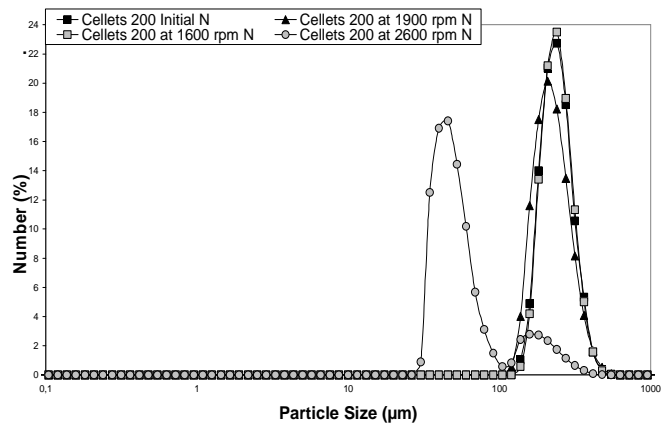


**Figure IV.13.** Number Particle Size Distribution of Cellets 200 Particles Before and After Treatments in Cyclomix

The volume mean diameter of the treated cellets 200 particles for each operating velocity of cyclomix and particle recovery after the trials can be seen in the figure IV.14 and IV.15. It can be seen that the volume mean particle size distribution decreases at high operating velocities because of the particle fragmentation.

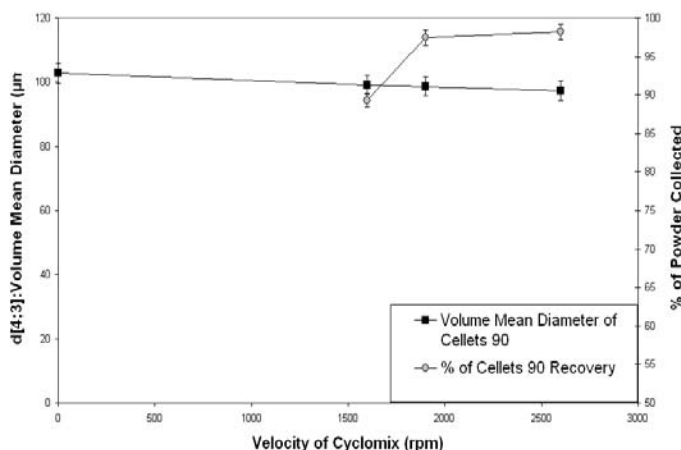


**Figure IV.14.** Volume Mean Diameter vs. % of Recovery for Treated Cellets 90 Particles in Cyclomix

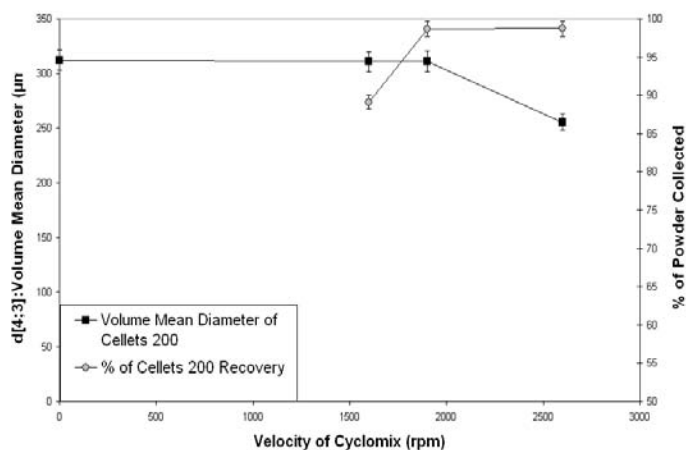


**Figure IV.15.** Volume Mean Diameter vs. % of Recovery for Treated Cellets 200 Particles in Cyclomix

ESEM has also been used to have visual analysis of the particles. As it can be seen in the fig.IV.16 there is no particle fragmentation either cellets 90 and cellets 200 particles at 1600 rpm treatments. At 1900 and 2600 rpm treatments, high mechanical forces cause some particle breakage.

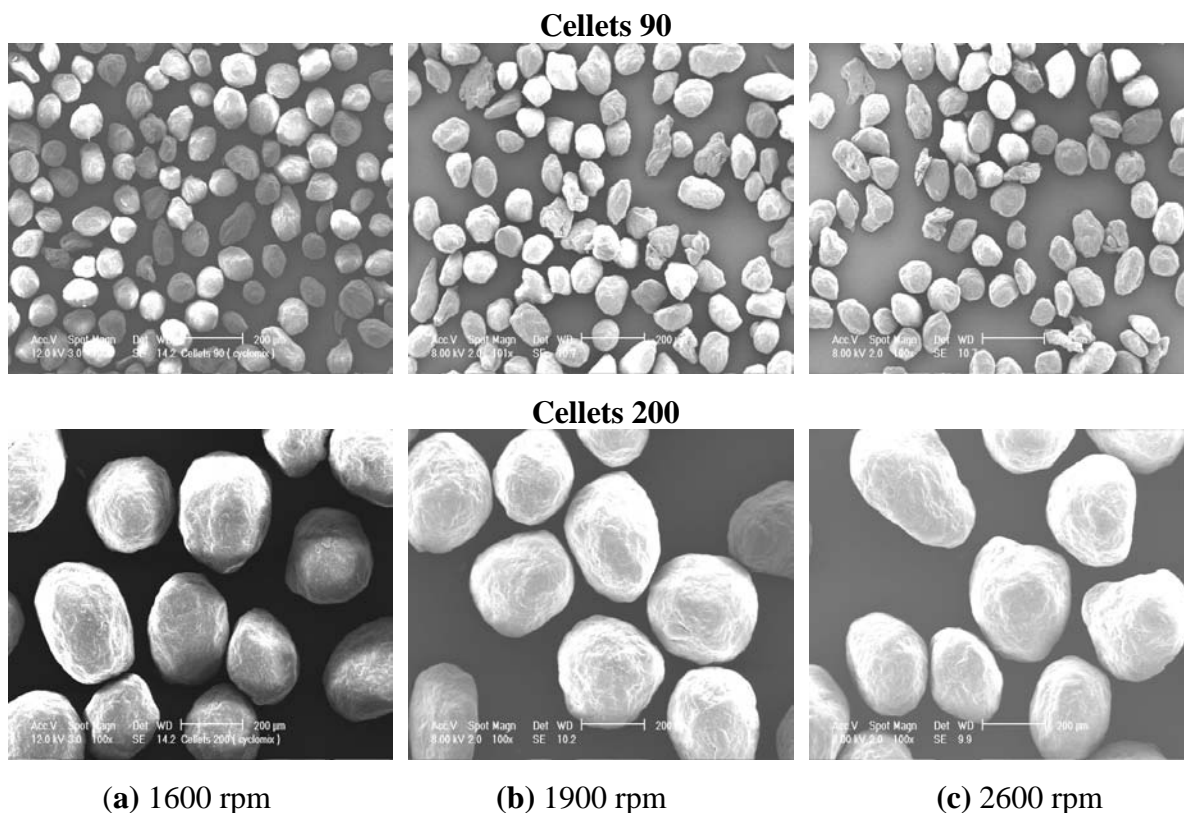


**Figure IV.16.** Surface Morphology of Cellets 90 and Cellets 200 Particles after Treatments in Cyclomix



To understand the effect of host particle size on coating strength of the particles we have to protect our host particles against particle breakage. For this reason, we chose rotational speeds where the host particles retain the initial particle size distribution. For the hybridizer trials 4000 rpm and for the cyclomix trials 1600 rpm has been chosen as the operating velocities. For turbula and basic mixing trials 4000 rpm has been chosen for pre-treatments of cellets particles in hybridizer.

## 2.2. Dry Coating of Cellets 90 and Cellets 200 with Talc

In the preliminary study, the operating conditions for dry coating of cellets particles with talc have been determined. Monolayer coating percentage in hexagonal packing of the cellets 90 and cellets 200 particles has been calculated (Appendix II). It was found that, 9.6 % talc for cellets 90 particles and 3 % talc for cellets 200 particles are needed for monolayer coating of the cellets particles. The operating conditions of the dry coating trials can be seen in the table IV.1.

**Table IV.1.** Operating Conditions of Dry Coating Treatments

Host Particles	Guest Particles	Equipment	Operating Velocity (rpm)	Operating Time (min)	Mass % of Guest Particles	Batch Size (g)	Cooling Jacket (°C)
Cellets 90	Talc	Hybridizer	4000	6	9.6 %	30	13
Cellets 200					3 %		
Cellets 90	Talc	Cyclomix	1600	6	9.6 %	500	13
Cellets 200					3 %		
PreTreated Cellets 90	Talc	Turbula	96	6	9.6 %	30	none
PreTreated Cellets200					3 %		

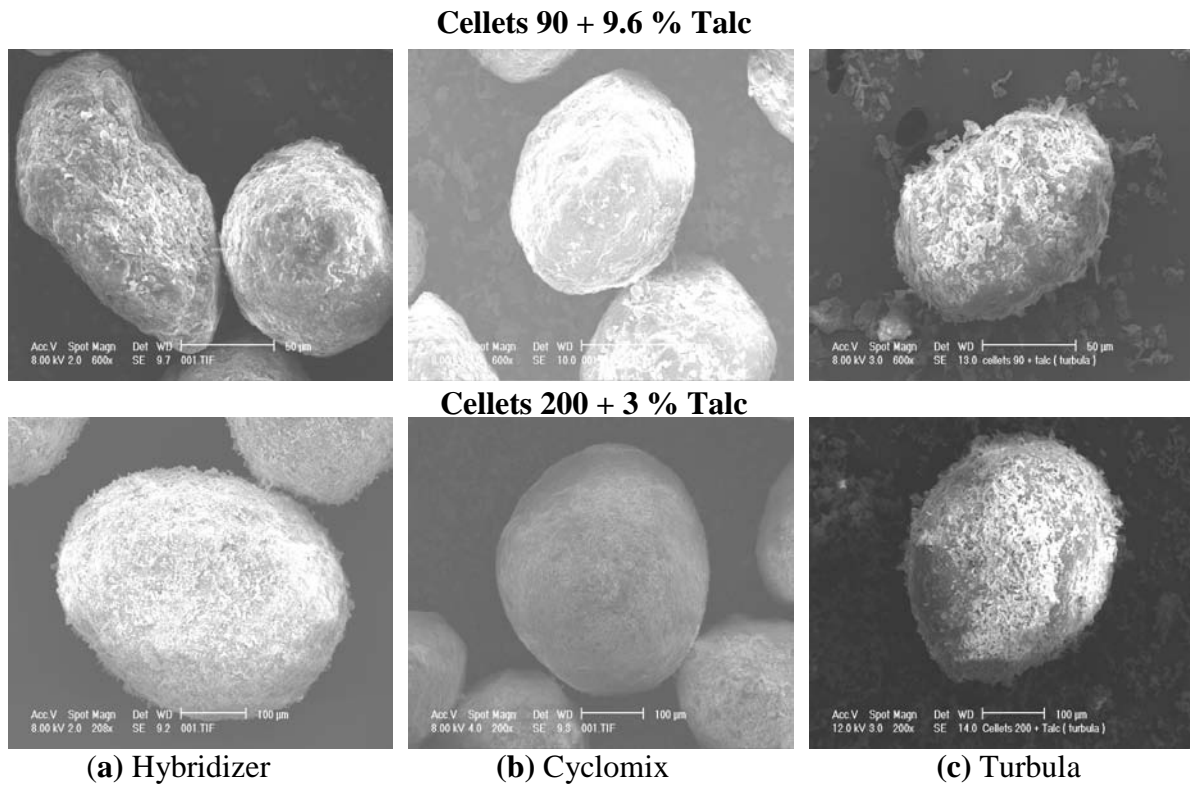
In Turbula trials, cellets 90 and cellets 200 particles were pre-treated in hybridizer at 4000 rpm rotational velocity. Afterwards, the pre-treated cellets particles have been processed with talc particles in a 1 L container (30 g) at 96 rpm operating velocity for 6 minutes by turbula.

In addition, the basic mixing method has been also used for dry coating of the particles. In basic mixing, cellets 90 and cellets 200 particles are pre-treated in hybridizer at 4000 rpm operating velocity and then mixed with talc particles by shaking them by hand as for the PMMA and talc model couple (chapter III).

Different characterization methods have been used before and after dry coating trials to understand the effect of host particle size on the end-use properties of the coated particles. More precisely, we are interested to understand the effect of host particle size on the coating strength of the particles and also on the modification of hydrophilic properties of the particles. ESEM has been used for morphological analysis of the particles before and after coating. AFM has also been used in order to understand the topographical properties of the particles and to find the adhesion forces between the particles. The adhesion force values also enable us to calculate the guest particle deposition on the host particle by the adhesion force model. Malvern Mastersizer laser diffraction granulometer has been used to analyse the coating strength properties of the particles. On the other hand, Dynamic vapour sorption (DVS) and contact angle methods have been used to understand the evolution of the hydrophilic properties of the particles after coating with talc particles.

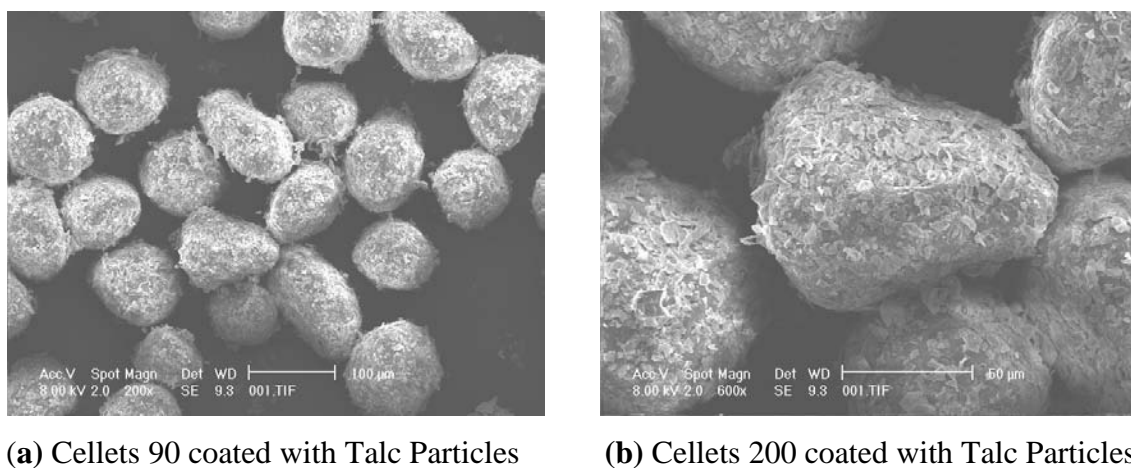
### **2.2.1. Characterization of Surface Morphology of the Particles**

Figure IV.17 shows the ESEM images of talc coated cellets 90 and cellets 200 particles in different equipments. It can be seen that there is no particle fragmentation of coated particles in any of the dry coating equipment. It was observed that, there are some talc agglomerates in the cellets 90 coated with 9.6% talc particles probably because of the high mass percentage of talc particles in the mixture. It can be seen that, there are many talc agglomerates in the turbula trials but on the other hand there are very few amount of talc agglomerates for hybridizer and cyclomix trials. This shows us the effect of applied mechanical forces on the particles by the equipments. It was also observed that for hybridizer and cyclomix trials, most of the talc particles are embedded on the surface of the cellets particles but for turbula trials it can be seen that talc particles are weakly attached on the surface of the host particles.



**Figure IV.17.** Surface Morphology of Monolayer Talc Coated Cellets 90 and Cellets 200 Particles in Different Equipments

The visual analysis has also been done for the coated particles from the basic mixing method. It can be seen that there are talc agglomerates on the surface of the cellets particles (fig. IV.18 & IV.19). It was also observed that the talc particles are just attached on the surface of the cellets particles because of the inter-particle forces between the particles.



**Figure IV.18.** Surface Morphology of Monolayer Talc Coated Cellets 90 and Cellets 200 Particles by Basic Mixing Method

The Scanning Electron Microscope is equipped with an Energy Dispersive Spectrometer (EDS). SEM/EDS provides chemical analysis of regions of minute particles (chapter II). The SEM/EDS was used to analyse the chemical composition of the coatings. Figure IV.19 shows the SEM/EDS results of an example of a talc coated cellets 90 particle in hybridizer. It can be seen that in one of the regions of the particle surface, we have silicon and magnesium which are the chemical components of talc. This shows the existence of talc particles on the surface. On the other hand, it was observed that in another region of the surface of the cellets 90 particle there was neither silicon nor magnesium so this part of the surface there is no talc particle. The result shows that we have obtained a discrete talc coating on the surface of cellets 90 particle. The same study has also been done for cyclomix and turbula trials and it was observed that for all equipments we have obtained discrete type of coating. (Appdix.VII)

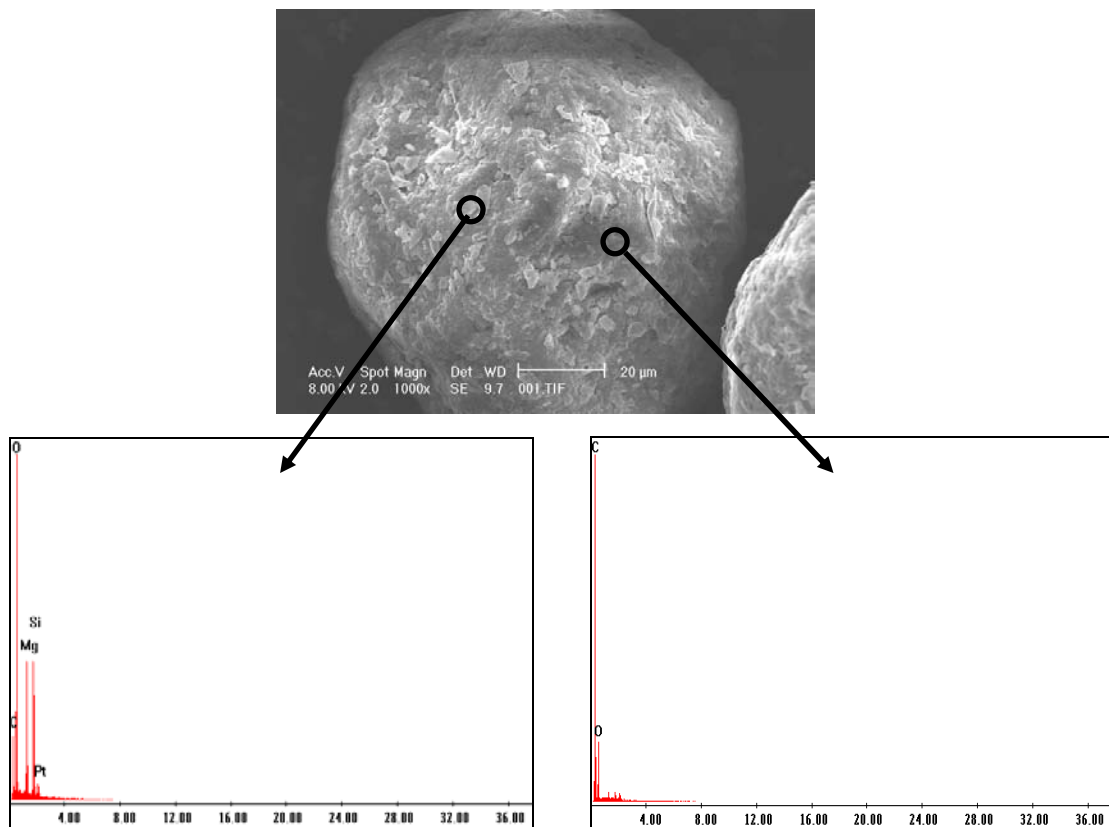


**Figure IV.19.** Chemical Analysis of the Surface of Talc Coated Cellets 90 Particle in Hybridizer

### 2.2.2. Characterization of the Particles by Atomic Force Microscopy

The topographical analysis of the coated and uncoated cellets 90 and cellets 200 particles have been done by using an Atomic Force Microscopy (AFM). The adhesion force between

the particles has also been found by using the AFM with contact mode and afterwards the guest particle deposition on the host particles has been calculated by using the adhesion force model. (Eqn.III.8)

### A. Topographical Analysis of the Particles

In the topographical analysis of the particles, the AFM has been used with different imaging magnitudes (from  $5 \times 5 \mu\text{m}^2$  to  $1 \times 1 \mu\text{m}^2$ ) on the initial and coated cellets 90 and cellets 200 particles (10 different representative particles). The tapping mode of the AFM is used for analysing surface topography of the samples. For each trial height, amplitude and phase values are registered simultaneously. The same experimental apparatus and conditions of PMMA and talc trials were used (chapter III) in particular the same ratio (0.8) between the free amplitude ( $A_F$ ) and the amplitude set point ( $A_{SP}$ ) since it gives images with good resolution also for the case of cellets and talc particles. The results of initial and coated cellets 90 and cellets 200 particles will be presented in the next part.

#### A.1. Topographical Analysis of the Initial Cellets 90 and Cellets 200 Particles

Surface topography of the initial cellets 90 sample has been studied by using 10 different representative particles (according to particle shape & size) with 3 different magnitudes of imaging ( $1 \times 1 \mu\text{m}$ ,  $2 \times 2 \mu\text{m}$ ,  $5 \times 5 \mu\text{m}$ ). Figure IV.20 shows the AFM cantilever while having a topographical analysis of a cellets 90 particle. Figures IV.21 and IV.22 show the height images of a cellets 90 particle in 2D and 3D formats. Height images with  $5 \times 5 \mu\text{m}^2$  imaging magnitude have been used for surface roughness analysis. According to these images, it was found that the average surface roughness ( $R_a$ ) is 165 nm and root mean square average of surface roughness (RMS) is 207 nm for initial cellets 90 particles. (table IV.2)

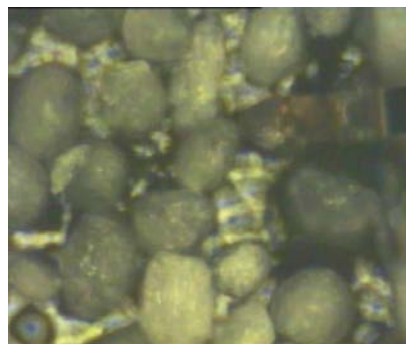


**Figure IV.20.** Cellets 90 Particles  
and Cantilever of AFM

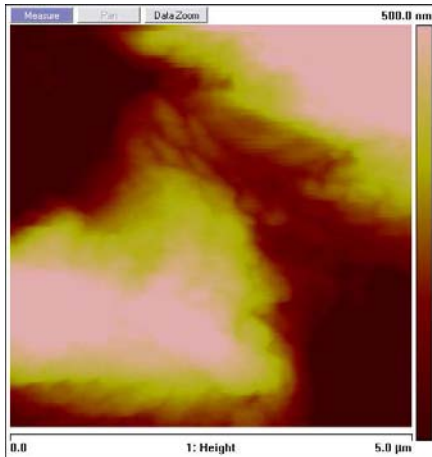


**Figure IV.21.** Height Image of  $5 \times 5 \mu\text{m}^2$  Surface of Cellets 90 Particle by AFM

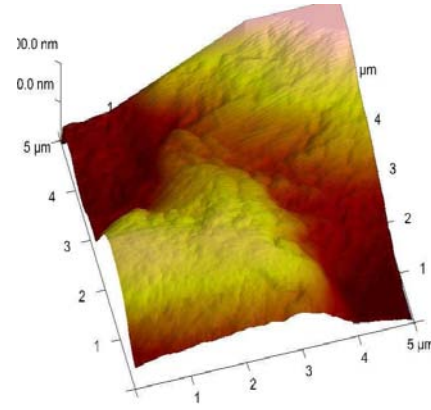


**Figure IV.22.** 3D Height Image of  $5 \times 5 \mu\text{m}^2$  Surface of Cellets 90 Particle by AFM

The topographical analysis of initial cellets 200 particles has also been studied. In the figure IV.23 cellets 200 particles and the cantilever of the AFM can be seen. Figure IV.24 and IV.25 show the height images of an initial cellets 200 particle with  $5 \times 5 \mu\text{m}^2$  imaging magnitude.



**Figure IV.23.** Cellets 200 Particles and Cantilever of AFM

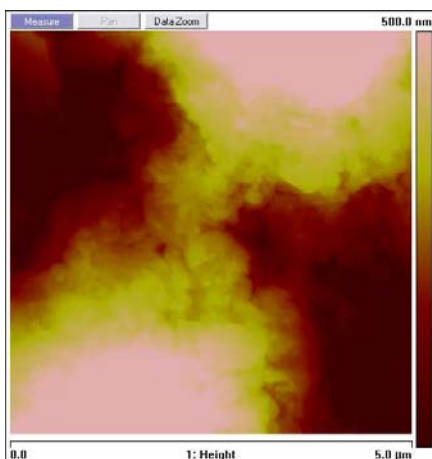


**Figure IV.24.** Height Image of  $5 \times 5 \mu\text{m}^2$  Surface of Cellets 200 Particle by AFM

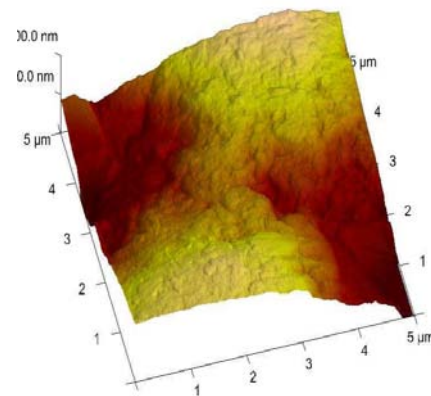


**Figure IV.25.** 3D Height Image of  $5 \times 5 \mu\text{m}^2$  Surface of Cellets 200 Particle by AFM

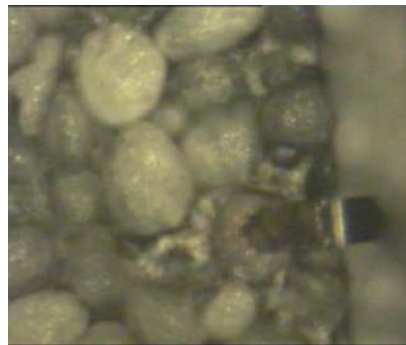
At the end of the topographical analysis, it was found that the Ra value is between 48 nm and 188 nm with an average 111 nm and RMS value is between 62 nm and 263 nm with an average 141 nm for the initial cellets 200 particles. For talc particles, the Ra and RMS values have been used from chapter III. The surface roughness values of the initial host and guest particles are presented in table IV.2.

**Table IV.2.** Surface Roughness Values of Initial Cellets and Talc Particles ( $5 \times 5 \mu\text{m}^2$ )

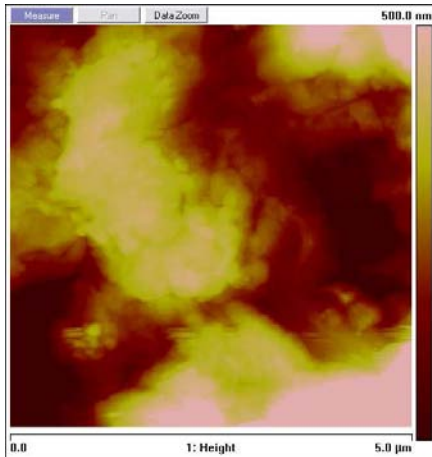
Material	$Ra_{\min} - Ra_{\max}$ (nm)	$Ra_{\text{ave}}$ (nm)	$RMS_{\min} - RMS_{\max}$ (nm)	$RMS_{\text{ave}}$ (nm)
<b>Cellets 90</b>	88 – 206	165	113 – 257	207
<b>Cellets 200</b>	48 – 188	111	62 – 263	141
<b>Talc</b>	100 – 220	131	140 – 270	186

### A.2. Topographical Analysis of the Coated Cellets 90 and Cellets 200 Particles

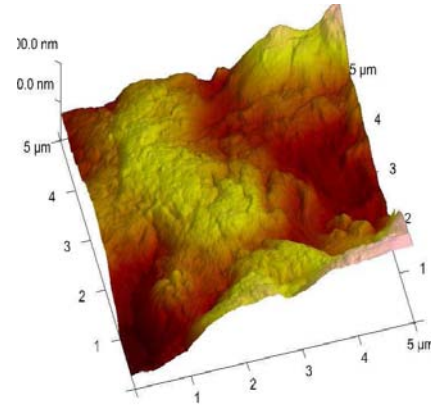
In this part, the aim is to understand the effect of talc coating on the surface roughness of the initial cellets 90 and cellets 200 particles. The topographical properties of 9.6 % talc coated cellets 90 and 3 % talc coated cellets 200 particles have been analysed by using 10 different particles in order to have representative results. Figure IV.26 shows the AFM cantilever while having a topographical analysis of a 9.6% talc coated cellets 90 particle. The height images of cellets 90 coated with 9.6% talc particle can be seen in the figure IV.27 and IV.28.



**Figure IV.26.** Cellets 90 coated with 9.6% Talc Particles and Cantilever of AFM

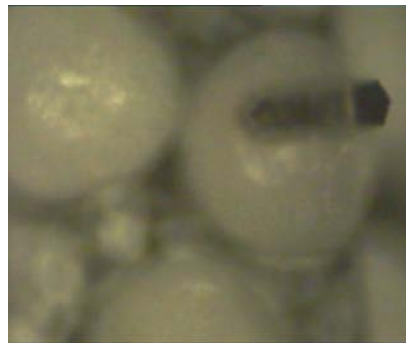


**Figure IV.27.** Height Image of 5x5  $\mu\text{m}^2$  Surface of Cellets 90 coated with 9.6% Talc Particles by AFM



**Figure IV.28.** 3D Height Image of 5x5  $\mu\text{m}^2$  Surface of Cellets 90 Coated with 9.6% Talc Particles by AFM

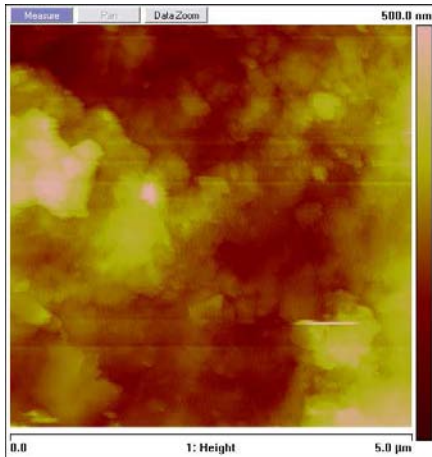
The Ra value has been determined between 72 nm and 131 nm and RMS varies between 91–165 nm for talc coated cellets 90 particles. It was observed that the surface roughness of cellets 90 particles decreases after coating with talc particles.



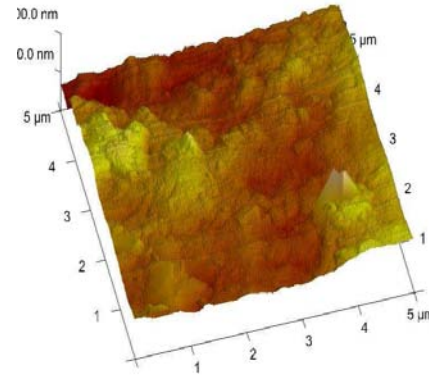
**Figure IV.29.** Cellets 200 coated with 3% Talc Particles and Cantilever of AFM

Figure IV.29 shows the cantilever and 3% talc coated cellets 200 particles while the AFM treatment. The height images of cellets 200 with talc particles can be seen in the figure IV.30 and IV.31.





**Figure IV.30.** Height Image of  $5 \times 5 \mu\text{m}^2$  Surface of Cellets 200 coated with 3% Talc Particles by AFM



**Figure IV.31.** 3D Height Image of  $5 \times 5 \mu\text{m}^2$  Surface of Cellets 200 Coated with 3% Talc Particles and Cantilever by AFM

It was found that the  $R_a$  value is between 24 nm and 73 nm and the RMS value is between 28 nm and 100 nm for coated cellets 200 particles. Table IV.3 shows the different surface roughness values of initial and talc coated cellets 90 and cellets 200 particles in hybridizer.

**Table IV.3.** Surface Roughness Values of Uncoated and Coated Particles ( $5 \times 5 \mu\text{m}^2$ )

Material	$R_{a_{\min}} - R_{a_{\max}}$ (nm)	$R_{a_{\text{ave}}}$ (nm)	$RMS_{\min} - RMS_{\max}$ (nm)	$RMS_{\text{ave}}$ (nm)
<b>Cellets 90</b>	88 – 206	165	113 – 257	207
<b>Cellets 200</b>	48 – 188	111	62 – 263	141
<b>Talc</b>	100 – 220	131	140 – 270	186
<b>Cellets 90 + 9.6% Talc</b>	72 – 131	96	91 – 165	125
<b>Cellets 200 + 3% Talc</b>	24 – 73	50	28 – 100	64

It was observed that the coating with talc particles affects the surface roughness of the host particles (cellets 90 and cellets 200). The valleys and holes on the surface (surface roughness) of the cellets particles could be either filled by talc particles or closed because of the slab geometry of the talc particles (fig.IV.32) and this would be the possible reason of the decrease in surface roughness of cellets particles after coating with talc particles.

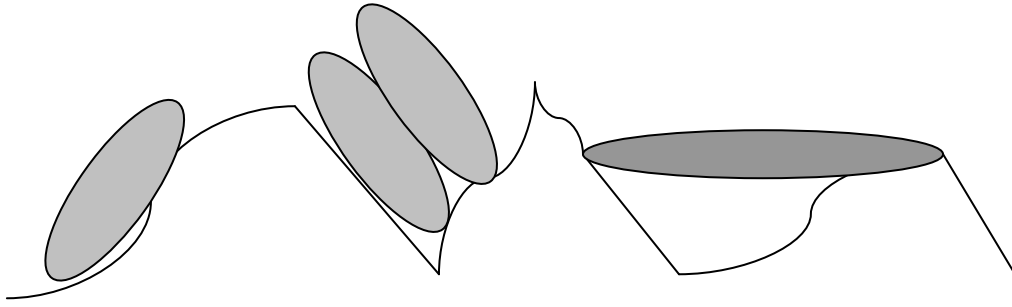


**Figure IV.32.** Possible Surface Coating of Cellets Particles with Talc Particles (Grey)

In order to be sure about the existence of talc particles on the surface of the host particles, the phase angle and height results of talc coated cellets particles have been compared.

**B. Phase Contrast Analysis of the Particles**

In order to be able to distinguish the talc particles on the surface of the cellets particles, the phase and height results have been compared for coated cellets particles. We suppose that phase contrast results would give us different phase angles in the coated particles. The results of initial and coated cellets particles will be presented in this part.

**B.1. Phase Contrast Analysis of the Initial Cellets 90 and Cellets 200 Particles**

Figure IV.33 and IV.34 show the height, phase angle and amplitude images of an initial cellets 90 and cellets 200 particles.

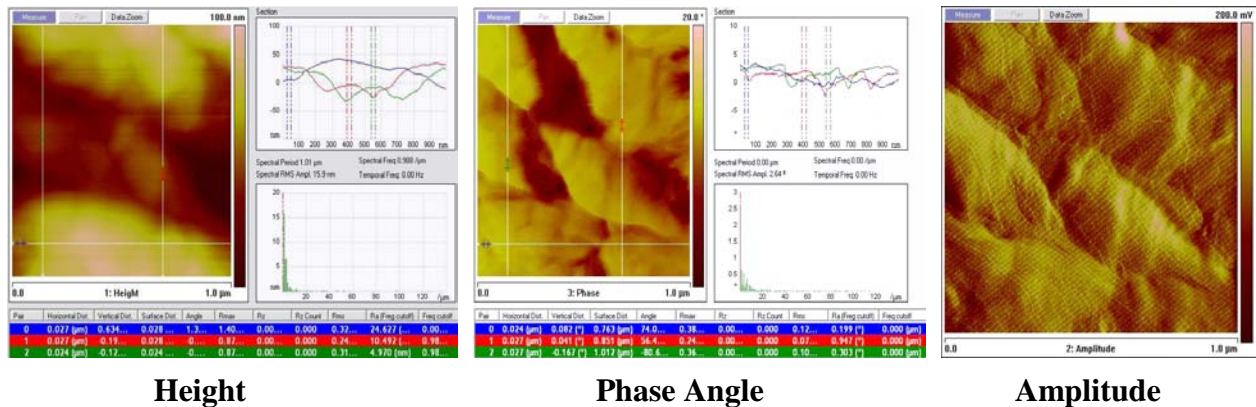
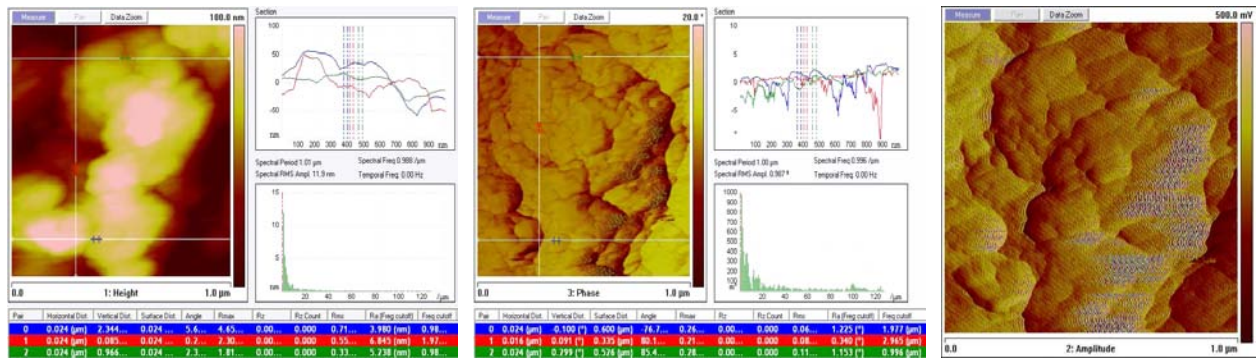


**Figure IV.33.** Height, Phase Angle and Amplitude Images of 1x1 μm<sup>2</sup> Surface of Cellets 90 Particle by AFM



Height

Phase Angle

Amplitude

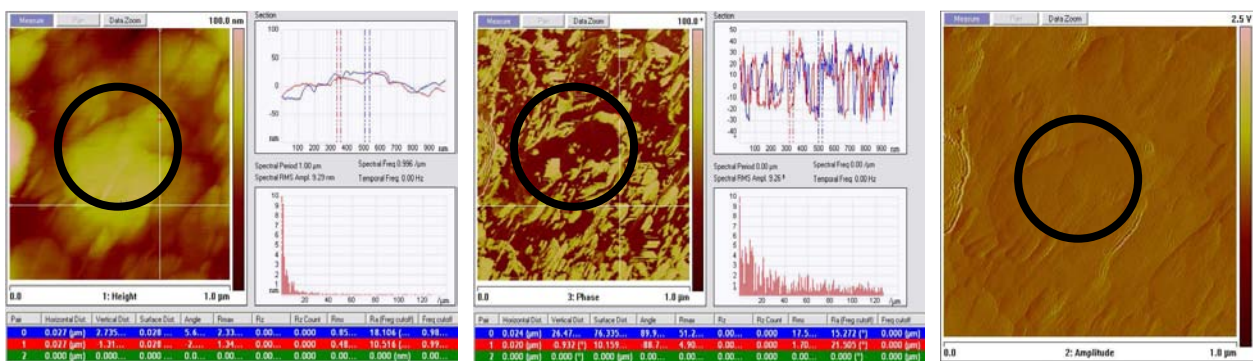
**Figure IV.34.** Height, Phase Angle and Amplitude Images of 1x1  $\mu\text{m}^2$  Surface of Cellets 200 Particle by AFM

It was found that the phase angle values vary between  $-90^\circ$  and  $15^\circ$  for cellets 90 and for cellets 200 particles the phase angle values are between  $-100^\circ$  and  $15^\circ$  (table IV.4).

It was observed that in the same section of images of height and phase angle, the variety is probably the reason of difference in height of the surface (surface roughness). It was also observed that the phase angle range of cellets 90 and cellets 200 particles are similar because basically they are the same material and only difference between them is the particle size distributions (table IV.4).

### B.2. Phase Contrast Analysis of the Talc Coated Cellets 90 and Cellets 200 Particles

The results of phase angle, height and amplitude values of talc coated cellets 90 and cellets 200 particles can be seen in the figure IV.35 and IV.36 for 1x1  $\mu\text{m}^2$  magnitude of imaging.



Height

Phase Angle

Amplitude

**Figure IV.35.** Height, Phase Angle and Amplitude Images of 1x1  $\mu\text{m}^2$  Surface of Cellets 90 Coated with 9.6% Talc Particles by AFM



It was observed that the phase angle range is higher for talc coated cellets 90 particles than talc coated cellets 200 particles because of probably higher mass percentage of talc particles (9.6%) for talc coated cellets 90 particles compared to talc coated (3%) cellets 200 particles. Moreover, the height and phase angle images of the particles have been analysed numerically in order to understand existence of talc particles on the surface of cellets 90 and cellets 200 particles like it has been done for PMMA and talc particles (chapter III). The numerical results of height and phase angle global profiles of the particles ( $5 \times 5 \mu\text{m}^2$  - 10 images) have been taken and they have been converted into a graph of height versus phase angle values. Each image has 256 pixel resolutions so there are  $256 \times 256 \times 10$  points for the height and phase angle graphs of each sample. Figure IV.37 and IV.38 show the signature of initial cellets 90, cellets 200 and talc particles.

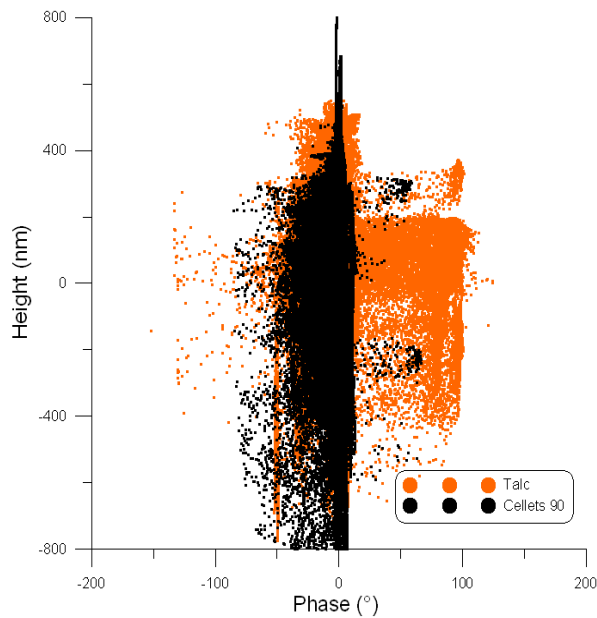


**Figure IV.37.** Height vs. Phase Angle Profiles for Initial Cellets 90 and Talc Particles

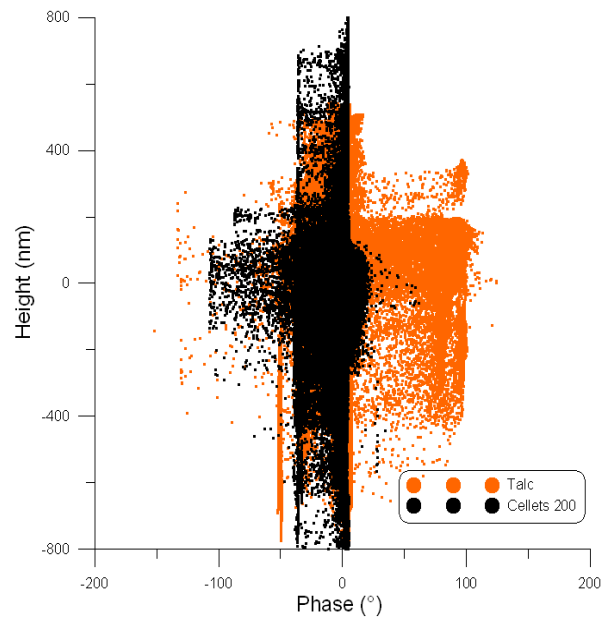


**Figure IV.38.** Height vs. Phase Angle Profiles for Initial Cellets 200 and Talc Particles

It was observed that cellets 90 and cellets 200 particles have similar phase angle signatures which is not unexpected because they are the same material with different particle sizes. On the other hand, the height and phase angle profiles of 9.6% talc coated cellets 90 particles and 3% talc coated cellets 200 particles with initial cellets 90, cellets 200 and talc particles can be seen in the figure IV.39 and IV.40.

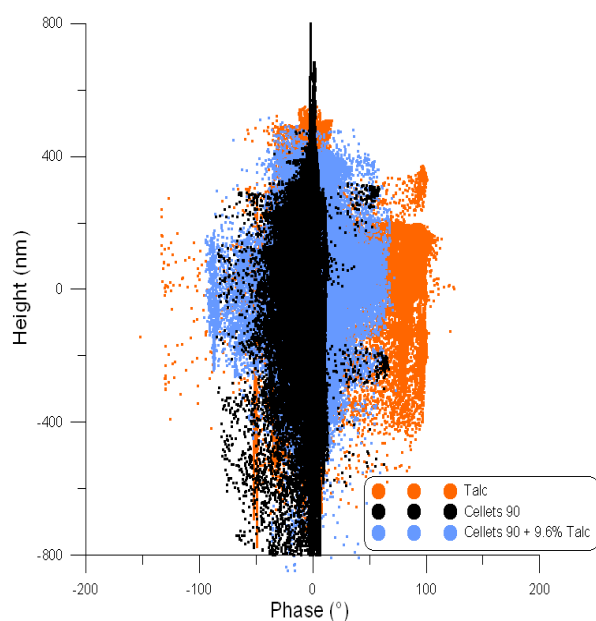


**Figure IV.39.** Height vs. Phase Angle Profiles for Initial and Coated Cellets 90 and Talc Particles

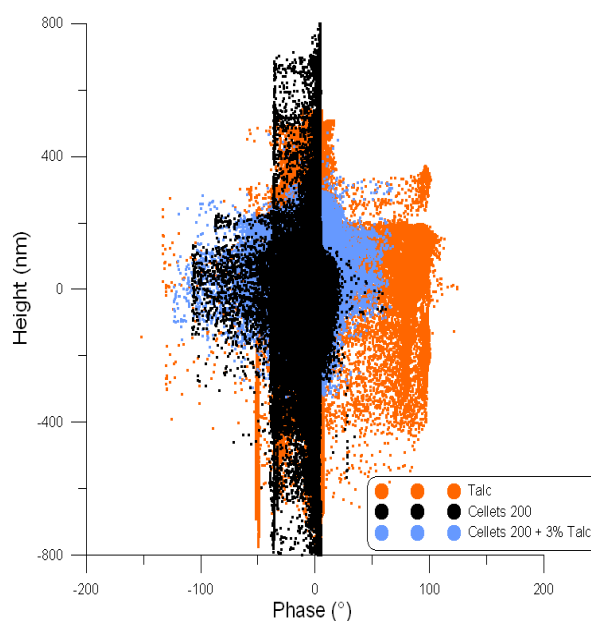


**Figure IV.40.** Height vs. Phase Angle Profiles for Initial and Coated Cellets 200 and Talc Particles

It was observed that, 9.6 % talc coated cellets 90 particles have some higher phase angle values than initial cellets 90 particles, which is characteristic of talc particles (table.IV.4). It can be seen from the figure IV.39 that between -400 nm – 400 nm height ranges and 15° and 65° and also between -95° and -90° phase angle of talc coated cellets 90 particles shows the existence of talc particles on the surface. On the other hand, it was observed that for talc coated cellets 200 particles there are also higher phase angle values than initial cellets 200 particles, which corresponds to existence of talc particles on the surface. It was observed that there are less phase angle points which are higher than initial cellets signature for talc coated cellets 200 particles compared to talc coated cellets 90 particles. It is probably the reason of difference in the mass percentages of talc particles in the mixtures.

### C. Measurement of Adhesion Forces Between the Particles

In the adhesion force analysis, talc particles have been glued by epoxy resin at the cantilever tip. It can be seen in the figure IV.41, before and after the adhesion force experiments the cantilever tip has been checked to make us sure the talc particles stay on the cantilever tip.

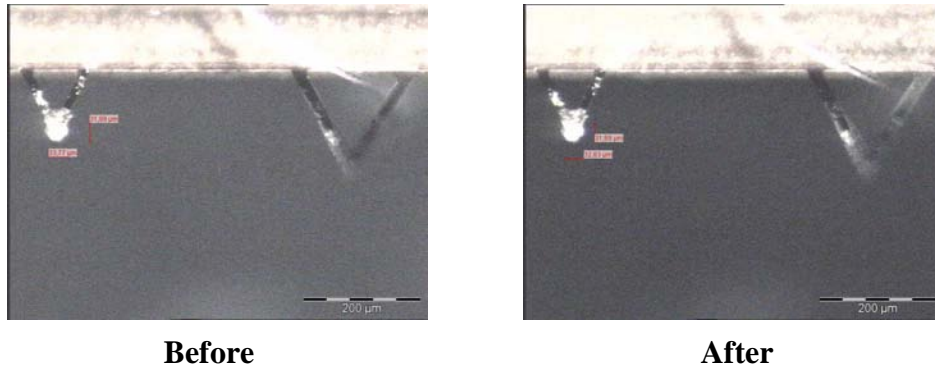


**Figure IV.41.** The Talc Particles on the Cantilever Tip Before and After the Analysis

In this study, the adhesion forces between talc particles and the coated and uncoated cellets particles have been determined. Basically, cellets 90 and cellets 200 particles have the same chemical composition, they have similar phase contrast signatures and a large common surface roughness range. On the other hand, the AFM measurements are very local so the difference in particle size is not a factor that affects the adhesion force measurements. Moreover, the talc particles on the cantilever tip are very fragile so in order to eliminate their erosion and avoid the modification of the cantilever tip (geometry, spring constant etc.) the treatments have been limited with essential experiments. So, the measurements of adhesion forces between initial cellets and talc particles have been done just between cellets 90 and talc particles and the values have been used both for cellets 90 and cellets 200 particles. For each powder sample, around 600–700 adhesion force curves have been obtained by analysing minimum 15 particles and 6 different surfaces. In the figure IV.42, an example of an adhesion force between talc particles at the cantilever tip and a sample of cellets 90, and the adhesion force between the talc particles at the cantilever tip and a sample of talc can be seen. The force peak corresponds to pull-off movement of the cantilever tip from the sample.

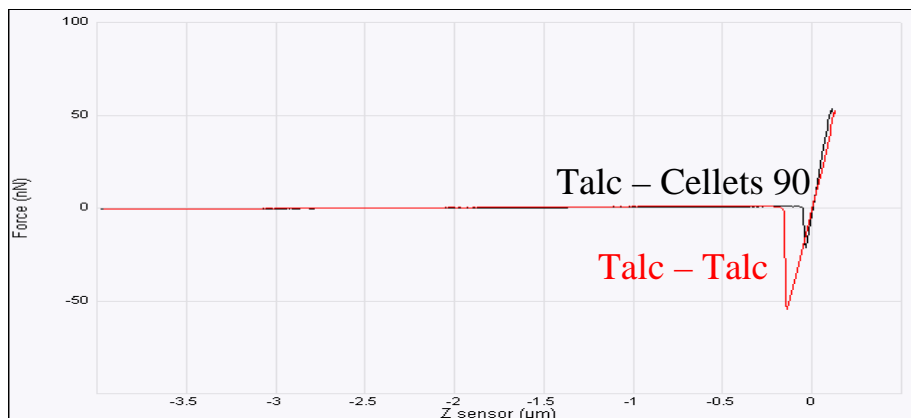


**Figure IV.42.** Adhesion Force Curves between Talc–Cellets 90 and Talc–Talc Particles

As it was presented in the chapter III, the adhesion forces between the talc particles vary between 5 nN and 220 nN with an average value of 55 nN. It was found that the average adhesion forces between talc and cellets 90 particles is 24 nN, the data range is between 0 nN and 190 nN. It was determined that 92.7% of the adhesion force values between talc and cellets 90 particles vary between 0–80 nN. The results show that the average adhesion force value between the talc particles is higher than the average adhesion force values between talc and cellets 90 particles. (table IV.5)

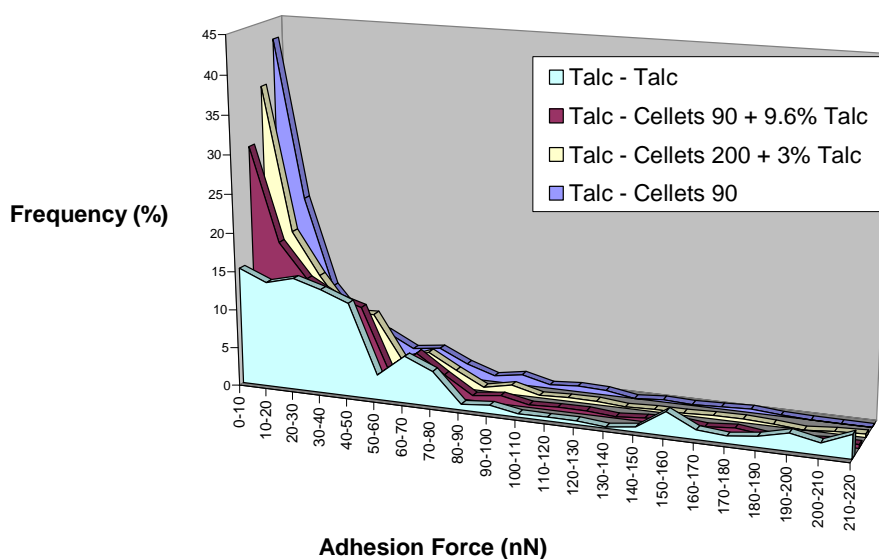


**Figure IV.43.** Distributions of Adhesion Forces between Talc, Cellets and Talc Coated Cellets Particles

On the other hand, the average adhesion forces between talc and talc coated cellets 90 and cellets 200 particles has been determined (table IV.5). It was found that the average adhesion force of cellets particles increases after coating with talc particles as expected. It was observed that the 80.9% of the adhesion force values of initial cellets 90 particles are between 0–80 nN and it decreases to 76.5% for 3% talc coated cellets 200 particles and 72.9% for 9.6% talc coated cellets 90 particles (figure IV.43). At the end, we have obtained 28 nN average adhesion force value for 3% talc coated cellets 90 particles and 32 nN for 9.6% talc coated cellets 90 particles.



**Table IV.5.** Adhesion Force Values for Uncoated and Coated Particles

<b>Material</b>	<b>Average Adhesion Force (nN)</b>	<b>Standard Deviation</b>
<b>Cellets 90</b>	24	2.8
<b>Talc</b>	55	5.2
<b>Cellets 90 + 9.6 % Talc</b>	32	1.5
<b>Cellets 200 + 3 % Talc</b>	28	2.9

### 2.2.3. Calculation of Talc Particle Deposition on the Surface of the Coated Particles

In this part of the study, the aim is to calculate the amount of talc particles on the surface of the cellets 90 and cellets 200 particles by using the model that has been used for calculation of adhesion forces between the fixed talc particles at the cantilever tip and different mass percentages talc coated PMMA particles. (Chapter III)

As it has been described in the chapter III, the model enables us to calculate the mass fraction of the guest particles on the surface of the host particle if the adhesion forces between the coated particles and the fixed guest particle at the cantilever tip is known.

In the AFM adhesion force measurement for each particle, 6 different surfaces have been chosen in order to have representative values as it was done for PMMA–talc model couple (chapter III). According to the average adhesion force values which have been obtained from each 6 different surfaces (an average of minimum 100 adhesion force values), the mass fraction of the talc particles for each particle has been calculated.

The adhesion force between the talc and cellets ( $F_0$ ) has been taken as 24 nN, and the adhesion force between the talc particles ( $F_1$ ) has been taken as 55 nN which are the measured average adhesion force values by AFM. Table IV.6 shows an example of the calculation of the mass fraction of talc particles according to the adhesion force between the fixed talc particles at the cantilever tip and each chosen surface of a 9.6 % talc coated cellets 90 particle. According to the table IV.6, it can be seen that the talc particles are not homogeneously distributed on the surface of the cellets 90 particles. It was also observed that the calculated talc percentage values are lower than 9.6%, which is the introduced mass percentage of talc particles in the mixture. The same study has been done for 15 different talc coated cellets 90 particles, it was calculated that the mass percentage of talc particles vary between 4.4 % and

9.2 % with an average of 7.8% talc particles. The non-analyzed zones on the cellets surface and agglomeration of talc particles (multilayer) could be possible reasons for this result.

**Table IV.6.** Calculated Amount of the Talc Particles on a 9.6 % Coated Cellets 90 Particle

Surface Number	Measured Average Adhesion Forces (nN)	Real Mass Fraction of Talc Particles
1 <sup>st</sup>	33.2	8.9 %
2 <sup>nd</sup>	29.1	5.2 %
3 <sup>rd</sup>	30.3	6.3 %
4 <sup>th</sup>	32.5	8.3 %
5 <sup>th</sup>	31.6	7.5 %
6 <sup>th</sup>	29.8	5.8 %
<b>Total Surface</b>	31.1	7 %

The amount of talc particle deposition on the cellets 200 particles has also been calculated. Table IV.7 shows the results of an example of measured adhesion force for each surface zone of the talc coated cellets 200 particle and mass fraction of talc particles for a 3 % talc coated cellets 200 particle can be seen.

**Table IV.7.** Calculated Amount of the Talc Particles on a 3 % Coated Cellets 200 Particle

Surface Number	Measured Average Adhesion Forces (nN)	Real Mass Fraction of Talc Particles
1 <sup>st</sup>	31.4	2.5 %
2 <sup>nd</sup>	27.9	2 %
3 <sup>rd</sup>	28.1	1.4 %
4 <sup>th</sup>	30.1	2.1 %
5 <sup>th</sup>	28.4	1.4 %
6 <sup>th</sup>	29.8	2 %
<b>Total Surface</b>	29.3	1.9 %

It was observed that for all 6 surface zones the calculated amount of talc is less than 3%. The same study has also been done for 15 representative talc coated cellets 200 particles. It was found that the range of calculated mass percentage of talc particles is between 0.4% and 2.4%.

The non analyzed zones of the particles could be one of the reasons and also analysing more particles would give us more reliable results.

#### 2.2.4. Calculation of the Van der Waals Forces Between the Particles

The objective of this part is to have a rough estimation of effect of host particle size on Van der Waals forces between the particles in order to understand the initial affinity of the particles. It is known that the surface roughness may have an important effect on the Van der Waals forces between the particles that we have chosen but in this preliminary estimation it won't be taken into account.

For an approximate calculation, the Hamaker constant for Cellets (90&200) has been taken from the literature as the Hamaker constant of microcrystalline cellulose as shown in table IV.12 and put inside the equation of the microscopic calculation for 2 spherical particles from table I.1 (chapter I).

It can be seen the calculated  $F_{vdw}$  values for each powder couple in table IV.8. For all calculations it is assumed that the particles are spherical and rigid and also the distance between the particles is much smaller than the particle diameter.

**Table IV.8.** The  $F_{vdw}$  Between Cellets (90&200) Particles & Cellets (90&200)–Talc Couples

Powder Couples	Hamaker Constants ( $10^{-19}J$ )	Estimated $F_{vdw}$ ( $10^{-7} N$ )
Cellets 90 with Cellets 90	1,12	3
Cellets 200 with Cellets 200	1,12	9
Talc with Talc	0,84	3
Cellets 90 with Talc	0,97	62
Cellets 200 with Talc	0,97	68

These estimated Van der Waals forces give some interesting trends. The adhesion between Cellets–Talc is greater than between the host particles and between the guest particles. Hence the dry coating process is helped by the initial adhesion properties of the chosen powders. It is also observed that the adhesion between Cellets–Talc is increasing with increasing size of the cellets diameter (expected from the equation for microscopic calculation of  $F_{vdw}$  between 2 spherical particles), more precisely with the increase of the size ratio of host particle and guest particle. The link between the initial “affinity” and the “mechanical coating strength” is not

straightforward. Actually the process action and the elastic–ductile properties of the materials must also play an important role and are still not taken into account. Nevertheless, in this simplified approach there is a link between the coating strength and the size of the host particle for all the studied processes.

### 2.2.5. Characterization of Coating Strength of the Particles

In this part of the study, the aim is to understand the effect of host particle size on the coating strength of the particles. In the first part, the coating strength results of 9.6 % talc coated cellets 90 and 3 % talc coated cellets 200 particles are compared. Afterwards, the coating strength results of the talc coated cellets particles from different equipments have been compared to understand the effect of equipment on the coating strength properties of the particles. The method used to evaluate the strength of the coating on the host particles is based on particle size analysis by Malvern Mastersizer laser diffraction granulometer in dry feed mode. Increasing the dispersing air pressure causes liberation of the guest particles from the surface of the host particles, and this liberation is detected by following the number size distribution.

#### A. Coating Strength of the Particles in Hybridizer Trials

Here the coating strength of the monolayer talc coated cellets 90 and cellets 200 particles in hybridizer are compared. The volume and number particle size distributions of talc coated cellets 90 particles can be seen in the figure IV.44 and IV.45. It was observed that from 0.5 bars to 2.5 bars pressure, the coated particles have the same particle size distributions with the initial cellets 90 particles.

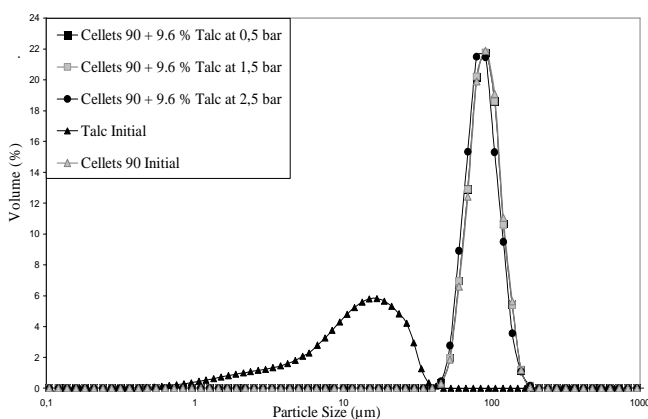


**Figure IV.44.** Volume Particle Size Distribution of 9.6 % Talc Coated Cellets 90 Particles in

Hybridizer

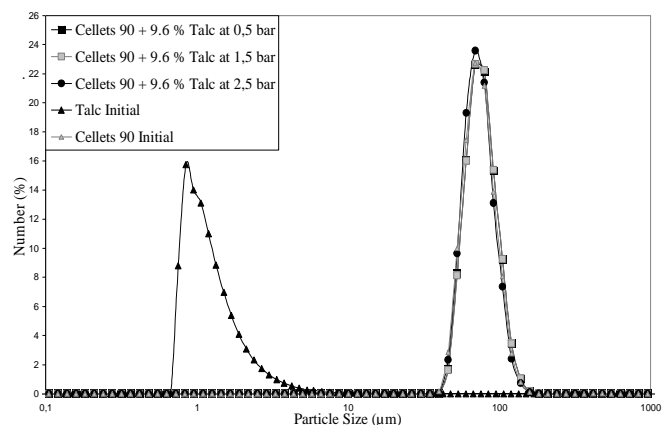


**Figure IV.45.** Number Particle Size Distribution of 9.6 % Talc Coated Cellets 90 Particles in

Hybridizer

On the other hand, it can be seen that when the dispersing pressure increases to 3.5 bars, there is a fine population of talc coated cellets 90 particles. It can be also observed from the figure IV.46 that at 4.0 bars pressure the volume of fine particle population is increasing compared to 3.5 bars pressure. It is also easy to distinguish these fine particle populations in number particle size distributions of the particles as shown in the figure IV.47.

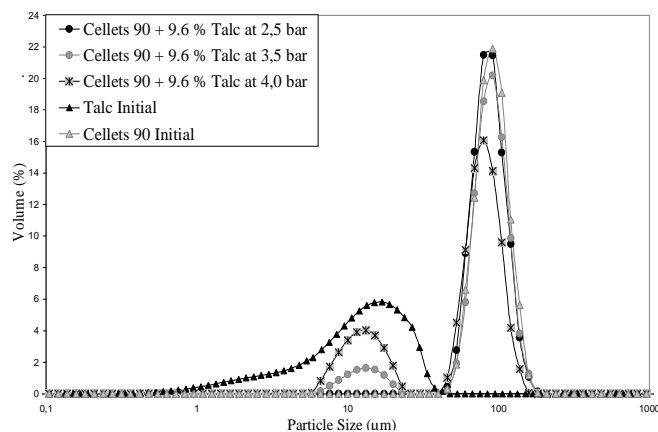


**Figure IV.46.** Volume Particle Size Distribution of 9.6 % Talc Coated Cellets 90 Particles in Hybridizer

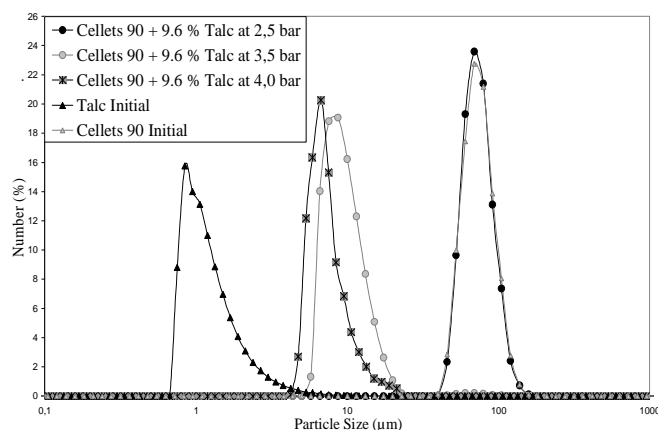


**Figure IV.47.** Number Particle Size Distribution of 9.6 % Talc Coated Cellets 90 Particles in Hybridizer

Volume and number particle size distributions of talc coated cellets 200 particles at 0.5, 1.5, 2.5 and 3.5 bars are presented in the figure IV.48 and IV.49. It can be seen that up to 3.5 bars pressure, there is no particle liberation because of the strong interactions between the particles.

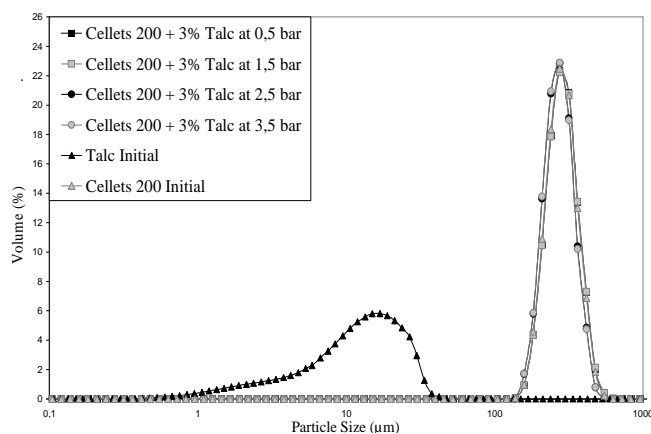


**Figure IV.48.** Volume Particle Size Distribution of 3 % Talc Coated Cellets 200 Particles in Hybridizer

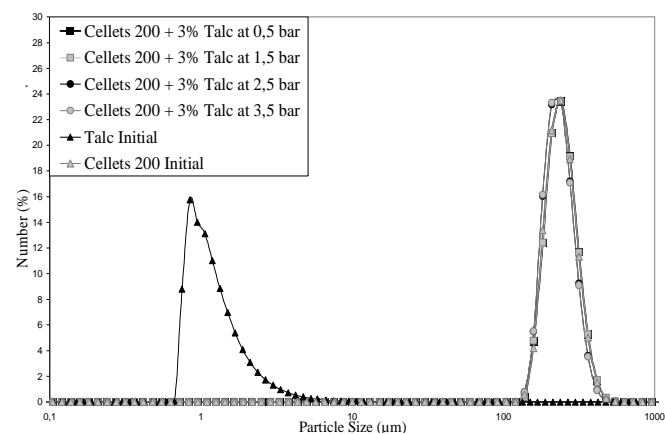


**Figure IV.49.** Number Particle Size Distribution of 3 % Talc Coated Cellets 200 Particles in Hybridizer

It was observed that at 4.0 bars pressure (maximum particle liberation pressure of the mastersizer), there is a fine population of particles around 15  $\mu\text{m}$  in the volume particle size distribution (fig.IV.50 and IV.51). This corresponds to the shift of the number particle size distribution of talc coated cellets 200 particles to the smaller particle size. It shows that the particle liberation pressure for talc coated cellets 200 particles is between 3.5 and 4.0 bars pressures.

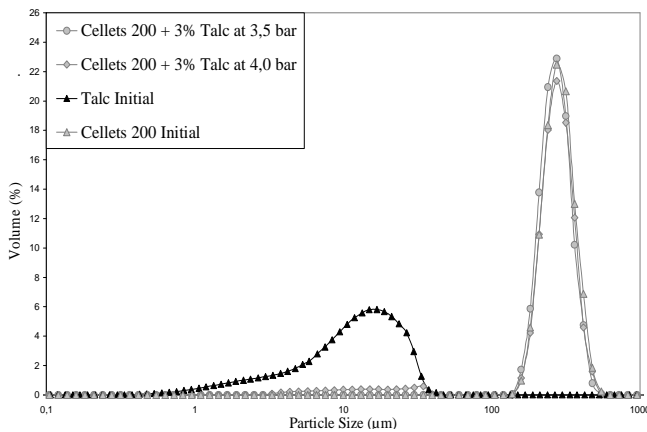


**Figure IV.50.** Volume Particle Size Distribution of 3 % Talc Coated Cellets 200 Particles in Hybridizer

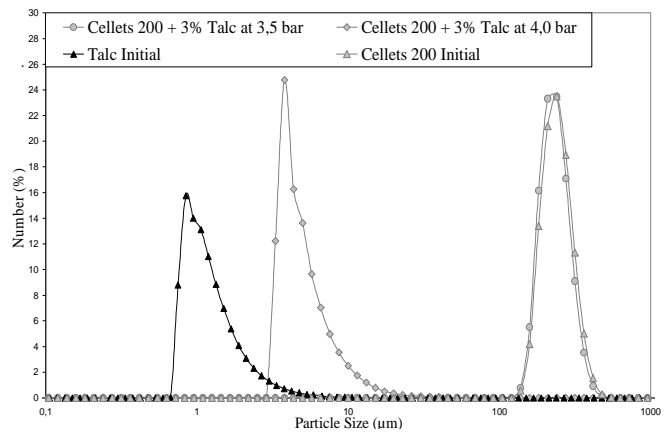


**Figure IV.51.** Number Particle Size Distribution of 3 % Talc Coated Cellets 200 Particles in Hybridizer

The particle liberation pressure of talc coated cellets 90 and cellets 200 particles are presented more precisely in the figure IV.52. It was found that at 3.4 bar pressure, talc coated cellets 90 particles start to be liberated (or broken) and move to the distribution of alone talc particles which is around 1  $\mu\text{m}$ . This indicates that cellets 90 coated with 9.6% talc particles by hybridizer remain coated until 3.4 bar pressure. On the other hand, the results of cellets 200 particles with 3% talc particle couple show that up to 3.8 bar dispersing pressure the particle size distributions are similar and are around 305  $\mu\text{m}$ . At 3.9 bar pressure the particle size distribution of the particle couple comes closer to the distribution of talc particles. This indicates that particle detachment (or fragmentation) for cellets 200 with 3% talc particles starts at 3.9 bar dispersing pressure.

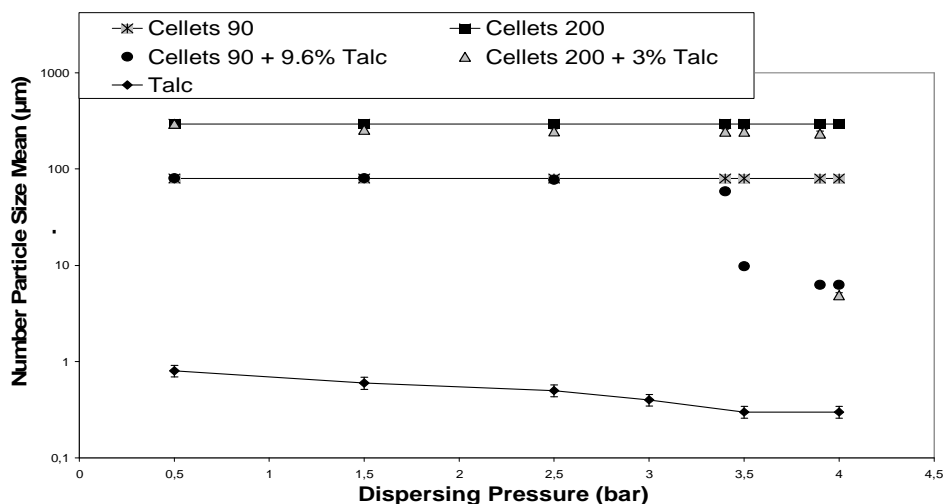


**Figure IV.52.** Number Particle Size Mean vs. Dispersing Pressure

For Talc Coated and Initial Cellets 90 and Cellets 200 Particles in Hybridizer

It can be seen that the dispersing air pressure for particle liberation is higher for talc coated cellets 200 particles compared to talc coated cellets 90 particles (Table IV.9). This is probably related to the particle size ratio between the host and guest particles which has an important role for inter-particle forces. On the other hand, it should be considered that both particle detachment and fragmentation may cause decrease in the particle size distribution of the particles.

**Table IV.9.** Dispersing Pressures and Air Velocities for Particle Detachment for Talc Coated Cellets 90 and Cellets 200 Particles in Hybridizer

Material	Particle Size Ratio (Host/Guest)	Dispersing Air Pressure	Air Velocity
Cellets 90 + 9.6% Talc	7.1	3.4 bar	118 m/s
Cellets 200 + 3% Talc	21.8	3.9 bar	124 m/s

### B. Coating Strength of the Particles in Cyclomix Trials

The coating strength properties of the monolayer talc coated cellets 90 and cellets 200 particles in cyclomix has also been studied. Figure IV.53 and IV.54 show the volume and number particle size distributions of coated and uncoated cellets 90 particles for 0.5, 1.5 and 2.5 bars air dispersing pressures.

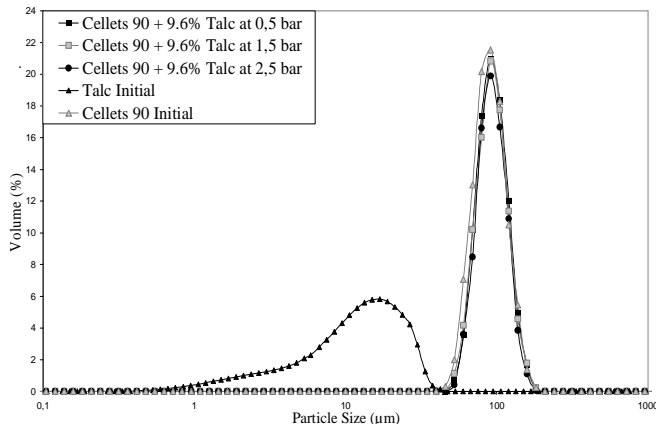


**Figure IV.53.** Volume Particle Size Distribution of 9.6 % Talc Coated Cellets 90 Particles in Cyclomix

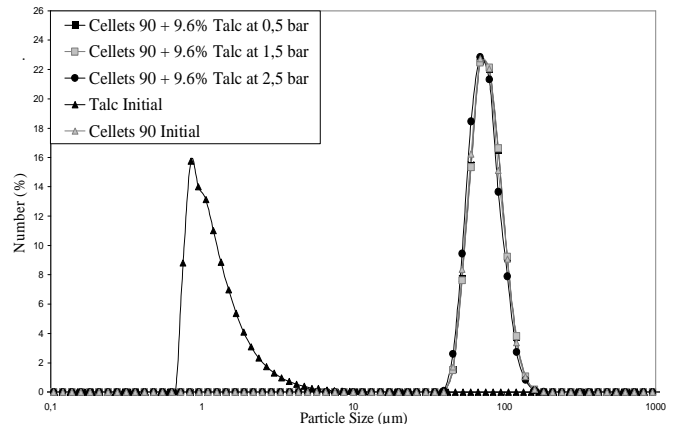


**Figure IV.54.** Number Particle Size Distribution of 9.6 % Talc Coated Cellets 90 Particles in Cyclomix

It was observed that up to 2.5 bars dispersing pressure 9.6% talc coated cellets 90 particles keep their particle size distribution. At 3.5 bars dispersing pressure it can be seen that some of the talc coated cellets 90 particles are smaller so the particle liberation pressure for coated cellets 90 particles in cyclomix is between 2.5 and 3.5 bars (figure IV.55 and IV.56).

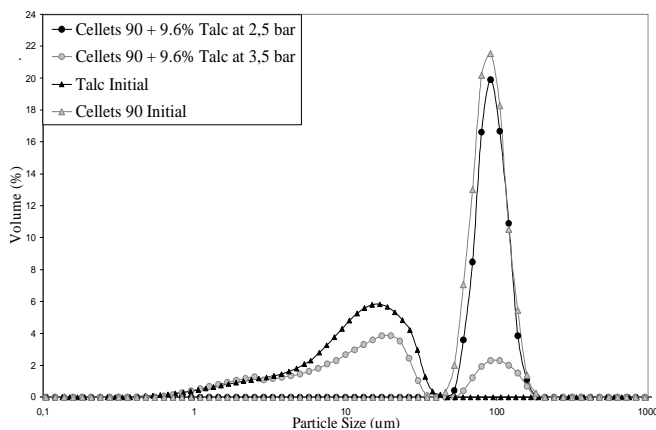


**Figure IV.55.** Volume Particle Size Distribution of 9.6 % Talc Coated Cellets 90 Particles in Cyclomix

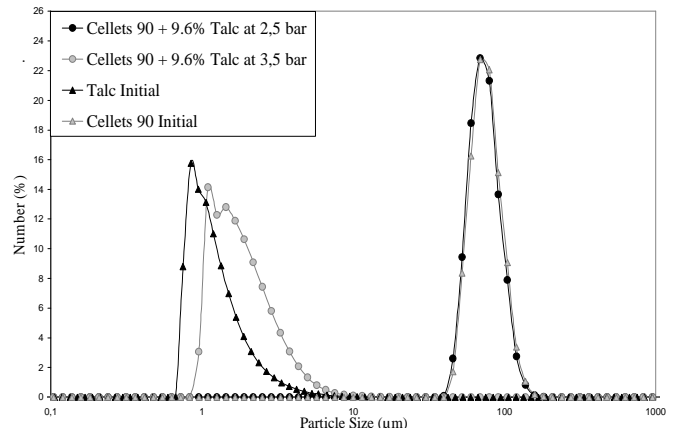


**Figure IV.56.** Number Particle Size Distribution of 9.6 % Talc Coated Cellets 90 Particles in Cyclomix

The same study has also been done for 3% talc coated cellets 200 particles in cyclomix. It can be seen that until 2.5 bars dispersing pressure talc coated cellets 200 particles also keep their particle size distributions like coated cellets 90 particles. (fig. IV.57 & IV.58)



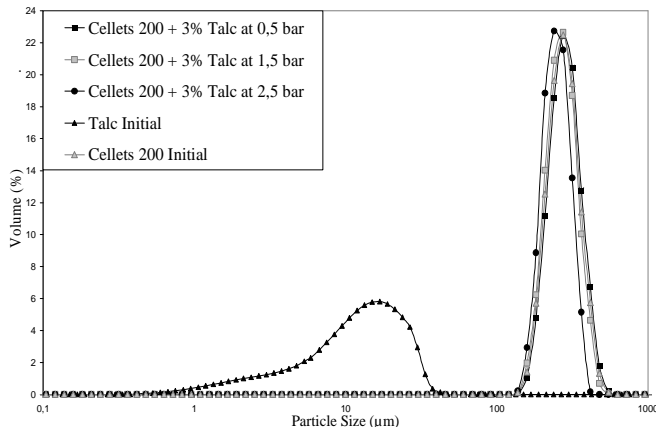


**Figure IV.57.** Volume Particle Size Distribution of 3 % Talc Coated Cellets 200 Particles in Cyclomix

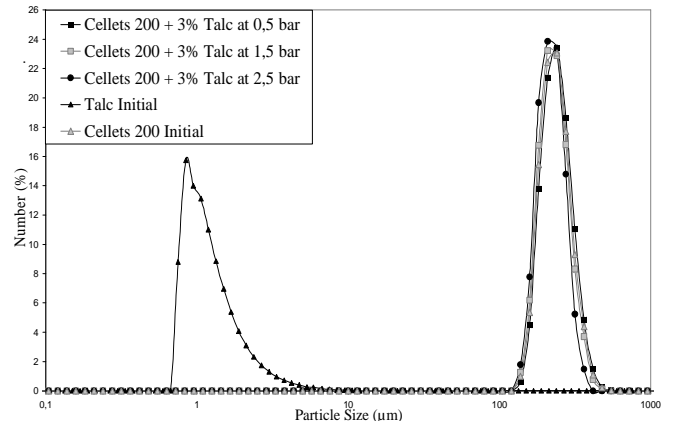


**Figure IV.58.** Number Particle Size Distribution of 3 % Talc Coated Cellets 200 Particles in Cyclomix

On the other hand, whenever the dispersing air pressure increases to 3.5 bar pressure, it can be seen in the figure IV.59 and IV.60 there is a fine population of coated cellets 200 particles. This shows us that the particle liberation (or fragmentation) pressure for coated cellets 200 particles is also between 2.5 and 3.5 bars pressures.

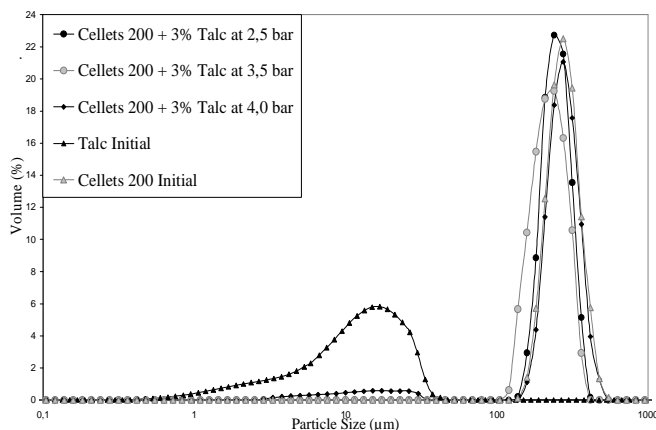


**Figure IV.59.** Volume Particle Size Distribution of 3 % Talc Coated Cellets 200 Particles in Cyclomix

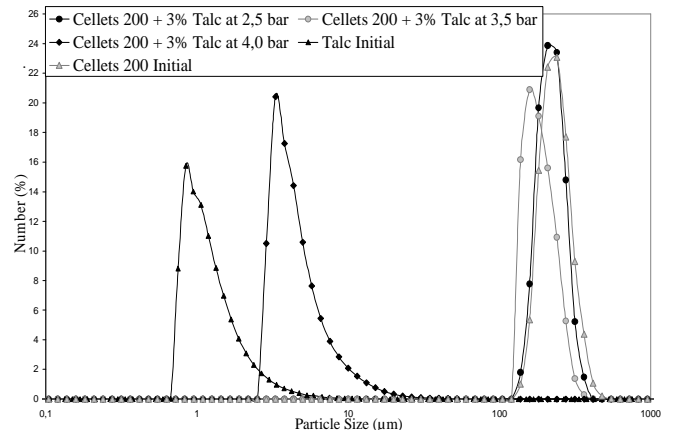


**Figure IV.60.** Number Particle Size Distribution of 3 % Talc Coated Cellets 200 Particles in Cyclomix

Afterwards, the particle size distributions of coated cellets 90 and cellets 200 particles in cyclomix have been analysed for each dispersing pressure between 2.5 and 3.5 bars in order to find the particle liberation pressures more precisely. It was found that the particle liberation (or fragmentation) pressure for 9.6 % talc coated cellets 90 particles in cyclomix is 2.9 bars and for 3 % talc coated cellets 200 particles the particle liberation pressure is 3.4 bars (fig. IV.61).

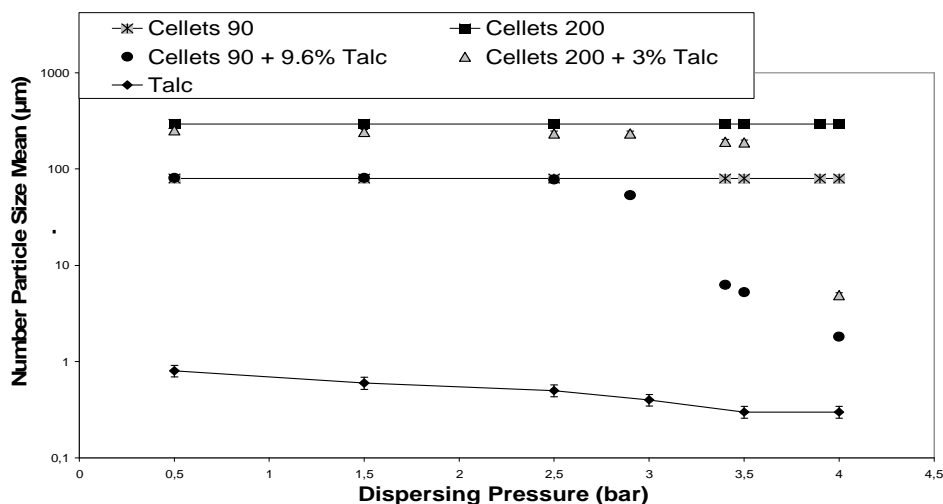


**Figure IV.61.** Number Particle Size Mean vs. Dispersing Pressure

For Talc Coated and Initial Cellets 90 and Cellets 200 Particles in Cyclomix

As it can be seen from the table IV.10 that the air pressure required for dispersion increases with increasing particle size ratio between the host and guest particles for cyclomix trials as it was observed for the hybridizer trials. The size ratio between the host and guest particles has effect on the inter-particle forces between the particles. In addition, it should be taken in account that the difference in particle size distribution could also be due to particle breakage.

**Table IV.10.** Dispersing Pressures and Air Velocities for Particle Detachment for Talc Coated Cellets 90 and Cellets 200 Particles in Cyclomix

Material	Particle Size Ratio (Host/Guest)	Dispersing Air Pressure	Air Velocity
Cellets 90 + 9.6% Talc	7.1	2.9 bar	109 m/s
Cellets 200 + 3% Talc	21.8	3.4 bar	118 m/s

### C. Coating Strength of the Particles in Turbula Trials

The volume and number particle size distributions of pre-treated cellets 90 particles (in hybridizer at 4000 rpm for 6 min) and then coated with talc particles by turbula at 0.5 and 1.5 bars dispersing pressures can be seen in the figure IV.62 and IV.63. It was observed that coated cellets 90 particles keep their particle size distribution at 0.5 bars but at 1.5 bars dispersing pressure there is a fine particle population. It shows that particle liberation (or breakage) pressure for talc coated cellets 90 particles by turbula is between 0.5 and 1.5 bar dispersing pressures.

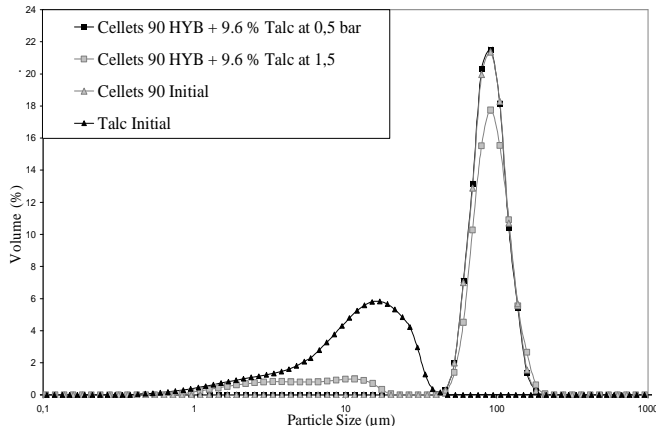


**Figure IV.62.** Volume Particle Size Distribution of 9.6 % Talc Coated Pre-treated Cellets 90 Particles in Turbula

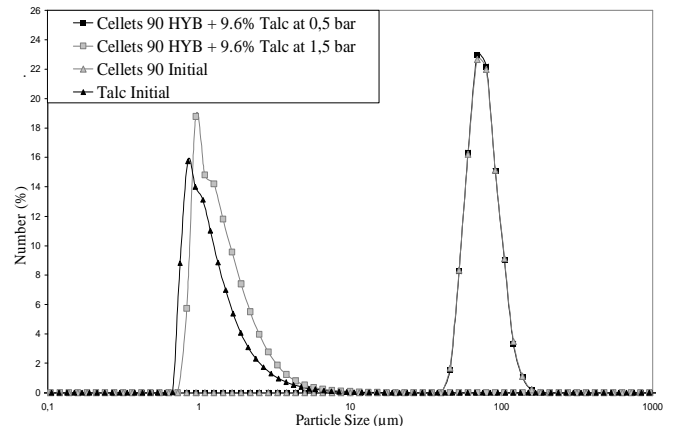


**Figure IV.63.** Number Particle Size Distribution of 9.6 % Talc Coated Pre-treated Cellets 90 Particles in Turbula

Figure IV.64 and IV.65 show the volume and number particle size distributions of coated cellets 90 particles at 1.5, 2.5 and 3.5 bars dispersing pressures. It can be seen that the volume of fine particle population increases with increasing dispersing pressure. On the other hand, it can be seen that at 2.5 and 3.5 bars dispersing pressures, the coated cellets 90 particles has the same number particle size distributions with initial talc particles.

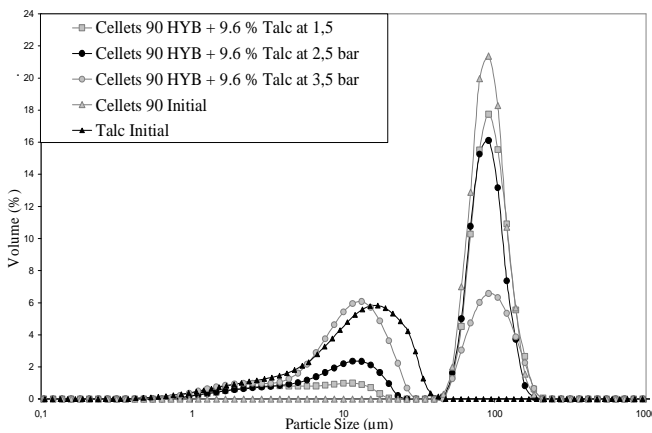


**Figure IV.64.** Volume Particle Size Distribution of 9.6 % Talc Coated Pre-treated Cellets 90 Particles in Turbula

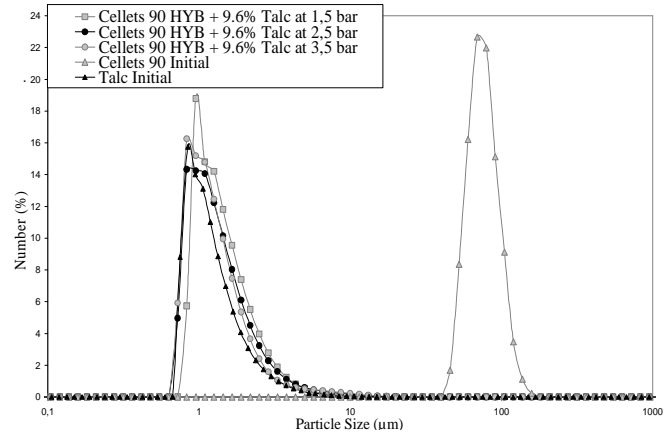


**Figure IV.65.** Number Particle Size Distribution of 9.6 % Talc Coated Pre-treated Cellets 90 Particles in Turbula

The coating strength analysis has also been done for pre-treated cellets 200 particles (in hybridizer at 4000 rpm for 6 min) and then coated with 3% talc particles by turbula. It can be seen that up to 1.5 bars dispersing pressure, the coated cellets 200 particles have the same particle size distribution with the initial cellets 200 particles. (fig. IV.66, IV.67.)

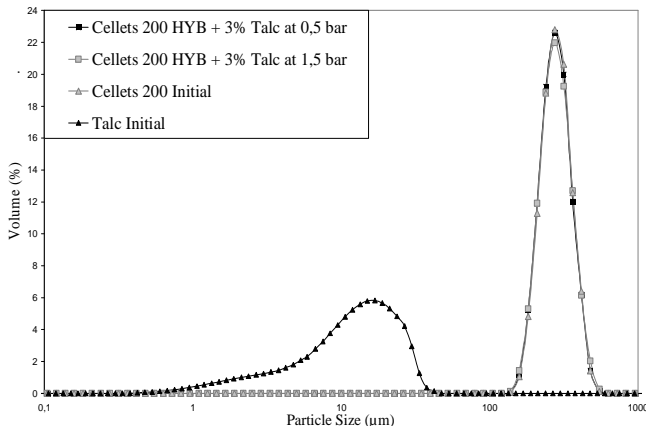


**Figure IV.66.** Volume Particle Size Distribution of 3 % Talc Coated Pre-treated Cellets 200 Particles in Turbula

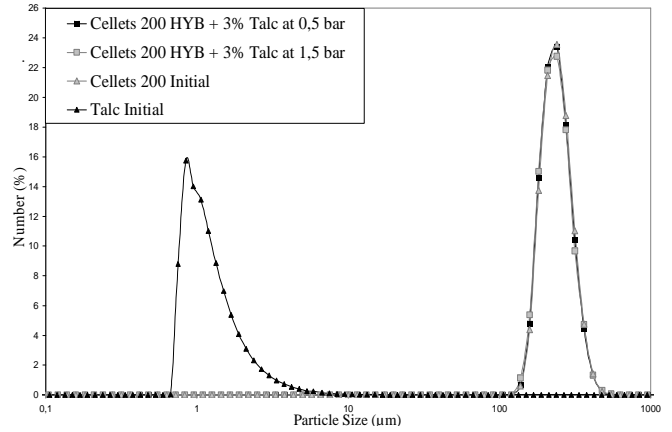


**Figure IV.67.** Number Particle Size Distribution of 3 % Talc Coated Pre-treated Cellets 200 Particles in Turbula

On the other hand, it was observed that the particle size distribution decreases at 2.5 bars dispersing pressure. This shows that the particle liberation (or fragmentation) pressure for coated cellets 200 particles is between 1.5 and 2.5 bars dispersing pressures. In addition, the volume of the fine particle population increases when the dispersing pressure increases to 3.5 bar pressure (fig. IV.68 and IV.69).

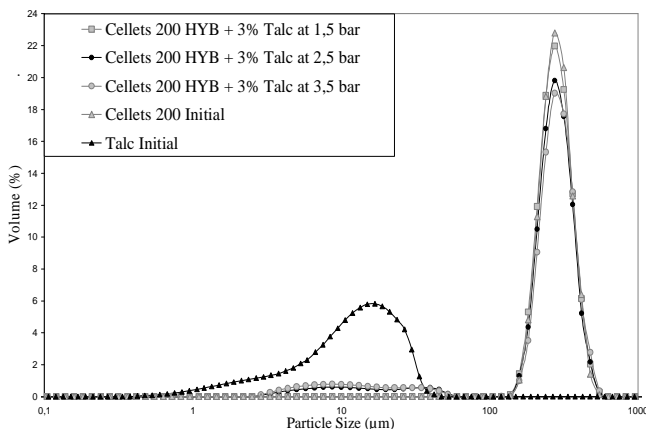


**Figure IV.68.** Volume Particle Size Distribution of 3 % Talc Coated Pre-treated Cellets 200 Particles in Turbula

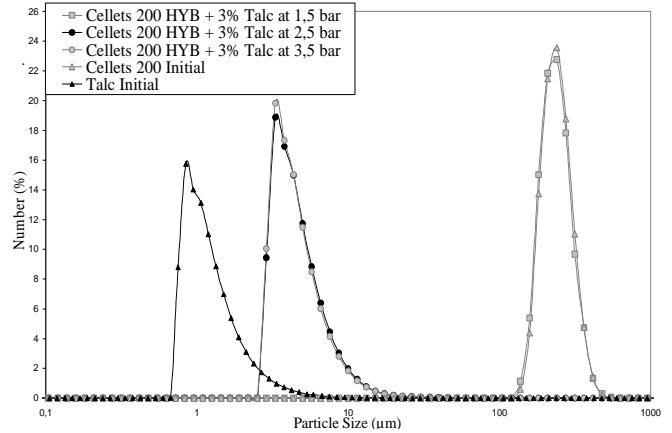


**Figure IV.69.** Number Particle Size Distribution of 3 % Talc Coated Pre-treated Cellets 200 Particles in Turbula

Figure IV.70 shows the particle size distributions of coated cellets 90 and cellets 200 particles precisely. It was found that the particle liberation pressure is 1.2 bars for coated cellets 90 particles and 1.8 bars for coated cellets 200 particles.

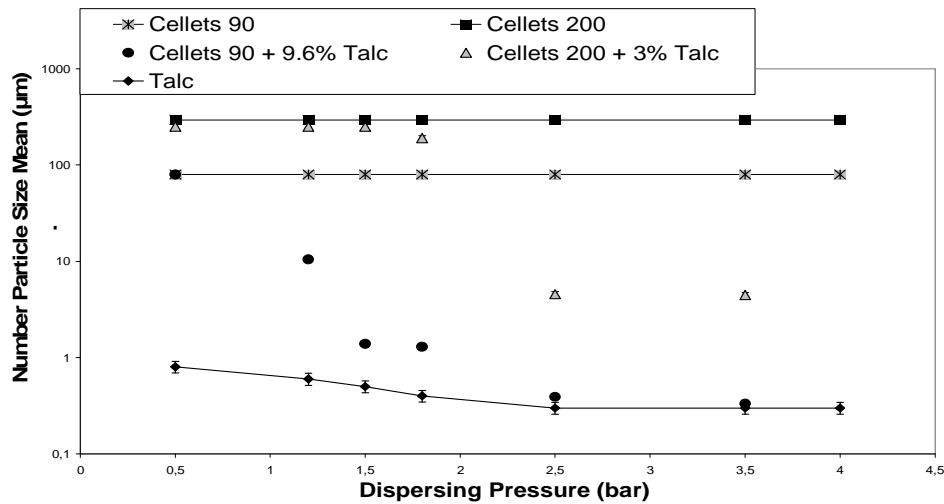


**Figure IV.70.** Number Particle Size Mean vs. Dispersing Pressure

For Talc Coated and Initial Cellets 90 and Cellets 200 Particles in Turbula

Table IV.11 shows the particle liberation pressures and corresponding air velocities for coated cellets 90 and cellets 200 particles more precisely. It was observed that particle liberation (or fragmentation) pressure is higher for coated cellets 200 particles compared to coated cellets 90 particles also in turbula trials. On the other hand, the particle breakage should also be considered as a reason of particle size decrease.

**Table IV.11.** Dispersing Pressures and Air Velocities for Particle Detachment for Talc Coated Pre-treated Cellets 90 and Cellets 200 Particles by Turbula

Material	Particle Size Ratio (Host/Guest)	Dispersing Air Pressure	Air Velocity
Pre-Treated Cellets 90 + 9.6% Talc	7.1	1.2 bar	60 m/s
Pre-Treated Cellets 200 + 3% Talc	21.8	1.8 bar	81 m/s

#### D. Coating Strength of the Particles in Basic Mixing Trials

The coating strength analysis has also been done for the coated cellets 90 and cellets 200 particles by basic mixing method. The volume and number particle size distributions of coated cellets 90 particles at 0.5 and 1.5 bars dispersing pressures can be seen in the figure IV.71 and IV.72. It can be seen that the coated cellets 90 particles keep their particle size distribution at 0.5 bars dispersing pressure but at 1.5 bars there is particle detachment (or

breakage). It shows that the particle liberation pressure is between 0.5 and 1.5 bars for coated cellets 90 particles by basic mixing method.

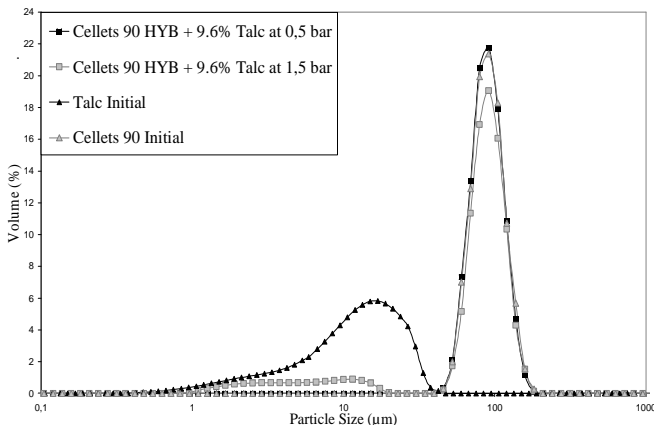


**Figure IV.71.** Volume Particle Size Distribution of 9.6 % Talc Coated Pre-treated Cellets 90 Particles by Basic Mixing Method

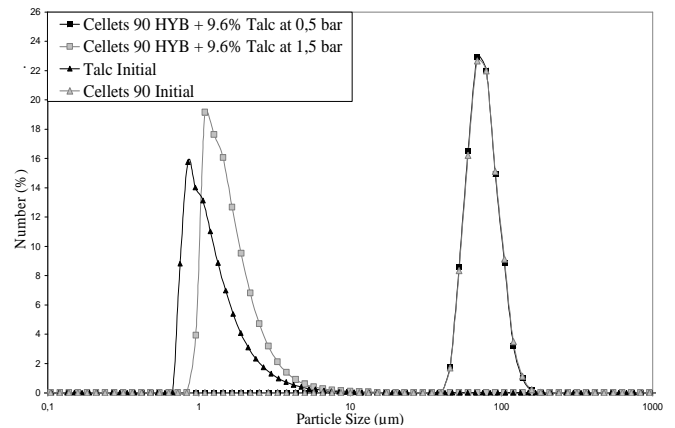


**Figure IV.72.** Number Particle Size Distribution of 9.6 % Talc Coated Pre-treated Cellets 90 Particles by Basic Mixing Method

Figure IV.73 and IV.74 show the particle size distributions of coated cellets 90 particles at higher dispersing pressures. It was observed that the volume of fine particle population, which has almost the same particle size with initial talc particles, increases at higher dispersing pressures as expected.

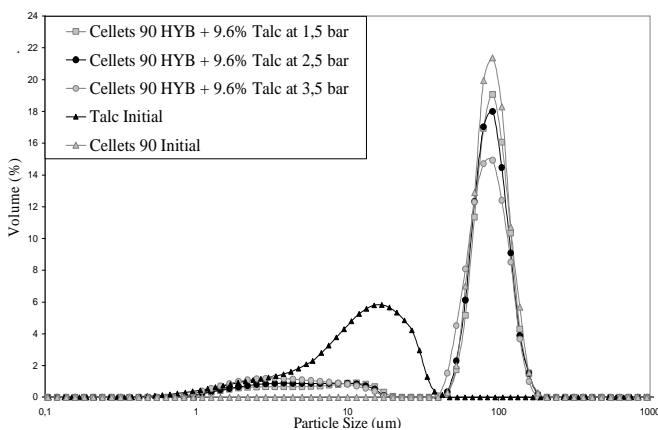


**Figure IV.73.** Volume Particle Size Distribution of 9.6 % Talc Coated Pre-treated Cellets 90 Particles by Basic Mixing Method

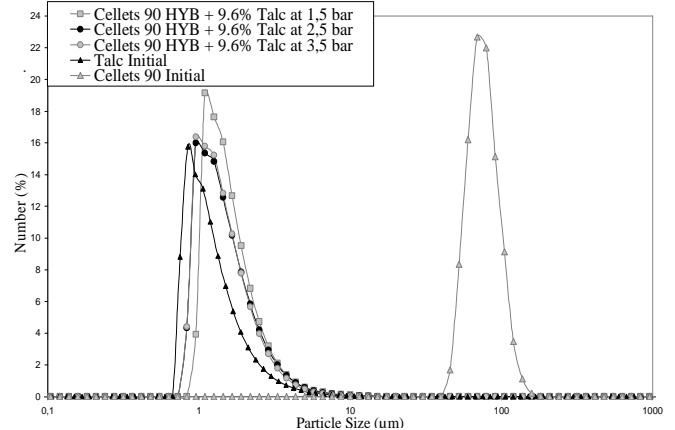


**Figure IV.74.** Number Particle Size Distribution of 9.6 % Talc Coated Pre-treated Cellets 90 Particles by Basic Mixing Method

The volume and number particle size distributions of coated cellets 200 particles at 0.5 and 1.5 bars dispersing pressures are shown in figure IV.75 and IV.76. It was observed that the

particle liberation pressure for coated cellets 200 particles is also between 0.5 and 1.5 bars dispersing pressures.

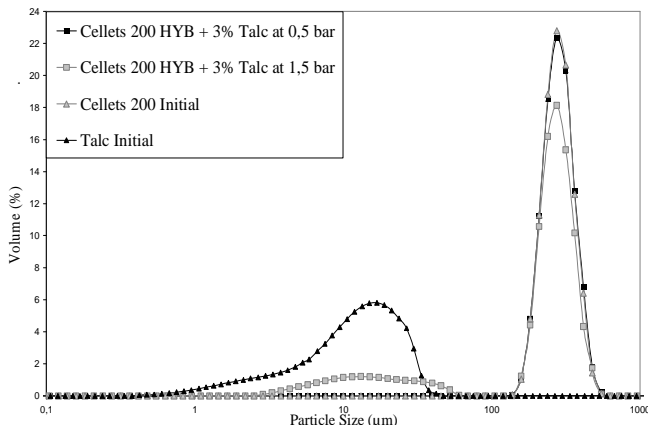


**Figure IV.75.** Volume Particle Size Distribution of 3 % Talc Coated Pre-treated Cellets 200 Particles by Basic Mixing Method

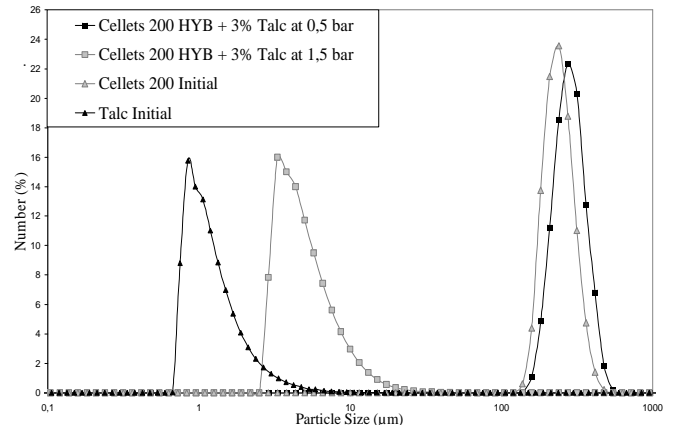


**Figure IV.76.** Number Particle Size Distribution of 3 % Talc Coated Pre-treated Cellets 200 Particles by Basic Mixing Method

At 2.5 and 3.5 bars dispersing pressures, the fine particle population increases also for the coated cellets 200 particles. (fig.IV.77 and IV.78). Contrary to the results of coated cellets 90 particles by basic mixing method, the fine particles of coated cellets 200 particles by basic mixing method have higher number particle sizes than initial talc particles.

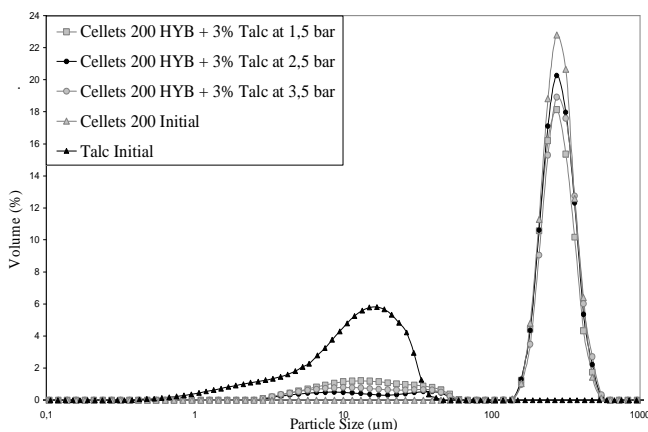


**Figure IV.77.** Volume Particle Size Distribution of 3 % Talc Coated Pre-treated Cellets 200 Particles by Basic Mixing Method

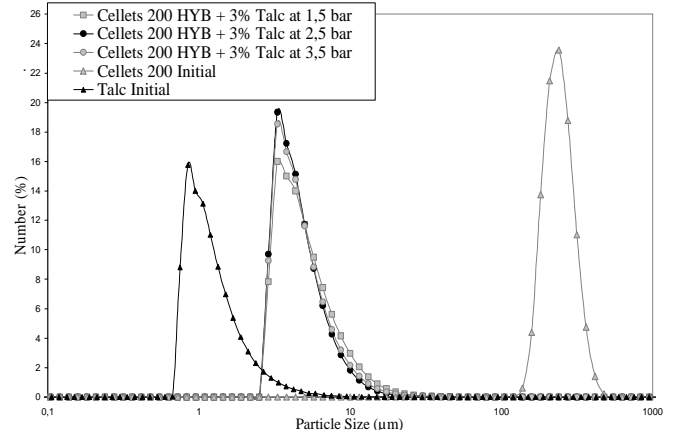


**Figure IV.78.** Number Particle Size Distribution of 3 % Talc Coated Pre-treated Cellets 200 Particles by Basic Mixing Method

It was found that, the particle liberation (or fragmentation) pressure is 0.7 bar for coated cellets 90 particles and 1.1 bars for coated cellets 200 particles by basic mixing method. (fig.IV.79)

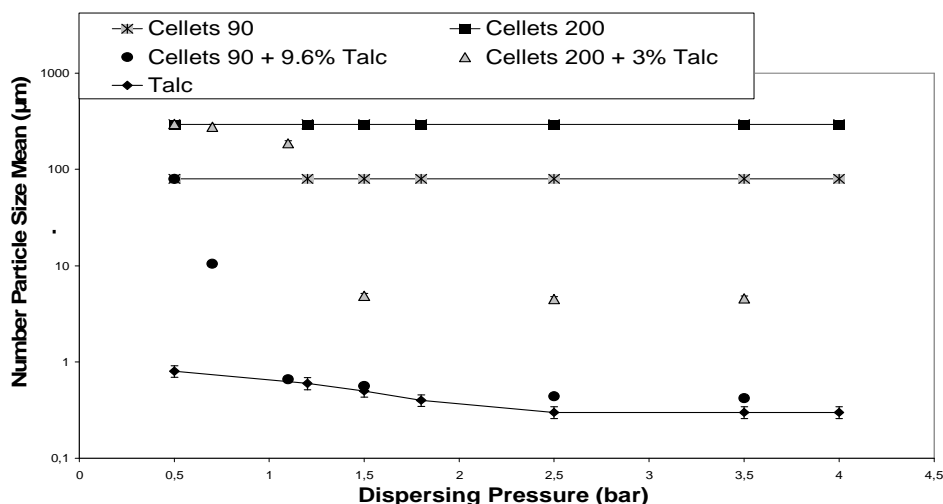


**Figure IV.79.** Number Particle Size Mean vs. Dispersing Pressure

For Talc Coated and Initial Cellets 90 and Cellets 200 Particles by Basic Mixing Method

Table IV.12 shows the particle liberation pressures and corresponding air velocities for coated cellets 90 and cellets 200 particles by basic mixing method. It was observed that particle liberation (or breakage) pressure increases with increasing size ratio between the host and guest particles as expected. The particle breakage with increasing dispersing pressures should also be considered like in hybridizer and cyclomix trials.

**Table IV.12.** Dispersing Pressures and Air Velocities for Particle Detachment for Talc Coated Pre-treated Cellets 90 and Cellets 200 Particles by Basic Mixing Method

Material	Particle Size Ratio (Host/Guest)	Dispersing Air Pressure	Air Velocity
Pre-Treated Cellets 90 + 9.6% Talc	7.1	0.7 bar	40 m/s
Pre-Treated Cellets 200 + 3% Talc	21.8	1.1 bar	56 m/s

In addition, it was observed that cellets 90 particles coated by the basic mixing method and in turbula trials have the same number particle size distributions with initial talc particles at 2.5



and 3.5 bar pressures. For hybridizer and cyclomix trials the coated particles never had the same number particle size distributions with initial talc particles. This difference probably shows the effect of the equipment on the coating strength of the particles. Figure IV.80 shows the particle liberation pressures of coated cellets 90 and cellets 200 particles in different equipments to the simple calculation of kinetic energy per mass values of the equipments.

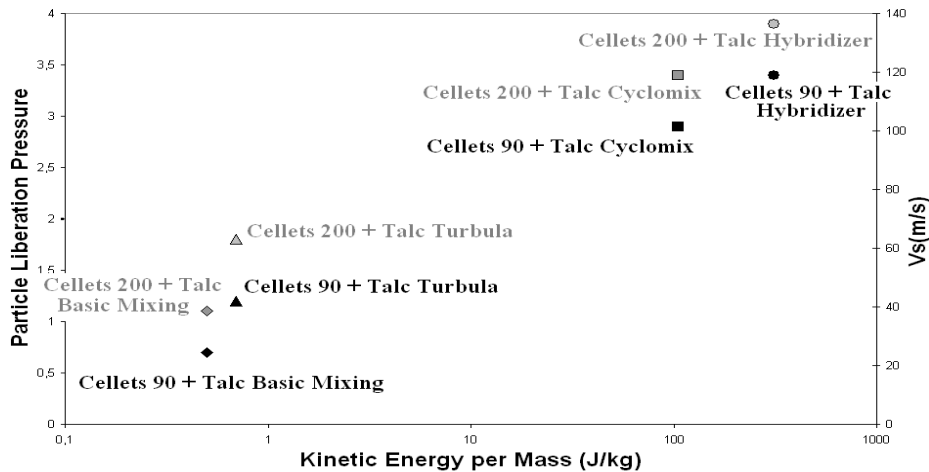


**Figure IV.80.** Particle Liberation Pressures for Coated Cellets 90 and Cellets 200 Particles in Different Equipments

The linear velocities (m/s) of the equipments from have been calculated by putting the rotational velocities (tours/second) in the equation III.9. Then, the kinetic energy per mass values have been calculated for each equipment by putting the calculated linear velocity values in the equation III.10.

It was observed that the coating strength between the cellets 200 and talc particles is stronger than the coating strength between the cellets 90 and talc particles for all the cases. It would be related to the difference in inter-particular forces between talc-cellets 90 and talc-cellets 200 particles. On the other hand, it can be seen that the particle liberation pressures are higher for the particles that were treated in high force mixers (hybridizer and cyclomix) compared to coated particles in turbula and basic mixing method since the high force mixers apply mechanical forces on the particles which causes strong interactions between the particles.

### 2.2.6. Characterizations of the Hydrophilic Properties of The Particles

In this part of the study, it is aimed to understand the effect of talc coating, which is a hydrophobic material, on the water affinity of the cellets 90 and cellets 200 particles. In order to understand the modification of the water affinity of the coated cellets 90 and cellets 200,

particles have been characterized before and after coating trials by different methods. Contact angle measurements with sessile drop technique (chapter II) was used for characterization of wettability property of the particles and dynamic vapour sorption (DVS) (chapter II) measurement have been realized in order to understand the water vapour adsorption and desorption behaviour of the particles.

#### A. Characterization of the Wettability of the Particles

The contact angle measurements have been done before and after coating of the particles in order to understand the effect of coating on the wettability of the particles. Figure IV.81 shows the contact angle measurements of individually treated and talc coated cellets 90 particles in hybridizer. It can be seen that the water droplet, on the treated (in hybridizer at 4000 rpm for 6 minutes) cellets 90 particles, almost disappears just after 3 seconds. On the other hand, it was observed that the water droplet keeps the initial contact angle even after 30 seconds on the 9.6% talc coated cellets 90 particles.

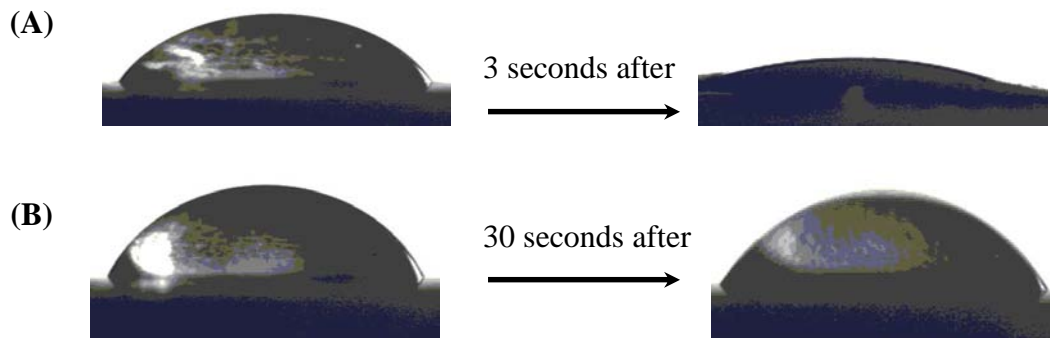


**Figure IV.81.** Contact Angle Measurements of (A) Individually Treated Cellets 90 Particles  
(B) Talc Coated Cellets 90 Particles in Hybridizer

Figure IV.82 shows the contact angle measurement of individually treated and talc coated cellets 200 particles in hybridizer. It can be seen that 5 seconds after putting the water droplet on the surface of the treated cellets 200 particles in hybridizer, the powder bed absorbs the water droplet. On the other hand, for 3% talc coated cellets 200 particles in hybridizer, the water droplet still stays on the surface of the powder bed after 30 seconds. The rest of the images of contact angle measurements for talc coated cellets 90 and cellets 200 particles in different dry coating equipments are presented in appendix VIII.

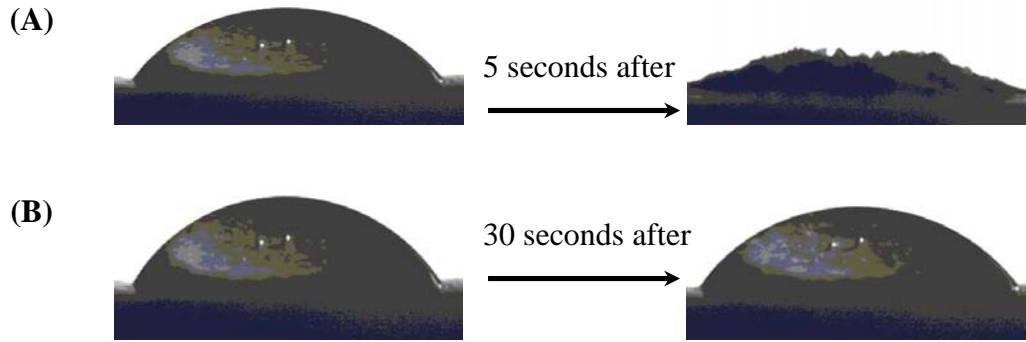


**Figure IV.82.** Contact Angle Measurements of (A) Individually Treated Cellets 200 Particles  
(B) Talc Coated Cellets 200 Particles in Hybridizer

The contact angle measurements have been done 3 times for each powder sample and at the end, the average contact angle values for uncoated and coated particles were found (Appendix VIII). It was observed that the average contact angle for individually treated cellets 90 particles in hybridizer is  $53.4^\circ$  and it increases to  $62.7^\circ$  after coating them with talc particles in hybridizer. Cellets 200 particles show the same characteristic that is the increase in contact angle after coating with talc particles. The results show that the coating of cellets particle with talc particles decreases the wettability of the particles because of the hydrophobic nature of talc.

### **B. Characterization of the Particles by Dynamic Vapour Sorption Method**

Dynamic vapour sorption method (DVS) has been used in order to understand the affinity of water vapour adsorption/desorption characteristics of the particles. In DVS measurements, the dry powder samples (around 100 mg) are equilibrated at 0% relative humidity to remove any surface adsorbed vapour and to establish a dry mass baseline. Afterwards, the isotherms were measured at  $25^\circ\text{C}$  by increasing/decreasing the relative humidity by 10% between 0% and 90% relative humidity. (Chapter II)

Figure IV.83, IV.84 and IV.85 show the adsorption/desorption isotherms of initial cellets 90, cellets 200 and talc particles.

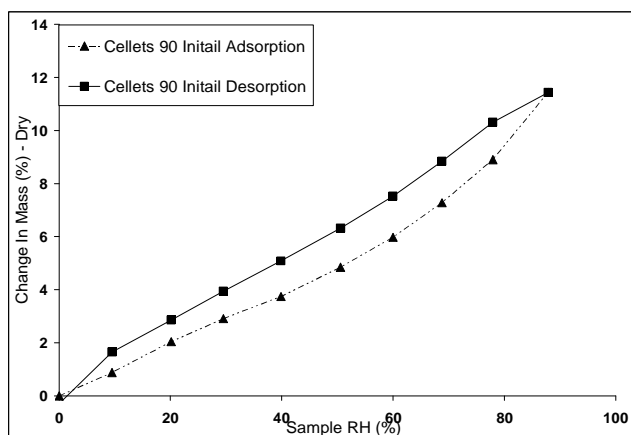


**Figure IV.83.** Water Vapour Adsorption/Desorption Isotherm of Initial Cellets 90 Particles (at 25°C)

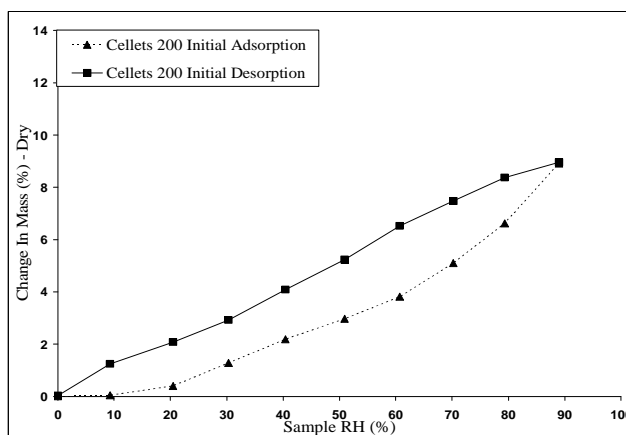


**Figure IV.84.** Water Vapour Adsorption/Desorption Isotherm of Initial Cellets 200 Particles (at 25°C)

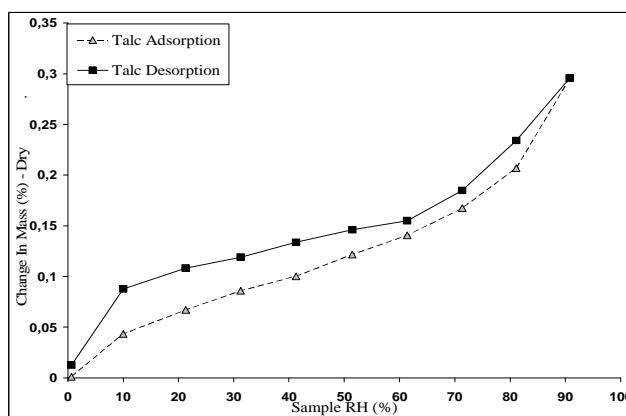


**Figure IV.85.** Water Vapour Adsorption/Desorption Isotherm of Talc Particles (at 25°C)

It was observed that the amount of water uptake for the cellets 90 and cellets 200 particles are different, which is probably reason of the difference in the total surface area. It shows that the same material with different particle size distributions may have different surface properties. It was also observed that the water uptake increases linearly with increasing relative humidity for cellets (90 & 200) and talc particles. It can be seen that the cellets 90 particles adsorbs 12% water vapour and cellets 200 particles adsorbs 8.5% water vapour at 90% relative humidity. On the other hand, it can be observed from figure IV.85 that the talc particles adsorb just 0.3% water vapour. It can be also seen that the both cellets (90&200) and talc particles releases all the water vapour that they hold at 0% relative humidity.

Figure IV.86 and IV.87 shows water vapour adsorption of the coated cellets 90 and cellets 200 particles in different dry coating equipments. It was observed that the water vapour adsorption percentage of cellets 90 particles decreases 21% (from 12% to 9.5%) after coating with talc particles in hybridizer. It can be also seen that the talc coated cellets 90 particles in cyclomix, turbula and by basic mixing method have similar water adsorption percentage (8.3%–8.5%) which is 30% less than water vapour adsorption percentage of initial cellets 90 particles. It shows that the coating with talc particles decreased the affinity of water vapour adsorption of cellets 90 particles. On the other hand, it wasn't observed a significant difference between the results of water vapour adsorption percentages of initial and coated cellets 200 particles. It was also observed that the water vapour adsorption percentage of coated cellets 90 and cellets 200 particles are higher than water vapour adsorption percentage of talc particles, since in all different dry coating trials, it has been obtained discrete type of coating so that the water vapour may penetrate the talc coating and reach the cellets particle.

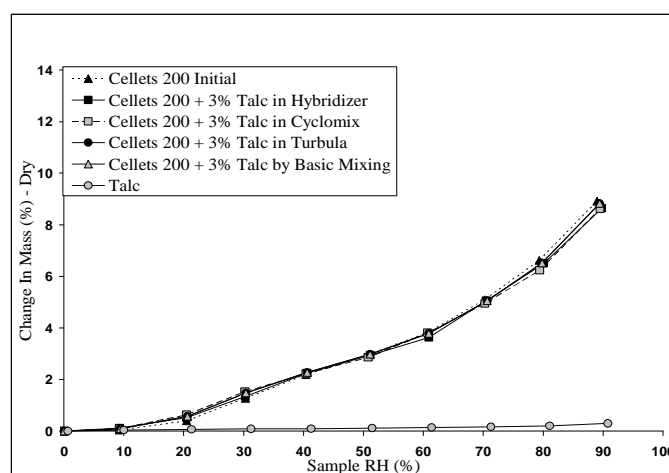
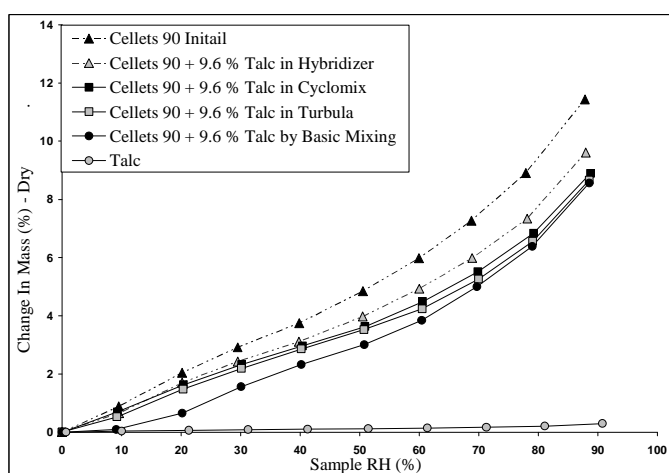


**Figure IV.86.** Water Vapour Adsorption Isotherm of Initial and Talc Coated Cellets 90 Particles (at 25°C) **Figure IV.87.** Water Vapour Adsorption Isotherm of Initial and Talc Coated Cellets 200 Particles (at 25°C)

As a perspective, it would be also interesting to study the water vapour adsorption kinetics of the particles, in different relative humidity, before and after coating in order to understand the effect of coating on the water vapour adsorption kinetics of the particles.

### 2.3. Conclusions

The effect of the host particle size on the end-use properties of the coated particles has been studied. The initial host particles (cellets 90 and cellets 200) have been treated individually in hybridizer and cyclomix. At the end of the preliminary study, the operating conditions of the dry coating trials have been determined by considering no particle fragmentation at the chosen operating velocities.

Different characterization methods have been used before and after coating the particles. Environmental Scanning Electron Microscopy (ESEM) has been used for morphological analysis of the particles. It was observed that there are some talc agglomerates in the turbula and basic mixing trials compared to trials in high force mixers (hybridizer & cyclomix). It shows that the generated mechanical energy is not sufficient to break the talc agglomerates in turbula and basic mixing trials. On the other hand, it was also observed that the talc particles are embedded in hybridizer and cyclomix trials because of the generated high mechanical energy but in turbula and basic mixing trials the talc particles are more like weakly attached on the surface of the host particles. In addition, the chemical composition analysis of the coated particles has been done by using ESEM equipped with Energy Dispersive Spectrometer (EDS). It was observed that, at the end of dry coating of cellets particles we have obtained discrete type of coating for each dry coating trial with different equipments.

The topographical analysis of the particles has been done before and after coating by using an AFM. It was observed that the average surface roughness is higher for cellets 90 particles compared to cellets 200 particles. It was also found that the surface roughness of cellets 90 and cellets 200 particles decreases after coating with talc particles. Filling up or closing of the holes and valleys on the surface of the cellets particles by talc particles could be a possible reason of decrease in surface roughness of cellets particles after coating with talc particles.

The phase angle results of cellets 90 and cellets 200 particles show that both cellets 90 and cellets 200 particles have similar phase angle signature because the only difference between them is the size of the particles. Moreover, it was observed that coating of cellets particles (90 & 200) with talc causes increase in the phase angle values which shows us the existence of talc particles on the surface since the signature of talc particles have higher phase angle values than cellets particles. On the other hand, the comparison of phase angle values show that the talc coated cellets 90 particles have more phase angle points in the higher phase angle range than initial cellets particles compared to talc coated cellets 200 particles. It is probably

the reason of coating with higher mass percentage of talc particles (9.6 %) for cellets 90 particles than talc coated cellets 200 particles (3%).

The adhesion forces between the particles have been measured by using AFM with contact mode. It was found that the average adhesion force between the talc particles is higher than the average adhesion force between talc and cellets particles. On the other hand, it was observed that the average adhesion force between cellets and talc particles increases for talc coated cellets particles as expected. The adhesion force model allowed us to calculate the talc particle deposition on the cellets 90 and cellets 200 particles by using the obtained adhesion force values from AFM measurements. It was found that the calculated amount of talc percentage on the surface of cellets particles are less than introduced amounts. The agglomeration of talc particles and non – analyzed surface zones of the particles could be possible reasons. AFM measurements with more particles would give more reliable results.

The Malvern Mastersizer laser diffraction granulometer have been used to study the coating strength of the particles. It was found that for all the dry coating trials with different equipments the coating strength between cellets 200 and talc particles are stronger than the coating strength between the cellets 90 and talc particles. It shows that the increasing size ratio between the host and guest particles increases the coating strength between the particles. In addition, it should be remembered that the decrease in particles size could be either particle detachment or breakage.

The hydrophilic properties of the particles before and after coating have been studied by contact angle and dynamic vapour sorption (DVS) measurements. The results of contact angle measurements show that coating of cellets particles (90 & 200) with talc particles increases the contact angle values which means that the wettability of the coated particles are less compared to the initial state. As an example, it was found that the contact angle value of individually treated cellets 90 particles in hybridizer is  $53.4^{\circ}$  and it is increased to  $62.7^{\circ}$  after coating with talc particles in hybridizer.

The DVS measurements showed that the water affinity of the cellets 90 particles decreases after coating with talc particles. It was found that at 90% relative humidity, the water vapour adsorption value is 12% for initial cellets 90 particles which decreases 21% after coating with talc particle in hybridizer and it decreases 30% for talc coated cellets 90 particles in cyclomix, turbula and by basic mixing methods. On the other hand, it was observed that there is no

significant difference between the results of water vapour adsorption percentage of initial and coated cellets 200 particles.

At the end, it was seen that the dry coating of particles can be done by using high shear mixers or even by simple stirring of the particles. It was observed that the particle size ratio is an important parameter that affects the coating strength proportionally, but also it should be remembered that, there are many other factors (viscoelastic properties, surface roughness, surface free energy etc.) that should be considered for analysing coating strength.



### **3. EFFECT OF GUEST PARTICLE SIZE ON THE END – USE PROPERTIES OF THE DRY COATED PARTICLES**

In the second part of the study, in order to understand the effect of guest particle size on the end–use properties of the particles, Cellets 200 ( $d_{[4;3]v}:305 \mu\text{m}$ ) particles have been coated with 2 different particle size distributions of talc particles ( $d_{[4;3]v}:14 \mu\text{m}$  and  $d_{[4;3]v}:4 \mu\text{m}$ ) by different dry particle coating equipments. In the first part, cellets 200 particles have already been coated with the talc particles that have  $14 \mu\text{m}$  volume mean diameter. In order to obtain talc particles with smaller size, the particles have been treated individually in hybridizer at 16000 rpm operating velocity (maximum operating velocity) for 6 minutes. At the end, we have obtained talc particles (talc 16000) that have  $4 \mu\text{m}$  volume mean diameter. The cellets 200 particles have been coated with talc 16000 particles ( $d_{[4;3]v}:4 \mu\text{m}$ ) and the results have been compared with the talc ( $d_{[4;3]v}:14 \mu\text{m}$ ) coated cellets 200 particles.

The preliminary study of the initial Cellets 200 particles has already been done in the first part of the study so in this part the same operating conditions have been used.

The theoretical monolayer coating percentage in hexagonal packing has also been calculated for cellets 200 with talc 16000 particles and the dry coating trials have been realized in different equipments.

#### **3.1. Dry Coating of Cellets 200 Particles with Talc and Talc 16000**

The monolayer coating percentage in hexagonal packing of the cellets 200 with different particle size distributions of talc particles have been calculated (Appendix II). It was found that, for cellets 200 with talc particles the monolayer coating percentage is 3 % and for cellets 200 with talc 16000 particles the monolayer coating percentage becomes 1.6%. The operating conditions of the dry coating trials can be seen in the table IV.13.

In Turbula trials, cellets 200 particles were pre-treated in hybridizer at 4000 rpm rotational velocity. Afterwards, the pre-treated Cellets 200 particles have been treated with talc and talc 16000 particles inside a 1lt container (30 g) at 96 rpm operating velocity for 6 minutes by turbula.

The cellets 200 with talc and talc 16000 particles have also been coated by basic mixing method. In basic mixing, cellets 200 particles are also pre-treated in hybridizer at 4000 rpm operating velocity and then mixed with guest particles by shaking them by hand as it was done in the first part of the study.

**Table IV.13.** Operating Conditions of Dry Coating Treatments

Host Particles	Guest Particles	Equipment	Operating Velocity (rpm)	Operating Time (min)	Mass % of Guest Particles	Batch Size (g)	Cooling Jacket (°C)
Cellets 200	Talc	Hybridizer	4000	6	3 %	30	13
	Talc 16000				1.6 %		
Cellets 200	Talc	Cyclomix	1600	6	3 %	500	13
	Talc 16000				1.6 %		
PreManip. Cellets200	Talc	Turbula	96	6	3 %	30	none
	Talc 16000				1.6 %		

In order to have the morphological analysis of the particles, the ESEM has been used before and after coating of the particles. The coating strength of the particles has been studied by using Malvern Mastersizer laser diffraction granulometer. In order to understand the effect of guest particle size on the coating strength of the particles, the results of the granulometer for coated cellets 200 particles with different particle size of talc particles have been compared with each other.

### 3.1.1. Characterization of Surface Morphology of the Particles

The figure IV.88 shows the ESEM images of coated cellets 200 particles with different particle size of talc particles in different dry coating equipments. It was observed that there is no particle breakage after dry coating treatments in any equipment. It can be seen that the talc particles on the surface of cellets 200 particles are more distinctive than talc 16000 particles on the cellets 200 particles because of their higher particle size distribution compared to talc 16000 particles and also higher mass percentage in the mixture. On the other hand, it was also observed that there are more talc agglomerates in the mixture in turbula trials than hybridizer

and cyclomix trials probably reason of the mechanical energy that the equipment applies on the particles in dry coating process.

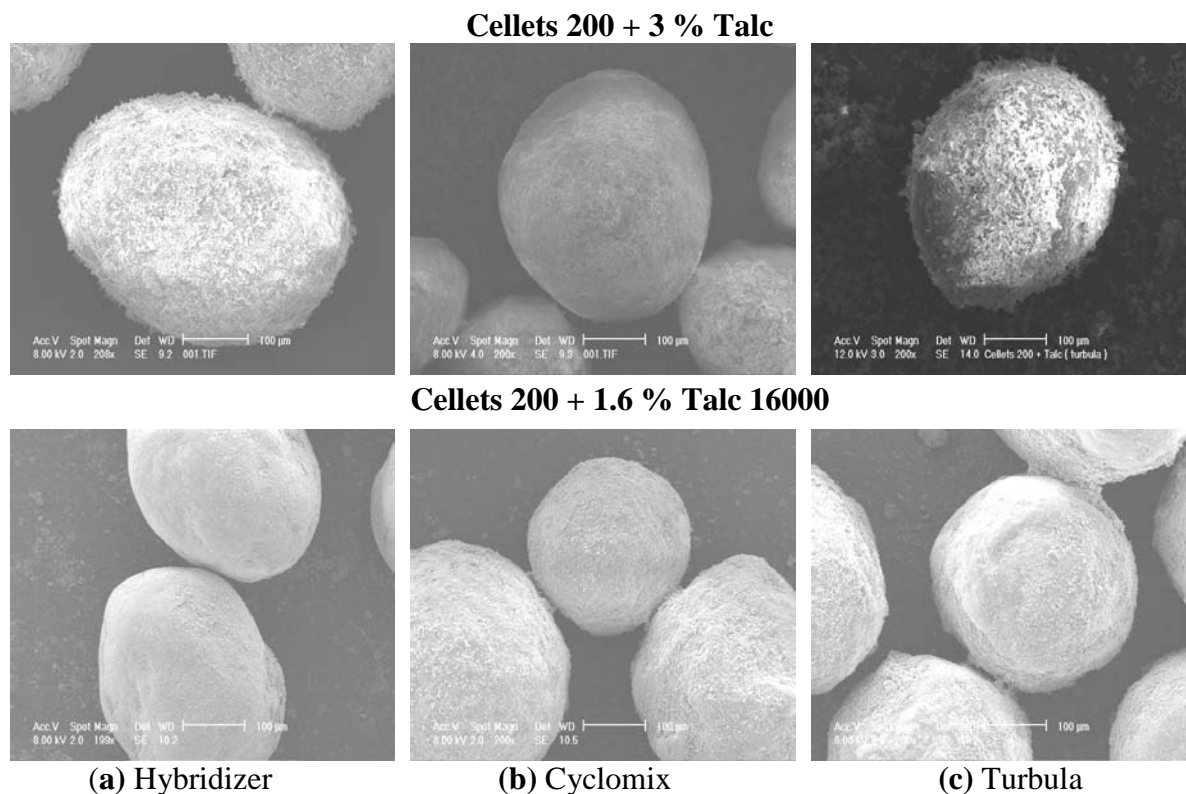


**Figure IV.88.** Surface Morphology of Coated Cellets 200 Particles with Talc and Talc 16000 Particles in Different Equipments

The visual analysis has been also done for the coated particles by basic mixing method. It can be seen that there are talc agglomerates on the surface of the cellets 200 particles (fig. IV.89 a & b). It was also observed that the talc particles are just attached on the surface of the cellets particles because of the inter-particle forces between the particles.

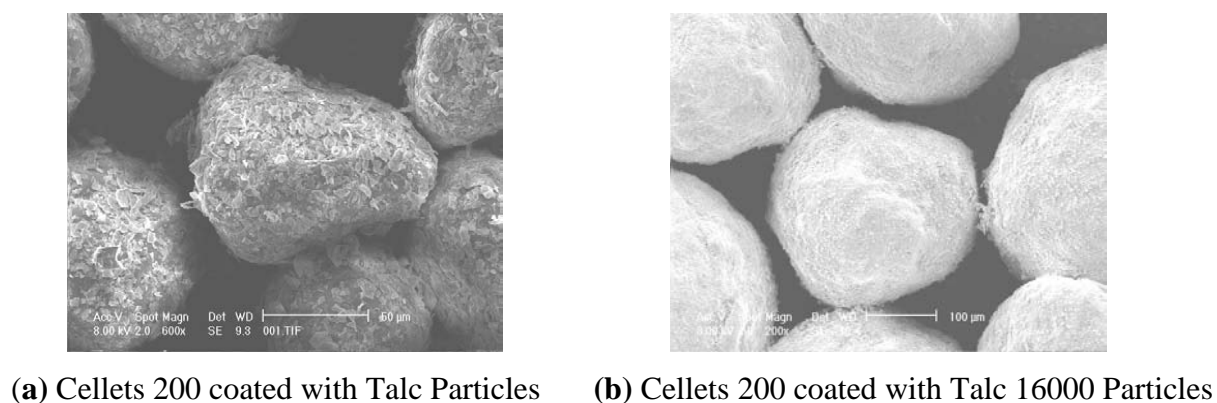


**Figure IV.89.** Surface Morphology of Coated Cellets 200 Particles with Talc and Talc 16000 Particles by Basic Mixing Method

The SEM/EDS was also used to analyse the chemical composition of the surface of the coated particles. Figure IV.89 shows the SEM/EDS results of a talc coated cellets 200 particle in cyclomix. It can be seen that, in some regions we have the components of talc particles (silicon and magnesium) but in some regions we don't have these components. It shows that we have obtained a discrete talc coating on the surface of cellets 200 particle.

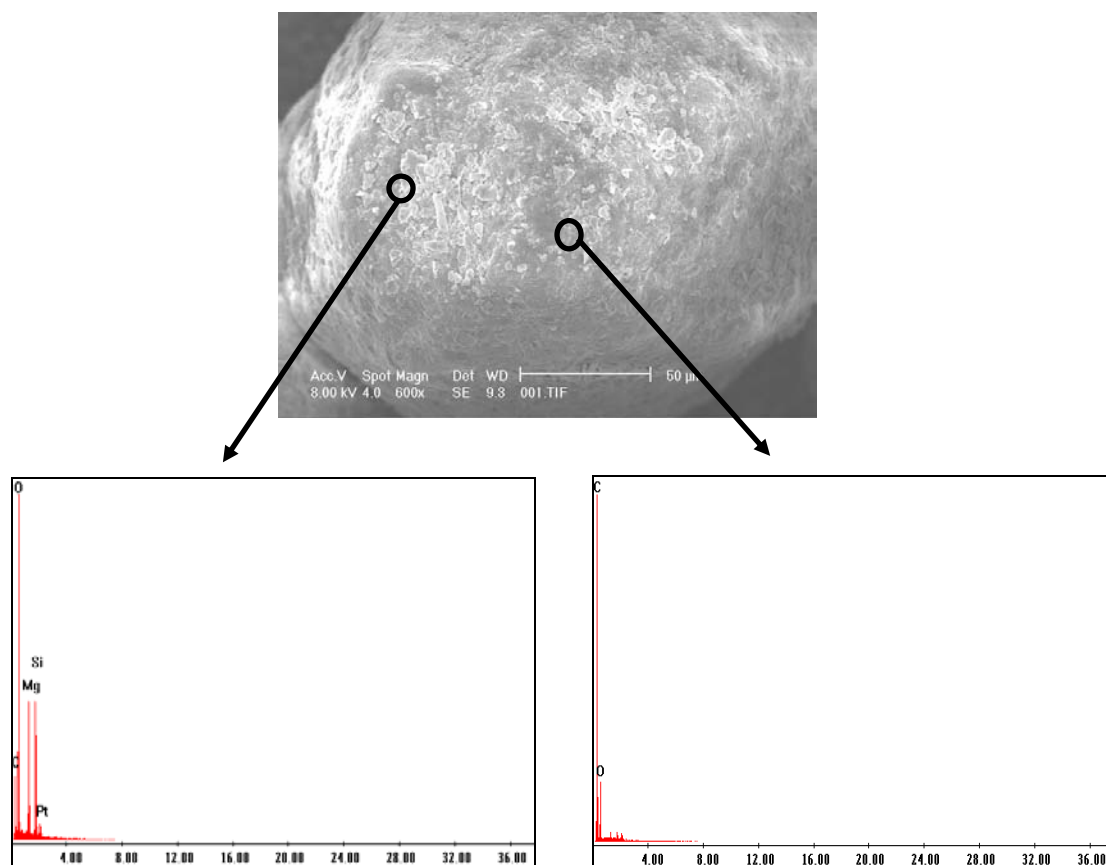


**Figure IV.90.** Chemical Analysis of the Surface of Talc Coated Cellets 200 Particle in Cyclomix

The same study has also been done for talc 16000 coatings in different equipments and it was observed that for all equipments we have obtained discrete type of coating for both talc and talc 16000 coatings. (Appendix.VII)

### 3.1.2. Characterization of Coating Strength of the Particles

In this part of the study, the Malvern Mastersizer in dry feed mode has been used to find the particle size distribution of the particles with different air dispersing pressures. The coating strength results of talc coated cellets 200 particles have been compared with talc 16000 coated

cellets 200 particles for each dry coating equipment. At the end, the effect of the equipment on the coating strength of the particles has also been studied.

### A. Coating Strength of the Particles in Hybridizer Trials

In this part, the coating strength of cellets 200 coated with two different particle size distributions of talc particles in hybridizer have been compared. The volume and number particle size distributions of talc 16000 coated cellets 200 particles can be seen in the figure IV.91 and IV.92.

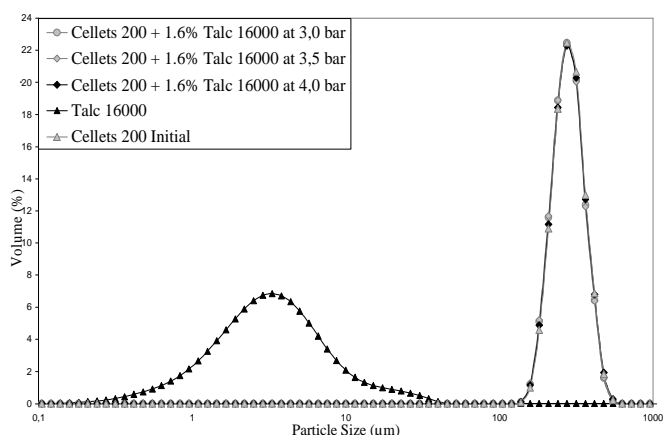


**Figure IV.91.** Volume Particle Size Distribution of 1.6 % Talc 16000 Coated Cellets 200 Particles in Hybridizer

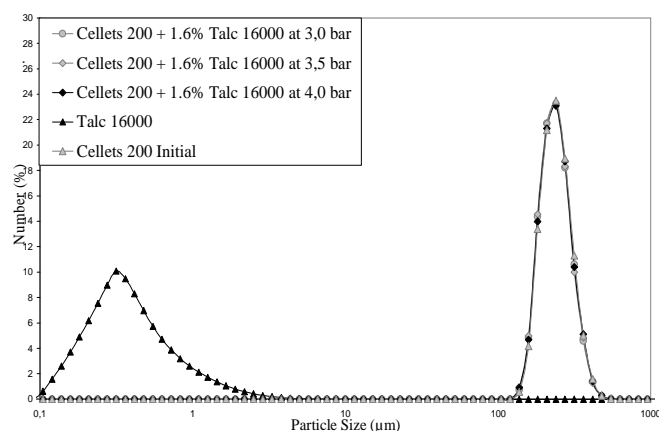


**Figure IV.92.** Number Particle Size Distribution of 1.6 % Talc 16000 Coated Cellets 200 Particles in Hybridizer

It can be seen that for all dispersing pressures, coated cellets 200 particles have the same particles size distributions. Even at 4.0 bar dispersing pressure (maximum air pressure of the granulometer) we didn't observe any fine particle populations. This results show that the coating strength of the talc 16000 coated cellets 200 particles in hybridizer, is high enough even at 4.0 bar dispersing pressure. The particle liberation pressure of the talc 16000 coated cellets 200 particles is higher than the dispersing air pressure range of the granulometer.

On the other hand, the particle liberation pressure for 3% talc coated cellets 200 particles have already been determined in the first part of the study. It was found that the particle liberation pressure is 3.9 bar and it corresponds to 124 m/s air velocity.

Table IV.14 shows the particle liberation pressures and corresponding air velocities for coated cellets 200 particles. It can be seen that for the same host particle with smaller size of guest particle has higher particle liberation pressure compared to the same guest particle with higher particle size distribution. It shows the particle size ratio between the host and guest particles

has an important role for inter-particle forces. On the other hand, it should be remembered that the decrease in particle size distribution of the particles may also correspond to particle fragmentation.

**Table IV.14.** Dispersing Pressures and Air Velocities for Particle Detachment for Talc and Talc 16000 Coated Cellets 200 Particles in Hybridizer

Material	Particle Size Ratio (Host/Guest)	Dispersing Air Pressure	Air Velocity
Cellets 200 + 3 % Talc	21.8	3.9 bar	124 m/s
Cellets 200 + 1.6 % Talc 16000	76.3	> 4.0 bar	> 124 m/s

### B. Coating Strength of the Particles in Cyclomix Trials

The coating strength of talc coated cellets 200 and talc 16000 coated cellets 200 particles in cyclomix have also been studied. Figure IV.93 and IV.94 show the volume and number particle size distributions of coated and uncoated particles at 0.5, 1.5 and 2.5 bars dispersing pressures.

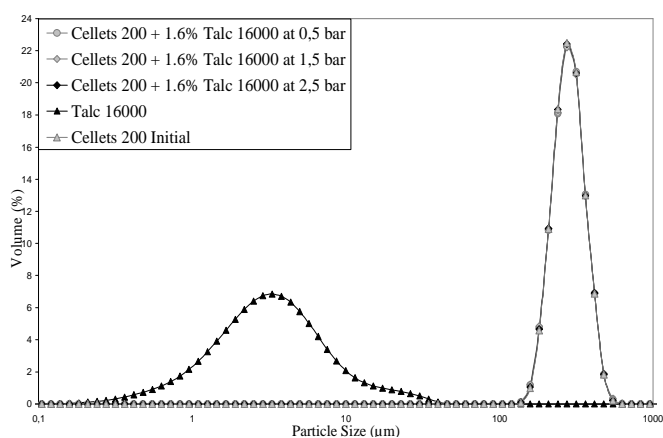


**Figure IV.93.** Volume Particle Size Distribution of 1.6 % Talc 16000 Coated Cellets 200 Particles in Cyclomix

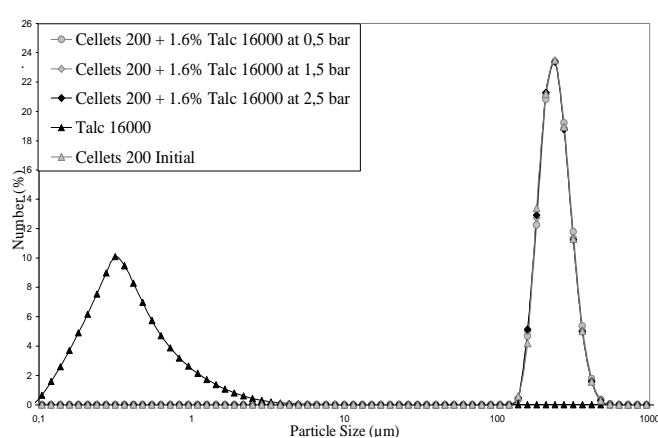


**Figure IV.94.** Number Particle Size Distribution of 1.6 % Talc 16000 Coated Cellets 200 Particles in Cyclomix

It was observed that the talc 16000 coated cellets 200 particles have the same particle size distributions at 0.5, 1.5 and 2.5 bars dispersing pressures. The particle size distributions of cellets 200 with talc 16000 particles at 3.5 and 4.0 bars can be seen in the figure IV.95 and IV.96. It was observed that at 4.0 bars there is fine population of the coated cellets 200

particles. It shows that the particle liberation pressure is between 3.5 and 4.0 bars for talc 16000 coated cellets 200 particles.

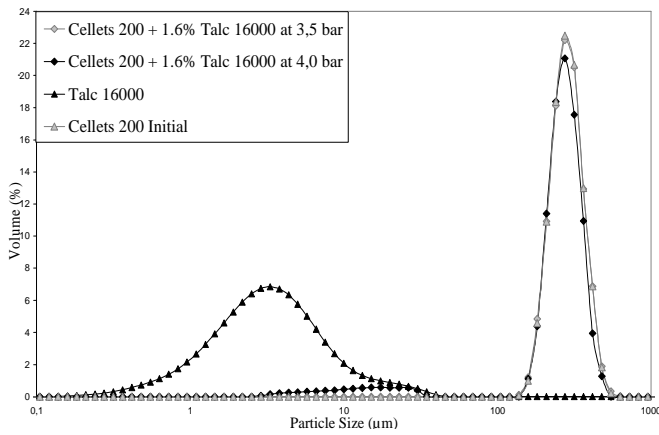


**Figure IV.95.** Volume Particle Size Distribution of 1.6 % Talc 16000 Coated Cellets 200 Particles in Cyclomix

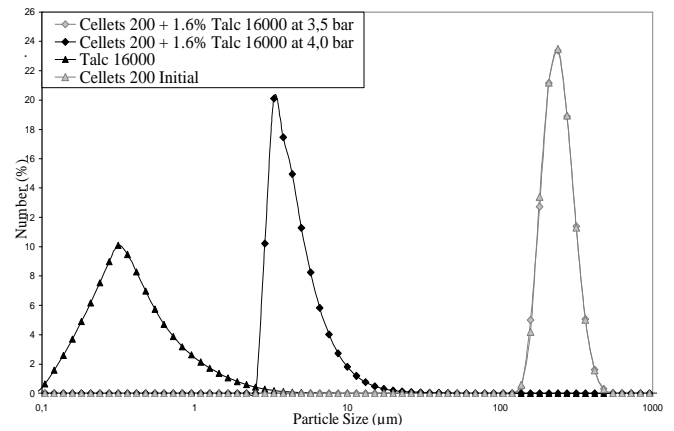


**Figure IV.96.** Number Particle Size Distribution of 1.6 % Talc 16000 Coated Cellets 200 Particles in Cyclomix

The particle size distributions of the talc 16000 coated cellets 200 particles have been analysed for each pressure between 3.5 and 4.0 bars in order to find the particle liberation pressure more precisely. The particle liberation pressure for talc coated cellets 200 particles was already found in the first part and it is 3.4 bars. It was found that the particle liberation pressure increases to 3.8 bars for talc 16000 coated cellets 200 particles. (fig.IV.97)

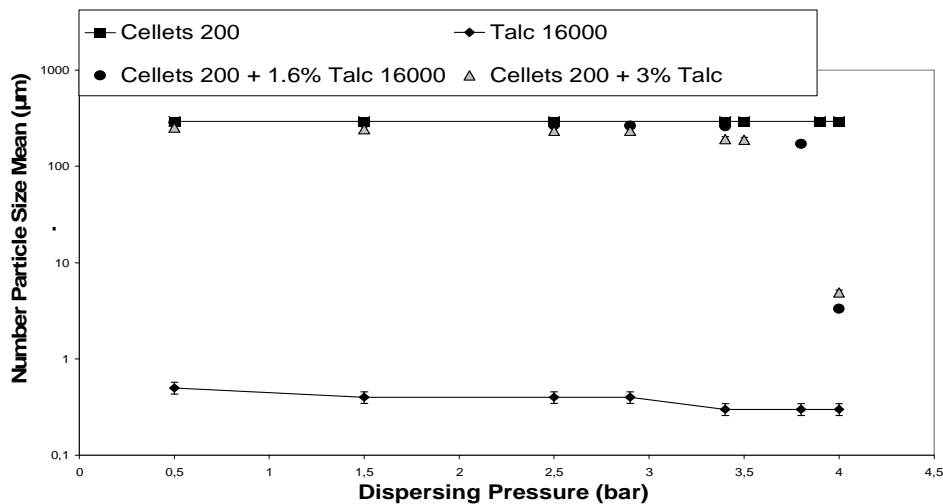


**Figure IV.97.** Number Particle Size Mean vs. Dispersing Pressure for Talc and Talc 16000 Coated Cellets 200 Particles in Cyclomix

Table IV.15 shows the particle liberation pressures for coated cellets 200 particles with talc and talc 16000 particles. Cyclomix trials also shows that the increasing particle size ratio between the host and guest particles causes higher coating strength property for the coated particles. In addition, the possible particle fragmentations in the granulometric analysis should also be considered as a reason for decrease in particle size distributions of the particles.

**Table IV.15.** Dispersing Pressures and Air Velocities for Particle Detachment for Talc and Talc 16000 Coated Cellets 200 Particles in Cyclomix

Material	Particle Size Ratio (Host/Guest)	Dispersing Air Pressure	Air Velocity
Cellets 200 + 3 % Talc	21.8	3.4 bar	118 m/s
Cellets 200 + 1.6 % Talc 16000	76.3	3.8 bar	123 m/s

### C. Coating Strength of the Particles in Turbula Trials

The volume and number particle size distributions of pre-treated cellets 200 particles (in hybridizer at 4000 rpm for 6 min) coated with talc 16000 particles at 0.5 and 1.5 bars can be seen in the figure IV.98 and IV.99.

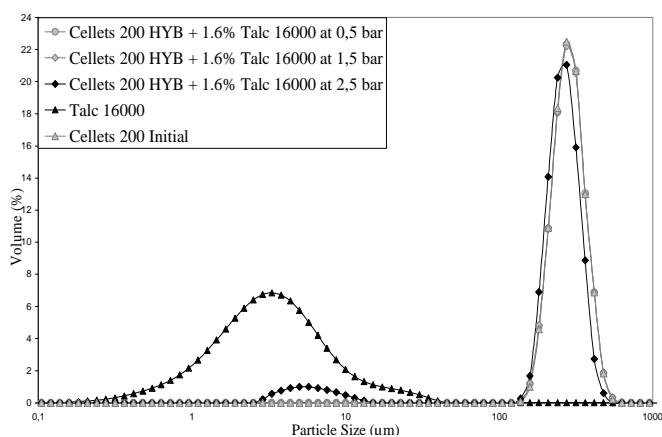


**Figure IV.98.** Volume Particle Size Distribution of 1.6 % Talc 16000 Coated Pre-treated Cellets 200 Particles in Turbula

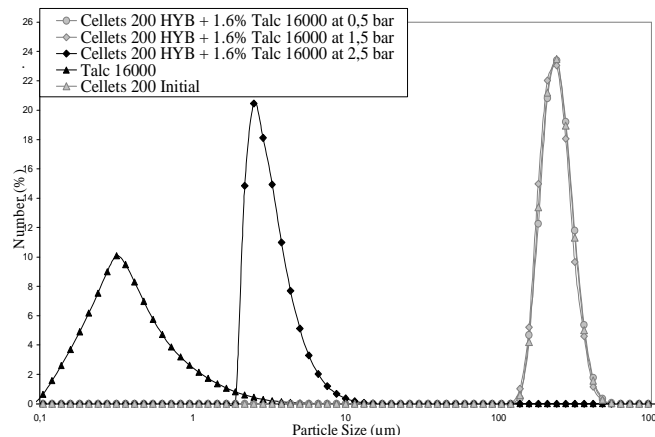


**Figure IV.99.** Number Particle Size Distribution of 1.6 % Talc 16000 Coated Pre-treated Cellets 200 Particles in Turbula

It was observed that coated cellets 200 particles keep their particle size distribution until 1.5 bars dispersing pressure. At 2.5 bars dispersing pressure, it can be seen that there is 2 different particle size populations for coated cellets 200 particles. It shows that the particle



liberation pressure is between 1.5 and 2.5 bars for 1.6% talc 16000 coated cellets 200 particles. On the other hand, it can be seen that the volume of fine population increases at 3.5 bars dispersing pressure as expected (figure IV.100, IV.101).

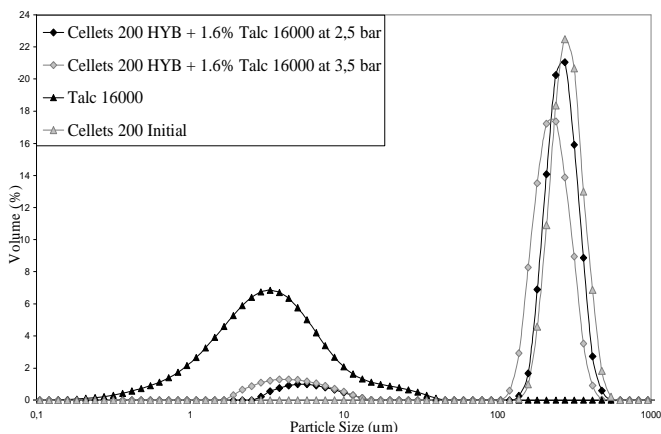


**Figure IV.100.** Volume Particle Size Distribution of 1.6 % Talc 16000 Coated Pre-treated Cellets 200 Particles in Turbula

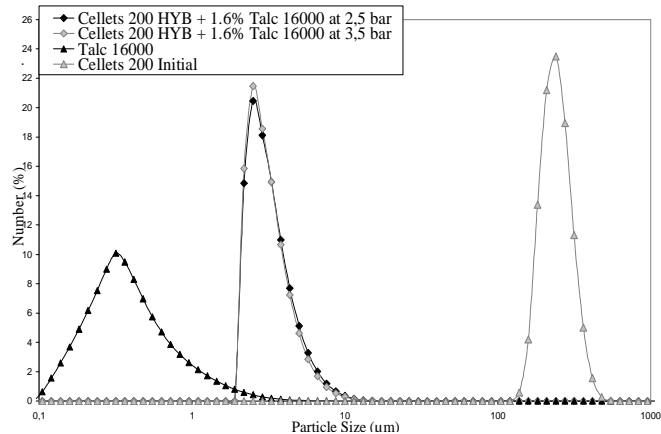


**Figure IV.101.** Number Particle Size Distribution of 1.6 % Talc 16000 Coated Pre-treated Cellets 200 Particles in Turbula

At the end, it was found that the particle liberation pressure is 2.1 bars for talc 16000 coated cellets 200 particles. The particle liberation pressure has already been determined for talc coated cellets 200 particles in turbula in the first part and it is 1.8 bars. (fig.IV.102)

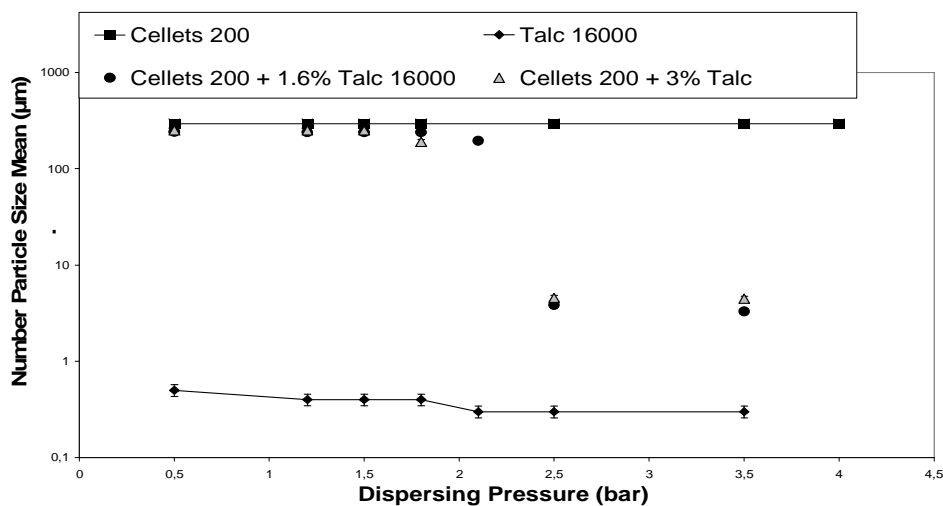


**Figure IV.102.** Number Particle Size Mean vs. Dispersing Pressure For Talc and Talc 16000 Coated Cellets 200 Particles in Turbula

Table IV.16 shows the particle liberation pressures for coated cellets 200 particles with talc and talc 16000 particles in turbula. It was observed that, the particle liberation (or fragmentation) pressure increases with increasing size ratio between the host and guest particles also in turbula trials.

**Table IV.16.** Dispersing Pressures and Air Velocities for Particle Detachment for Talc and Talc 16000 Coated Cellets 200 Particles in Turbula

Material	Particle Size Ratio (Host/Guest)	Dispersing Air Pressure	Air Velocity
Pre-Treated Cellets 200 + 3 % Talc	21.8	1.8 bar	81 m/s
Pre-Treated Cellets 200 + 1.6 % Talc 16000	76.3	2.1 bar	89 m/s

**D. Coating Strength of the Particles in Basic Mixing Trials**

The coating strength of the pre-treated cellets 200 particles coated with talc particles have already been determined in the first part of the study. It was found that the particle liberation pressure is 1.1 bars for the particles. In this part, the coating strength of the pre-treated cellets 200 particles coated with talc 16000 particles have been studied. The volume and number particle distributions of 1.6 % talc 16000 coated cellets 200 particles at 0.5 and 1.5 bars pressures can be seen in the figure IV.103 and IV.104.

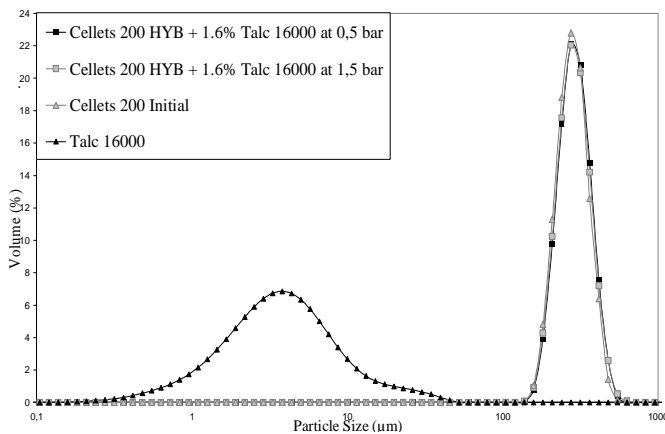


**Figure IV.103.** Volume Particle Size Distribution of 1.6 % Talc 16000 Coated Pre-treated Cellets 200 Particles by Basic Mixing Method

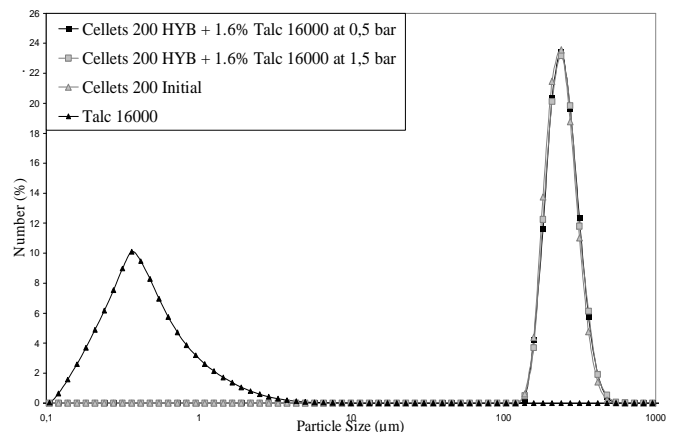


**Figure IV.104.** Number Particle Size Distribution of 1.6 % Talc 16000 Coated Pre-treated Cellets 200 Particles by Basic Mixing Method

It was observed that there is no particle detachment up to 1.5 bars dispersing pressures. On the other hand, it can be seen that there is a population of fine particles at 2.5 bars dispersing pressure (fig. IV.105 and IV.106) and volume of that population increases at 3.5 bar pressure.

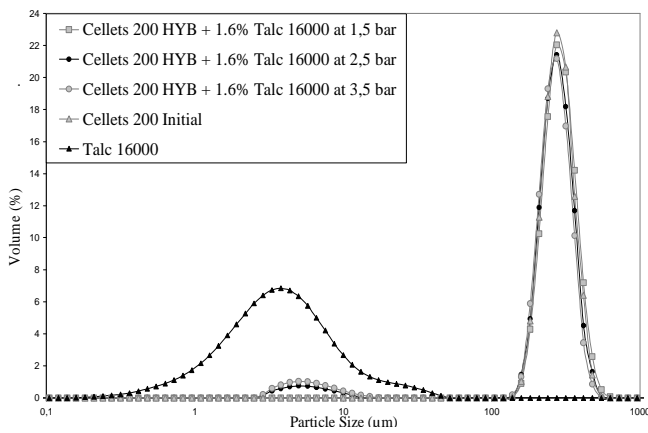


**Figure IV.105.** Volume Particle Size Distribution of 1.6 % Talc 16000 Coated Pre-treated Cellets 200 Particles by Basic Mixing Method

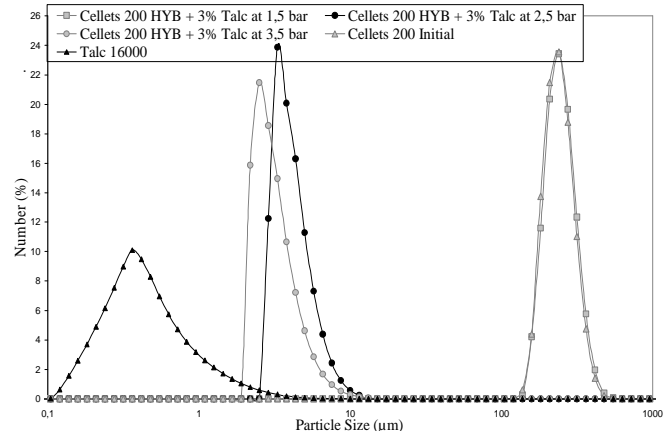


**Figure IV.106.** Number Particle Size Distribution of 1.6 % Talc 16000 Coated Pre-treated Cellets 200 Particles by Basic Mixing Method

In order to find the particle liberation for talc 16000 coated cellets particles more precisely, the particle size analysis have been realized between the 0.5–1.5 bars pressure range. It was found that the particle liberation pressure is 1.6 bars for talc 16000 coated cellets 200 particles. (fig. IV.107)

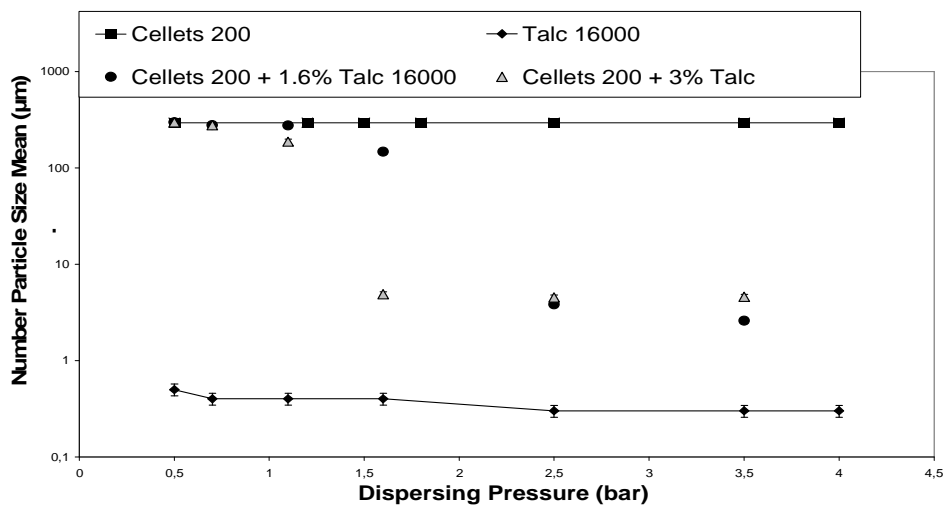


**Figure IV.107.** Number Particle Size Mean vs. Dispersing Pressure For Talc and Talc 16000 Coated Cellets 200 Particles by Basic Mixing Method

The particle liberation pressures and the corresponding air velocities for the coated particles can be seen more precisely in the table IV.17. It can be seen that the particle liberation pressure is higher for talc 16000 coated cellets 200 particles compared to talc coated cellets 200 particles also for the basic mixing trials. It shows the effect of particle size ratio between the host and guest particles on the coating strength of the particles.

**Table IV.17.** Dispersing Pressures and Air Velocities for Particle Detachment for Talc and Talc 16000 Coated Cellets 200 Particles by Basic Mixing Method

<b>Material</b>	<b>Particle Size Ratio (Host/Guest)</b>	<b>Dispersing Air Pressure</b>	<b>Air Velocity</b>
<b>Pre-Treated Cellets 200 + 3 % Talc</b>	21.8	1.1 bar	56 m/s
<b>Pre-Treated Cellets 200 + 1.6 % Talc 16000</b>	76.3	1.6 bar	74 m/s

At the end, it was observed that the coating strength between the cellets 200 and talc particles is higher than the coating strength between the cellets 200 and talc 16000 particles for all dry coating trials with different equipments (table IV.18).

**Table IV.18.** Dispersing Pressures and Air Velocities for Particle Detachment for Talc and Talc 16000 Coated Cellets 200 Particles in Different Equipments

<b>Material</b>	<b>Equipment</b>	<b>Dispersing Air Pressure (bar)</b>	<b>Air Velocity (m/s)</b>
<b>Cellets 200 + 3 % Talc</b>	Hybridizer	3.9	124
<b>Cellets 200 + 1.6 % Talc 16000</b>		>4.0	>124
<b>Cellets 200 + 3 % Talc</b>	Cyclomix	3.4	118
<b>Cellets 200 + 1.6 % Talc 16000</b>		3.8	123
<b>Pre-Treated Cellets 200 + 3 % Talc</b>	Turbula	1.8	81
<b>Pre-Treated Cellets 200 + 1.6 % Talc 16000</b>		2.1	89
<b>Pre-Treated Cellets 200 + 3 % Talc</b>	Basic Mixing	1.1	56
<b>Pre-Treated Cellets 200 + 1.6 % Talc 16000</b>		1.6	74

In addition, it was observed that the particle liberation pressures are higher for the particles that were treated in hybridizer and cyclomix compared to coated particles in turbula and basic mixing method because of the difference in the supplied mechanical energy on the particles by the equipment.

### **3.2. Conclusions**

Cellets 200 particles have been coated with two different particle size distributions of talc particles in different dry coating equipments. The preliminary study has been done for the cellets 200 particles in order to understand the fragmentation behaviour of the particles in different equipments and afterwards the operating conditions for the dry coating trials have been determined.

Visual analysis has been done before and after coating of the particles by ESEM. It was observed that in turbula and basic mixing trials there are some agglomerates of guest particles because of the lack of generated mechanical forces by the equipment probably.

The ESEM/EDS analysis has also taken a place in order to understand the chemical composition of the surface of the particles. The results show that we have obtained discrete coating for both cellets 200 with talc and cellets 200 with talc 16000 coatings in all dry coating trials with different equipments.

The coating strength of the particles has been studied by using the granulometer. The results show that the coating strength is higher between the cellets 200 and talc 16000 particles compared to cellets 200 with talc particles. It shows that coating strength between the particles increases with increasing particle size ratio between the host and guest particles. On the other hand, it should be remembered that the decrease in the particle size distribution in granulometric analysis could be also reason of particle fragmentation. In order to have better analyse of granulometric results it would be a nice idea to recover the particles after granulometric analysis and visually analyse them again by ESEM then it would be possible to understand if the decrease in particle is reason of particle detachment of fragmentation.

#### 4. CONCLUSIONS

In this study, cellets particles with two different particle size distributions ( $d_{[4;3]_v}$ :100  $\mu\text{m}$  and  $d_{[4;3]_v}$ :305  $\mu\text{m}$ ) have been coated with two different particle size distributions of talc particles ( $d_{[4;3]_v}$ :14  $\mu\text{m}$  and  $d_{[4;3]_v}$ :4  $\mu\text{m}$ ) by different dry coating equipments in order to understand the effect of host and guest particle size on the end-use properties of the particles. The theoretical monolayer coating percentage in hexagonal packing has been calculated for the particles.

In the first part, cellets particles with two different particle sizes have been coated with talc particles. In the second part, cellets 200 particles have been coated with two different particle size distributions of talc particles. The operating conditions of the equipments for dry coating trials have been determined in the preliminary study of the particles. Afterwards, cellets particles have been coated with talc particles in different dry coating equipments.

Different characterization methods have been used before and after coating of the particles. The visual analysis showed that for all the dry coating trials we have obtained discrete type of coating.

The AFM has been used to have the topographical analysis (surface roughness, chemical composition, elasticity etc.) of the particles. It was observed that cellets 90 and cellets 200 particles have similar phase angle signatures because basically they are the same material but with different size distributions. On the other hand, it was found that cellets 90 particles have higher surface roughness values than cellets 200 particles. The surface roughness of both cellets 90 and cellets 200 particles decrease after coating with talc particles.

The Van der Waals forces have an important role on particle adhesion and may give an idea of the initial adhesion affinity between the powders. A rough estimation of the Van der Waals forces between the particles has been calculated. It was observed that the Van der Waals forces between Cellets–Talc is greater than between the host particles (cellets) and between the guest (talc) particles. It shows that the guest particles have much more affinity to have adhesion with host particles than with guest particles so the dry coating has also been helped by the initial adhesion affinity properties of the chosen particles. On the other hand, it should be remembered that there are many other factors (process action, elastic – ductile properties, surface energy etc.) that have effects on the mechanical coating strength of the particles.

The adhesion forces between the particles have been measured by using AFM with contact mode. Afterwards, the guest particle deposition on the host particles has been calculated by

using the adhesion force model. The results show that calculated amount of talc particles is less than introduced amount. The possible reasons could be agglomeration of talc particles, non-analyzed surface zones.

The Malvern Mastersizer laser diffraction granulometer have been used to study the coating strength of the particles. The coating strength of the particles depends on the way the host and guest particles are brought into contact and on the physico-chemical interactions between them. It was observed that the larger the size ratio of host and guest particles the stronger the coating strength for all the different processes used. On the other hand, it should be considered that there are many factors influencing adhesion: particle size and shape, surface roughness, material hardness and elasticity and the work of adhesion and surface free energy. Surface roughness is one of the most important characteristic influencing the adhesion because it is strongly related to the geometry of contact.

The water affinity of the particles before and after coating has been studied by contact angle and dynamic vapour sorption (DVS) measurements. The contact angle results show that the cellets (90&200)-talc composite particles have lower wettability than individually treated cellets 90 and cellets 200 particles because of very hydrophobic characteristic of talc particles. The DVS results shows that the talc coated cellets 90 particles in any dry coating equipment has lower water vapour adsorption percentage compared to initial cellets 90 particles. On the other hand, it was seen that the water vapour adsorption percentages of initial and coated cellets 200 particles are the same.

As conclusion, it was observed that the coating of the host particles by guest particles can be achieved by high energy impact coating devices and also even by simple stirring method. It was seen that the particle size ratio between the host and guest particles affects proportionally the mechanical coating strength of the particles. On the other hand, it was also observed that the particle size ratio between the host and guest particles, hasn't affected the water affinity and wettability properties of the composite particles.





## CONCLUSIONS & PERSPECTIVES



In this study, dry particle coating has been successfully used for the synthesis of materials with new/improved end–use properties.

***In the first part:*** it is aimed to understand the effect of the dry particle coating equipment and operating conditions on the end-use properties of the particles. Three different dry coating equipments (Hybridizer, Cyclomix, Turbula) with different operating conditions have been used. Some key parameters that affect the end–use properties of the particles have been studied for a model couple of PMMA (d[4;3]<sub>v</sub>:160 μm) coated with two different mass percentages of talc (d[4;3]<sub>v</sub>:14 μm) particles. The feasibility of the dry coating process has been examined, both quantitatively and qualitatively, and the results have been compared with coating by simple mechanical mixing (basic mixing method).

The hybridizer, cyclomix and turbula have different characteristics according to their working mechanism/principle and type of mechanical energy that they apply on the particles. In order to understand the fragmentation behaviour of the particles and to define the operating conditions for each equipment, the particles have been treated individually in “preliminary study” with different operating conditions for the dry coating trials.

The theoretical monolayer coating percentage in hexagonal packing has been calculated for the particles. It was found that 5 % talc is needed for monolayer coating of PMMA particles. 1% has been chosen as the second coating percentage in order to understand the effect of coating percentage of talc on the end–use properties of the particles. Afterwards, dry coating of PMMA with talc particles has been done in different equipments.

***In the hybridizer trials,*** it was observed that due to intense impaction forces in hybridizer, the materials underwent severe size reduction in the preliminary study. It was seen that the particle size of the PMMA particles was reduced to less than 10 μm at high rotational velocities. On the other hand, talc particles could keep their particle size for each operating velocities. In addition, it was observed that the particle recovery varies from 60% and goes up to 90% for 9600 rpm operating velocity.

Visual analysis shows that we have obtained discrete type of talc coating for each operating velocities of the hybridizer trials. Moreover, the amount of talc particles on the surface of the PMMA particles is greater for the 5 % talc coating than 1 % talc coating, as it was expected.

In order to have the topographical analysis of the particles (surface roughness, phase difference etc.) and to find the adhesion forces between the particles the Atomic Force Microscopy (AFM) has been used with tapping mode. It was found that the talc particles have

higher surface roughness ( $R_{a_{ave}}$ :131 nm,  $RMS_{ave}$ :186 nm) values than initial PMMA particles ( $R_{a_{ave}}$ :86 nm,  $RMS_{ave}$ :118 nm). On the other hand, it was observed that talc coating increases surface roughness of the PMMA particles. Moreover, it was found that 5% talc coated PMMA particles have higher surface roughness values than 1% talc coated PMMA particles, as it can be expected.

On the other hand, in AFM analysis, the phase angle values have been also determined for initial and coated particles. It was found that the talc particles have larger phase angle range (between  $-130^\circ$  and  $110^\circ$ ) than PMMA (between  $-100^\circ$  and  $40^\circ$ ) particles. The reason is probably the difference in the surface roughness but also the difference in softness between PMMA and talc particles. It was found that coating of PMMA with talc particles causes to have higher phase angle values for coated particles.

The adhesion forces between the particles have been found by using the AFM on contact mode. In the AFM trials, the adhesion forces between the uncoated/coated PMMA particles, talc particles and talc particles that were fixed on the cantilever tip have been determined. It was observed that the adhesion forces between the talc particles are higher than the adhesion forces between talc and PMMA particles. This results show that, the talc particles have much more affinity to adhere with talc particles rather than PMMA particles.

Afterwards, the talc particle deposition on the PMMA particles has been calculated by using a adhesion force model. It was obtained the calculated values of talc particle deposition are very close to 1% and 5% values. To explain the difference, the non analyzed zones of the particles may be one of the reason and also the loss talc particles after treatment in the hybridizer has to be considered. On the other hand, agglomeration of talc particles on the surface of the PMMA particle (more than monolayer coating) can be one of the reasons. It is sure that more AFM experiments would give more reliable results.

The coating strength of the composite particles has been studied by using a Malvern Mastersizer laser diffraction granulometer. It was observed that the particle liberation pressure increases with increasing rotational velocity, which is probably related to the energy that the system supplies to the particles in order to break the agglomerates and coat the host particles. On the other hand, while analysing the granulometric results of the particles, it should be remembered that the decrease in particle size could be reason of particle detachment and also particle fragmentation.

A tapped density tester and Freeman Technology Powder Rheometer (FT4) have been used in order to study the flowability properties of the particles and the effects of operating velocity, coating percentage and equipment on the flowability properties of the powders. It was observed that the flowability of the PMMA particles decreases at high operating velocities since the particles are either all broken or there are some fragments of the particles at these velocities, which causes increase in the contact surface of the particles.

The results of tapped density tester and the FT4 show that the dry coated PMMA particles with talc particles (1% and 5%) have better flowability properties than grinded PMMA particles at all of the operating velocities.

***In the cyclomix trials***, the results of the preliminary study showed that there is no particle fragmentation at even high operating velocities of cyclomix, which is defined also as a high force mixer, like hybridizer. The difference in the results of preliminary study of the particles from hybridizer and cyclomix should be the way of operating the particles and type of mechanical forces they apply on the particles. In hybridizer, the mechanical impact forces take an important place in the treatments, but on the other hand, cyclomix uses shearing forces mainly. The results of preliminary study also showed that there is a high percentage of particle recovery (> 94%) for each operating velocity of the cyclomix.

The ESEM observations show that the particles keep their particle size and shape and at the end of the dry coating trials in cyclomix, discrete particle coating have been obtained for all operating conditions.

In the coating strength analysis of the particles, it was observed that, similar to the hybridizer trials, the coating strength of the coated particles in cyclomix increases with increasing operating velocity, since the generated mechanical energy by the equipment is probably related to operating velocity.

The analysis of flowability properties of the treated particles in cyclomix shows that either just treated PMMA particles or PMMA coated with talc particles have very good flowability. The possible reason of this result should be having no particle fragmentations in cyclomix trials. On the other hand, it was observed that the talc coated PMMA particles have always better flowability than individually treated PMMA particles in cyclomix.

***In the turbula trials***, the PMMA particles have been pre-treated in hybridizer to be able to compare the results with other mixers. The preliminary study shows that mixing of particles

in turbula doesn't affect the particle characteristics (size and shape) of the pre-treated PMMA particles in hybridizer.

The visual analysis shows that there is discrete type of talc coating on the PMMA particles after coating them with talc particles in turbula. Moreover, it was also observed that there are some talc agglomerates in the mixture, because of the insufficient mechanical forces in turbula trials.

The results of the granulometer show that particle liberation pressure decreases with increasing mass percentage of talc particles in the mixture for all the cases.

Tapped density and FT4 results show that both 1% and 5% talc coated pre-treated PMMA particles in turbula have better flowability than just pre-treated PMMA particles because of the lubricant property of talc particles.

***In the basic mixing trials***, like the other coated PMMA particles from different equipments, the visual analysis shows that we have obtained discrete coating after coating of particles by basic mixing. So, it means that coating of the host particles by guest particles can be achieved by high energy impact coating devices and also even by simple stirring method.

It was observed that the coating strength of the particles is inversely proportional to the mass percentage of talc particles for the particles that are generated by basic mixing method. Increasing mass percentage of talc particles in the mixture creates more talc agglomerates on the surface of the PMMA particles. In the granulometric analysis, having more agglomerates on the surface (more impact shock contact surface) make them easier to be broken after having impacts with other particles or with the walls of the granulometer.

The flowability analysis also shows that the talc coated PMMA particles by basic mixing method have better flowability than pre-treated PMMA particles in hybridizer.

***The effect of equipment on the end-use properties of the particles***, has been studied at the end. It was observed that the coating strength of the particles that were treated in hybridizer and cyclomix are much stronger compared to the particles that were coated in turbula and by basic mixing method. The effect of mechanical energy that the high force mixers (hybridizer & cyclomix) apply on the particles to break up the agglomerates and coat the host particles, probably has an important role in this result.

The flowability results show that the flowability of the talc coated particles in hybridizer and cyclomix is better than the coated particles in turbula and basic mixing trials. Since, contrary to high force mixers, turbula and basic mixing method can not supply sufficient mechanical

energy to break-up the talc agglomerates and disperse them well on the surface of the PMMA particles.

***In the second part;*** the effect of particle size ratio between host and guest particles on the end-use properties of the particles has been studied. In this part, two different particle sizes of cellets particles have been coated with two different particle sizes of talc particles in hybridizer, cyclomix, turbula and by basic mixing methods.

In the preliminary study, the particles have been individually treated with different operating conditions of each equipment. The operating conditions have been chosen according to the principle that the particles should keep their particle size in order to understand the effect of particle size ratio on the end-use properties of the particles. Afterwards the particles have been coated with theoretical monolayer coating percentage of talc particles in different equipments.

The visual analysis and also chemical analysis of the coating surface (ESEM/EDS) showed that, for all of the dry coating trials, we have obtained discrete type of coating like in the first part of the study. It would be reason of the equipment, operating conditions or the characteristics of the particles.

The topographical analysis by using the AFM has been done for initial and talc coated cellets 90 and cellets 200 particles. It was found that the surface roughness of the cellets 90 particles gets lower after coating with talc particles. On the other hand, it was observed that the surface roughness of the cellets 200 particles also decreased after coating with talc particles. The possible reason should be the filling and closing up the gaps and valleys on the surface of the cellets particles by talc.

The initial affinity of the particles has been studied by roughly calculating the Van der Waals forces between the particles. It was found that the guest particles have much more affinity to adhere on the host particles than to guest particles. On the other had, it should be considered that the initial affinity of the particles and particle adhesion is not straightforward.

By using the AFM, the adhesion forces between the particles have also been found. It was observed that the adhesion forces between talc particles are much higher than talc and cellets particles. It was also seen that after coating of cellets particles with talc, the adhesion force increases because of contacts between talc-talc particles.

The mass percentage of talc particles on the surface of the cellets particles have been calculated by using the results of the AFM and the adhesion force model. It was observed that

the introduced mass percentages of talc particles are higher than the calculated amounts on the cellets 90 and cellets 200 particles. Agglomeration of talc particles and non-analyzed surface zones of host particles could be considered as some possible reasons for this result.

The coating strength of the particles was one of the end-use property that has been studied. It was seen that coating strength of the particles increases with increasing particle size ratio between the particles, either by decreasing guest particle size, or increasing host particle size, for all the cases. On the other hand, it should be remembered that there are many parameters that affect the particle adhesion, like surface roughness, hardness, elasticity and surface free energy. Surface roughness is one of the most important characteristic of the particles that influences the adhesion between the particles, because it is strongly related to the geometry of contact.

Contact angle and DVS methods have been used in order to understand the water affinity of the particles before and after coating with talc particles. It was observed that the talc coated cellets 90 and cellets 200 particles have lower wettability compared to individually treated cellets 90 and cellets 200 particles for all dry coating trials with different equipment. It was seen that, there is no significant effect of talc coating on the water affinity of the cellets 200 particles but on the other hand, it was observed that the water affinity of the cellets 90 particles decreases, after coating with talc particles in any dry coating equipment because of hydrophobic characteristic of talc.



### **Future Perspectives**

In this research, dry particle coating has been successfully used for the synthesis of particles and the modification of the coating strength, flowability and water affinity properties of the particles have been studied. There are however many other applications where dry particle coating technology can be used for the production of improved composites. One such area is in the dispersing kinetics of the coated particles which is another research and has been studying by Guillaume Lefebvre in RAPSODEE.

In the area of particle adhesion, there are numerous factors that still need to be studied. First, the ability of the dry coating to de-agglomerate and effectively disperse the guest particles should be investigated both experimentally and theoretically. A study in order to model and predict whether a guest particle would de-agglomerate based on the forces they are subjected to in the devices would greatly simplify the choice of equipment and operating conditions for chosen particles.

The methodology of the coating strength analysis with the laser granulometer would be improved by recovery of the samples after the experiments and visually analyse them in order to be sure if the change in particle size is because of the particle detachment or breakage of the particles.

To study the effect of coating on the mechanical properties of a single particle would be also another interesting approach. An equipment that is called Micromanipulator allows to find the single mechanical properties of the particles. It also enables the operator to find the adhesion forces between two single particles and afterwards the results would be compared with the AFM in order to have two different approaches to the particle adhesion phenomena.

Dry particle coating process is very charming because of its certain advantages compared to traditional coating methods in the industry. So, different dry coating applications with specific powder couples (food, metallurgy, cosmetic etc.) and a scale up study of the dry coating process would be necessary and interesting for the industrial applications.



# APPENDICES



## List of Appendices

N°	Title	Page
<b>I</b>	Examples of dry coating applications	241
<b>II</b>	Calculation of mass percentage of guest particles for monolayer coating	252
<b>III</b>	Coating strength of talc coated PMMA particles by basic mixing method	255
<b>IV</b>	Effect of talc coating on the electrostatic properties of PMMA particles	257
<b>V</b>	Characteristics of different AFM probes	260
<b>VI</b>	Calculation of adhesion energy between PMMA & Talc particles	262
<b>VII</b>	Chemical analysis of the particle surface with energy dispersive spectrometer	266
<b>VIII</b>	Contact angle measurements of Talc coated Cellets particles	270
<b>IX</b>	European Union 6 <sup>th</sup> Framework Program Biopowders Project	274



---

**EXAMPLES OF DRY PARTICLE COATING APPLICATIONS**
**1. By Mechanofusion**

Host Particles	Guest Particles	Equipment	Objectives	Author
PMMA (5µm)	TiO <sub>2</sub> (15 nm)	Mechanofusion	- Improvement of flowability of PMMA - Improvement of wettability of PMMA	Yokoyama et al., 1987
Polystyrene resin (10 µm)	Black Carbon		- Rounding of the particles - Improvement of flowability	
PMMA (0,5 µm)	Polytetrafluoroethylene (PTFE ; 10 µm)		- Decreasing electrostatic charge of PMMA	
PMMA (50 µm)	Black Magnetic Spheres (0.17 µm)	Mechanofusion	- Evaluation of coating mechanism of particles	Alonso et al., 1989 (b)
PMMA (50 µm)	Silver (1 µm)	Mechanofusion	- Creation of super conductive materials by coating - Understand the effect of size of metal particles and their concentration on conductivity	Alonso et al., 1990 et 1991
Magnesium Niobate (PMN)	Magnesium Stearate (MgSt)	Mechanofusion	- Microencapsulation of ceramic powders - Improving of solid phase reactivity	Mort et al., 1992

Host Particles	Guest Particles	Equipment	Objectives	Author
Ag-Ni Alloy (386 $\mu\text{m}$ )	Ni (1 $\mu\text{m}$ )	Mechanofusion	- Development of electro – conductive material for industry	Satoh et al., 1992
Glass Spheres (23 $\mu\text{m}$ ) PMMA (12 $\mu\text{m}$ ) Silica powder (26 $\mu\text{m}$ )	TiO <sub>2</sub> (0,015 $\mu\text{m}$ )	Mechanofusion	- Characterization of composite particles - Analyzing the difference in surface energy after coating	Naito et al., 1993 (b)
Fe <sub>0,91</sub> Mn <sub>0,09</sub> Si <sub>2</sub> (5 – 8 $\mu\text{m}$ )	Black Carbon (0,02 – 0,3 $\mu\text{m}$ )	Mechanofusion	- Improvement of thermo – conductivity of the particles	Kita et al., 1997
Cu (30 $\mu\text{m}$ )	$\alpha$ -Al <sub>2</sub> O <sub>3</sub> (0,15 $\mu\text{m}$ )	Mechanofusion	- Preparation of metal oxide composites by mechanofusion - Study of surface state and compactness of the coating	Kaga et al., 1997
Al <sub>2</sub> O <sub>3</sub> (45 $\mu\text{m}$ )	Cu (0,2 $\mu\text{m}$ )			
Ni (8 $\mu\text{m}$ )	CoO (0,3 $\mu\text{m}$ )	Mechanofusion	- Creation of new composite materials for fuel cells (MCFCs).	Fukui et al., 2001
Fe (150 $\mu\text{m}$ )	Al <sub>2</sub> O <sub>3</sub> (9 $\mu\text{m}$ )	Mechanofusion	- Dry coating of Fe with Al <sub>2</sub> O <sub>3</sub> particles in order to compare the temperature resistance of the composite particles before and after coating	Jay et al., 2006



## 2. By Magnetically Assisted Impact Coater (MAIC)

Host Particles	Guest Particles	Equipment	Objectives	Author
PMMA (200 $\mu\text{m}$ )	Alumina (20 $\mu\text{m}$ )	MAIC	- Effect of some parameters (particle size, collision frequency, treatment time) on dry coating	Ata et al., 1993
PMMA Alumina Nickel Hydroxide	Titanium Alumina Argent Cobalt Oxide	MAIC	- Feasibility of MAIC for dry coating process - Influence of some parameters (hardness of material, particle size, particles adhesion) on coating	Singh et al., 1997 a) et b)
Starch (15 $\mu\text{m}$ )	Silica (0,3 $\mu\text{m}$ )	MAIC	- Modification of flowability and water affinity properties of starch and cellulose - Optimization of process parameters : process time, particle size ratio, velocity of magnetic particles	Ramlakhan et al., 2000
Cellulose (180/40 $\mu\text{m}$ )	Silica (0,3 $\mu\text{m}$ )			
PMMA (200 $\mu\text{m}$ )	Alumina (0,05, 0,2, 0,4 et 1 $\mu\text{m}$ )			
PMMA (200 $\mu\text{m}$ )	Alumina (0,7 $\mu\text{m}$ )	MAIC	- Optimization of dry coating process time	Singh et al., 2001

### 3. By Theta Composer

Host Particles	Guest Particles	Equipment	Objectives	Author
PMMA (50 $\mu\text{m}$ ) Calcium Carbonate (2,38 $\mu\text{m}$ )	Iron Oxide (0,21 $\mu\text{m}$ )	Theta Composer	- Evaluation of coating performance of theta composer	Miyanami et al., 1994
Cellulose (149 - 180 $\mu\text{m}$ )	Carbazochrome Sodium Sulfonate (CCSS) (5,4 $\mu\text{m}$ )	Theta Composer	- Multilayering & preparation of ethyl cellulose microcapsules - Control of dissolution and liberation of CCSS microcapsules	Fukumori et al., 1998
Food Fibre sorbitol + glucose (80 $\mu\text{m}$ )	Hydrophilic Silica (8 $\mu\text{m}$ )	Theta Composer	- Modification of surface properties of food fibres : flowability and water affinity - Influence of operating conditions on water adsorption, flowability, particle size and dispersion of the particles	Watano et al., 2000
Copper (69,1 $\mu\text{m}$ )	Alumina (0,4 $\mu\text{m}$ )	Theta Composer	- Determination and optimization of operating conditions of theta composer by analysing necessary energy of guest particle immobilization	Iwasaki et al., 2002
$\alpha\text{-Al}_2\text{O}_3$ Fiber (116,7 $\mu\text{m}$ )	$\gamma\text{-Al}_2\text{O}_3$ (27 - 56 nm) CuO (16 - 32 nm)	Theta Composer	- Influence of initial particle charge & process time on the process	Coowanitwong et al., 2003

Host Particles	Guest Particles	Equipment	Objectives	Author
Silica (9,3 $\mu\text{m}$ )	Zinc Oxide (0,02 $\mu\text{m}$ )	Theta Composer	- Optimizing the dry coating process	Iwazaki et al., 2003
Copper (69.1 $\mu\text{m}$ )	$\gamma$ -Alumina – 1 ( 0.4 $\mu\text{m}$ ) $\gamma$ -Alumina – 2 (1.3 $\mu\text{m}$ )	Theta Composer	- Optimization of operating conditions - Effect of guest particles amount on the particle hardness	Iwazaki et al.2004
Cellulose (150 – 177 $\mu\text{m}$ )	Sodium Phosphate (5.4 $\mu\text{m}$ ) Riboflavine (3.3 $\mu\text{m}$ ) Indometacine (6.7 $\mu\text{m}$ ) Naproxen (5.2 $\mu\text{m}$ ) Nifedipine (2.1 $\mu\text{m}$ )	Theta Composer	- Study the quality of the coating - Improvement of flowability of the particles	Yoshikawa et al. 2005

## 4. By Hybridizer

Host Particles	Guest Particles	Equipment	Objectives	Author
Nylon 12 (5 $\mu\text{m}$ )	PMMA (0.3 $\mu\text{m}$ ) Titanium dioxide (0.3 $\mu\text{m}$ )	Hybridizer	- Modification of wettability and water penetration ratio properties of the particles - Comparison with OM Dizer	H. Honda et al., 1987
Nylon 12 Polyethylene Hypoxia Resin (5 $\mu\text{m}$ )	Graphite fluorure	Hybridizer	- Preparation of microspheres by dry coating method - Comparison with a binary mixing powder method	H. Honda et al., 1988
Starch	Phenbutazone Prednisolone Theophylline Indometacin Phenacetine Aspirin	Hybridizer	- Preparation of hybrid powders for pharmaceutical industry by dry coating method - Evolution of crystalline structure and surface of hybrid powders according to process time in hybridizer	Ishizaka et al., 1989
Nylon 12 (5 $\mu\text{m}$ ) Polyethylene (5 $\mu\text{m}$ ) Polyethylene (2-10 $\mu\text{m}$ )	PMMA (0,4 $\mu\text{m}$ ) Silica (0,6 $\mu\text{m}$ )	Hybridizer	- Effect of electrostatic charge of powders on the composite particles - Study the mechanism of adhesion in the preparation of Polyethylene/Silica powders	H. Honda et al., 1989
Candelilla Wax	Zinc Phosphate	Hybridizer	- Improvement of dissolution in water property of the particles	Nakaya et al., 1991

Host Particles	Guest Particles	Equipment	Objectives	Author
Polyethylene (5 µm) Nylon 12 (5 µm)	Silica (0,4 µm) PMMA (0,4 µm)	Hybridizer	- Analysing the surface morphology of coated particles and modification of electrostatic charges of the powders - Study of adhesion mechanism in dry coating process and necessary energy for preparation of coated particles	H. Honda et al., 1991
Boride molybdenum (MoB ; 3,2 µm)	Nickel (0,2 µm)	Hybridizer	- Dry coating of particles in order to improve thermal resistance of the particles	Oki et al., 1992
Titanium (Ti) (150 µm)	Calcium Phosphate (Hydroxyapatite)	Hybridizer	- Dry coating of porous biomaterials	Oki et al., 1992
Polyethylene (5 et 10 µm)	Silica (0,3 - 0,6 – 0,9 µm)	Hybridizer	- Improving the performance of column chromatography (CLHP)	F. Honda et al., 1992
Starch	Indometacin (γ)	Hybridizer	- Effect of dry coating on the dissolution of Indometacine	Ishizaka et al., 1993 (a)
Polyethylene (FB)	N-methylol acrylamide (N-MMA ; solide monomère réactif)	Hybridizer	- Polymerization of composite particles - Effect of rotational velocity and mass fraction on the ratio of polymerisation	Ishizaka et al., 1993 (b)

Host Particles	Guest Particles	Equipment	Objectives	Author
Polyethylene (5 et 10 $\mu\text{m}$ )	Silica (0,3 – 0,6 et 0,9 $\mu\text{m}$ )	Hybridizer	- Estimation of adhesion energy (electrostatic & London Van der Waals interactions) on the formation of monolayer guest particle coating	H. Honda et al., 1994
Polyethylene (10 $\mu\text{m}$ )	Hydroxyapatite (HA)	Hybridizer	- Evaluation of separation capacity of composite proteins and their mechanical stability	F. Honda et al., 1995
Hydroxyapatite (HAP) (9,32 $\mu\text{m}$ )	Zirconium (PSZ) (0,12 $\mu\text{m}$ )	Hybridizer	- Formation of agglomerates of HAP/PSZ and study of structure and their mechanical resistance	Matsuno et al., 1996
Polyethylene (13,1 $\mu\text{m}$ )	Silica (0,3 $\mu\text{m}$ ) Titanium (0,017 $\mu\text{m}$ )	Hybridizer	- Preparation and characterization of surface of multilayered composite particles	F. Honda et al., 1997
Polyethylene (10 et 40 $\mu\text{m}$ )	Cattle Bone Powder (CBP)	Hybridizer	- Utilisation of CBP composite particles for purification of proteins	F. Honda et al., 1998
Titanium (< 150 $\mu\text{m}$ ) PMMA Insulator materials	Hydroxyapatite Eudragit Conductor materials	Hybridizer	- Improvement of biomaterials for using in pulverisation - Improvement of dissolution - Improvement of conductivity	Shmidt et al., 1998

Host Particles	Guest Particles	Equipment	Objectives	Author
Polyethylene (40 et 180 $\mu\text{m}$ )	Red Bengara Powder (0,14 $\mu\text{m}$ )	Hybridizer	<ul style="list-style-type: none"> <li>- Modification of colour and luminosity of the particles by dry coating</li> <li>- Effect of mass fraction, operation time, operating velocity and average particle size of host particles on degree of homogeneity of the mixture</li> </ul>	Shinohara et al., 2000
Tungsten carbide (WC ; 6 $\mu\text{m}$ )	Cobalt ( Co ; 1,6 $\mu\text{m}$ ) Aluminium Oxide ( $\text{Al}_2\text{O}_3$ ; 0,5 $\mu\text{m}$ ) Titanium carbide (TiC ; 0,9 $\mu\text{m}$ )	Hybridizer	<ul style="list-style-type: none"> <li>- Effect of particle size on the mixing quality</li> <li>- Effect of mixing quality on the mechanical properties of the composite particles</li> </ul>	Kangwantrakool et al., 2001
Tungsten carbide (WC ; 6 $\mu\text{m}$ )	Cobalt ( Co ; 1,4 $\mu\text{m}$ ) Aluminium Oxide ( $\text{Al}_2\text{O}_3$ ; 0,5 $\mu\text{m}$ ) Titanium carbide (TiC ; 0,9 $\mu\text{m}$ )	Hybridizer	<ul style="list-style-type: none"> <li>- Evaluation of hardness of the composite materials according to different mass fractions of guest particles and comparison with WC – Co alloys</li> </ul>	Kangwantrakool et al., 2002
Nylon (10 $\mu\text{m}$ )	Polyethylene (5 $\mu\text{m}$ ) $\text{Fe}_3\text{O}_4$ (200 nm)	Hybridizer	<ul style="list-style-type: none"> <li>- Improving magnetic properties of the particles</li> </ul>	Li et al., 2003

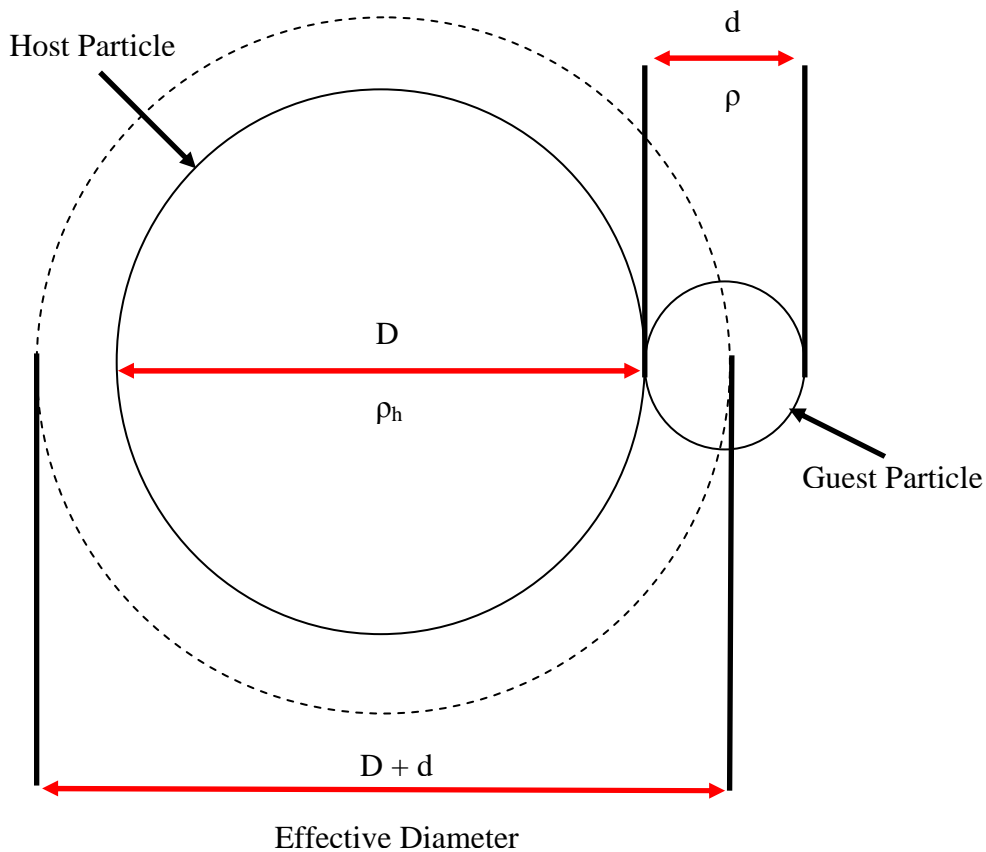
Host Particles	Guest Particles	Equipment	Objectives	Author
Tungsten carbide (WC ; 6 $\mu\text{m}$ )	Cobalt ( Co ; 1,4 $\mu\text{m}$ ) Aluminium Oxide ( Al <sub>2</sub> O <sub>3</sub> ; 0,5 $\mu\text{m}$ ) Titanium carbide (TiC ; 0,9 $\mu\text{m}$ )	Hybridizer	- Sintering study and its effect on the microstructure and mechanical properties of the WC – Co/TiC – Al <sub>2</sub> O <sub>3</sub> particles	Kangwantrakool et al., 2003
Glass Spheres (300 $\mu\text{m}$ ) PMMA (200 $\mu\text{m}$ ) $\gamma$ -Alumina (80 $\mu\text{m}$ ) Silica – Alumina (40 $\mu\text{m}$ )	Silica carbide (SiC ; 3,2 $\mu\text{m}$ )	Mechanofusion, MAIC and Hybridizer	- Discrete coating of materials by dry coating techniques in order to increase the agglomeration temperature of the host particles by coating them with high temperature resistant materials (SiC)	Mohan et al., 2003
Activated Carbon (1-50 $\mu\text{m}$ ) Starch ( $\leq$ 50 $\mu\text{m}$ )	Praziquantal (1-50 $\mu\text{m}$ )	Hybridizer	- Optimisation of taste masking and improving the liberation kinetics of Praziquantal by dry coating technique	Pieper et al., 2004
Grinded Magnesium (75 $\mu\text{m}$ )	Carnuba Wax (15 $\mu\text{m}$ )	MAIC, Hybridizer and Mechanofusion	- Protecting pyrotechnic properties of magnesium powder by dry coating - Improving the humidity resistance of magnesium by dry coating	Mujumdar et al., 2004



Host Particles	Guest Particles	Equipment	Objectives	Author
Cohesive Starch (15 µm)	Hydrophilic/hydrophobic Silica	MAIC and Hybridizer	- Improving the flowability of starch by dry coating method	Yang et al., 2005
Active principle (50 µm)	Magnesium Stearate (2 µm)	Hybridizer	- Evolution of interparticular forces between host and guest particles	Vilela et al., 2005
TiB2 (6 – 13 µm)	BN (0.6 µm)	Hybridizer	- Study the influence of rotational velocity and operating time on the end use properties of the particles	Feng et al., 2005
Polyethylene (85 µm)	Silica 0,3 – 0,5 et 1 µm	Hybridizer	- Effect of process and filling rate of the hybridizer on quality of coating	Uchiyama et al., 2006
Silica Gel (55 µm)	Magnesium Stearate (5 µm)	Hybridizer and Cyclomix	- Modification of flowability and wettability properties of powders - Study of powder ageing	Ouabbas et al., 2008 (a)
Silica Gel (55 µm) Corn Starch (13 µm)	Aerosil R200 (0.12 nm) Aerosil R974 (0.12 nm) MgSt (5 µm)	Hybridizer and Cyclomix	- modification of wettability & flowability of powders - Study of particle coating strength - Study of discharging kinetics of particles	Ouabbas et al., 2008 (b)

## CALCULATION OF MASS PERCENTAGE OF GUEST PARTICLES FOR MONOLAYER COATING

The number of guest particles on host particles in order to have a monolayer coating can be calculated by using the ratio of particle size and density between the host and guest particles.



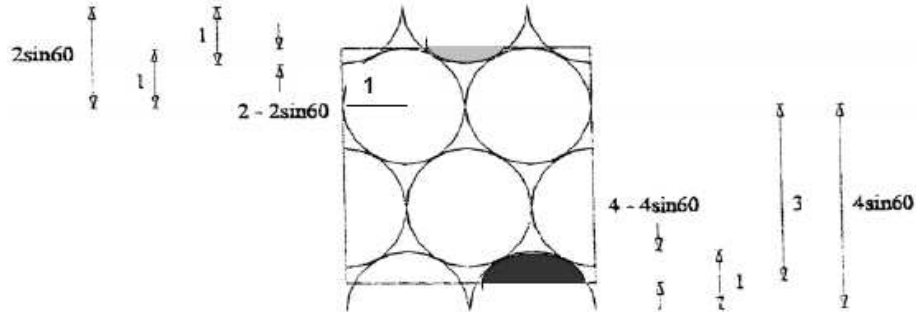
**Figure A.1.** Concept of the Monolayer Coating Model

Figure A.1 shows the concept of the model basically. The model considers that all particles (host & guest) are spherical, have the same diameter and there is no particle deformation in the dry coating trials.

In order to calculate the percentage of guest particles on the host particle surface, there are two hypotheses;

- The particle size ratio between the host and guest particles is in the range of 'ordered mixture' concept ( $10 < x < 100$ )
- The guest particles appear as hexagonal packing on the surface of the host particle

The hexagonal packing of the particles can be simply calculated by using trigonometry as it can be seen from Figure A.2.



**Figure A.2.** Concept of Hexagonal Packing

There are 3 circles, 2 half circles in the section and the black and grey coloured parts can also be calculated. The surface of the sphere that has the diameter of “D + d” can be calculated as;

$$SA = \pi(D + d)^2 \quad \text{(Eqn.A.1)}$$

The projected surface area spherical guest particles can be calculated as;

$$CSA = \frac{\pi}{4} d^2 \quad \text{(Eqn.A.2)}$$

If the number of guest particles in the mixture is n and the number of host particles is N, then the number of contacts (z) between a host and guest particles become;

$$z = \frac{SA}{CSA} C_{2D} \quad \text{(Eqn.A.3)}$$

Where,  $C_{2D}$  refers to compactness in 2 dimensions in hexagonal packing. The number of contacts can also be represented as the ratio between the number of guest and host particles in the mixture;

$$\frac{n}{n_h} = \frac{3.6\pi \left(1 + \frac{d}{D}\right)^2 D^2}{\pi \left(\frac{d}{D}\right)^2 D^2} = \frac{3.6 \left(1 + \frac{d}{D}\right)^2}{\left(\frac{d}{D}\right)^2} \quad \text{(Eqn.A.4)}$$

Where;

$m$  : mass of guest particles (g)

$M$  : mass of host particles (g)

$d$  : diameter of guest particles ( $\mu\text{m}$ )

$D$  : diameter of host particles ( $\mu\text{m}$ )

$\rho$  : density of guest particles ( $\text{g}/\text{cm}^3$ )

$\rho_h$  : density of host particles ( $\text{g}/\text{cm}^3$ )

The mass of host particles ( $M$ ) and the mass of guest particles ( $m$ ) can be calculated by using the equations A.5 and eqn.A.6;

$$M = \rho_h \frac{\pi}{6} D^3 N \quad (\text{Eqn.A.5})$$

$$m = \rho \frac{\pi}{6} d^3 n \quad (\text{Eqn.A.6})$$

Then the ratio between the number of guest and host particles in the mixture becomes;

$$\frac{m}{M} = 3.6 \left( \frac{d}{D} \right) \left( \frac{\rho}{\rho_h} \right) \left( 1 + \left( \frac{d}{D} \right)^2 \right) \quad (\text{Eqn.A.7})$$

This expression can be also converted into the mass fraction of guest particles in the mixture ( $W_c$ );

$$W_c = \frac{m}{m + M} \quad (\text{Eqn.A.8})$$

## COATING STRENGTH OF TALC COATED PMMA PARTICLES BY BASIC MIXING METHOD

Figure A.3, A.4 and A.5 shows the number particle distribution and particle liberation pressure of 1% and 5% talc coated PMMA particles by basic mixing method.

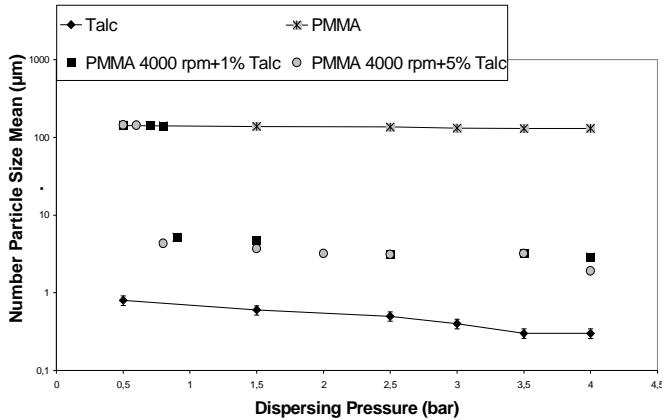


**Figure A.3.** Number Particle Size Mean vs. Dispersing Pressure for Coated and Uncoated PMMA at 4000 rpm by Basic Mixing

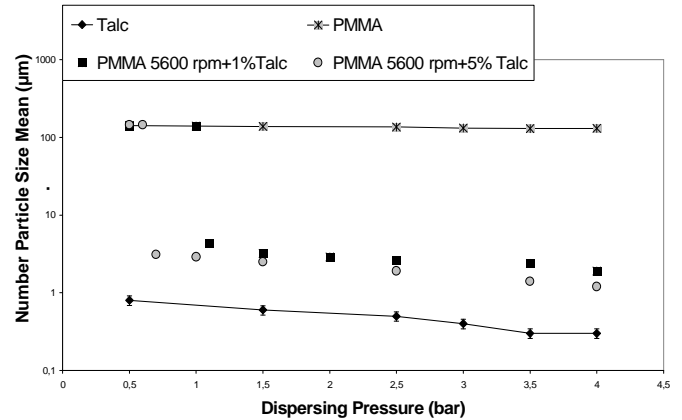


**Figure A.4.** Number Particle Size Mean vs. Dispersing Pressure for Coated and Uncoated PMMA at 5600 rpm by Basic Mixing

It is observed that the particle liberation pressure is 0.9 bars for 4000 rpm treated PMMA with 1% talc particles and it decreases to 0.8 bar for 5% talc coating. For PMMA at 5600 rpm with 1% talc the particle liberation pressure is 1.1 bar and it decreases to 0.7 bar for 5% talc coating

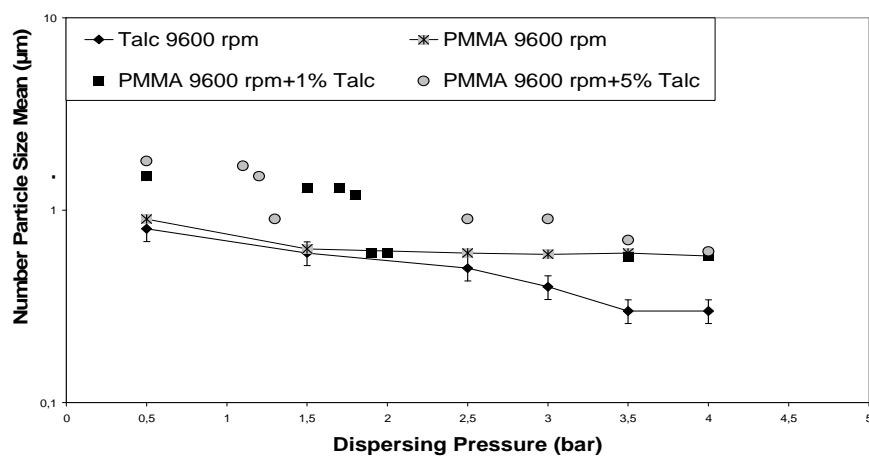


**Figure A.5.** Number Particle Size Mean vs. Dispersing Pressure for Coated and Uncoated PMMA at 9600 rpm by Basic Mixing

PMMA treated at 9600 rpm with 1% talc coating, the particles start to detach (or break up) at 1.9 bar and for 5% talc coating the particle liberation pressure is 1.3 bar. According to these results, for the particles that are treated by basic mixing method, the particle liberation pressure decreases with increasing talc percentage in the coating.(table A.1)

**Table A.1.** Dispersing Pressures and Air Velocities for Particle Detachment for 1% and 5% Talc Coated PMMA Particles by Basic Mixing

<b>Material</b>	<b>Dispersing Air Pressure</b>	<b>Air Velocity</b>
<b>PMMA at 4000 rpm + 1% Talc</b>	0.9 bar	48 m/s
<b>PMMA at 5600 rpm + 1% Talc</b>	1.1 bar	56 m/s
<b>PMMA at 9600 rpm + 1% Talc</b>	1.9 bar	84 m/s
<b>PMMA at 4000 rpm + 5% Talc</b>	0.8 bar	44 m/s
<b>PMMA at 5600 rpm + 5% Talc</b>	0.7 bar	39 m/s
<b>PMMA at 9600 rpm + 5% Talc</b>	1.3 bar	64 m/s

## EFFECT OF TALC COATING ON THE ELECTROSTATIC PROPERTIES OF PMMA PARTICLES

As it has been discussed previously, it was observed some accumulation of PMMA particles in hybridizer trials. It was observed that, generally the uncoated PMMA particles stayed on the walls of stator, inside the recirculation tube and the small space between the rotor and stator (fig. A.6)

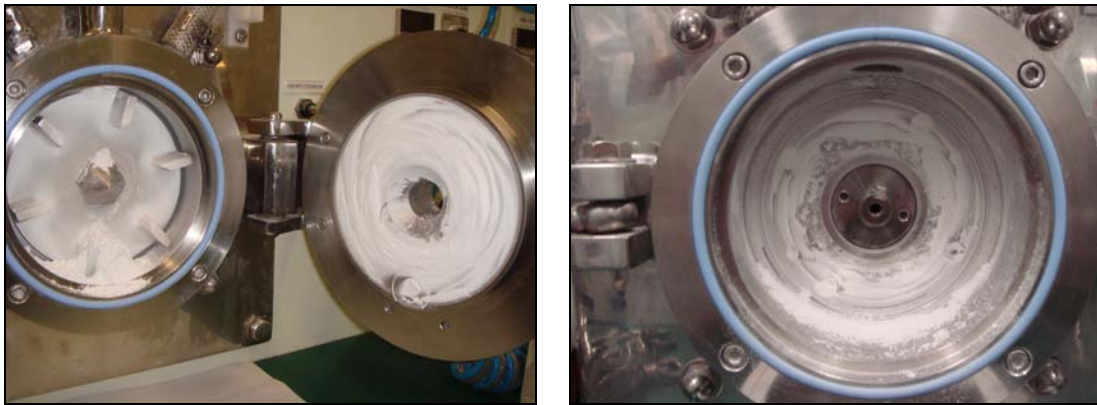


**Figure A.6.** Rotor and Stator of the Hybridizer after PMMA Treatment

In order to understand the particle accumulation inside hybridizer, the electrostatic properties of the particles have been analysed by diminution of particle charge method. Diminution of electrostatic charge of particles measurements are made using a high voltage corona discharge to deposit a small patch of charge on the material to be tested with a fast response field mill electrostatic field – meter used to measure how quickly the deposited charge migrates away by the decrease in the surface voltage (Chubb, 2002). A physical arrangement for diminution of electrostatic charge of particles measurement is shown in Figure A.7.

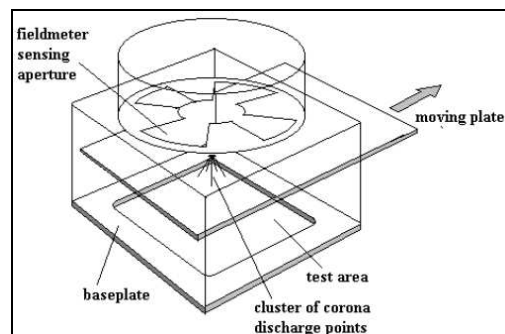


**Figure A.7.** Experimental Setup of Diminution of Electrostatic Charge Measurements (Chubb, 2002)

The corona discharge is created by a brief pulse of high voltage (in the range  $\pm 2.5$  to  $\pm 10$  kV) applied to a cluster of discharge points mounted on a moveable plate a short distance above the surface to be tested. The corona discharge deposits a local patch of charge on to the surface without contact. As soon as charge has been deposited the moveable plate is moved away (in 20 – 30 ms). A fast response field mill electrostatic field-meter, that has been shielded by this plate, is used to measure, without contact, the voltage developed on the surface by this charge and how quickly this voltage falls (to % 40 of the initial value) as the charge migrates away (Chubb, 2002).

The measurements have been done at 20°C temperature and 18–26 % relative humidity. Figure A.8 shows the evaluation of surface voltage according to time.

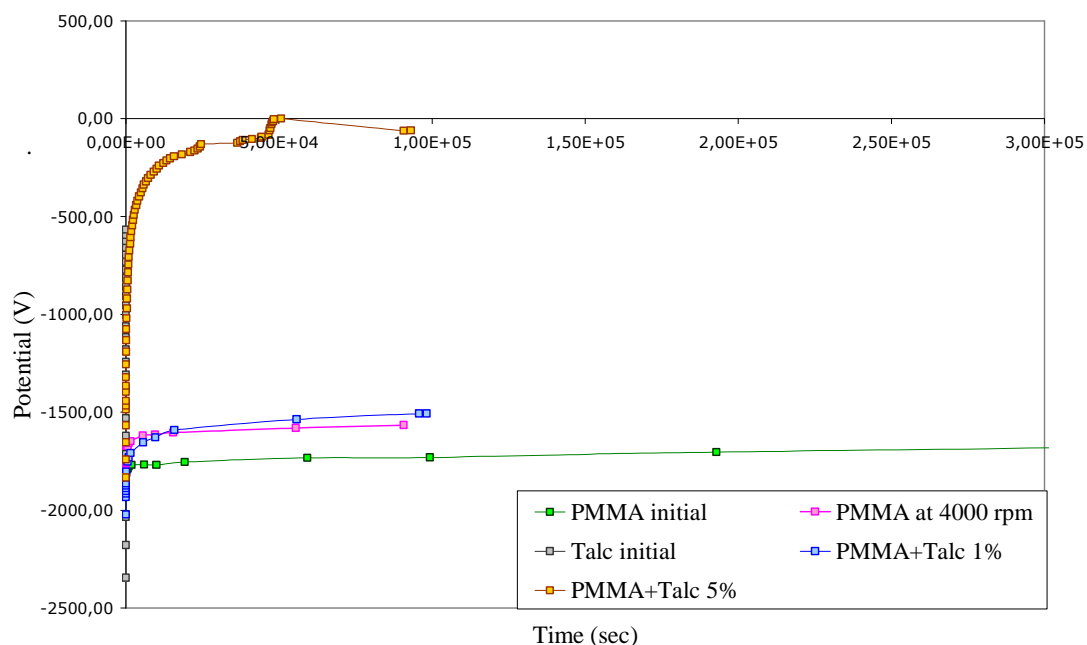


**Figure A.8.** Discharging Time for Initial and Coated Materials

The results show that, the discharging time of initial talc particles is very short (in 7 seconds). On the other hand, initial PMMA particles need 3.5 months and treated PMMA particles at 4000 rpm need 1 month for discharging. The results of coated PMMA particles show the effect of talc coating that is the increasing mass percentage of talc particles in the mixture decreases discharging time of the composite particles. The discharging time for each material can be seen in the table A.2.



**Table A.2.** Discharging Time for Initial and Coated Materials

<b>Material</b>	<b>Time of Discharging</b>
Talc Initial	7.3 second
PMMA Initial	74.5 days
PMMA at 4000 rpm	30.2 days
PMMA + 1 % Talc at 4000 rpm	11.9 days
PMMA + 5 % Talc at 4000 rpm	19 minutes

As conclusion, it was observed that the talc coating has an important role on the modification of discharge time of composite particles. It shows that both lubricant and electrostatic discharging properties of talc particles decreases particle accumulation in hybridizer trials.

## CHARACTERISTICS OF DIFFERENT AFM PROBES

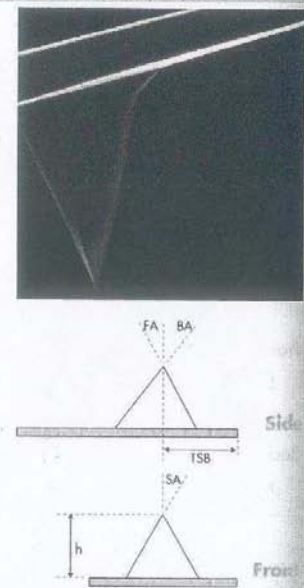
### 1. Characteristics of Tapping Mode Probe (MP11120) and Cantilever

#### MPP-11120

Tap300 Metrology Probes

#### Tip Specifications

Geometry:	Anisotropic
Tip Height:	1.5 $\mu$ m - 20 $\mu$ m
Front Angle:	15° $\pm$ 2°
Back Angle:	25° $\pm$ 2°
Side Angle:	17.5° $\pm$ 2°
Tip ROC:	<10nm
Tip ROC Max:	12.5nm
TSB Nom:	1.5 $\mu$ m
TSB Range:	5 $\mu$ m - 25 $\mu$ m
Tilt Comp:	-
Spike Ht Nom:	-
Spike Ht Range:	-
Spike W:	-
Spike W Range:	-
Overhang:	-
Effective Neck:	-



Model	Mounting	Notes	Qty/pk
MPP-11120-10	Unmounted	Tap300: 40N/m, 300kHz, Symmetric Tip, Al Reflective Coating	10
MPP-11120-50	Unmounted	Tap300: 40N/m, 300kHz, Symmetric Tip, Al Reflective Coating	50
MPP-11120-70	Unmounted	Tap300: 40N/m, 300kHz, Symmetric Tip, Al Reflective Coating	70
MPP-11120-100	Unmounted	Tap300: 40N/m, 300kHz, Symmetric Tip, Al Reflective Coating	100
MPP-11120-W	Unmounted	Tap300: 40N/m, 300kHz, Symmetric Tip, Al Reflective Coating	375
MPP-11123-10	CP	Tap300: 40N/m, 300kHz, Symmetric Tip, Al Reflective Coating	10
MPP-11123-50	CP	Tap300: 40N/m, 300kHz, Symmetric Tip, Al Reflective Coating	50

#### Silicon Probes

#### Cantilever Specifications

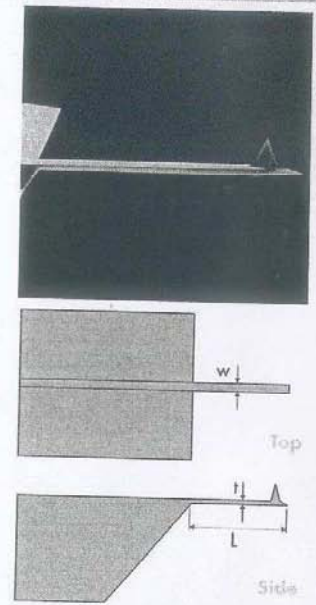
Material: 0.5 - 2  $\Omega$ cm Phosphorus (n) doped Si

Thickness, Nom: 4 $\mu$ m

Thickness, Range 3.5 $\mu$ m - 4.5 $\mu$ m

Front Side Coating: None

Back Side Coating: 40 +/- 10nm of Al



Shape	Freq. (kHz)			k (N/m)			Length ( $\mu$ m)			Width ( $\mu$ m)		
	Nom.	Min.	Max.	Nom.	Min.	Max.	Nom.	Min.	Max.	Nom.	Min.	Max.
A Rectangular	300	200	400	40	20	80	125	115	135	35	30	40

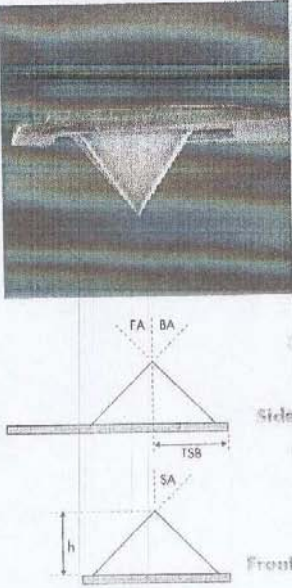
Notes:

## 2. Characteristics of Contact Mode Probe (NP) and Cantilever

### NP Series Probes

#### Tip Specifications

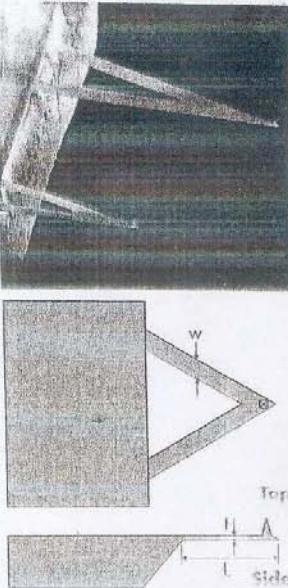
**Geometry:** Cast  
**Tip Height:** 2.5µm - 3.5µm  
**Front Angle:** 35° ± 2°  
**Back Angle:** 35° ± 2°  
**Side Angle:** 35° ± 2°  
**Tip ROC:** 20nm  
**Tip ROC Max:** 60nm  
**TSB Nom:** 4µm  
**TSB Range:** 3µm - 5.5µm  
**Tilt Comp:** -  
**Spike Ht Nom:** -  
**Spike Ht Range:** -  
**Spike W:** -  
**Spike W Range:** -  
**Overhang:** -  
**Effective Neck:** -



### Silicon Nitride Probes

#### Cantilever Specifications

**Material:** Silicon Nitride  
**Thickness, Nom:** 0.6µm  
**Thickness, Range:** 0.4µm - 0.7µm  
**Front Side Coating:** None  
**Back Side Coating:** Bottom Layer: 15nm of Cr, Top Layer: 60nm of Au



Model	Mounting	Notes	Qty/Pk
NP.10	Unmounted	4 Cantilevers 0.06 - 0.58 N/m; Au Reflective Coating	10
NP.20	Unmounted	4 Cantilevers 0.06 - 0.58 N/m; Au Reflective Coating	20
NP.1	Unmounted	4 Cantilevers 0.06 - 0.58 N/m; Au Reflective Coating	100
NP	Unmounted	4 Cantilevers 0.06 - 0.58 N/m; Au Reflective Coating	500

Shape	Freq. (kHz)			k (N/m)			Length (µm)			Width (µm)		
	Nom.	Min.	Max.	Nom.	Min.	Max.	Nom.	Min.	Max.	Nom.	Min.	Max.
A Triangular	57	40	75	0.58			115	100	130	25	20	30
B Triangular	20	14	26	0.12			196	180	212	41	33	49
C Triangular	56	40	75	0.32			115	100	130	17	13	21
D Triangular	18	12	24	0.06			196	180	212	23	18	28

**Notes:**

---

## CALCULATION OF ADHESION ENERGY BETWEEN PMMA & TALC PARTICLES

Dry particle coating devices impart energy to systems of host and guest particles by the application of mechanical forces, causing the particles to impact each other. Impacting guest particles can either adhere to the host particle or rebound becoming detached from the host particle, depending on the magnitude of the adhesion forces between the host and the guest particles after impactation. Therefore, in this part it was aimed to theoretically calculate the adhesion energy between PMMA and talc particles. According to this information, it would be possible to predict the initial affinity of the two materials adhering to each other after an impactation.

Ramlakhan et al. (2001) presented a model to describe adhesion of particles due to elastic-plastic impacts with a surface. The model considers elastic deformation in the two impacting bodies and plastic deformation in the softer of the two bodies. For a guest particle G, impacting on a host particle H, the criteria which allows the particle to rebound is given by:

$$(Q_I - Q_P) > Q_A \quad \text{(Eqn.A.9)}$$

Where  $Q_I$  is the impacting energy due to an impacting velocity ( $v$ ),  $Q_P$  is the energy dissipation in plastic deformation,  $Q_A$  is the adhesion energy between guest and host particles after collision.

The model is based on elastic and plastic deformations on one of the impacting bodies, with only elastic deformation occurring in the other. There are two stages of the first phase for the interaction between the impacting bodies. The first stage is characterized by the purely elastic deformations of the two bodies due to impactation. The impact progresses until the pressure between the two bodies reaches the elastic yield limit of the softer of the two bodies. For the model to be valid the impactation velocity ( $v$ ) must be larger than the elastic limiting velocity ( $\varphi$ ):

$$\varphi = \left( \frac{2\pi}{3K} \right)^2 \left( \frac{2}{5\rho} \right) y^{2.5} \quad \text{(Eqn.A.10)}$$

Where  $y$  is the elastic yield limit of the softer of the two bodies,  $\rho$  is the density of the impacting particle and  $K$  is defined by the eqn.A.11;

$$K = \frac{4}{[3\pi(k_1 + k_2)]} \quad (\text{Eqn.A.11})$$

With;

$$k_i = \frac{(1 - \nu_i^2)}{(\pi E_i)} \quad (\text{Eqn.A.12})$$

Where  $\nu_i$  is the Poisson ratio and  $E_i$  is the Young's modulus of particle i. The properties of the materials, which would be used for the calculations, are given in table A.3.

**Table A.3.** Properties of the Materials

Properties	PMMA (160 $\mu\text{m}$ )	Talc (15 $\mu\text{m}$ )
Elastic Yield Limit (Pa)	$10 \times 10^6$	$5 \times 10^6$
Density ( $\text{kg/m}^3$ )	1190	2691
Poisson's Ratio	0.5	0.268
Young's Modulus (Mpa)	3300	7380
Hardness (Mohs)	1.50	1
Dispersive Surface Energy ( $\text{mJ/m}^2$ )	38	41.2

By using the eqn.A.12, k value for PMMA ( $k_1$ ) was found  $7.21 \times 10^{-11}$  and k value for talc ( $k_2$ ) was found  $4.01 \times 10^{-11}$ . Afterwards the K was found  $3.78 \times 10^9$  by using  $k_1$  and  $k_2$  values in the eqn.A.11.

Therefore the elastic limiting velocity is:

$$\varphi = \left( \frac{2\pi}{3 * 3.78 * 10^9} \right)^2 \left( \frac{2}{5 * 1190} \right) (5 * 10^6)^{2.5} = 0.00031 \text{ m/s}$$

The second stage continues until the two particles have zero relative velocity. During this stage, there is growth of a region of plastic deformation of the softer of the two particles. This area of plastic deformation is surrounded by an annulus in which only elastic deformation occurs. Using conservation of energy, the total kinetic energy of the impaction  $Q_1$  can be expressed as:

$$Q_I = \left( \frac{v^2 m}{2} \right) = Q_e + Q_{pe} + Q_p \quad (\text{Eqn.A.13})$$

Where  $Q_e$  is the energy stored as elastic deformations in the annular region and  $Q_{pe}$  is the energy stored as elastic deformations in the area of plastic deformation.  $v$  is the impacting velocity and  $m$  is the mass of the impacting guest particle which is talc in our system. In this calculation  $v$  has been chosen as 1 m/s and afterwards the  $Q_I$  was found  $1.9 \times 10^{-12}$  j.

The energy used to produce the plastic deformation and the energy stored as elastic energy in the area of plastic deformation can be expressed as:

$$Q_I = \left( \frac{\left( \left( 2mv^2 - \frac{1}{8} m\phi^2 \right)^{0.5} - \left( \frac{15}{8} m\phi^2 \right)^{0.5} \right)^2}{2} \right) \quad (\text{Eqn.A.14})$$

For our system  $Q_p$  was found  $1.88 \times 10^{-12}$  j. Then, it is possible to find the energy for rebound by using the eqn.A.9:

$$Q_I - Q_p = 1.9 \times 10^{-12} - 1.88 \times 10^{-12} = 2 \times 10^{-14} \text{ j}$$

The adhesion energy of the two particles that holds particles together after impaction is found from the expression:

$$U_T = U_M + U_S \quad (\text{Eqn.A.15})$$

Where  $U_T$  is the total adhesion energy and is equal to  $Q_A$ ,  $U_M$  is the adhesion due to mechanical energy and  $U_S$  is the adhesion due to surface energy.  $U_M$  and  $U_S$  is defined by following equations.

$$U_M = P_0 \left( \frac{P_1^{2/3} + 2P_0 P_1^{-1/3}}{3K^{2/3} R_c^{1/3}} \right) \quad (\text{Eqn.A.16})$$

$$U_S = \Delta\gamma\pi \left( \frac{R_c P_1}{K} \right)^{2/3} \quad (\text{Eqn.A.17})$$

Where  $P_0$  is the external force applied to the contacting particles ( $P_0=mg$ ),  $m$  is the mass of the guest particle,  $g$  is the gravitational force,  $\Delta\gamma$  is the surface adhesive energy per unit area and  $R_c$  is the contact geometry parameter.

$P_0$  was found  $3.8 \cdot 10^{-11}$  N for our system.  $\Delta\gamma$  and  $R_c$  was found by using the following equations:

$$\Delta\gamma = 2(\gamma_1^d \gamma_2^d)^{0.5} \quad \text{(Eqn.A.18)}$$

$$\frac{1}{R_c} = \frac{1}{R_1} + \frac{1}{R_2} \quad \text{(Eqn.A.19)}$$

Where  $\gamma_i^d$  is the dispersive energy component of particle i,  $R_1$  is the radius of host particle and  $R_2$  is the radius of the guest particle. For our system,  $\Delta\gamma$  was found  $0.079$  J/m<sup>2</sup> and  $R_c$  was found  $6.45 \cdot 10^{-6}$ .

The projected radius of plastic deformation that the particle undergoes is found by the following expression:

$$P_1 = P_0 + 3\Delta\gamma\pi R_c + \left[ (P_0 + 3\Delta\gamma\pi R_c)^2 - P_0^2 \right]^{1/2} \quad \text{(Eqn.A.20)}$$

The  $P_1$  value was found  $9.6 \cdot 10^{-6}$  N for our system. Afterwards it is possible to calculate  $U_T (= Q_A)$  by using eqn.A.15, eqn.A.16 and eqn.A.17 in order to predict whether talc particle would adhere to or rebound from the surface of PMMA particle.

$$U_T = U_M + U_S = 0.26 \cdot 10^{-2} + 1.6 \cdot 10^{-14} = 0.26 \cdot 10^{-2} \text{ j} = Q_A$$

The  $Q_I - Q_P$  relation has already been found and it was  $2 \cdot 10^{-14}$  j. It shows that the talc particles have initial affinity to adhere on the surface of the PMMA particles, because;

$$(Q_I - Q_P) < Q_A$$

## CHEMICAL ANALYSIS OF THE PARTICLE SURFACE WITH ENERGY DISPERSIVE SPECTROMETER (EDS)

The EDS was used to analyse the chemical composition of the talc coated cellets 90 and cellets 200 particles in order to understand the type of coating (discrete, continuous).

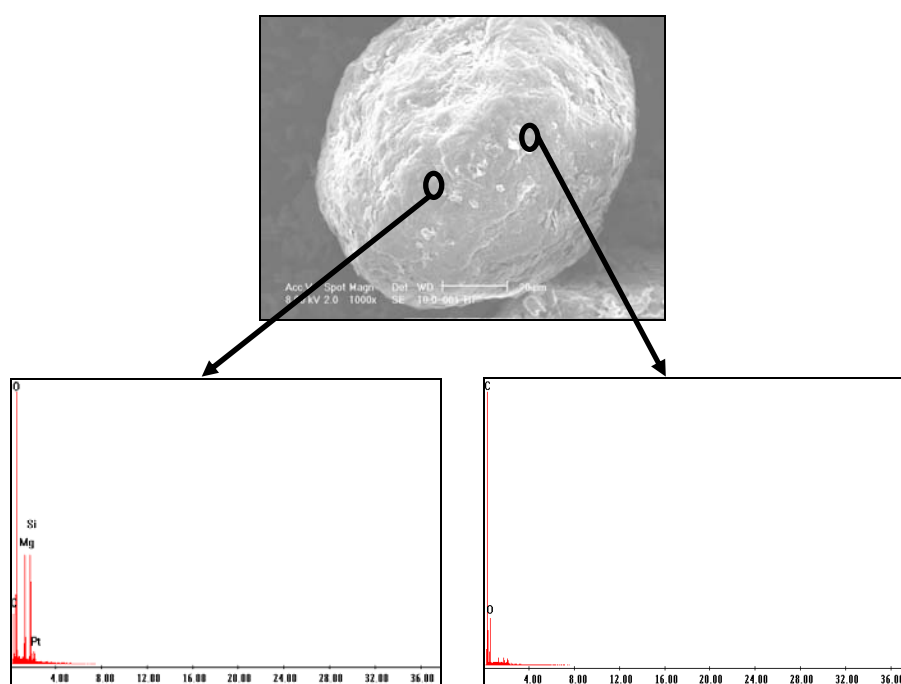


**Figure A.9.** Chemical Analysis of Talc Coated Cellets 90 Particle in Cyclomix

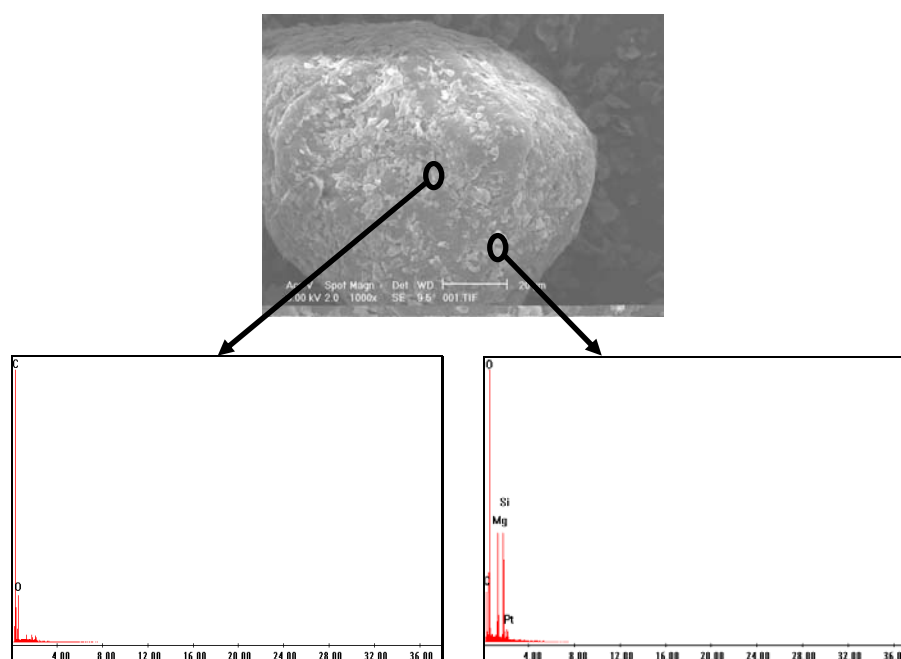


**Figure A.10.** Chemical Analysis of Talc Coated Cellets 90 Particle in Turbula



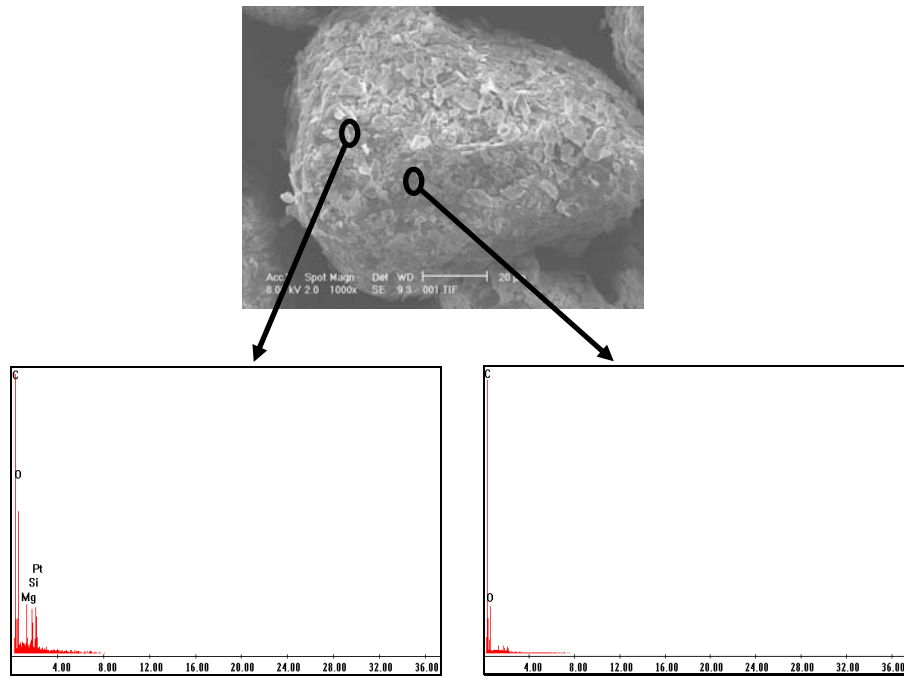


**Figure A.11.** Chemical Analysis of Talc Coated Cellets 90 Particle by Basic Mixing

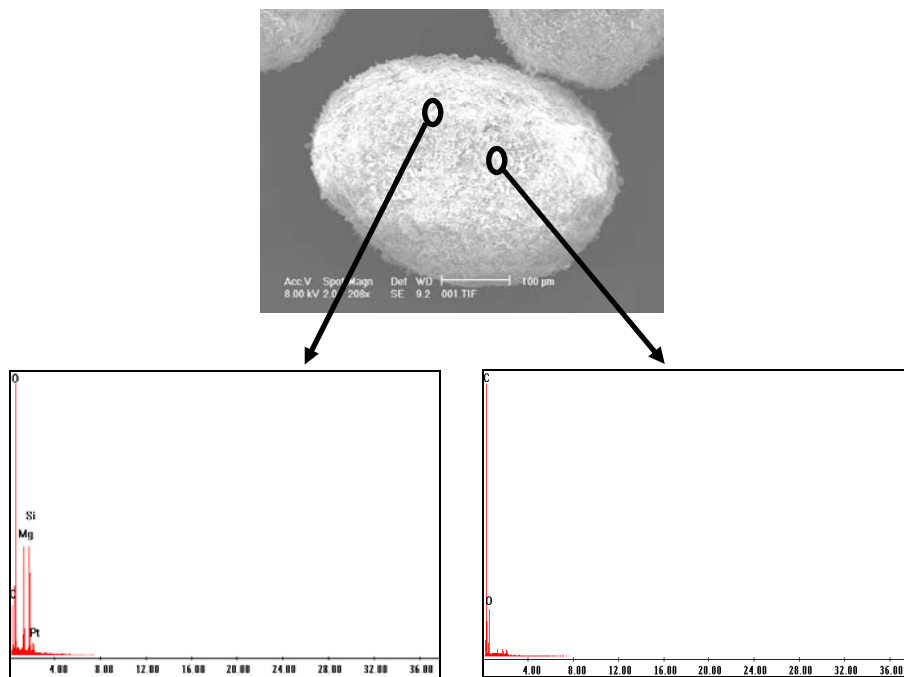


**Figure A.12.** Chemical Analysis of Talc Coated Cellets 200 Particle in Hybridizer

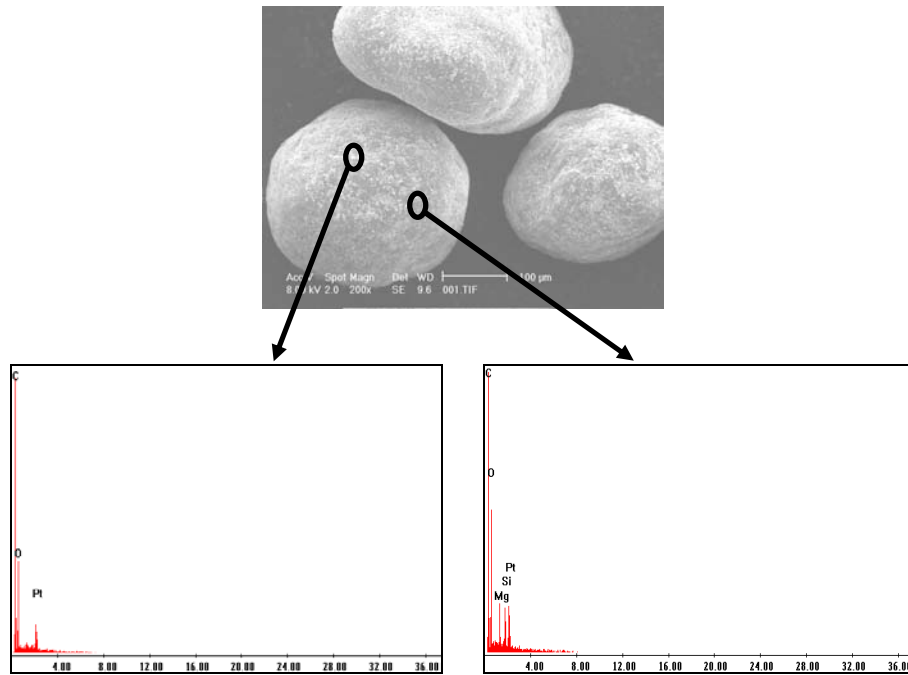


**Figure A.13.** Chemical Analysis of Talc Coated Cellets 200 Particle in Turbula

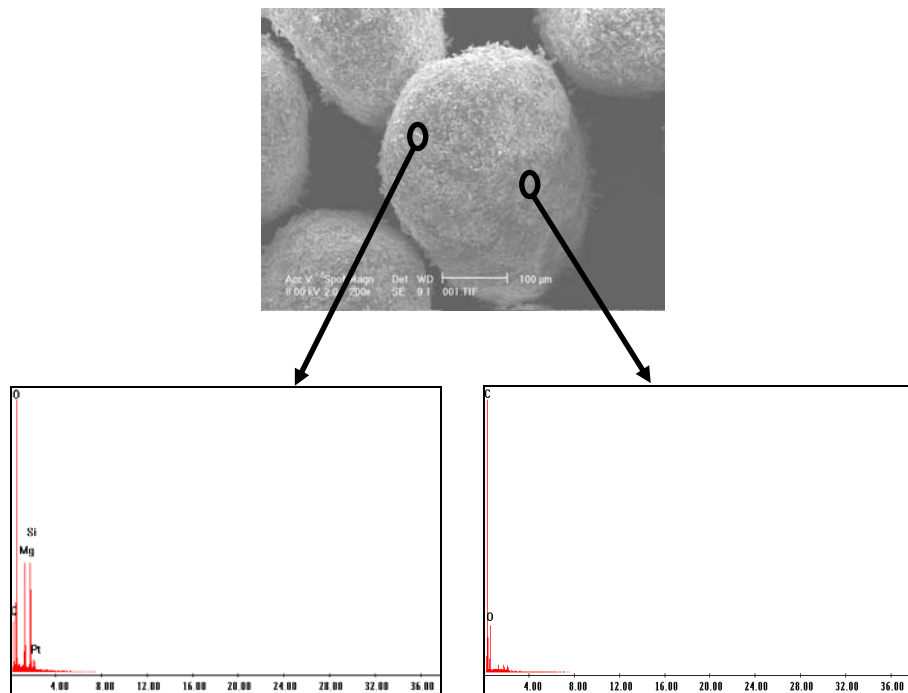


**Figure A.14.** Chemical Analysis of Talc Coated Cellets 200 Particle by Basic Mixing Method

It was observed that there are silicon and magnesium peaks in some regions of surface of both coated cellets 90 and cellets 200 particles for all the cases. It shows that there are talc particles in these surface zones but on the other hand, there are

some surface regions where there is just carbon and oxygen peaks. It shows us that, we have obtained discrete type of talc coating on both cellets 90 and cellets 200 particles in all different coating equipments.

**CONTACT ANGLE MEASUREMENTS OF TALC COATED CELLETS PARTICLES**

The contact angle measurements of talc coated cellets particles have been done with sessile drop technique in order to understand the effect of talc coating and dry coating equipment on the wettability property of the composite particles.

Figure A.15 and A.16 show the images contact angle measurements for talc coated cellets 90 and cellets 200 particles in different dry coating equipments. It was observed that there is no significant difference between coated cellets 90 and cellets 200 particles. Moreover, it can be seen that there is no significant difference between the coated particles in hybridizer, cyclomix or basic mixing technique. It was observed that the water droplet stays on the particles surface even after 30 seconds.

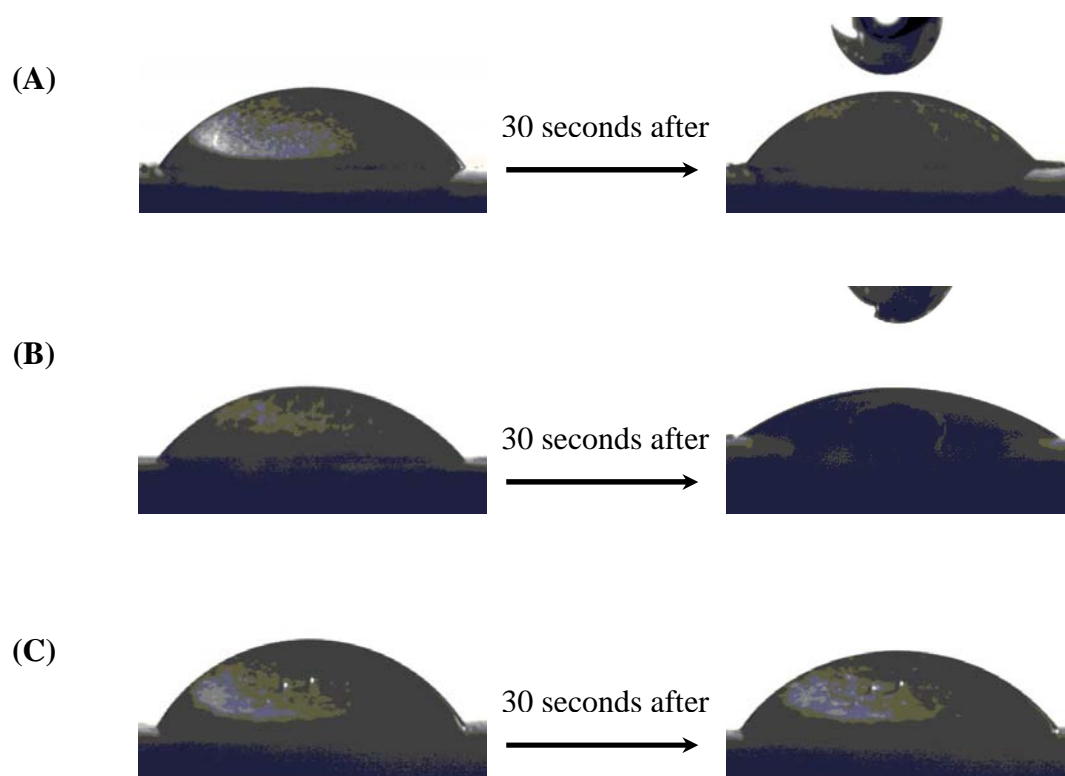


**Figure A.15.** Contact Angle Measurements of (A) Coated Cellets 90 Particles in Cyclomix (B) Coated Cellets 90 Particles in Turbula (C) Coated Cellets 90 Particles by Basic Mixing

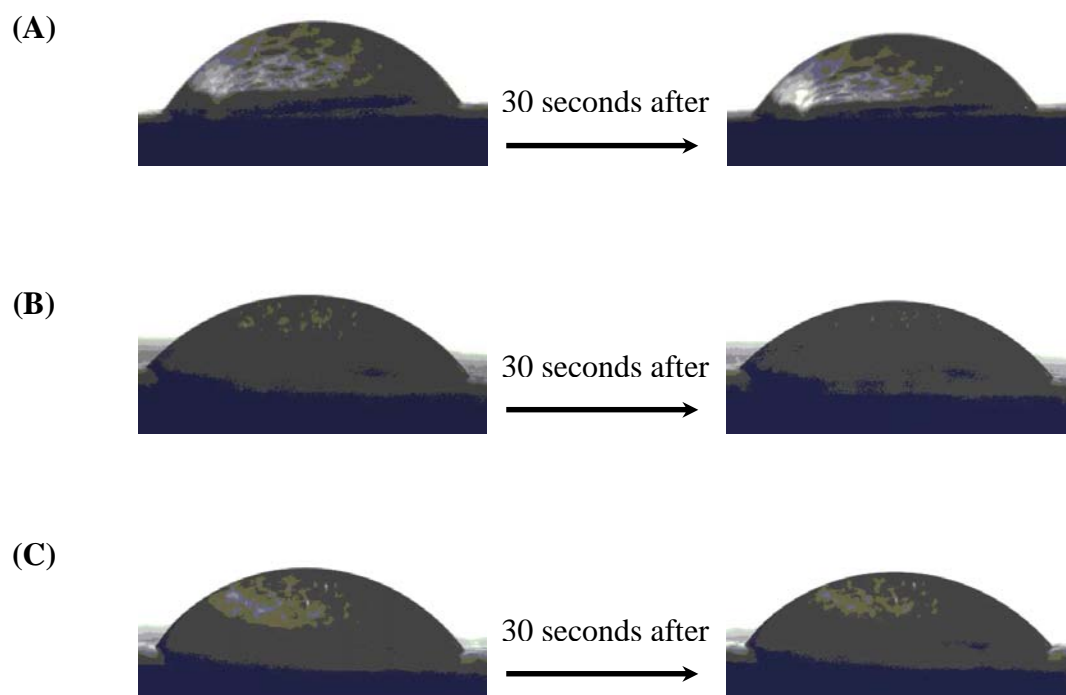


**Figure A.16.** Contact Angle Measurements of (A) Coated Cellets 200 Particles in Cyclomix (B) Coated Cellets 200 Particles in Turbula (C) Coated Cellets 200 Particles by Basic Mixing

**Table A.4.** Average Contact Angle Values of the Particles

SAMPLE	Ave. Contact Angle ( $\theta^\circ$ )
Talc	$66 \pm 3.3$
Cellets 90 Hybridizer	$53.4 \pm 7.1$
Cellets 200 Hybridizer	$57.6 \pm 5.4$
Cellets 90 + 9.6 % Talc Hybridizer	$62.7 \pm 4.8$
Cellets 200 + 3 % Talc Hybridizer	$63.8 \pm 3.3$
Cellets 90 Cyclomix	$54.4 \pm 6.2$
Cellets 200 Cyclomix	$54.5 \pm 4.3$
Cellets 90 + 9.6 % Talc Cyclomix	$62.3 \pm 2.7$
Cellets 200 + 3 % Talc Cyclomix	$64.4 \pm 5.5$
Pre-Treated Cellets 90 + 9.6 % Talc Turbula	$64.9 \pm 7.1$
Pre-Treated Cellets 200 + 3 % Talc Turbula	$61.3 \pm 1.8$
Pre-Treated Cellets 90 + 9.6 % Talc Basic Mixing	$60.1 \pm 8.6$
Pre-Treated Cellets 200 + 3 % Talc Basic Mixing	$61.6 \pm 4.3$

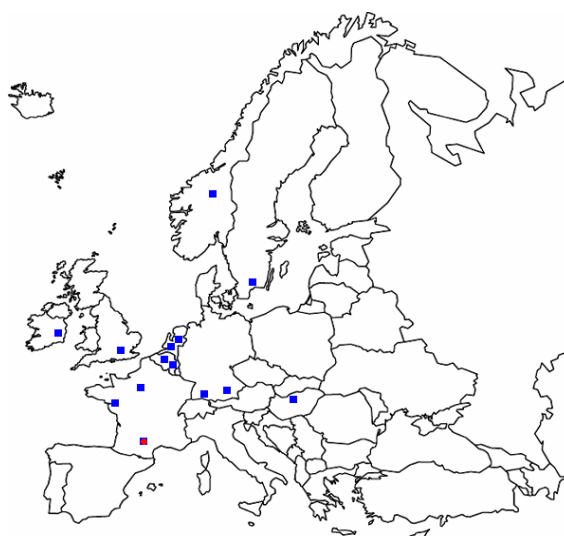
---

## EUROPEAN UNION 6<sup>th</sup> FRAMEWORK PROGRAM BIOPOWDERS PROJECT

This work has been supported by the EU 6<sup>th</sup> framework program “Biopowders” Marie Curie research training network. The focus of the project is to highlight industry problems, knowledge barriers and research and development opportunities in relation to food powders. It highlights the priority research needs for development of new and improved powder products and processes. It is envisaged that this will act as a necessary step in fostering the potential for future research ideas and collaborative research.

This work has been presented in several conferences;

- International Congress on Particle Technology, Nuremberg, Germany, 27-29 March 2007
- Mini conference of Biopowders Project (Research Methodology & research project management), Delft, Netherlands, 13-17 March 2007
- Mini conference of Biopowders Project (Advances in Powder Technology), Budapest, Hungary, 13-14 September 2007
- International Symposium Reliable Flow of Particulate Solids IV, Tromso, Norway, 10-12 June 2008
- Particulate System Analysis 08, Warwickshire, United Kingdom, 2-4 September 2008
- Mini conference of Biopowders Project (Biopowders), Massy, France, 18-19 September 2008



The work has also been published in several communications;

- OTLES S., CHAMAYOU A., GALET L., LECOQ O., DODDS J., (2008), Adhesive Forces and Surface Modification in Dry Particle Coating, In Proc: Particulate Systems Analysis, Warwickshire, UK
- OTLES S., CHAMAYOU A., GALET L., LECOQ O., DODDS J., (2008), Dry Particle – High Impact – Coating of Biopowders – Coating Strength of Biopowders, In Proc:International Symposium Reliable Flow of Particulate Solids IV, Tromso, Norway (This paper was also submitted in Powder Science and Technology)
- OTLES S.,CHAMAYOU A., GALET L., LECOQ O., DODDS J., (2007), Flowability Improvement of Biopowders by Dry Particle – High Impact – Coating, Advances in the Powder Technology, ISBN 978-963-9696-23-5
- OTLES S., CHAMAYOU A., GALET L., LECOQ O., DODDS J., (2007), Biopowders Surface Modification by Dry Particle – High Impact – Coating, In Proc: International Congress on Particle Technology, Nuremberg, Germany





## REFERENCES



**Ahmad S., Agnihotry A.**

Synthesis and characterization of in situ prepared PMMA nanocomposites, *Bulletin of Material Science*, 30, 31-35, 2007

**Alonso M., Satoh M., Myanami K.**

Powder coating rotary mixer rocking motion, *Powder Technology*, 56, 135-141, 1988.

**a) Alonso M., Satoh M., Myanami K.**

Mechanism of the combined coating–mechanofusion processing of powders, *Powder Technology*, 59, 45-52, 1989

**b) Alonso M., Satoh M., Myanami K.**

Kinetic of fines transfer among carriers in powder coating, *Powder Technology*, 59, 217-224, 1989

**Alonso M., Satoh M., Myanami K.**

The effect of random positioning on the packing of particles adhering to the surface of a central particle. *Powder Technology* 62, 35-40, 1990

**Alonso M., Alguacil F.J.**

Dry mixing and coating powders, *Revista de Metalurgia*, 35, 315-328, 1999

**Alonso M., Alguacil F.J.**

Stochastic modelling of particle coating, *Aiche Journal*, 47, 1303-1308, 2001

**Anczykowski B., Kruger D., Fuchs H.**

Cantilever dynamics in quasinoncontact force microscopy: Spectroscopic aspects, *Physical Review B* 53, 23, 15485-15488, 1996

**Ata A., Rabinovich I., Singh R.K.**

Magnetically assisted impaction coating process to synthesize engineered particulates with controlled surface characteristics, *Material Research Society Symposia Proceedings*, 501, 1998

**Balard H., Comard M.P., Calvet C., Dodds J.A.**

Study of surface properties of polymer absorbed on a solid surface using inversed gas chromatography techniques, *Materials Sciences Technology Conference*, 9-11 October Newaska, 2000

**Bannister P., Harnby N.**

A colorimetric technique for assessing the mixture quality of fine particle mixtures, *Powder Technology*, 36, 275-270, 1983

**Berrquand A., Mazeran P.E., Laval J.M.**

Influence of volume and surface properties on phase contrast in tapping mode atomic force microscopy, *Surface Science*, 523, 125-130, 2003

**Boisgard R., Michel D., Aime P.**

Hysteresis generated by attractive interaction : oscillating behaviour of a vibrating tip-microlever system near a surface, *Surface and Science*, 401, 199-205, 1998

**Bunham N.A., Behred O.P., Oulevery F., Gremaud G., Gallo P.J., Gourdon D., Dupas E., Kulik A.J., Pollock H.M., Briggs G.A.D.**

How does a tip tap?, *Nanotechnology*, 8, 67-75, 1997

**Butt H.J., Capella B., Kappl M.**

Force measurements with atomic force microscope: technique, interpretation and applications, *Surface Science Reports*, 59, 1-152, 2005

**Cappella B., Dietler G.**

Force-distance curves by atomic force microscopy, *Surface Science Reports*, 34, 1-104, 1999

**Castellanos A.**

The relationship between attractive interparticle forces and bulk behaviour in dry and uncharged fine powders, *Advances in Physics*, 54, 263-376, 2005

**Chatelet J.**

Application du laser à la granulométrie, *Techniques de l'ingénieur, Electronique dossier N° E4410*, 1996

**Chen Y., Yang J., Dave R.N., Pfeffer R.**

Fluidization of cohesive particles by surface modification. *CHOPS 05*, 2006

**Chen W., Dave R.N., Pfeffer R., Walton O.**

Numerical simulation of mechanofusion system, *Powder Technology*, 146, 121-136, 2004

**Chen X., Roberts C.J., Zhang J., Davies M.C., Tendler S.J.B.**

Phase contrast and attraction repulsion transition in tapping mode atomic force microscopy, *Surface Science*, 519, 593-598, 2002

**Chubb J.N.**

New approaches for electrostatic testing of materials, *Journal of Electrostatics*, 54, 233-244, 2002

**Cleaver J.A.S., Tyrrell J.W.G.**

The influence of relative humidity on particle adhesion-a review of previous work and the anomalous behaviour of Soda-lime Glass, *Kona*, 22, 9-22, 2004

**Cleaver J.A.S., Tyrrell J.W.G.**

Energy dissipation in tapping mode atomic force microscopy, *Applied Physics Letters*, 20, 2613-2615, 1998

**Coowanitwong N., Wu C.Y., Cai M., Ruthkosky M., Rogers J., Feng L.**

Surface modification of Al<sub>2</sub>O<sub>3</sub> fiber with binary nanoparticles using a dry-mechanical coating technique, *Journal of Nanoparticles Research*, 5, 247-258, 2003

**During U.**

Extracting interaction force and complementary observes in dynamic probe microscopy, *Applied Physics Letters*, 9, 1203-1205, 2000

**Egermann H., Orr N.A.**

Ordered mixtures-Interactive mixtures, *Powder Technolgy*, 36, 117-118, 1983

**Elvira C., Fanovich A., Fernandez M., Fraile J.**

Evaluation of drug delivery characteristics of microspheres of PMMA–PCL–cholesterol obtained by supercritical-CO<sub>2</sub> impregnation and by dissolution–evaporation techniques. *Journal of Controlled Release*, 99, 231–240, 2004

**Fatah N.**

Etude et comparaison des poudres microniques et nanométriques: Approche microscopique pour le calcul des propriétés interparticulaires, *Proceedings du congrès Sciences et Technologie des Poudres STP07, Albi, 23-25 May 2007*

**Freeman R.**

Measuring the flow properties of consolidated, conditioned and aerated powders-A comparative study using a powder rheometer and a rotational shear cell, *Powder Technology*, 174, 25-33, 2007

**Fukumori Y., Ichikawa H., Ueda M.**

Preparation of controlled release microencapsules by high-speed elliptical rotor type powder mixer, 3<sup>rd</sup> Congress in Particle Technology, UK, 1998

**Garcia R., San Paulo A.**

Dynamics of vibrating tip near or in intermittent contact with a surface, *Physical Review*, 20, 13381-13384, 2000

**Garcia R., San Paulo A.**

Attractive and repulsive tip-sample interaction regimes in tapping mode atomic force microscopy, *Physical Review*, 7, 4961-4967, 1999

**Gotzinger M., Peukert W.**

Dispersive forces of particle-surface interactions: direct AFM measurements and modelling, *Powder Technology*, 130, 102-109, 2003

**Hamaker H.C.**

The London-Van der Waals attraction between spherical particles, *Physica IV*, 10, 1059-1072, 1937

**Hassanpour A., Kwan C.C., Ng B.H., Rahmania N., Ding Y.L., Ghadiri M.**

Effect of granulation scale-up on the strength of granules, *Powder Technology*, 1-9, 2008

**Hersey J.A.**

Ordered mixing: a new concept in powder mixing, *Powder Technology*, 11, 41-44, 1975

**Hersey J.A.**

Preparation properties ordered mixtures, Australian Journal of Pharmaceutical Sciences, 6, 29-31, 1977

**Honda H., Ono T., Ishizaka T., Matsuno T., Katano M.**

Surface modification of powders by the high speed impact treatment method, Journal of the Society of Powder Technology Japan, 24, 593-599, 1987

**Honda H., Matsuno T., Koishi M.**

Preparation of a graphite fluoride modified-polymer microsphere by a high speed impact treatment method, Journal of the Society of Powder technology Japan, 25, 597-602, 1988

**Honda H., Matsuno T., Koishi M.**

The effect of powder properties on dry impact blending preparation method, Journal of the Society of Powder technology Japan, 25, 666-671, 1989

**Honda H., Kimura M., Honda F., Matsuno T., Koishi M.**

Preparation of composite and encapsulated powder particles by dry impact blending, International Journal of Chemistry and Biotechnology, 1991

**Honda F., Honda H., Koishi M.**

Application of non-porous silica untramicrospheres to high performance liquid chromatographic column packings, Journal of Chromatography, 609, 49-59, 1992

**Honda H., Kimura M., Honda F., Matsuno T., Koishi M.**

Preparation of monolayer particle coated powder by the dry impact blending process utilizing mechanochemical treatment, Colloids and Surfaces A, Physicochemical and engineering Aspects, 82, 117-128, 1994

**Honda F., Honda H., Koishi M., Matsuno T.**

Double-layered composite particles as a complex stationary phase for high-performance liquid chromatography, Journal of Chromatography A, 775, 13-27, 1997

**Honda F., Honda H., Koishi M., Matsuno T.**

Properties of cattle bone powder-coated composite particles as high-performance and open column liquid chromatographic column packings, Journal of Chromatography A, 813, 21-33, 1998

**Horiuchi S., Kajita T., Tachibana S.**

Preparation of pigment-polymer hybrid particles for plastic colorants by dry-impact blending method, Journal of Applied Polymer Science, 74, 1762-1772, 1999

**Ishizaka T., Honda H., Kikuchi Y., Ono K., Katano T., Koishi M.**

Preparation drug diluent hybrid powder by dry processing, Journal of Pharmacy and Pharmacology, 41, 361-368, 1989

**a) Ishizaka T., Honda H., Koishi M.**

Drug dissolution from indometacine-starch hybrid powders prepared by dry impact blending method, Journal of Pharmacy and Pharmacology, 45, 770-774, 1993

**b) Ishizaka T., Kikuchi Y., Ono K.**

Hybridization of particles with reactive solid monomers by the dry impact blending method, 6<sup>th</sup> International Symposium on Agglomeration, Japan, 1993

**Israelachvili J.**

Intermolecular and surface forces, Academic Press Inc., 1996

**Kablitz C, Harder K., Urbanetz N.**

Dry coating in a rotary fluid bed. European Journal of Pharmaceutical Sciences, 27, 212–219, 2006

**Kangwantrakool S., Shinohara K.**

Preparation of new WC-Co/TiC-Al<sub>2</sub>O<sub>3</sub> composite materials with mechanically coated particles, Journal of Chemical Engineering of Japan, 34, 1486-1492, 2001

**Kangwantrakool S., Shinohara K.**

Hot hardness of WC-Co/TiC-Al<sub>2</sub>O<sub>3</sub> composite materials, Journal of Chemical Engineering of Japan, 35, 893-899, 2002

**Kangwantrakool S., Shinohara K.**

Sintering behaviour of mechanically coated WC-Co/TiC-Al<sub>2</sub>O<sub>3</sub> particles by high speed rotational impact blending, International Journal of Refractory Metals & Hard Materials, 21, 171-182, 2003

**Kawashima, Y., Serigano, T., Hino, T., Yamamoto M., and Takeuchi, H.**

International Journal of Pharmaceuticals, 173,243-251, 1998

**Kwan C.C., Ding Y., Williams R.A., Ghadiri M.**

Effects of operating parameters of high shear granulator on the evolved properties and structure of calcium carbonate granules, PSA, Stratford, 21-23 September 2005

**Kuan C.F., Yen W., Chen C., Yuen S.**

Synthesis, characterization, flame retardance and thermal properties of halogen-free expandable graphite/PMMA composites prepared from sol-gel method, Polymer Degradation and Stability, 1357-1363, 2008

**Laarhoven B., Wiers S.C.A., Schaafsma S.H., Meesters G.M.H.**

Attrition strength of different coated agglomerates, Chemical Engineering Science, 63, 1361-1369, 2008

**Lazghab M.**

Wettability assessment of finely divided solids, Powder Technology, 157, 79-91, 2005

**Lifshitz, E. M.**

The Theory of Molecular Attractive Forces Between Solids, Soviet Phys. JETP. 2: 73-83, 1956

**Limmer S J, Seraji S, Wu Y, Chou T P, Nguyen C., Cao G.**

Advanced Functional Materials, 12-59, 2002

**Louey M.D., Mulvaney P., Stewart P.J.**

Characterization of adhesional properties of Lactose carriers using AFM, *Journal of Pharmaceutical and Biomedical Analysis*, 25, 559-567, 2001

**Ma X., Zhou B., Deng Y., Wang C., Pan Y.**

Study of CaCO<sub>3</sub>/PMMA nanocomposite microspheres by soapless emulsion polymerization, *Colloids and Surfaces A.*, 312, 190-194, 2008

**Magonov N., Elings V., Whangbo H.**

Phase imaging and stiffness in tapping mode atomic force microscopy, *Surface Science*, 375, 385-391, 1997

**Marth M., Maier M., Honerkamp J., Brandsh R., Bar G.**

A unifying view on some experimental effects in tapping mode atomic force microscopy, *Journal of Applied Physics*, 85, 7030-7036, 1999

**Massimilla L., Donsi G.**

Cohesive forces between particles of fluid-bed catalysts, *Powder Technology*, 15, 253-260, 1976

**Mendicino R., Bowers A., Catanzariti A.**

Antibiotic coated intramedullary rod, *Tips, Quips and Pearls*, 2008

**Mujumdar A., Wei D., Dave R.N., Pfeffer R., Wu C.Y.**

Improvement of humidity resistance of magnesium powder using dry particle coating, *Powder Technology*, 140, 86-97, 2004

**Mulryan H.T.**

Talc, *Encyclopaedia Kirk-Othmer*, 22, 523-531

**Naidich, Y. V. and Lavrinenko, I. A.**

Capillary adhesion forces between solid particles with an intermediate liquid layer at the contact, *Powder Metallurgy and Metal Ceramics*. 6, 709-710, 1967

**a) Naito M., Kondo A., Yokoyama T.**

Applications of comminution techniques for the surface modification of powder materials, *ISIJ International*, 33, 915-924, 1993

**b) Naito M., Yoshikawa M., Tanaka T., Kondo A.**

Analysis powder composite process by mechanical method, *Kona*, 11, 229-234, 1993

**Ouabbas Y., Dodds J.A., Chamayou A., Galet L., Baron M.**

Particle-particle coating in a cyclomix impact mixer. 3<sup>rd</sup> International Granulation Workshop EFCE, Sheffield, 28-29 June 2007

**Ouabbas Y., Chamayou A., Galet L., Baron M., Thomas G., Grosseau P., Guilhot B.**

Surface modification of silica particles by dry coating: characterization and powder ageing, *Powder Technology*, 2008



**Paqueton H., Ruste J.**

Microscopie électronique à balayage-images, applications et développements, Techniques de l'ingénieur, Techniques d'analyses, 2006

**Pfeffer R., Dave R.N., Dongguang W., Ramlakhan M.**

Synthesis of engineered particulates with tailored properties using dry particle coating, Powder Technology, 117, 40-67, 2001

**Pieper W.**

The nara hybridization design our own particle, Powder Handling and Processing, 8, 232-234, 1996

**Pieper W., Mattern C.**

Optimization of taste masking pharmaceutical compounds by hybridization technique, Powder Handling and Processing, 16, 136-138, 2004

**Podzcek F., Newton J.M., James M.B.**

Variation in the adhesion force between a drug and carrier particles as a result of changes in the relative humidity of the air, International Journal of Pharmaceutics, 149, 151-160, 1997

**Podzcek F. Newton J.M., James M.B.**

Adhesion and friction between powders or aluminium surface determined by a centrifuge technique, Powder Technology, 83, 201-209, 1995

**Rabinovich, Y. I., Esayanur, M. S., Moudgil B. M.**

Capillary forces between two spheres with a fixed volume liquid bridge: theory and experiment, Langmuir. 21, 10992-10997, 2005

**Rahmanian N., Ghadiri M., Ding Y.**

Effect of scale operation on granule strength in high shear granulators, Chemical Engineering Science, 63, 915-923, 2008

**Ramlakhan M, Wu C.Y., Watano S., Dave R.N., Pfeffer R.**

Dry particle coating using magnetically assisted impaction coating: modification of surface properties and optimization of system and operating parameters, Powder Technology, 112, 137-148, 2000

**Roberts C.J.**

What can we learn from atomic force microscopy adhesion measurements with single drug particles, European Journal of Pharmaceutical Sciences, 24, 153-157, 2005

**Sabastian A., Salapaka M.V., Chen D.J., Cleveland J.P.**

Harmonic and power balance tools for tapping mode atomic force microscope, Journal of Applied Physics, 89, 6473-6480, 2001

**San Paulo A., Garcia R.**

Tip-surface forces, amplitude and energy dissipation in amplitude modulation (tapping mode) force microscopy, Physical Review, 19, N° 193411, 2001

**Seville J.P.K, Tuzun U., Clift R.**

Processing of particulate solids, Brian Blackie Academic & Professional, 1997

**Shinohara K., Liang H., Uchiyama T.**

Mixing lightness characteristics fine particles coated by high rotational impact blending, Journal of the Ceramic Society of Japan, 108, 402-406, 2000

**Schmidt B., Yoshihara I., Pieper W.**

Production of hybrid particles in the micrometer range by mechanical surface modification of particles without any binding agent, Freiburger Forschungshefte, 841, 148-161, 1998

**Schubert, H.**

Handbuch der Verfahrenstechnik, Wiley-VCH, Weinheim, 2003

**Singh R.K., Ata A., Gerald J.F., Rabinovich L., Hendrickson W.**

Dry coating method using magnetically assisted impaction in a randomly turbulent fluidized bed, Kona, 15, 1997

**Sreejith P.S., Ngoi B.K.A.**

Dry machining: Machining of the future, Journal of Materials Processing technology, 101, 287-291, 2000

**Tao S.L., Lubeley M.W., Desai T.A.**

Bioadhesive poly(methyl methacrylate) microdevices for controlled drug delivery, J. Control. Release, 88, 215-228, 2003.

**Tang W.J., Fu Z.Y., Zhang J.Y., Wang W.M., Wang H., Wang Y.C., Zhang Q.J.**

Fabrication and characteristics of  $TiB_2/Al_2O_3$  core/shell particles by hybridization. Powder Technology, 167, 117-123, 2006

**Tanno, K.**

Current status of the Mechanofoesion process for producing composite particles, Kona, 74, 1990.

**Thiel W.J., Nguyen L.T., Stephenson P.L.**

Fluidized bed granulation of ordered powder mixture reduces the potential for ordered segregation, Powder Technology, 34, 75-80, 1982

**Thomas G., Ouabbas Y., Grosseau P., Baron M., Chamayou A., Galet L.**

Modelling the mean interaction forces between powder particles-Application to silica gel-magnesium stearate mixture, Applied Surface Science, Submitted 2008

**Toussaint, A., De Wilde M.**

A comprehensive model of sintering and coalescence of unpigmented latexes, Progress in Organic Coatings. 30, 113-126, 1997

**Vallet-Regi M., Granado S., Arcos D., Gordo M., Caban M.V.**

Preparation, characterization, and in vitro release of Ibuprofen from  $Al_2O_3/PLA/PMMA$  composites, J. Biomed. Mater. Res., 39, 423-428, 1998.

---

**Veeco Ltd.**  
AFM Manual

**Veeco Ltd.**  
Multimode Picoforce Manual

**Vilela A., Chamayou A., Accart P., Rolland C., Baron M., Dodds J.A.**  
The evaluation of the strength of interactions between magnesium stearate and an active pharmaceutical substance coated by mechanical action, In Proceedings: 8<sup>th</sup> International Symposium on Agglomeration, Thailand, 298-294, 2005

**Vilela A., Concepcion L., Accart P., Chamayou A., Baron M., Dodds J.A.**  
Evolution of the mechanical resistance of powder-powder coating by modulated dry feed particle size analysis, Particle and Particle Systems Characterization, 23, 128-132, 2006

**Visser J.**  
Particle adhesion and removal, Particulate Sciences and Technology, 13, 169-196, 1995

**Wang L.**  
The role of damping in phase imaging in tapping mode atomic force microscopy, Surface Science, 429, 178-185, 1999

**Watanabe T., Ohno I., Wakiyama N., Kusai A., Senna M.**  
Stabilization of amorphous indomethacine by co-grinding in a ternary mixture, International Journal of Pharmaceutics, 241, 103-111, 2002

**Watanabe T., Hasegawa S., Wakiyama N., Akira K., Senna M.**  
Comparison between polyvinylpyrrolidone and silica nanoparticles as carriers for indomethacine in a solid dispersion, International Journal of Pharmaceutics, 250, 283-286, 2003

**Watano S., Imada Y., Miyanami K., Wu C.Y., Dave R.N., Pfeffer R., Yoshida T.**  
Surface modification of food fiber by dry particle coating, Journal of Chemical Engineering of Japan, 33, 848-854, 2000

**Watano, S., Pfeffer, R., DavC, R. N. and Dunphy, W.**  
Dry particle coating by a newly developed rotating fluidized bed coater, Advanced Technologies for Particle Processing: AIChE Conference, Vol. I, 598-565, November 1998.

**Whangbo M.H., Bar G., Brandsch R.**  
Description of phase imaging in tapping mode atomic force microscopy by harmonic approximation, Surface Science, 411, 794-801, 1998

**Yang J., Sliva A., Banerjee A., Dave R.N., Pfeffer R.**  
Dry coating for improving the flowability of cohesive powders, Powder Technology, 158, 21-33, 2005

**Yeung C.C., Hersey J.A.**

Ordered powder mixing course fine particulate systems, *Powder Technology*, 22, 127-131, 1977

**Yip C.W., Hersey J.A.**

Perfect powder mixtures, *Powder Technology*, 16, 189-192, 1977

**Yokoyama T., Uehara K., Naito M.**

The angmill mechanofusion system and its applications, *Kona*, 5, 59-68, 1987

**Yoshihara I., Pieper W.**

Hybridization-technology for surface modification of powders without binders, *Swiss Pharma*, 21, N° 6, 1999

**Youles J.**

Engineered particles through mechano chemical action. *Powder Handling & Processing*, 15, 132-134, 2003

**Zhu A., Shi Z., Cai A., Zhao F., Liao T.**

Synthesis of core-shell PMMA SiO<sub>2</sub> nanoparticles with suspension dispersion polymerization in an aqueous system and its effect on mechanical properties of PVC composites, *Polymer Testing*, 27, 540-547, 2008

## Abstract

Powder coating is an important process for many different industries. It focuses on modifying the surface properties and/or functionality of powders that the natural product does not offer. Surface modification of particles can be done by wet and dry coating methods. However, wet coating methods have become less desirable recently because of environmental concerns over the resulting waste streams and possible VOC emissions. Dry powder coating is an alternative technology avoiding the previous drawbacks, and with the advantages of having small processing time, of being environmentally friendly and with relatively low energy costs.

Dry particle coating consists of three main terms: powder couple, process and the end-use properties of the composite particles. The objective of this study is to have a fundamental knowledge on dry particle coating to better understand the interactions between these terms and also classify the criteria that affect the end-use properties of the particles. In this work, two different model couples have been treated by different equipments and the end-use properties of the composite particles have been compared with each other by using several characterization techniques. In the first part of the study, we focus on the processes and their operating conditions influencing the coating phenomena and to the development of the AFM technique to derive coating coverage information. In the second part the influence of the size of the host and guest particles on the end-use properties are studied.

**Key Words:** Biopowders, Dry Particle Coating, Composite Particles, Interparticular Forces, Coating Strength, Atomic Force Microscopy

## Résumé

L'enrobage des poudres est un procédé important dans le monde industriel. Ce procédé consiste en la modification des propriétés de surface et/ou des propriétés fonctionnelles de poudre qui ne possède pas ces propriétés initialement. La modification de la surface des particules peut être effectuée par enrobage en voie humide ou sèche. Cependant, l'enrobage humide devient de moins en moins souhaitable en raison de préoccupations environnementales due au rejet de COV. Ainsi, l'enrobage à sec paraît être la technologie alternative adaptée pour éviter les inconvénients précédents tout en ayant des avantages tel qu'un faible temps de traitement, un faible coût énergétique ou encore d'être plus respectueux de l'environnement.

L'enrobage à sec met en avant trois termes importants : le couple de poudre, le procédé et les propriétés d'usage des particules composites. L'objectif de cette étude est d'améliorer la connaissance fondamentale du procédé d'enrobage à sec pour mieux comprendre les interactions entre ces termes et aussi de classer les critères qui affectent les propriétés d'usage des particules composées. Dans ce travail, deux différents couples modèles ont été traités avec différents équipements et les propriétés d'usage des particules ainsi obtenues ont été étudiées grâce à des techniques de caractérisation diverses. Dans la première partie de ce travail, nous avons d'une part, étudié le procédé et les conditions opératoires qui influencent le phénomène d'enrobage et d'autre part développé la technique AFM pour obtenir des informations sur la nature de l'enrobage effectué. La seconde partie quant à elle, traite de l'influence de la taille des particules hôtes et invitées sur les propriétés d'usage.

**Mots Clés:** Biopoudres, Enrobage à Sec, Particules Composés, Solidité d'enrobage, Microscopie de Force Atomique